The 2013 AIAA/Cessna Aircraft Company/Raytheon Missile Systems Design/Build/Fly Competition Flyoff was held at TIMPA Field in Tucson, AZ on the weekend of April 19-21, 2013. This was the 17th year the competition was held. Of the 90 entries this year, 81 teams submitted written reports to be judged and were eligible to participate in the flyoff. Sixty teams attended the flyoff, of which 55 completed the technical inspection (five teams attended even though their airplanes had irreparable damage prior to the competition). Over 600 students, faculty, and guests were present. The weather was sunny and warm allowing for non-stop flying. Of the 186 official flight attempts, 95 resulted in a successful score divided among 54 teams. Twelve teams successfully completed all three missions. The quality of the teams, their readiness to compete, and the execution of the flights continues to improve each year.

The contest theme this year was the Joint Strike Fighter. The first mission was a Short Take-off mission with no payload followed by a Stealth mission with internal payload only and a Strike mission which consisted of 6 possible payload configurations with various combinations of internal and external stores. The configuration for each mission 3 attempt was determined by a role of the dice by each team immediately prior to their flight attempt. As usual, the total score is the product of the flight score and written report score. More details on the mission requirements can be found at the competition website: http://www.aiaadbf.org .

First Place went to the University of California Irvine, Second Place went to San Diego State University and Third Place went to Rensselaer Polytechnic Institute. A full listing of the results is included below. The Best Paper Award, sponsored by the Design Engineering TC for the highest report score, went to Cornell University with a score of 96.00.

We owe our thanks for the success of the DBF competition to the efforts of many volunteers from Cessna Aircraft, Raytheon Missile Systems, and the AIAA sponsoring technical committees: Applied Aerodynamics, Aircraft Design, Flight Test, and Design Engineering. These volunteers collectively set the rules for the contest, publicize the event, gather entries, judge the written reports, and organize the flyoff. Thanks also go to the corporate Sponsors: Raytheon Missile Systems and Cessna Aircraft Company, and also to the AIAA Foundation for their financial support. Special thanks go to Raytheon Missile Systems for hosting the flyoff this year.

Finally, this event would not be nearly as successful without the hard work and enthusiasm from all the students and advisors. If it weren't for you, we wouldn't keep doing it.

Russ Althof
For the DBF Governing Committee

Cornell University

2012-2013 Aircraft Design Report

Cessna/Raytheon/AIAA Design/Build/Fly Competition

02/25/2013

Table of Contents

1   Executive Summary

The following report details the design, analysis, manufacturing and testing processes conducted by the Cornell University Design Build Fly project team in its development of a custom, radio-controlled aircraft for the 2012-2013 AIAA/Cessna/Raytheon Design/Build/Fly competition. The goal of this team is to produce an aircraft that can successfully complete each of the three missions specified by the competition rules, meet all listed requirements, and maximize the team's total flight score. The first mission is an empty timed flight, and the two subsequent missions are payload flight missions. For the payload missions, the plane must be capable of housing model rockets that are ballasted to specific weights both internally through a lower bay door and externally under its wings. In addition to inherent structural loading and flight handling requirements, the aircraft must be able to take off within a 30' x 30' square and must meet imposed propulsion limitations for each mission. The overall score is based on the aircraft's empty weight, wingspan, length, payload capacity, and empty and fully loaded flight times.

An analysis of the competition's scoring revealed that the aircraft's flight time would affect our overall score more than any other scoring parameter. The team identified the driving design requirements for this year's competition as maximizing flight speed, carrying the minimum required number of internal stores, and taking off within the allotted 30'x30' square. We considered several aircraft configurations and ultimately chose a conventional design, as it provides a high payload capacity and known stability characteristics. The selected design concept features an aerodynamic fuselage, a single tractor motor configuration, a taildragger landing gear, a conventional tail, and a two-by-two internal payload arrangement.

After reaching a conceptual design, the team broke up into five subteams: aerodynamics, stability and controls, structures, propulsion, and payloads. Each of these subteams identified the design goals of their respective subsystem. Through detailed design and analysis, the subteams optimized their subsystems to best meet the relevant design criteria and conducted testing to validate the design of their subsystems. The successful fabrication and flight test of our first prototype aircraft has enabled us to compare expected and actual performance parameters. Subsequent design iterations will optimize the current design to achieve the maximum possible flight score at competition. Figure 1.1 tabulates scoring estimates for the final aircraft design. We look forward to our second year of participation in the Design/Build/Fly competition!

Mission 1		Mission 2		Mission 3	
Laps flown	8	Stores carried	4	3 lap time (s)	105
Estimated max.	8	Estimated max.	10	Estimated min.	105
Empty weight (lb)	Wingspan (ft)	Length (ft)	FLIGHT SCORE		
4.37	5.50	3.52	12.1		

Figure 1.1 Scoring estimates for final aircraft prototype (report score not included)

2   Management Summary

The Cornell Design Build Fly team is comprised of 20 undergraduate and graduate students with a shared passion for aeronautics and aircraft design. As a team, we spent the first several weeks of the fall semester familiarizing ourselves with this year's competition rules and requirements, conducting a scoring analysis to identify driving design requirements, and developing a conceptual design. We then divided into several sub-groups for the preliminary design, detailed design, fabrication and testing phases of the project.

2.1   Team Organization

For the technical portion of the project, our team consists of five main subteams: aerodynamics, stability and controls, structures, propulsion, and payloads. Each of these groups is responsible for handling a particular aspect of design and analysis for the aircraft. Figure 2.1 illustrates the personnel assigned to each subteam. The team leads assigned members to subteams based on their interests and past experience. Subteam leaders keep their respective subteams on schedule, facilitate communication between subteams, and serve as mentors for the less experienced members of their subteams.
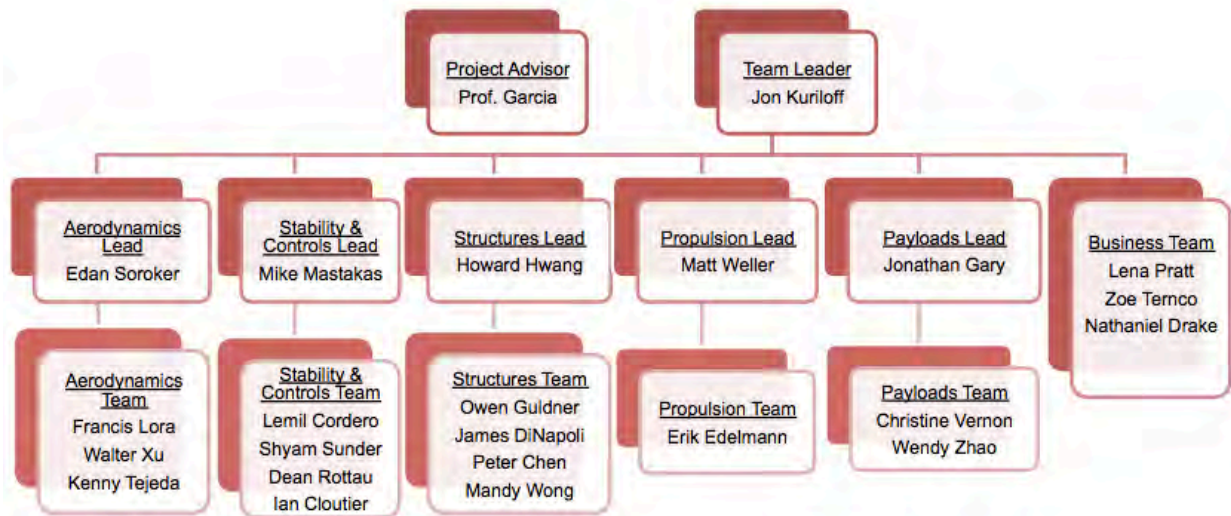
Figure 2.1 Team organizational chart

2.2   Milestone Chart

Our team made use of a milestone chart throughout the project in order to identify key deadlines in the design process and manage the project from a systems standpoint (Figure 2.2). The milestone chart displays planned and actual dates for different elements of the design process as well as key milestones. It also enabled us to highlight deficiencies with our current schedule so that we may improve the process for future years.

| Week of / Design phase | 08/26 | 09/09 | 09/23 | 10/07 | 10/21 | 11/04 | 11/18 | 12/02 | 12/30 | 01/13 | 01/27 | 02/10 | 02/24 | 03/10 | 03/24 |

Figure 2.2 2012-2013 Cornell DBF Milestone Chart

3   Conceptual Design

In the conceptual design phase of the project, our team carefully reviewed the mission and scoring requirements for the 2013 competition, conducted a detailed scoring analysis, and researched aircraft configurations in order to determine what aircraft configuration would yield the maximum possible score for this year's competition.
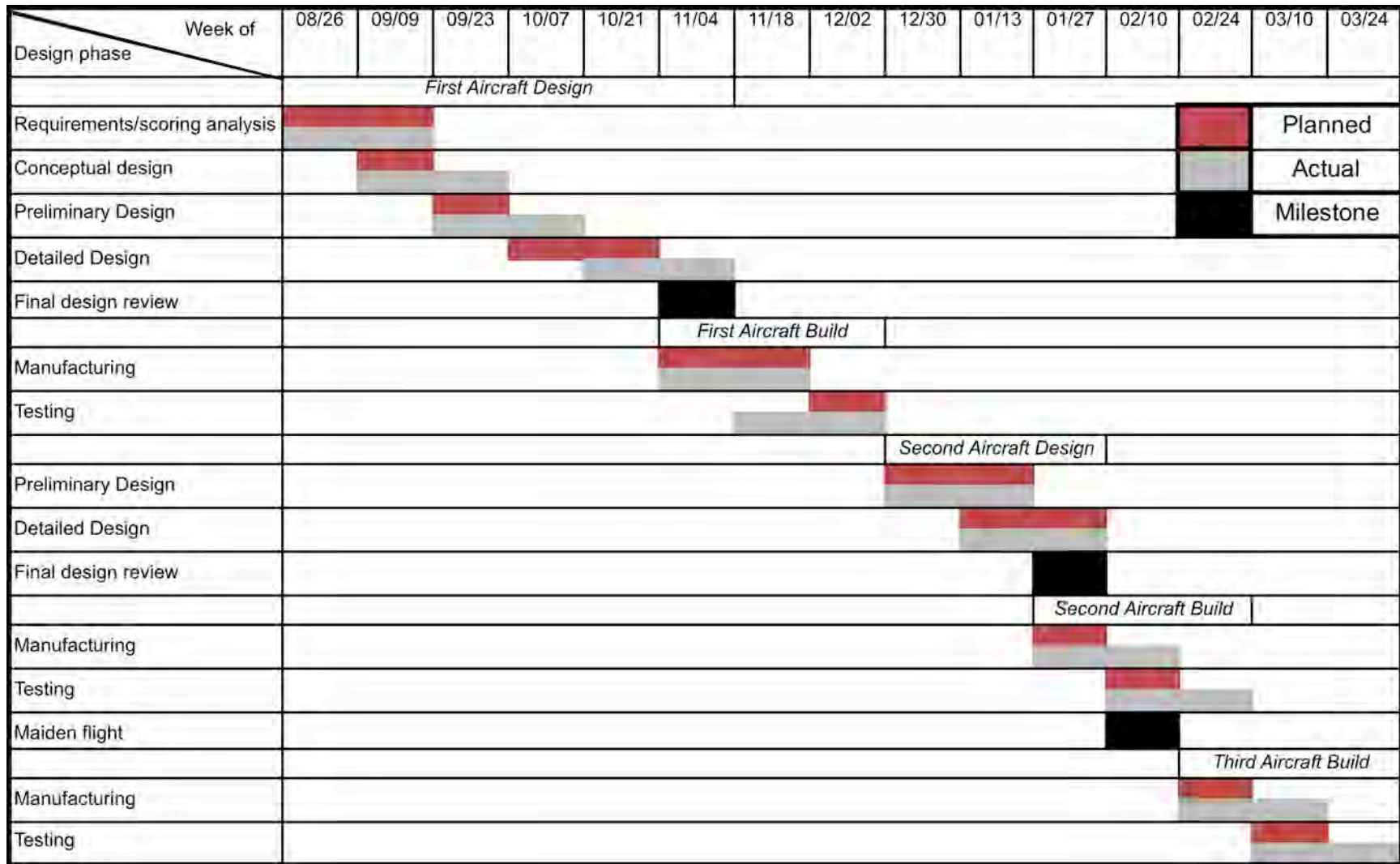
3.1   Mission Scoring and Requirements

The 2013 AIAA DBF competition consists of three independent flight missions. The highest possible score is attained by successfully completing all three missions, adhering to all of the competition constraints, and optimizing for weight, speed, size, and payload capacity.

3.1.1   General Requirements

Several requirements hold for all missions. The aircraft must be able to complete a rolling takeoff within a 30ft by 30ft box. It must also be able to land without sustaining any significant damage. All payloads must be loaded into the flight vehicle in less than five minutes. The same course must be flown for each mission, as shown in Figure 3.1.
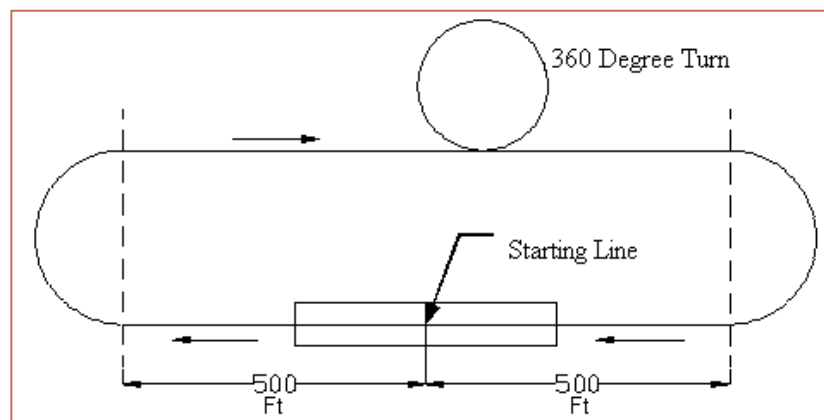
Figure 3.1 Flight course layout

A number of general requirements also apply to the propulsion system. Electric motors must be used and battery chemistry is restricted to either NiMH (Nickel-Metal-Hydride) or NiCd (Nickel-Cadmium). The propulsion batteries must not exceed 1.5 pounds. Additionally, the current in any propulsion components must not exceed 20 amps.

3.1.2   Scoring Summary

The team's score will be determined by the following formula:

*Total score = Written Report Score * Total Flight Score / Raw Aircraft Cost*

Judges determine the team's report score, which can vary from 0 to 100. The total flight score is the sum of the individual mission scores. The details of these scores are outlined in mission descriptions. Rated Aircraft Cost (RAC) is calculated from the equation:

$$RAC = \frac{\sqrt{Empty\ Weight * Size\ Factor}}{10}$$

Empty weight is the greatest weight of the aircraft with the payloads removed. This weight is measured in units of pounds after each successful mission flight. The size factor is measured in feet and is given by the equation:

$$SF = X_{max} + 2 * Y_{max}$$

X_{max} is the aircraft's greatest dimension in the direction of flight and Y_{max} is the greatest dimension in the direction perpendicular to the direction of flight.

3.1.3 Mission 1 – Short Takeoff

The objective of this mission is to have the aircraft complete as many laps as possible around the flight course within a 4-minute flight time. The scoring timer starts when the throttle is advanced for takeoff and ends after four minutes, counting only the number of full laps completed by the aircraft. The aircraft must take off within a 30' x 30' area on the runway. A lap is complete when the aircraft crosses the starting line. Finally, the aircraft must have a successful landing to receive a mission score. The performance in mission one will be normalized over all teams successfully completing the mission by the following formula:

$$M1\ Score\ = 2 \times \frac{Number\ of\ Laps\ Flown\ by\ Team}{Maximum\ Number\ of\ Laps\ Flown\ in\ Competition}$$

3.1.4 Mission 2 – Stealth Mission

This mission calls for the aircraft to take off within the specified area and fly three laps around the course before landing again in the specified area. During the mission, the aircraft carries internal stores, simulating stealth attack missions flown by military aircraft. Actual military aircraft use internal storage when carrying munitions in order to minimize their radar cross-sections when infiltrating hostile airspace.

Access to the storage bay must be from below the aircraft, via bay doors, in order to simulate the bomb bay doors on actual military aircraft. The rules do not require the doors to be mechanized. Additionally, to simulate actual storage of munitions, the stores must be held such that they are in line with the aircraft's flight axis, with the tails pointing aft and the noses pointing

forward. They must also be mounted via a permanent mounting rack that allows for them to be positioned such that there is a proper release trajectory for munitions. The stores may not contact each other or any other part of the aircraft body. All mounting points must secure the stores by their main bodies. All stores are Estes Mini-Max rockets ballasted to 0.25 lb. The aircraft is required to carry at least one store, and may carry any number of them in addition. Also, the external surface of the aircraft cannot be modified for this mission.

The mission score is based solely on the number of stores flown. The score is normalized across all teams by using the highest competition-wide performance in this mission. The aircraft must successfully land to be scored. This mission is scored as follows:

$$M2\ Score\ =\ 4 \times \frac{Number\ of\ Stores\ Carried\ by\ Team}{Maximum\ Number\ of\ Stores\ Carried\ in\ Competition}$$

3.1.5   Mission 3 – Strike Mission

This mission is designed to simulate a fighter jet embarking on a strike flight. The mission calls for carrying different combinations of stores together, potentially both external and internal. The exact payload configuration is decided by a roll of one die to be performed by the team upon entering the assembly area during competition. Therefore, the aircraft must be capable of supporting any of the six possible payload configurations in order to ensure completion of the mission, as shown in Figure 3.2.

Payload Configuration (Number on Die)		1	2	3	4	5	6
Internal	Mini-Max	4	-	2	-	-	-
Left Wing	Mini Honest John	-	-	-	2	-	-
	High Flyer	-	1	-	-	1	1
	Der Red Max	1	1	1	-	1	1
Right Wing	Mini Honest John	-	-	2	2	2	1
	High Flyer	-	1	-	-	-	1
	Der Red Max	1	1	-	-	-	-

Figure 3.2 Mission three payload configurations

As seen from the table, all configurations include external stores to be placed on the wings, and some require internal stores as well. The external stores must be fully external to the aircraft without submerging into the wing. While not actually fired in the mission, they must mount to the airplane such that they potentially could be fired. Therefore, the store fins must lie below all points on the lower surface of the wings, and all mounting points must secure the stores by their main bodies. The external stores may not overlap with or block the deployment area of internal stores. Also, all stores must be separated by at least 3 inches (between centerlines), as well as be at least 3 inches away from the aircraft centerline. The goal of this mission is to complete three

laps around the flight course, with a randomly chosen payload configuration from above, in the shortest amount of time. The mission score is calculated as follows:

$$M3\ Score = 6 \times \frac{Fastest\ Time\ Flown\ in\ Competition}{Team\ Time\ Flown}$$

3.2   Design Requirements

In order to better understand the driving design requirements of this year's competition, we conducted an extensive analysis of the competition scoring. This analysis determined the impact each scoring variable would have on the overall score. Variables were broken down into length, wingspan, empty weight, number of stores flown in mission two, and 3-lap time. Research from past years yielded rough estimates for size parameters and empty weight. Using these values and estimated maximum scores in each of the three missions, we generated a theoretical total maximum score. We then used MATLAB to simulate a percent permutation analysis of how a deviation in each parameter would decrease the overall score. For each of the five variables, the program graphed the score over a percentage reduction in that particular variable, while keeping the other scoring variables constant, as shown in Figure 3.3. By doing so, we were able to isolate how each of the five variables would drive down the maximum score individually.
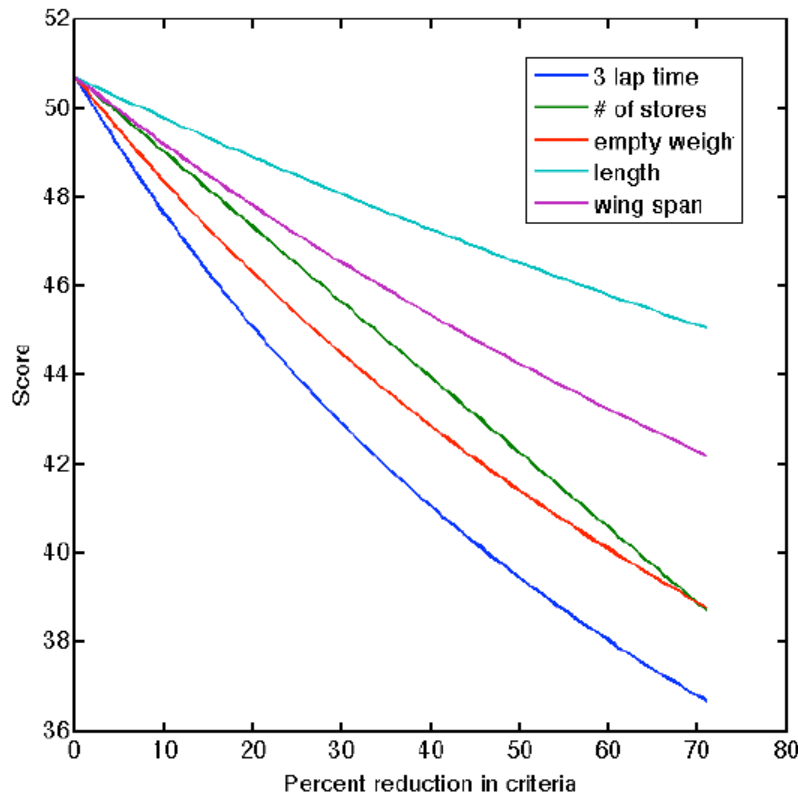

Figure 3.3 MATLAB scoring analysis

The output graph (Figure 3.3) allowed us to rank design parameters as they relate to the score. Moving from the line with the highest to lowest derivative, the team found that the three-lap time was the most important parameter, followed by empty weight, number of stores carried, wingspan, and length, respectively. Taking the rankings into consideration, we determined that focusing on maximizing speed would have the greatest positive effect on the score, even if it were detrimental to another parameter. For instance, a focus on speed would most likely negatively affect the number of stores carried. However, a reduction in the number of stores carried would not negatively affect the total score as much as an increase in the 3-lap time would.

By evaluating how each scoring variable would impact the total flight score, we were able to translate the competition requirements into the critical overall design requirements of the aircraft (Figure 3.4). We concluded that the score was positively correlated with speed, weight and size, while negatively correlated with the number of stores carried. It was then determined that the aircraft should be designed around speed above all else. In order to achieve this goal, the aircraft would have to maximize propulsion, minimize drag, and maximize maneuverability. By incorporating these design traits, the aircraft would maximize the scoring variables that would benefit the total score the most. In addition to these design goals, aircraft stability, accommodation of all possible mission three payloads and the ability to take off within the designated takeoff distance were considered essential requirements. Using these design characteristics, the team began comparing aircraft configurations.

Competition requirements	Design requirements
Complete flight course laps as fast as possible	Maximize propulsive system
	Low drag at cruise
	High maneuverability
Accommodate all payload configurations	Fuselage must hold at least four internal stores
Take off within 30x30 ft square	High wing area
	High static thrust
Take off and land successfully for all missions	Adequate static and dynamic stability

Figure 3.4 Translation of competition requirements into key design requirements

3.3   Concept Selection Process

We began the process of selecting concepts for the aircraft's systems by conducting independent and collaborative brainstorming. Team members spent time studying the competition requirements and the results of our scoring analysis. Each member then drew upon intuition and past experience in order to conceive and showcase ideas for designs that would score best in this year's competition. We made extensive use of aircraft sketches like those shown in Figure 3.5 as aids for the brainstorming process.
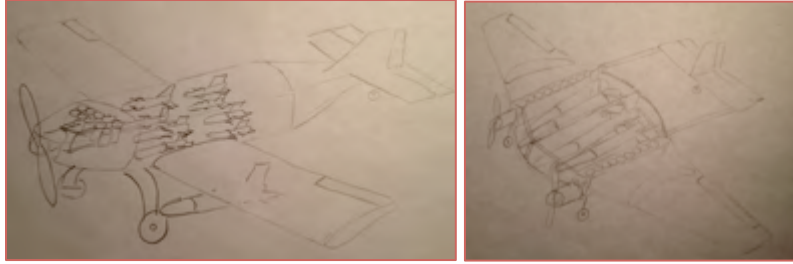
Figure 3.5 Brainstorming sketches

In order to carefully evaluate concepts being considered for the aircraft's systems, the team made use of decision matrices for the selection of each configuration. The categories in which concepts were evaluated were plane configuration, motor configuration, landing gear configuration, payload configuration and tail configuration. For each system, the team compared configurations by rating them based on parameters deemed critical to the success of the given system. The team then weighted the parameters for each decision matrix based on importance and normalized the weights to sum to one for each matrix. The component weights in this matrix are primarily derived from the initial design goals, placing higher weights on components that were deemed more important in the scoring analysis. This objective selection process enabled the team to select the configurations that would maximize the aircraft's score in competition.

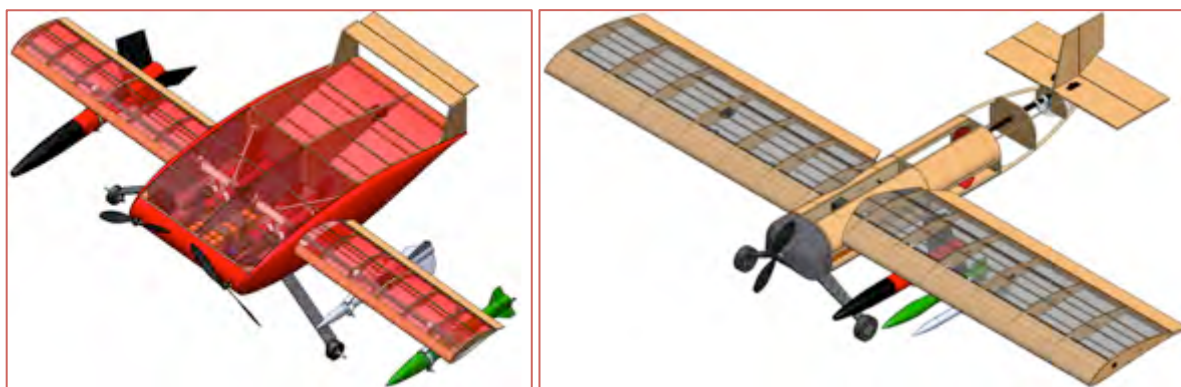### 3.3.1 Plane Configuration (Figure 3.5)

The categories considered for the selection of a plane configuration were lift-to-drag ratio, maneuverability, weight, stability, payload integration, and manufacturability. After the scoring analysis, the team decided that the plane configuration should be aimed at achieving the optimal lift-to-drag ratio, the most maneuverability, and the least weight. With these goals in mind, a conventional aircraft proved to be the most favorable combination of these requirements and scored well in all categories. The lifting body configuration also scored well, particularly because all the drag surfaces of a lifting body also generate lift which leads to a high lift-to-drag ratio.

Plane Configuration	%	Canard	Biplanes	Lifting Body	Conventional
Lift/Drag	30	3	2	4	3
Maneuverability	20	5	4	4	3
Weight	20	2	3	3	3
Stability	15	3	4	2	5
Payload Integration	10	1	3	4	4
Manufacturability	5	3	3	2	4
Total	100	3	3.05	3.4	**3.65**

Figure 3.5 Aircraft configuration decision matrix

Based on the results of this initial decision matrix and the completion of accompanying brainstorming, researching, and morphological charts, we chose to pursue the two top-scoring design configurations: conventional and lifting body. Doing so enabled us to quantitatively identify which design would perform better and eliminate uncertainties associated with the decision process. After developing initial prototypes for both designs as shown in Figure 3.6, we concluded by means of a comparative design trade that the conventional aircraft would yield a higher score at competition. The lifting body design also presented inherent difficulties with stability, manufacturability, and low aspect ratio body performance. Thus, the design outlined in the remainder of this report corresponds to the conventional aircraft configuration.

Figure 3.6 Lifting body design (left) & conventional design (right)

3.3.2   Motor Configuration (Figure 3.7)

The team went through the process of selecting a motor configuration with a focus on obtaining the best thrust to weight ratio and highest top speeds while taking up the least amount of space. After the scoring analysis, the team found that having one tractor motor in front of the fuselage would best fit these requirements. The tractor motor configuration with one motor running at 20 amps was found to give better thrust for its weight, as well as accommodate static stability, when compared to two motors with 20 amps and the same total battery size. This finding was augmented by how well one tractor would integrate with other subsystems.

Motor Configuration	%	Single Tractor	Single Pusher	Double Tractors	Counter-Rotate
Thrust to Weight	50	5	3	4	3
Stability	30	3	1	4	2
Size	20	4	3	2	2
Total	100	**4.2**	2.4	3.6	2.5

Figure 3.7 Motor configuration decision matrix

3.3.3 Landing Gear Configuration (Figure 3.8)

The categories considered for landing gear selection were weight, integration, and takeoff capability. The taildragger was ultimately selected as the best configuration for these criteria, especially since it would weigh less than a tricycle gear with similar functionality. The taildragger also provides more lift during takeoff for a low angle of attack aircraft and is easiest to integrate with a steering system. Skids were considered entirely impractical for the takeoff and landing requirements.

Landing Gear	%	Tricycle	Taildragger	Skids
Weight	50	1	2	3
Integration	25	2	3	1
Takeoff capability	25	2	3	1
Total	100	1.5	**2.5**	2

Figure 3.8 Landing gear decision matrix

3.3.4 Payload Configuration (Figure 3.9)

One of the major decisions the team had to make in the conceptual design phase was how to arrange the internal payloads. Initial qualitative design trades indicated that reducing weight and increasing speed were more important than high numbers of stores, so this matrix deals only with four store configurations. While there are a large number of potential configurations, they can all be placed into categories given by basic properties (shape and dimension). The winning configuration was two rows of two rockets, all in one horizontal plane. This configuration minimizes frontal area, which thereby minimizes drag and maximizes speed. The arrangement also minimizes the weight of the securing structures by bringing the stores closer to their enclosing body, which ultimately makes integration easier.

Payload arrangement (internal)	%	4x1	2x2 (diamond)	Triangle + 1	2x1 + 2x1	3x1 + 1
Drag	60	3	2	3	4	3
Weight	20	3	4	3	3	2
Integration	20	2	2	3	3	1
Total	100	2.8	2.4	3	**3.6**	2.4

Figure 3.9 Payload arrangement decision matrix

3.3.5 Tail Configuration (Figure 3.10)

The team considered three options for a tail configuration: conventional, T-tail, and V-tail. The ideal tail would provide sufficient stability for the aircraft while minimizing drag and weighing as little as possible. The conventional tail configuration selected has well known stability characteristics and doesn't pose significant manufacturability or weight concerns.


Tail Configuration	%	T-tail	V-tail	Conventional
Weight	30	4	2	4
Drag	40	1	3	2
Recovery	20	5	4	4
Manufacturability	10	1	3	4
Total	100	2.7	2.9	**3.2**

Figure 3.10 Tail configuration decision matrix

3.4 Selected Concept

Figure 3.9 shows an illustration of the aircraft's selected conceptual design. The slim and lightweight profile of the fuselage allows the aircraft to obtain a high cruise velocity by minimizing drag and lowering the required wing area. A single tractor motor maximizes the aircraft's overall thrust and power output. A taildragger configuration positions the aircraft to take off fully-loaded within the minimum required distance by generating additional lift from the wing at a high angle of attack. The conventional tail configuration provides adequate aircraft stability and recovery while minimizing weight and drag. The selected aircraft concept was optimized to be as fast as possible, lightweight, robust and capable of meeting all mission requirements and constraints.
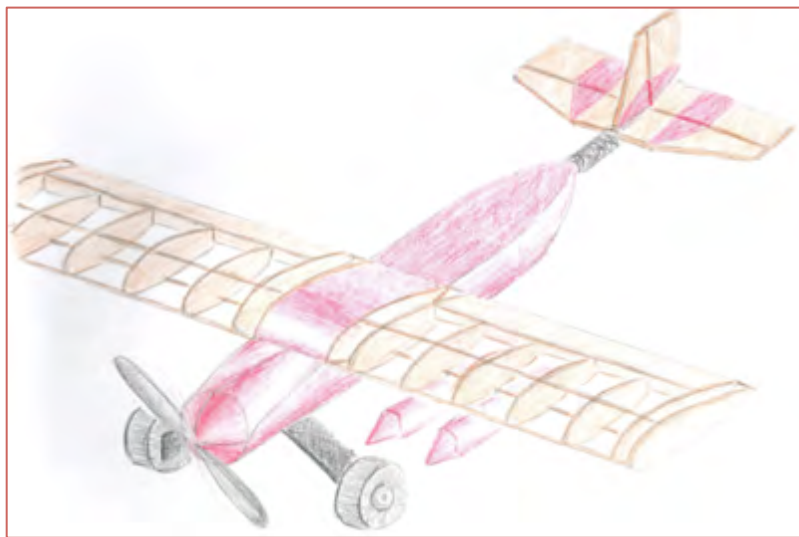
Figure 3.9 Illustration of selected aircraft concept

4 Preliminary Design

In the preliminary design phase, our team used the results from conceptual design to determine sizing and performance parameters for the aircraft's relevant systems. Through successive design iterations, we optimized the aircraft to best meet critical requirements.

4.1 Design and Analysis Methodology

The design and analysis of any aircraft is circular by nature; since the various systems and subsystems of an aircraft are dependent on one another, our team relied on an iterative process in order to develop an aircraft that would obtain the highest possible score at competition. The design wheel shown in Figure 4.1 illustrates the methodology utilized by our team. In this circular process, requirements are set by competition rules and prior design trade studies, concepts are developed in order to best meet said requirements, and analysis of the design leads to new trade studies, requirements and concepts.
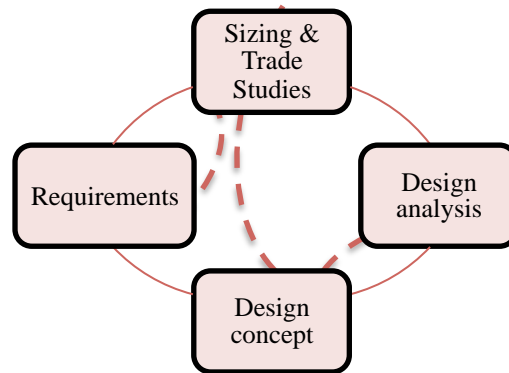

Figure 4.1 The design wheel

Upon entering the preliminary design phase, our team had already defined and prioritized many of the broader vehicle requirements and had developed an initial conceptual design. We began preliminary design by conducting several design trades, after which we began the process of determining layout, sizing and performance parameters. Initial guesses were followed by subsequent iterations until the design was optimized to best meet the requirements (Figure 4.2).
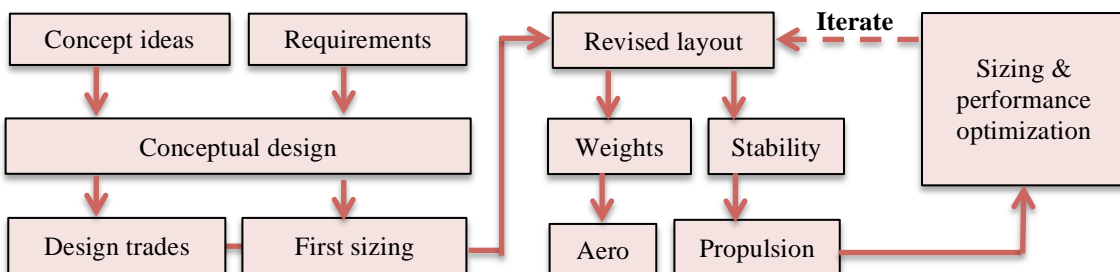

Figure 4.2 Preliminary design process diagram

4.2 Design and Sizing Trades

Throughout the process of developing the aircraft's systems, we made use of design and sizing trade studies in order to investigate how the attributes of certain systems would affect the vehicle's overall flight score. These trade studies began with initial estimates for sizing and performance parameters, and were updated successively as the design progressed. The mission model discussed in Section 4.3 facilitated the analyses necessary for each trade study. The three trade studies presented in this section demonstrate how the number of internal stores carried for mission two, the number of propulsion battery cells used, and the position of the tail relative to the wing would respectively affect overall flight score.

4.2.1 Variation of score with number of internal stores carried

As a driving constraint for several of the aircraft's systems, the number of stores to be carried for mission two needed to be identified early in the design process. Figure 4.3 shows the configuration of the internal stores used in this trade study. This configuration yields the best flight score because it requires the least additional structure and minimum frontal area.

Figure 4.3 Internal store configurations

We estimated that the aircraft empty weight would increase by 0.25 lb and the overall aircraft length would increase by 10 inches for every two additional internal stores added. Our conservative model ignored the increase in drag resulting from a longer fuselage when calculating flight scores. Using appropriate inputs to the mission model discussed in Section 4.3, we determined that flight score varies inversely with number of internal stores carried (Figure 4.4). This trade study led us to design around carrying only four internal stores for mission two, the minimum number required for mission three.
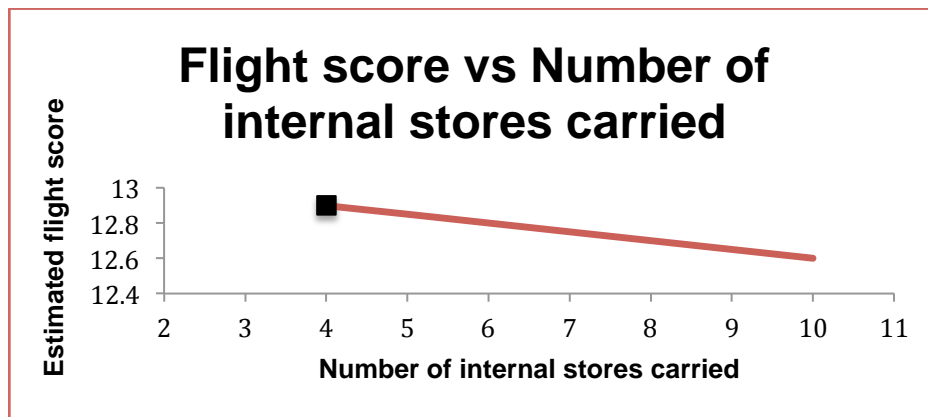

Figure 4.4 Affect of internal stores on flight score

4.2.2 Variation of score with number of propulsion battery cells used

The team conducted calculations on theoretical propulsion systems utilizing between ten and 28 cell batteries. The 28-cell limit was imposed by weight restrictions. We adjusted motor/propeller combinations in the mission model, along with aircraft weight and cell count, to output the best possible flight score for a given number of battery cells. Figure 4.5 shows that, from a scoring standpoint, the increase in speed overshadows the extra weight. Additionally, this study did not account for changes in wing size. Lower cell count would result in decreased static thrust, and would therefore necessitate a larger wing area in order to satisfy the takeoff distance constraint. This trade study led us to employ a 28-cell propulsion battery.
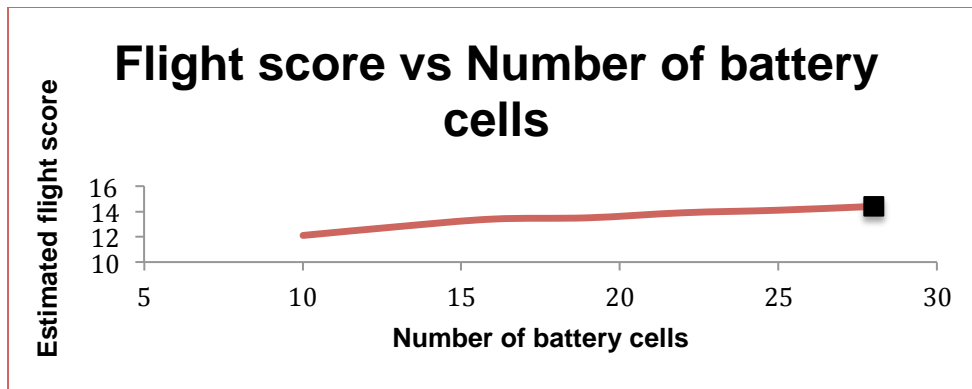
Flight score vs Number of battery cells

Figure 4.5 Affect of battery size on flight score

4.2.3 Variation of score with tail position

In this trade study, we use the mission model to determine the optimal tail location for maximizing flight score. We assumed a fixed weight, static margin, and wing geometry and then varied the horizontal tail position relative to the wing. We concluded that the increase in drag on the tail and decrease in overall flight speed was small compared to the corresponding decrease in the aircraft size factor. This led us to place the tail as close to the wing as possible while still accounting for fuselage taper, wing downwash and trimming considerations.
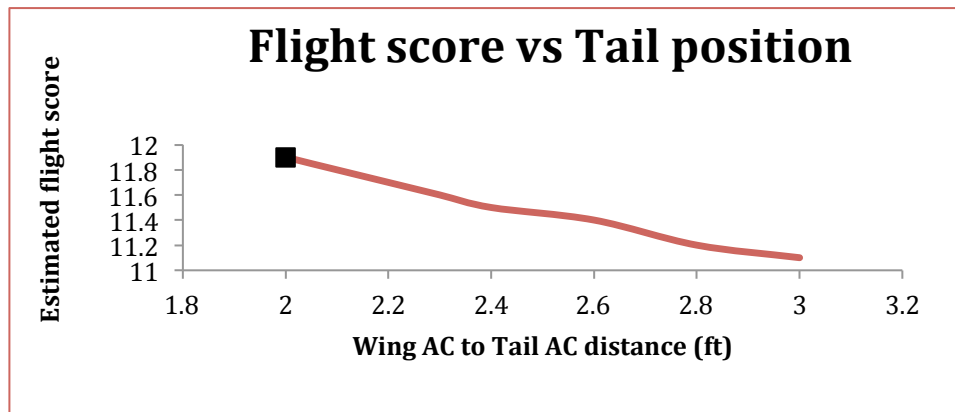
Flight score vs Tail position

Figure 4.6 Affect of tail position on flight score

4.3　Mission Model – Capabilities and Uncertainties

The team developed a comprehensive mission model using MATLAB programming software with the primary goal of optimizing aircraft systems to best meet competition requirements. The program facilitated the sizing of aircraft components, performance estimates, and flight score calculations based on inputted aircraft parameters and a model of the aircraft's flight trajectory. The flight course is simulated using four discrete flight phases: takeoff, climb, cruise and turn, as shown in figure 4.7.
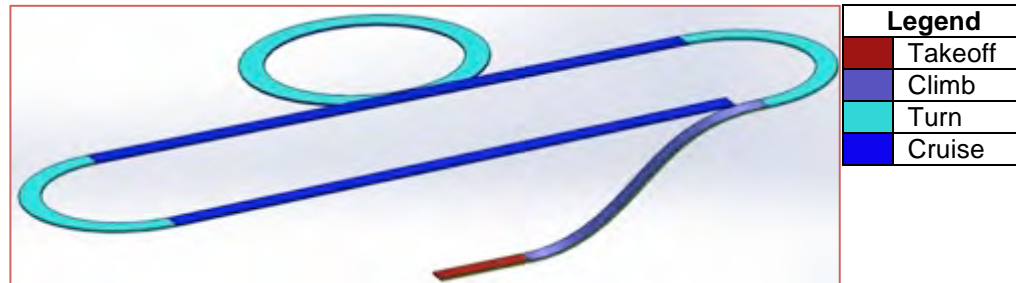
Figure 4.7 Flight course simulated in mission model

Each flight phase has unique constraints governing its equations of motion in the mission model, as summarized in Figure 4.8. The model shown is used for missions one through three. The mission model also accounts for accelerated flight between the climb and cruise phases of the flight course, as well as following the turn phases of flight. We used a turn load factor of five for mission one and three for mission three such that the loading experienced by the aircraft is the same for all missions.

Flight phase	Description	Constraints modeled
Takeoff	Acceleration from standstill until lift equals weight	AoA = constant
Climb	Climb from ground to safe flight altitude	AoA = constant
Cruise	Level, unaccelerated flight at optimal angle of attack	L = W, T = D
Turn	Sustained, constant speed, level turns at maximum allowable load factors (different for each mission)	L = nW, T = D
AoA = angle of attack, L = lift, W = weight, T = thrust, D = drag, n = load factor		

Figure 4.8 Summary of flight phases simulated in mission model

The mission model presented here possesses several uncertainties that limit the scope of its accuracy. Since all inputs to the model are only estimates and not representative of actual aircraft performance, the outputs obtained from the program are only estimates as well. The model does not account for wind conditions during flight; doing so adds significant variability to performance estimates. Battery voltage is treated as constant and equal to the nominal cell value throughout flight. Finally, the model neglects ground rolling friction, interference drag, and compressibility effects. In order to account for these uncertainties, we use the model as a tool in conjunction with extensive testing, which ensures that we ultimately attain the best results.

4.4   Propulsion Characteristics

The propulsion subteam was responsible for selecting all of the electronics used to power and control the aircraft. Operating under the design requirements listed in Figure 4.9, the subteam's objective was to determine the system of batteries, motor and propellers that would enable the fastest possible flight times. The propulsion system also needed to meet the additional battery weight and current limit requirements. The team paid careful attention to choosing a system that would provide high static thrust while also enabling a high cruise speed.

Overall design requirements	Subteam design requirement
Maximize propulsive system	Maximize battery pack voltage
	Maximize efficiency of motor and propeller system
High static thrust	Select a high static thrust motor and propeller system

Figure 4.9 Propulsion subteam design requirements

4.4.1   Battery selection

During conceptual design, we determined that the benefits of maximizing power far outweighed the costs of the corresponding increase in weight. The goal of the propulsion battery pack design, therefore, was to choose a configuration that would enable maximum power output. We determined the optimal operating current to be as close to twenty amps as possible. NiMH battery chemistry was chosen over NiCd chemistry due to its higher energy density and better resistance to memory effects. Operating at twenty amps for four minutes requires 1330 milliamp-hours of capacity. The closest commercially available range of cell capacity (1500-1600mAh) was chosen to further narrow our selection. Due to a lack of high quality data for RC battery performance, we chose to conduct our own performance tests on our top three candidate batteries. We tested the batteries by applying a small resistance across the battery terminals. The resulting battery current and voltage were recorded using an Eagle Tree Systems data logger. Figure 4.10 shows a sample of the output graphs created by the logging software.
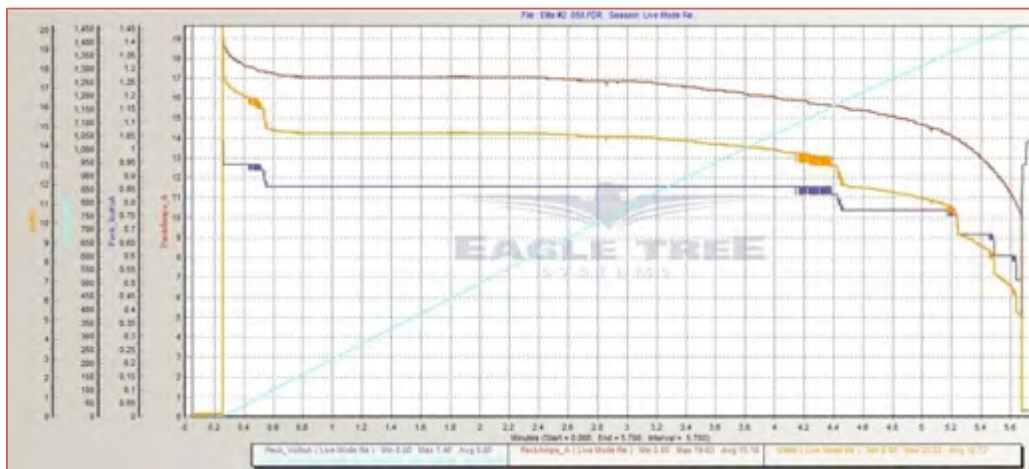
Figure 4.10 Sample data logging for RC battery performance

We reduced the data collected to the information listed in Figure 4.11.

Cell Type	Elite #1	Elite #2	VB Power #1	VB Power #2	Tenergy #1	Tenergy #2
Rated mAh	1500	1500	1600	1600	1600	1600
Cells in 1.45lb	28	28	26	26	26	26
Average Power per cell over 4 min (W)	14.6	14.6	N/A	15.6	15.3	14.3
Power @ 4.5 min (W)	10.9	11.8	N/A	7.4	11.1	13
Power to weight ratio (W/kg)	661	663	N/A	663	677	633
Average available power (W)	408		405		414	

Figure 4.11 Summary of battery test data

Based on the results of this test, we determined that the differences in performance across battery manufacturers were negligible. We selected the Elite 1500 batteries because of their exceptionally flat discharge profile and their proven track record of reliability. Our battery packs will utilize 28 of these cells at a nominal voltage of 33.6 V. High quality NiMH batteries have C-ratings of approximately 10. Therefore, with our selection of at least 1500mAh cells, we can expect to consistently output up to fifteen amps without problems. Past team experience has shown that exceeding this rating by five amps will not cause a problem in the short term, and testing later confirms this assumption.

4.4.2   Motor selection

The team sought to select a motor and propeller system that would achieve the fastest possible lap time while meeting the relevant competition constraints, following the process shown in Figure 4.12. This process began with a known battery voltage and allowable current. By examining a database of propeller thrust and power coefficients, we determined that a pitch to diameter ratio (p/D) of 2:3 would provide the best mix of high and low speed performance. This allowed us to later optimize for mission specific thrust requirements. We then chose a motor, propeller sizes and a corresponding RPM range to yield high top speeds while concurrently meeting takeoff thrust requirements.

Input voltage & current → Choose (p/D) ratio → Select motor → Select propellers

Figure 4.12 Propulsion system selection process

The selection process was executed iteratively using a web-based RC propulsion system calculator. We narrowed down motors based on their ability to handle the necessary power and RPM, and then based on their efficiency and weight. Of the top motor candidates (Figure 4.13), we chose the Neu 1110-3Y for its high power to weight ratio within our operating regime.

Brand	Model	Battery Power (W)	Efficiency (%)	Power to Propeller (W)	Power/Weight Ratio (W/kg)
Neu	1110-3Y	240	89.6	215.04	**270.90**
Axi	5330/18	240	80.6	193.44	145.18
Hacker	A50-14L	240	79.7	191.28	168.26
Scorpion	S4025-16	240	90.5	217.2	210.77
Turnigy	G110-295	240	87.8	210.72	180.85

4.13 Motor selection candidates

4.4.3   Propeller optimization

After selecting a motor, we utilized the mission model discussed in 4.3 to determine which propeller would yield the greatest flight score for each mission. Figure 4.14 shows static propulsion parameters for the best performing propellers in our operating regime. Since the aircraft accelerates and decelerates frequently during the flight course, higher pitch propellers with higher maximum flight speeds did not attain as high lap speeds as mid-range propellers. Ultimately, we selected the 12x8 APC thin electric for all three missions due to its dominant performance with respect to static and dynamic thrust. We will validate this selection by conducting flight tests with a range of propellers.

Propeller	Thrust (lbf)	Power (lbf·ft/s)	Current draw (amps)	RPM
11x10 APC E	3.77	384	24.9	32,400
12x8 APC E	5.68	360	22.0	34,600
13x6.5 APC E	6.36	398	27.1	30,800

4.14 Propeller selection candidates

Figure 4.15 depicts the thrust generated by the 12x8 propeller and current drawn from the batteries as a function of airspeed. Figure 4.16 graphs the power required to sustain lift for each mission (based on estimated weight values) and the power available from the propulsion system as functions of airspeed. As shown, the power required curves converge to equal power available at an approximate airspeed of 100 ft/s.
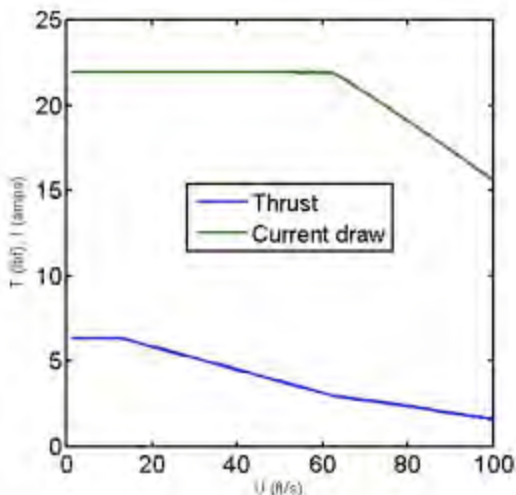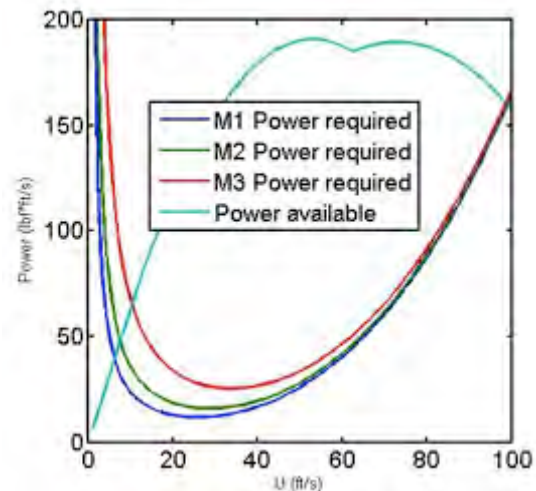

Figure 4.15 Thrust and current draw

Figure 4.16 Power required and available

The aerodynamics subteam was responsible for systematically determining the aerodynamic characteristics of the aircraft while operating under the design requirements shown in Figure 4.17. They were tasked with selecting airfoil shapes for the wing and tail, sizing the wing, and predicting lift and drag characteristics using both analytical and numerical methods.

Overall design requirements	Subteam design requirement
Low drag at cruise	Low drag airfoil at cruise conditions
	Low fuselage parasitic drag
High wing area	Size wing for takeoff

4.17 Aerodynamics subteam design requirements

4.5.1   Airfoil selection

The airfoil cross section of the aircraft's wing has a great bearing on aerodynamic performance. The aerodynamics subteam used worldofkrauss.com as our primary airfoil database and cross-referenced airfoils with airfoiltools.com. We began our search with 1,756 airfoils. We then proceeded to filter this list using the following search criteria:

- **Max C_L of 1.2-1.5** in order to create a lower bound to remove low performing airfoils.

- **Max Thickness 8%-13%** to remove extremely thin airfoils that would be hard to manufacture, and thick airfoils, which were generally less efficient. These percentages were used based on previous report data and sample airfoils.

- **Max Camber 1.5-8** to get airfoils that could perform near 0 angle of attack and to get rid of hyper cambered airfoils, which would be difficult to manufacture.

The filter criteria produced 332 airfoils. Of those airfoils, we eliminated all airfoils that had an onset of stall within 0 and 9 degrees, sharp trailing edges and other difficult to manufacture shapes, odd C_L curves at a range of Re numbers, and low lift airfoils. The process of elimination left us with 12 airfoils. We then compared the remaining airfoils using XFLR5 and further reduced the list to four airfoils: the DAE-31, FX 76-MP-120, MH-114, and SD-7062 (Figure 4.18).
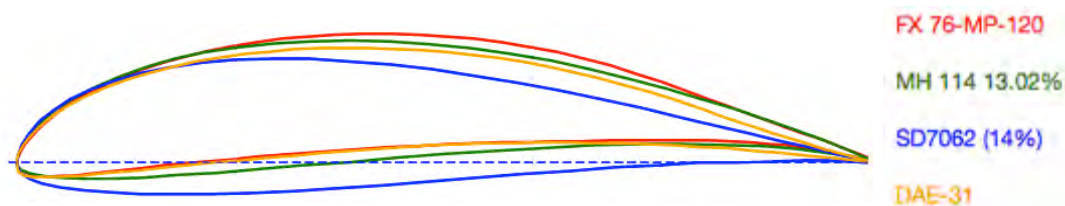

Figure 4.18 Airfoil comparison

Based on the conceptual design, the scoring analysis, and the mission requirements, we used the following critical criteria to determine the best airfoil to use for the wing:

- **Maximum lift coefficient**, C_L > 1.0 at 75% of the stall angle at takeoff (40%). A greater C_L would decrease the wing area and the amount of structure.

- **Minimum drag coefficient** with weighted attention to cruise (30%). By reducing drag during cruise, we increase flight speed.
- **Maximum C_L/C_D** at cruise and lower angles of attack (20%). Increased cruise efficiency would optimize our performance.
- **Minimum moment coefficient** (10%). A smaller pitching moment coefficient reduces the required control surface area and the longitudinal length of the aircraft.

Using XFLR5 to compare and confirm predicted airfoil results, we created a decision matrix to select an airfoil (Figure 4.19). Based on these criteria, we selected the MH-114 airfoil for our wing. Figure 4.20 shows XFLR5-generated plots of aerodynamic performance characteristics for the airfoils considered at cruise conditions.

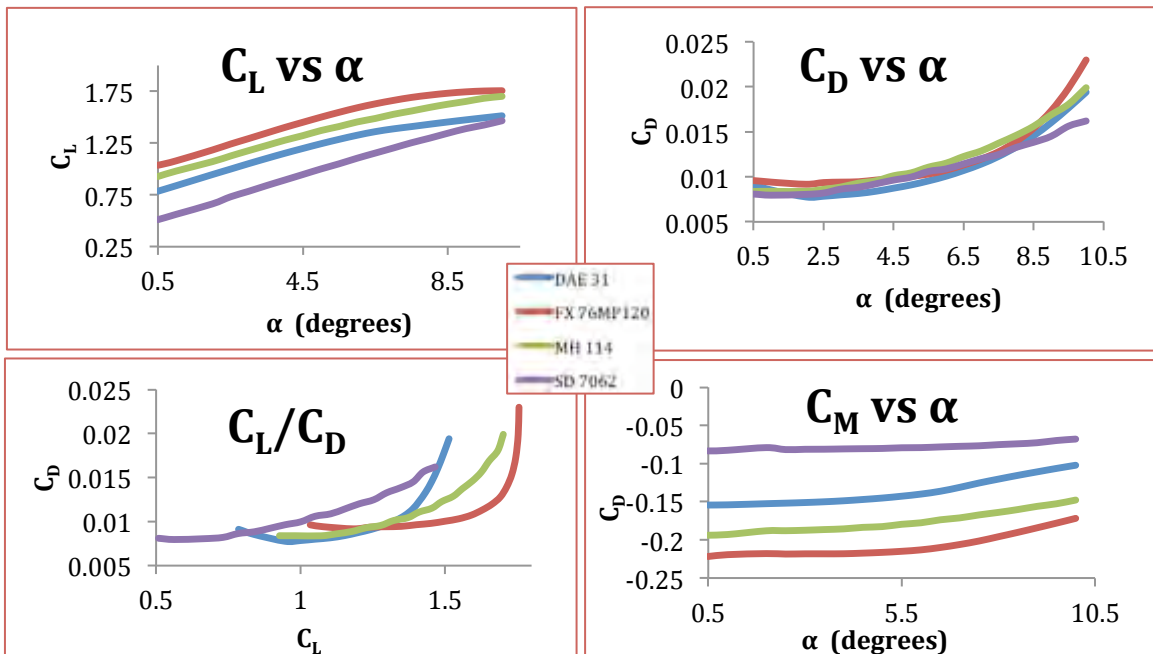| Airfoil	%	DAE-31	FX 76-MP-120	MH-114	SD-7062
C_L	40	4	5	4.5	3
C_D	30	4	3	4	4.5
C_L/C_D	20	3.5	4	4	2
C_M	10	4	1	2	5
Total	100	3.9	3.8	4	3.45

Figure 4.19 Airfoil selection decision matrix

Figure 4.20 2D airfoil performance parameters

We also carefully considered whether to use an airfoil shape or a flat plate in the design of the tail. Based on a performance and weight comparison, we found that using a flat plate for the tail increases total flight score. The marginal increase in performance from an airfoil shape was offset by the increase in aircraft weight, requiring a larger wing area and increased drag.

4.5.2 Aerodynamic sizing and performance parameters

We conducted sizing estimates for the wing using lift and drag calculations tabulated in the mission model, inputted propulsion parameters, and weight estimates. We optimized the wing to be as small as possible while enabling the aircraft to take off in the required distance fully loaded. We built in an initial safety factor of 1.3 to account for uncertainties in thrust and weight estimates. Figure 4.21 lists the inputs and formulas used by the mission model to calculate lift and drag, and the descriptions of each term used. These calculations are taken from sections of Shevell and Raymer's aircraft design texts. Lift and drag calculations are dependent on airspeed and angle of attack, which are controlled by the flight conditions in the mission model.

Inputs			
Term	Description	Term	Description
ρ	Density of air (slug/ft^3)	$\bar{c}$	Mean aerodynamic chord (ft)
U	Airspeed (ft/s^2)	μ	Viscosity of air (slug/ft·s)
a_0	2D airfoil lift curve slope (1/degrees)	u	Correction for non-elliptic loading
AR	Aspect ratio	s	Fuselage correction factor
α_{ZL}	Angle of attack for zero lift (degrees)	S	Planform area (ft^2)
$m.t.$	Maximum airfoil thickness (%)	C_{DpLG}	Landing gear parasite drag
d_f	Diameter of fuselage (ft)	L_f	Length of fuselage (ft)
Formulas	
---	---
$q = 0.5\rho U^2$	Dynamic pressure (lbf/ft^2)
$C_{L\alpha,w,h} = a_0/\left(1 + 57.3\left(a_0/\pi AR_{w,h}\right)\right)$	3D airfoil lift curve slope (1/degrees)
$C_{L,w,h} = C_{L\alpha,w,h}\left(\alpha - \alpha_{ZL,w,h}\right)$	Lift coefficient
$L = C_{Lw}qS_w + C_{Lh}qS_h$	Lift from wing and tail (lbf)
$K_{w,h} = 1 + 2.61(m.t./100)$	Wing and tail parasite pressure drag correction factor
$K_f = 1.4 - 0.05\left(L_f/d_f\right)$	Fuselage parasite pressure drag correction
$Re = \rho U\bar{c}/\mu$	Reynolds number
$C_f = 1.328/\sqrt{Re}$	Skin friction coefficient (laminar flow)
$C_{Dp,w,h} = 2KC_f$	Wing and tail parasitic drag
$C_{Dpf} = K_f C_f$	Fuselage parasitic drag
$k_{w,h} = 0.38C_{Dp}$	Wing and tail induced pressure drag correction factor
$C_{D,w,h} = [k + (\pi ARus)^{-1}]C_L^2 + C_{Dp}$	Wing and tail drag coefficient
$C_{DpLG} = \frac{1}{4}(frontal\ area)/S_w$	Landing gear drag coefficient
$D = \left(C_{Dw} + C_{DpLG} + C_{DpST}\right)qS_w$ $+C_{Dh}qS_h + C_{Dpf}qS_f$	Drag from wing, tail, fuselage, landing gear and external stores (lbf)

Figure 4.21 Lift and drag mission model calculations

Figure 4.22 illustrates the parasitic drag buildup by subsystem for missions one and two. The wing surfaces account for the largest portion of the parasite drag and are followed closely by contributions from the landing gear.

Component	C_{Dp}	% of Total
Fuselage	0.0078	13.6%
Wing	0.0266	46.3%
Tail	0.0044	7.65%
Landing Gear	0.0187	32.5%
Total	**0.0575**	**100%**

Figure 4.22 Missions one and two parasitic drag buildup

For mission three, the drag experienced by the aircraft varies for each of the six configurations. Using a procedure outlined in Raymer for calculating parasitic drag caused by external stores, we were able to determine the overall drag buildup. Figure 4.23 lists the external store parasitic drag coefficients for each configuration. In all cases, the contributions from external stores amount to no more than 6-10% of the total drag buildup.

Configuration	1	2	3	4	5	6
Der Red Max	0.0047	0.0047	0.0023	0	0.0023	0.0023
Mini Honest John	0	0	0.0017	0.0035	0.0017	0.0009
High Flyer	0	0.0017	0	0	0.0009	0.0017
Total	**0.0047**	**0.0064**	**0.0040**	**0.0035**	**0.0049**	**0.0049**

Figure 4.23 Mission three external store parasitic drag buildup (stores only)

In Figure 4.24, we summarize the critical lift and drag characteristics of the fully loaded aircraft: overall lift, drag, angle of attack and airspeed at the end of takeoff and at cruise.

| Flight phase	Lift (lbf)	Drag (lbf)	(L/D)	Angle of attack (°)	Airspeed (ft/s)
Takeoff	7.50	0.86	8.72	9.0	31.7
Cruise	7.50	1.63	4.60	-5.57	98.5

Figure 4.24 Aircraft lift and drag characteristics

4.5.3 Lift and drag simulation

We utilized Solidworks Flo Simulation software in order to validate the theoretical performance parameters calculated in the mission model. This software applies finite element analysis to the airflow around an approximate 3D model of our aircraft (Figure 4.25). From this simulation, we were able to tabulate aerodynamic performance parameters and compare them to the theoretical results we obtained (Figure 4.26).
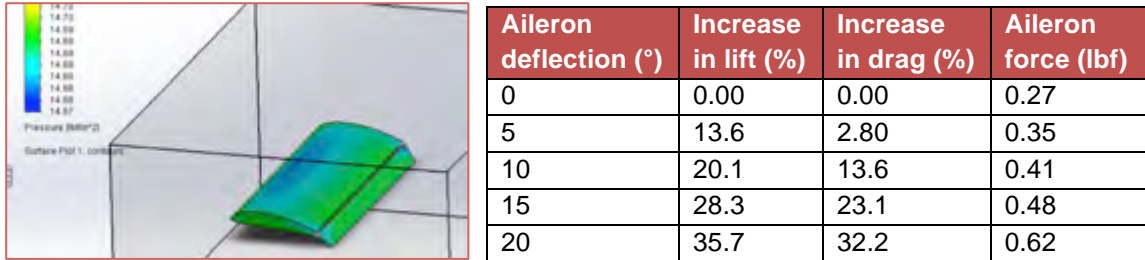

Figure 4.25 Full aircraft flow simulation
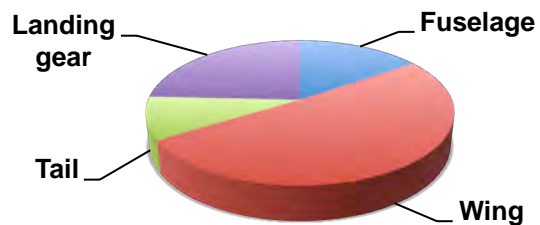
Figure 4.26 Simulated component drag buildup

We ran this simulation at approximate cruise conditions. The main discrepancy between theoretical and simulated performance predictions arises from the fuselage contributions. The methods used in the mission model do not account for lift forces generated by the fuselage (positive or negative). We also used Flo Simulation to validate the use of flaperons for generating additional lift during takeoff. Figure 4.27 illustrates the effectiveness of flaps for several angles of deflection. As shown, proper use of flaps can produce up to 25% additional lift during takeoff, which would lower the aircraft's required wing area and increase flight score.

Aileron deflection (°)	Increase in lift (%)	Increase in drag (%)	Aileron force (lbf)
0	0.00	0.00	0.27
5	13.6	2.80	0.35
10	20.1	13.6	0.41
15	28.3	23.1	0.48
20	35.7	32.2	0.62

Figure 4.27 Flap flow simulation (left); Flap effectiveness (right)

4.6   Stability Characteristics

In order to successfully navigate the flight course for each of the three missions, our aircraft must possess certain stability characteristics. The stability and controls subteam was responsible for determining the sizing parameters of the horizontal and vertical tail as well as the control surfaces in order to ensure stability and maneuverability during flight. The subteam's design requirements are outlined in Figure 4.28. The major challenges faced by the subteam included trimming the aircraft for all flight conditions and controlling the aircraft in tight turns.

Overall design requirements	Subteam design requirement
Adequate static and dynamic stability	Size horizontal and vertical tail for adequate stability
High maneuverability	Size control surfaces for high maneuverability

Figure 4.28 Stability and controls design requirements

4.6.1   Tail sizing parameters

Given the results of the trade study on tail position, we sought to position the tail close to the rear of the fuselage while achieving adequate static stability and without hindering aerodynamic performance. Based on historical data, we predicted that a static margin between 5-15% for all missions would produce an aerobatic aircraft but ensure its ability to recover from stalls. We sized the horizontal and vertical tails using the inputs and formulas listed in Figure 4.29. We selected the horizontal tail's geometry such that it would generate a desirable static margin. The empirical calculation of the fuselage moment coefficient is based on a method developed by Robert Gilruth (NACA TR711) and other calculations are taken from Shevell.

Inputs (new)	
Term	Description
K_{Mf}	Empirical factor for fuselage/wing combinations
η	Tail effectiveness (~90% for conventional tails)
l_H	Distance from wing aerodynamic center (AC) to tail AC
x	Distance from CG to wing AC
$\bar{V}_V$	Vertical tail volume coefficient (chosen based on empirical data)
Formulas	
$$\left(\frac{\partial C_M}{\partial C_L}\right)_f = \frac{K_{Mf} d_f^2 L_f}{57.3 \cdot S_w \bar{c}_w C_{L\alpha w}}$$	Fuselage moment coefficient
$$\frac{\partial \epsilon}{\partial \alpha} = \frac{2 C_{L\alpha w}}{\pi AR_w}$$	Rate of change of downwash from wing
$$N.P. = 100 \cdot \frac{\frac{C_{L\alpha h}}{C_{L\alpha w}}\left(1 - \frac{\partial \epsilon}{\partial \alpha}\right)\frac{S_h}{S_w}\frac{l_H}{\bar{c}_w}\eta - \left(\frac{\partial C_M}{\partial C_L}\right)_f}{\left(1 + \frac{C_{L\alpha h}}{C_{L\alpha w}}\right)\left(1 - \frac{\partial \epsilon}{\partial \alpha}\right)\frac{S_h}{S_w}\eta}$$	Neutral point - overall AC of aircraft (%)
$S.M. = N.P. - 100 \cdot (x/\bar{c}_w)$	Static margin (%)
$S_V = b S_w \bar{V}_V / l_H$	Vertical tail area (ft^2)

Figure 4.29 Horizontal and vertical tail sizing formulas

We considered both wing placement and dihedral as potential options for generating additional roll stability. We ruled out the use of dihedral because of the manufacturing complexities associated with adding dihedral. To provide roll stability, the team chose to use a high-wing design. A high-wing design produces a keel effect, which results in increased roll stability. This design has the added benefit of providing adequate clearance in the fuselage to accommodate payloads and wing mounting.

Figure 4.30 shows estimated center of gravity (CG) locations for each mission and configuration relative to the aircraft's fore and aft limits. The location can be adjusted to the desired static margin for each configuration by moving the propulsion batteries fore and aft.
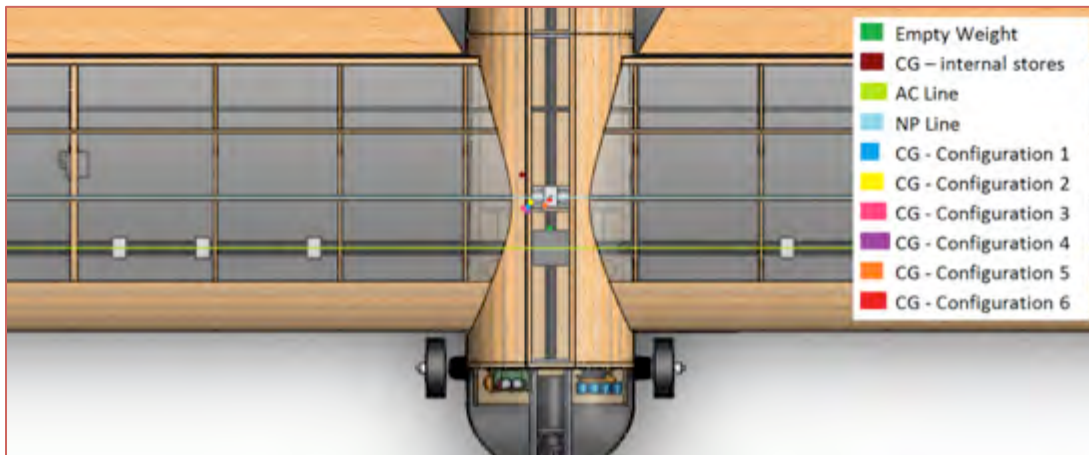
Figure 4.30 Mission CG locations

4.6.2 Control surface sizing parameters

Our team sought to size the aircraft's three control surfaces – ailerons, elevator and rudder – such that the aircraft would possess adequate roll, pitch, and yaw control. The design of the control systems ensured that the aircraft would be maneuverable and could be trimmed properly in all flight situations. We chose a conventional rudder for yaw control and sized the rudder as 50% of the vertical tail area based on estimates from Raymer. The team considered two methods of roll control: standard trailing edge ailerons and roll spoilers. While spoilers offer a considerable amount of proverse yaw, thus minimizing the amount of yaw correction required during coordinated turns, they also induce a large amount of drag, which contradicts our design goals. We ultimately chose to implement ailerons that span the full length of the wing. This decision allows for easy manufacturing and for the implementation of flaps as high-lift devices. We sized the aileron as 15% of the total wing area based on empirical estimations provided by Raymer. We calculated a flap effectiveness parameter of 0.25 with the given inputs.

To ensure longitudinal static control, or pitch control, we needed to size the elevator such that the overall moment coefficient of the vehicle could be trimmed to zero over the entire domain of flight. We initially sized the elevator as 50% of the horizontal tail area based on estimations from Raymer. With this sizing completed, we were able to determine optimal tail location, tail area and static margin. The mission model calculates the controlled moment coefficient of the aircraft as well as the trim required from elevator deflection using the formulas listed in Figure 4.31.

Inputs (new)	
Term	Description
$x_e/\bar{c}_h$	Ratio of elevator length to horizontal tail length
e	Elevator deflection (degrees)
C_{Mw}	Wing moment coefficient about wing AC
Formulas	
$r = \sqrt{x_e/\bar{c}_h}$	Elevator effectiveness
$C_{Le} = C_{L\alpha h}(S_h/S_w)r$	Elevator lift coefficient
$C_{Le} = -\{(l_H - x)/\bar{c}_w\}C_{Le}$	Elevator moment coefficient
$C_{L\alpha} = C_{L\alpha w} + C_{L\alpha h}(S_h/S_w)$	Overall lift curve slope (1/degrees)
$\alpha_{ZL} = \dfrac{C_{L\alpha w}\alpha_{ZL,w} + C_{L\alpha h}(S_h/S_w)\alpha_{ZL,h}}{C_{L\alpha w} + C_{L\alpha h}(S_h/S_w)}$	Overall angle for zero total lift (degrees)
$C_L = C_{L\alpha}(\alpha - \alpha_{ZL}) + C_{Le}e$	Overall, controlled lift coefficient
$C_M = C_{L\alpha w}(\alpha - \alpha_{ZL})(x/\bar{c}_w) + C_{Mw} + C_{Me}e$ $-C_{L\alpha h}(\alpha - \alpha_{ZL})(S_h/S_w)\{(l_H - x)/\bar{c}_w\}$	Overall, controlled moment coefficient

Figure 4.31 Controlled lift and moment coefficient calculations

The mission model produced the trim plots shown in Figure 4.32. The plot on the left graphs the aircraft's lift coefficient versus the moment coefficient at the wing aerodynamic center

for several different elevator deflections at a fixed static margin. The plot on the right graphs the trimmed elevator deflection versus lift coefficient for several different static margins.
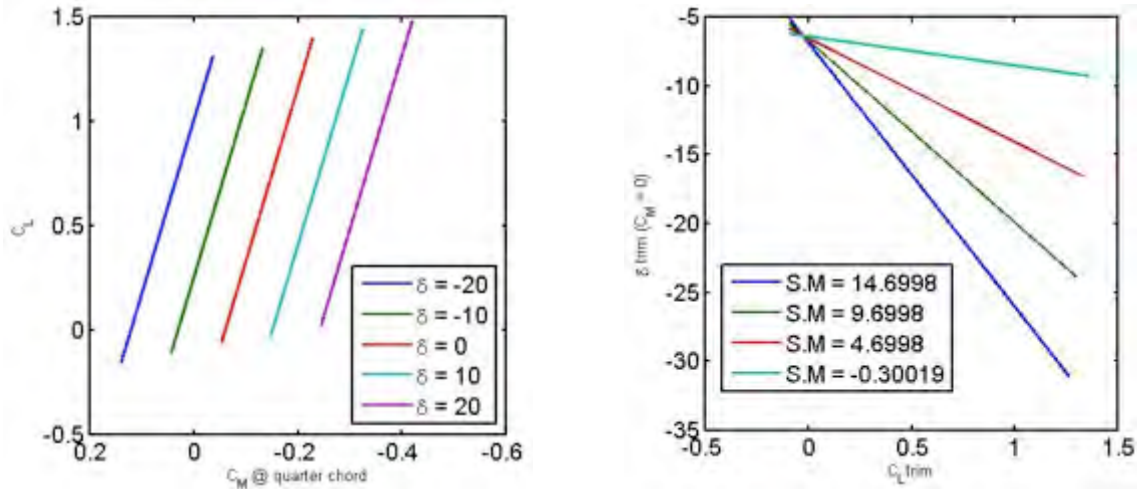
**Figure 4.32** Trim plots: C_L vs C_M (left), δ_{trim} vs $C_{L,trim}$ (right)

As shown in the right plot, larger static margins require more elevator deflection to balance the aircraft longitudinally. Since our elevator deflection is limited to a maximum of 25 degrees in both directions by the travel of our servos, we selected a static margin such that the aircraft could be trimmed during takeoff with 20 degrees of elevator deflection. The relevant parameters chosen for tail sizing during preliminary design are listed in Figure 4.33.

Parameter	$S.M.$	l_H	S_V
Value	8.2%	2.25 ft	0.55 ft^2

Figure 4.33 Relevant parameters chosen for tail design

4.6.3 Stability Derivatives

We calculated the stability derivatives of our aircraft using AVL software developed at MIT by Drela and Yougren. Figure 4.34 shows the model inputted into AVL for our aircraft.
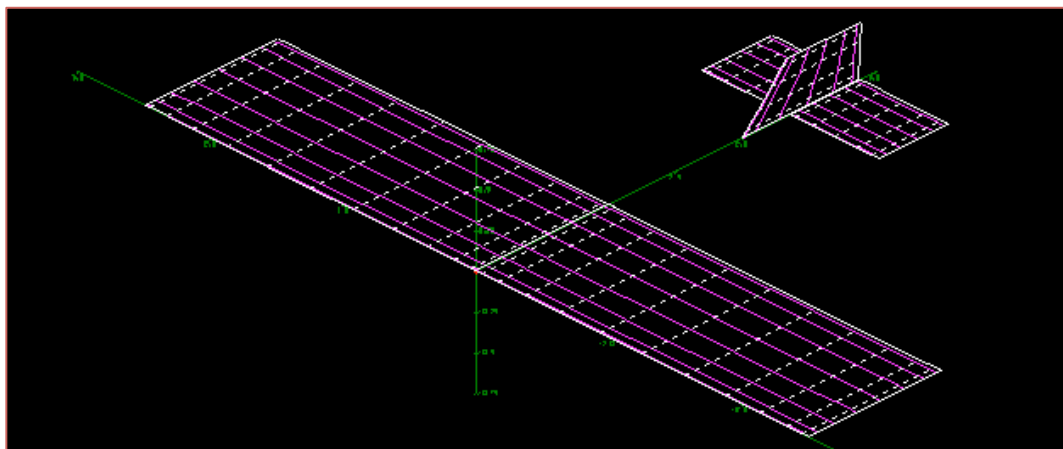
Figure 4.34 Aircraft geometry inputted into AVL

AVL outputs dimensionless aerodynamic derivatives based on the inputted geometry, which are used to calculate stability and control derivatives. In Figure 4.35, we list the AVL values converted for the coordinate system pictured in Figure 4.36. In general, these values are representative of a statically stable aircraft. The positive value of $C_{\ell\beta}$ indicates that the aircraft lacks dihedral stability. We later validate through testing that the aircraft is controllable in roll.

CORNELL	Roll rate		Yaw rate	
	C_{Yp}	-0.0539	C_{Yr}	0.11
	$C_{\ell p}$	-0.402	$C_{\ell r}$	0.0568
Angle of attack		C_{np}	0.00314	C_{nr}	-0.0472
$C_{L\alpha}$	4.23	Pitch rate		Aileron deflection	
$C_{M\alpha}$	-0.192	C_{Lq}	5.42	$C_{\ell\delta a}$	0.00703
Sideslip		C_{Mq}	-4.36	$C_{n\delta a}$	-0.00023
$C_{Y\beta}$	-0.121	Elevator deflection		Flap deflection	
$C_{\ell\beta}$	0.0062	$C_{L\delta e}$	0.00601	$C_{L\delta f}$	0.0386
$C_{n\beta}$	0.0498	$C_{M\delta e}$	-0.0128	$C_{M\delta f}$	-0.00394

Figure 4.35 Dimensionless aerodynamic derivatives (radians^{-1})
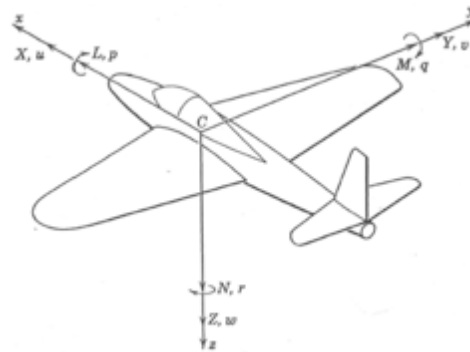
Figure 4.36 Aircraft coordinate system

4.7   Mission Performance Estimates

Figure 4.37 provides estimates for the aircraft's performance in each of the three missions. We used the mission model with inputted estimates for aircraft geometry and performance parameters in order to calculate the values listed below. We predict that our aircraft's lap time will be the fastest in both missions one and three because it has been optimized for speed throughout the design process. We predicted a maximum number of internal stores to be carried for mission two based on the weight and length resulting from additional stores and given takeoff and propulsion limitations.

Mission 1		Mission 2		Mission 3	
Laps completed	9	Stores carried	4	Time flown	103
Max laps completed	9	Max stores carried	10	Min time flown	103
M1 score	**2**	M2 score	**1.6**	M3 score	**6**

Figure 4.36 Estimates of aircraft mission performance

5 Detailed Design

In the following section of this report, we document the dimensional and performance parameters, structural characteristics, and systems design, selection and integration of the final aircraft design. The detailed design process embodies our primary objective of maximizing flight time by minimizing structural weight.

5.1 Dimensional Parameters

Figure 5.1 lists the pertinent dimensional parameters of the final aircraft design. It includes overall aircraft dimensions and dimensions of key subsystems.

		Horizontal Tail		Fuselage	
		Span	16.0"	Length	29.7"
Overall dimensions		MAC	6.30"	Width	6.00"
Length	42.2"	Area	82.6 in^2	Height	4.13"
Width	66.0"	Airfoil	Flat plate	**Main landing gear**	
Height	14.9"	Incidence	0.00°	Length	0.93"
Wing		**Vertical Tail**		Width	13.6"
Span	66.0"	Span	6.50"	Height	4.82"
MAC	12.0"	MAC	7.76"	Wheel diameter	2.25"
Area	720 in^2	Area	50.1 in^2	**Ground AoA**	
Aspect Ratio	5.00	Airfoil	Flat plate	9.00°	
Airfoil	MH 114	Wing AC to horizontal tail AC distance			26.9"
Incidence	0.00°	Wing AC to vertical tail AC distance			24.6"
Flaperons (2)		**Elevator**		**Rudder**	
Span	29. 9"	Span	16.0"	Span	5.71"
Percent chord	15.0%	Percent chord	47.6%	Percent chord	37.0%
Maximum δ_F	20°	Maximum δ_E	25°	Maximum δ_R	20°

Figure 5.1 Dimensional parameters of final design

5.2 Structural characteristics

In Figure 5.2, we summarize the structures subteam's design goals as they relate to overall design requirements. The structures subteam sought to minimize the structural weight of the aircraft while providing adequate strength and rigidity for high wing loading during turns and the shock impact of landing.

| Overall design requirements	Subteam design requirement
Low drag at cruise	Minimize weight of airframe structure
	Minimize airframe footprint
High maneuverability	Endure high wing loading during turns
Hold at least four stores	Design attachments to accommodate four internal stores

**Figure 5.2** Structures design requirements

5.2.1 Load paths

Central to the aircrafts structure are two hollow carbon fiber tubes. A single 0.5" tube runs along the span of the wing at quarter chord. To further ensure the torsional rigidity of the wing, a thinner 0.19" secondary spar spans the wing at 75% of chord. Perpendicular to the wing spar, we have a 0.375" tube running through all six bulkheads of the fuselage and tail. These spars and the connections between them form the aircraft's main load paths (Figure 5.3).
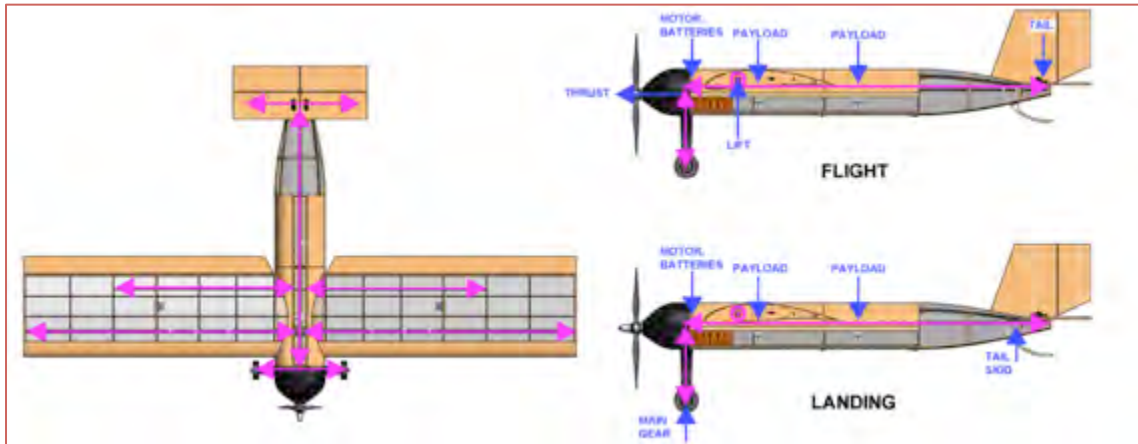
Figure 5.3 Structural load paths

5.2.2 Structural analysis

We analyzed the structural elements of the aircraft for failure modes during two flight phases: turning and landing. In doing so, we made the assumption that the carbon fiber spars spanning the wing and fuselage bear all of the structural loading. The empty aircraft undergoes a load factor of five during turns and an approximate load factor of four to simulate the shock of landing. Figure 5.4 illustrates the loading applied to the fuselage and wing spars. The fuselage spar experiences a shock force from landing and lift and weight forces further aft. The wing undergoes elliptical loading from lift and a central point load from the aircraft weight.
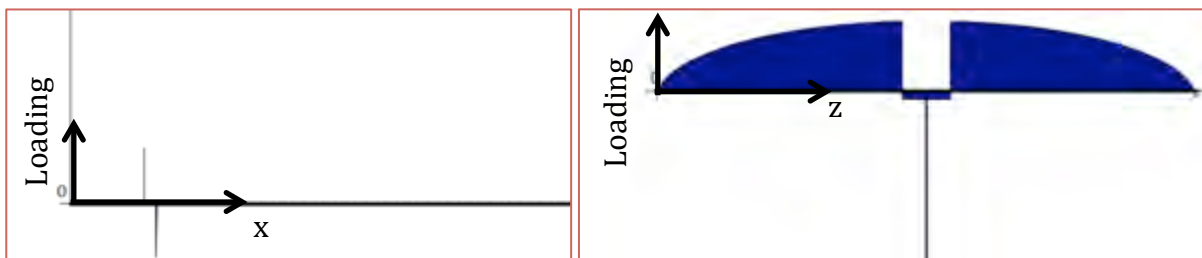
Figure 5.4 Loading diagrams for landing (left) and turning (right)

Based on inputted geometry and structural properties, we generated shear, moment and octahedral stress diagrams along the lengths of the wing and fuselage spars, respectively (Figure

5.5). We found that the structure has a factor of safety of 5.2 during landing and 58 during turning. This analysis does not account for spar deflection, which may cause other structural components to fail well before the spar would fail. We later validate the structural integrity of the aircraft through ground and flight testing.
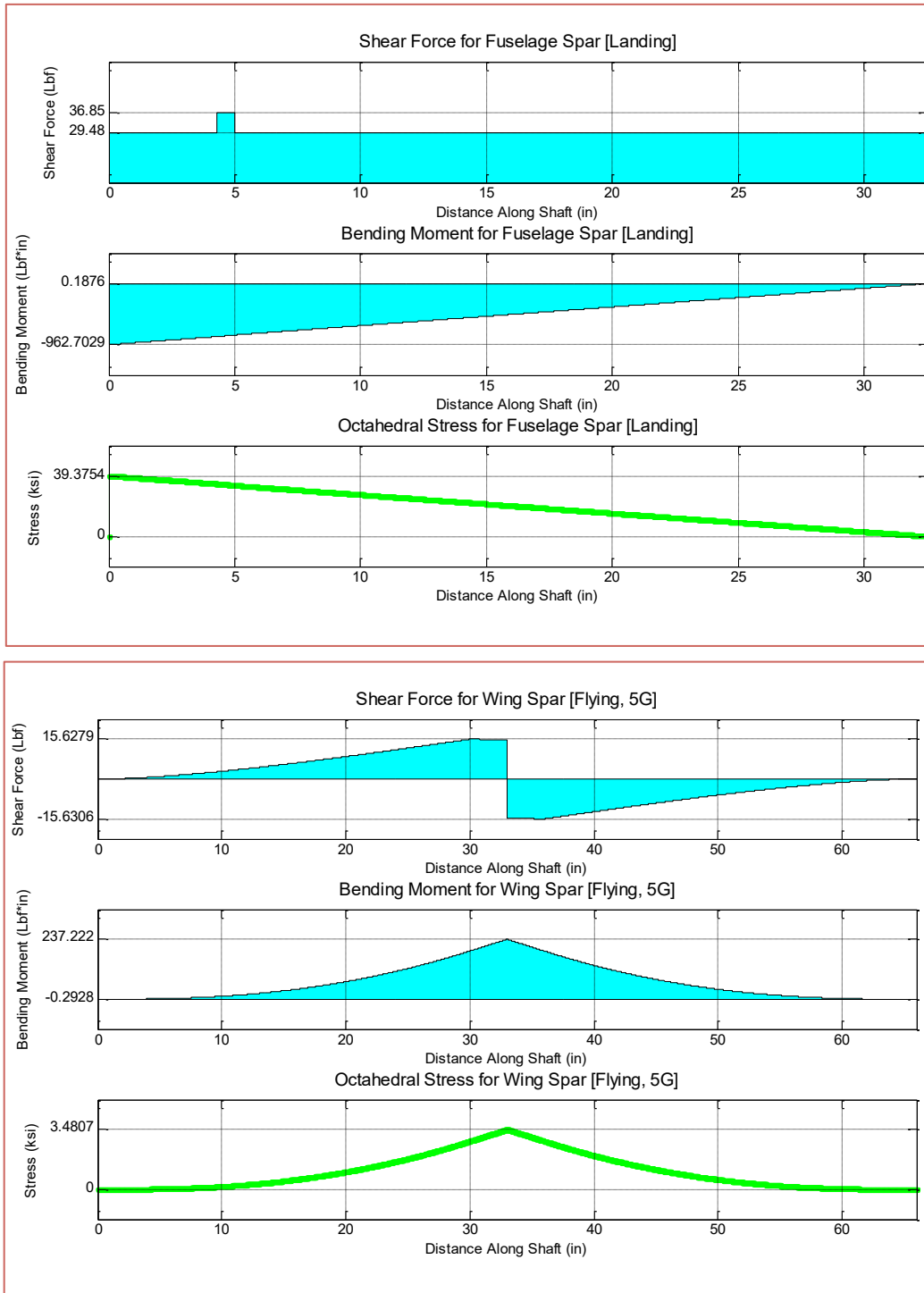
Figure 5.5 Structural diagrams for fuselage spar (top) & wing spar (bottom)

5.3   Aircraft Systems Design, Component Selection and Integration

This section of the report describes the design, selection and integration of the aircraft's key subsystems. The components discussed include the fuselage, wing, wing mount, bay door, empennage, nose cone, and electronics.

5.3.1   Fuselage design (Figure 5.6)

The design of the fuselage revolved around the accommodation of internal stores for missions two and three. Our primary objectives were to keep the fuselage as light as possible and to minimize its frontal area. We arranged the layout of internal stores and electronics such that we maximized the usage of space in the fuselage. The main structural element of the fuselage is a circular carbon fiber spar running lengthwise through the aircraft. Thin bulkheads and beams add rigidity to the structure and form the profile of the fuselage. A front landing gear mounts to a thicker bulkhead at the front end of the fuselage.
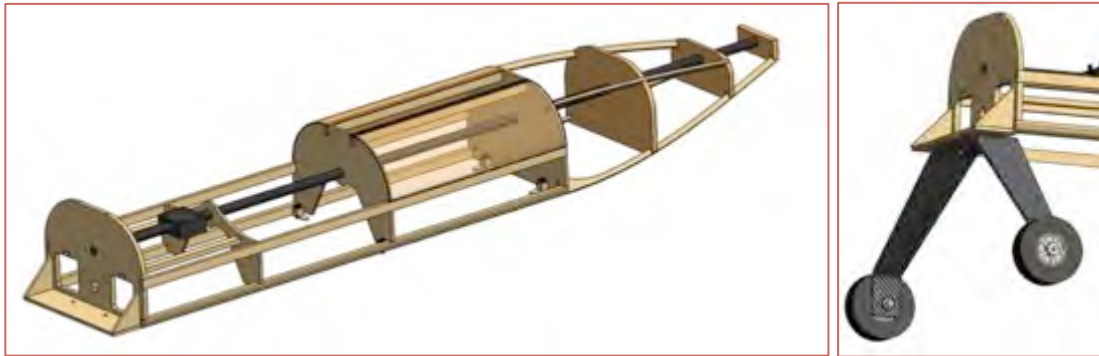
Figure 5.6 Fuselage design

5.3.2   Bay door design (Figure 5.7)

We designed the bay door with the intent of minimizing its weight and complexity. It needs to be removable and must enable four internal stores to drop out of the aircraft unobstructed. The bay door is a single, flat piece of wood. It is held in place by a lip on the fore end of the fuselage and four simple latches distributed along its length. It lines up with the bottom, rounded edges of the fuselage for aerodynamic purposes.

Figure 5.7 Bay door design

5.3.3   Wing design (Figure 5.8)

The wing design is based off of a balsa build-up consisting of ribs and stringers. In order to strengthen the design and reduce the number of ribs needed, two carbon fiber spars are used: a ½" diameter spar at quarter-chord and a .196" spar at 75% chord. The larger spar also serves as the attachment point for the payloads and as the attachment point between the wing and the fuselage. The wing is constructed using one-piece, full-span spars for added strength and rigidity.
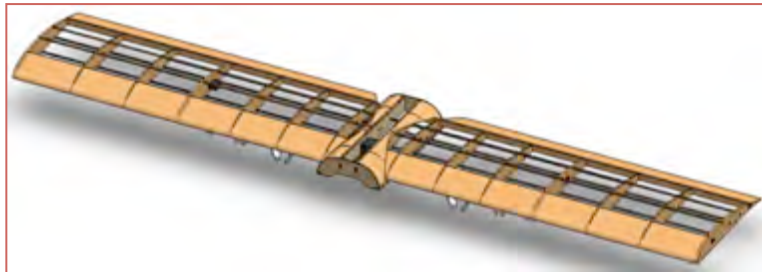
5.3.4   Wing attachment design (Figure 5.9)

The interface between the wing and fuselage was a critical element of our design from both structural and ergonomic standpoints. Since we chose to construct a one-piece wing, the wing needed to be able to attach from above. We also sought to maintain an aerodynamic profile between the wing and fuselage. The wing features a blended central section that fits into a gap in the top of the fuselage. A polycarbonate block on the main wing spar mounts via four screws to a similar block on the fuselage spar, guaranteeing structural integrity even when subjected to high wing loading. The fins of the internal stores fit through gaps in the central wing structure, thus maximizing the utility of internal space. The design allows for easy wing attachment, a secure wing connection, and an aerodynamic profile.
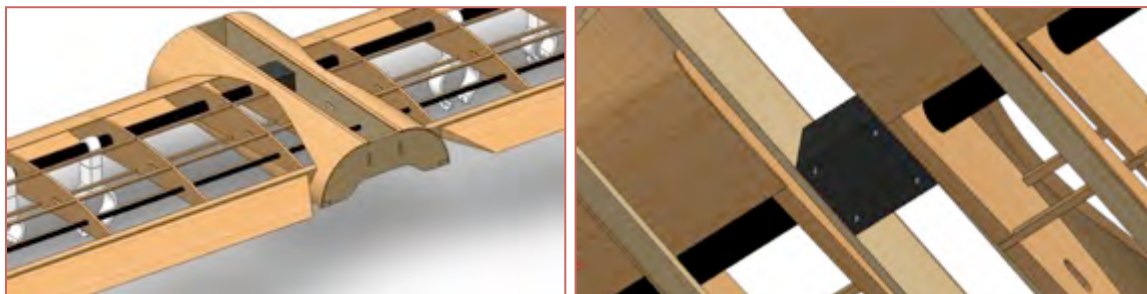
Figure 5.9 Wing attachment design

5.3.5   Empennage design (Figure 5.10)

We aimed for an empennage that would complement our overall design goals and maximize competition score. The empennage is designed to be lightweight yet structurally sound and resistant to flex. To minimize weight, a single carbon fiber spar runs through the entire fuselage of the plane and acts as the foundation for both the fuselage and empennage. To

maintain the aerodynamic profile of the fuselage and eliminate the formation of vortices in the fuselage wake, a series of bulkheads are located along the length of the spar and connected by stringers on the sides for support and shape. The horizontal and vertical tails connect to the spar by means of a tail cap and two tail mounts. To save weight, we designed a tail skid that mounts to the carbon fiber spar and serves as the second ground contact point for the aircraft.
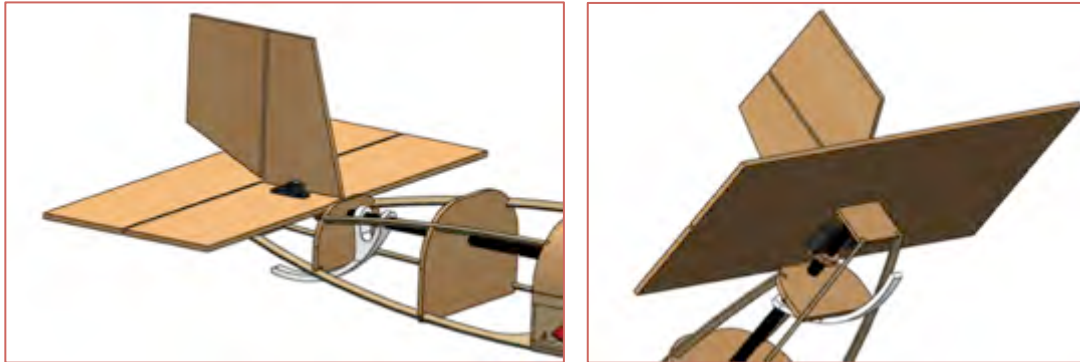
Figure 5.10 Empennage design

5.3.6   Nose cone design (Figure 5.11)

The main objectives of the nose cone design were to provide space for the motor and other electronics in the aircraft, to provide an aerodynamic profile, and to be as light as possible. It was not designed to bear any structural loading other than the drag force acting on it during flight. We also wanted an easily removable design such that the electronics were accessible for testing and building. A single-piece composite layup best served our needs, as it was lightweight yet retains shape well. We modeled the nose cone to maximize space for electronics and to achieve a high aerodynamic efficiency. The nose cone fits around wooden pieces on the fuselage and is held in place by a latch.
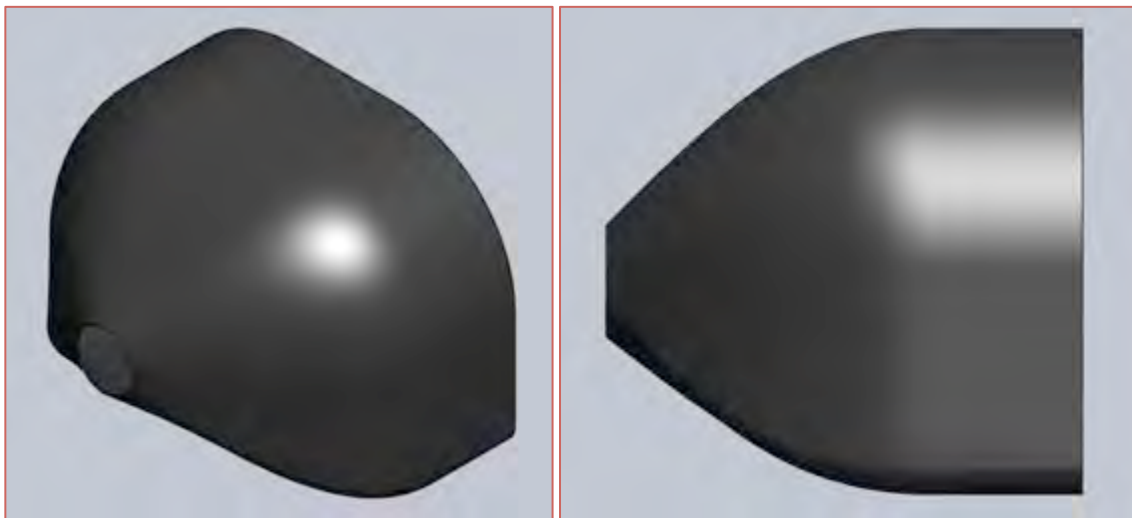
Figure 5.11 Nose cone design

5.3.7 Electronics selection

The aircraft utilizes standard servo motors to control the ailerons, elevator and rudder during flight. We initially sorted through a database of servos based on the class of servos typically used for aircraft in our estimated weight range. We then validated the amount of torque required for the servos through hinge moment calculations generated in the mission model. These calculations neglected wind contributions, so we included a factor of safety when determining the minimum torque required. We ultimately used a decision matrix to choose the optimal servo motor based on weight, torque and size (Figure 5.12). Consequently, the Hyperion DS11-AMB was chosen for actuating the aircraft's control surfaces. The performance of the servos in flight is later validated through testing.

Servo	%	DS11-AMB	DS11-SCB	DS450	DS 6125
Weight	0.55	1.00	1.05	1.10	0.38
Torque	0.35	1.00	0.81	0.74	1.57
Width	0.1	1.00	1.00	1.15	1.15
Total	1	**1.00**	0.96	0.98	0.88

Figure 5.12 Servo selection decision matrix

The competition requires that a separate battery power the receiver and servos. Using the servos that were specified above and the known maximum flight time of four minutes, we calculated an appropriate required battery capacity as shown in Figure 5.13.

Servo current (mA)	Total current (mA)	Flight time (hr)	Capacity (mAh)
400	1200	0.067	80

Figure 5.13 Receiver battery capacity sizing

In addition to the conservative estimate of full time maximum current, we implemented a safety factor of 1.5 to arrive at a capacity of 120mAh. We chose the KAN125 battery cell to fill this role in a four-cell pack. We chose the Phoenix HV ICE II electronic speed controller because it was the lightest and most efficient controller that could handle the high voltage of our propulsion system. We selected the Spektrum 6115e as the receiver based on its weight and compatibility with all other electronic components. Figure 5.14 shows a summary of the electronic components selected for the aircraft.

Component	Servo motor	Receiver battery	Electronic speed controller (ESC)	Receiver
Name	Hyperion DS11-AMB	KAN125	Phoenix ICE 2 HV 40	Spektrum 6115e

Figure 5.14 Summary of selected electronic components

5.4   Payloads Systems Design, Component Selection and Integration

The overarching design goals for the aircraft's payloads systems are summarized in Figure 5.15. The most critical objectives for the design of all internal and external payloads attachments are weight minimization and simplicity. The design, selection and integration of each payload system reflects these design goals.

Overall design requirements	Subteam design requirement
Low drag at cruise	Find internal store layout that minimizes frontal area
	Minimize weight of store attachments
Adequate stability	Minimize rolling tendency caused by external stores
Hold at least four stores	Design attachments to accommodate four internal stores

Figure 5.15 Payloads systems design goals

5.4.1   Internal store attachment

We sought to design an attachment between the aircraft and internal stores for mission two that would be simple, lightweight, and durable. It was necessary that the attachment constrain the stores from translating or rotating. We considered and tested various materials and methods, including clips, Velcro, hinges, magnets, ties, and rubber bands. The final system selected consists of a plastic clip lined with rubber and clamped closed with a nylon screw (Figure 5.15). We found that the clip created a rigid structure, establishing a secure housing for the store. An additional advantage to this method was that the clip could be fabricated via rapid prototyping, allowing precise control over the design and repeatability.
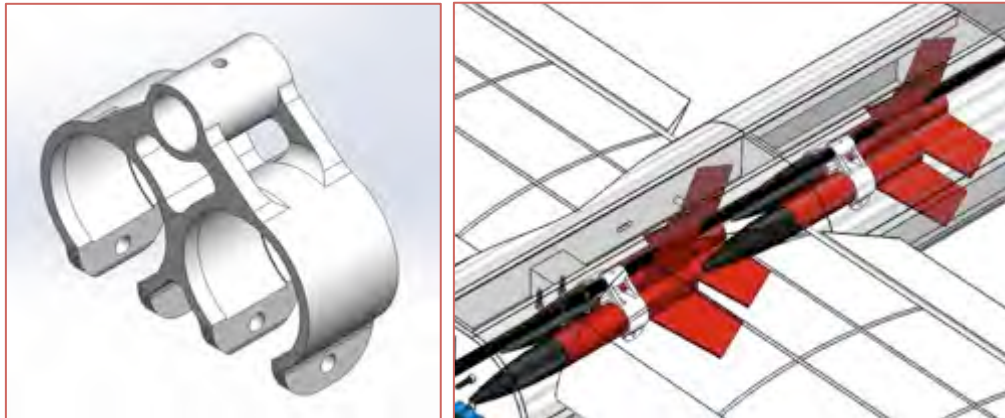
Figure 5.15 Internal store attachment clips

These clips then connect to a collar surrounding the carbon fiber spar running through the fuselage. In order to save weight and simplify the design, we wanted the collar to have two clips attached to it, connecting to a store on each side of the spar. Because of the staggered configuration of the stores, there was limited space where two purely cylindrical portions of the stores were next to each other. Attaching the stores at only one location enables quick access to the stores and meets our spatial constraints (Figure 5.16).
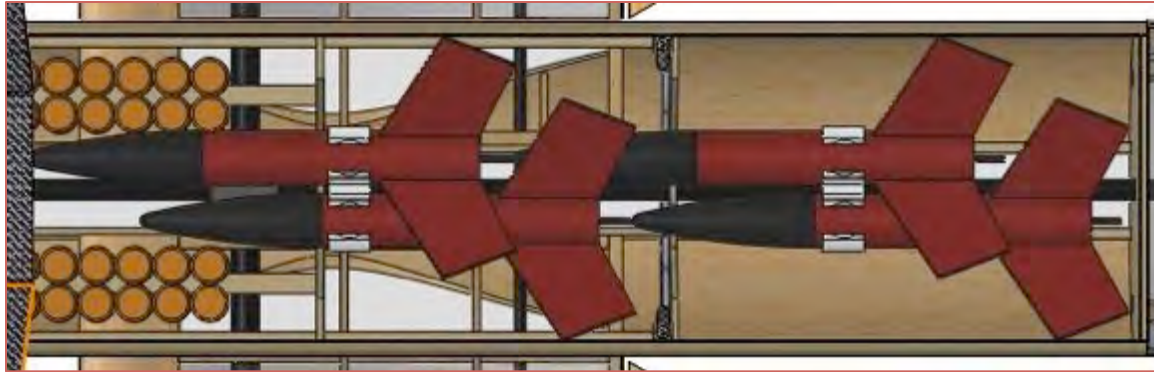
Figure 5.16 Final layout of internal stores (bottom view)

5.4.2 External store attachment

The design of external store attachment systems was driven by weight and the constraint of withstanding high structural loading. Since these stores need to be mounted on the wing, it was apparent that the loading should be directed through the main wing spar. We sought to design removable wing pylons so that we could minimize aircraft weight and drag for the first two competition missions. Doing so dictated that the mounting system must consist of two pieces per store: one permanently attached to the wing spar, and one removable. We proceeded to move forward with a "collar/clip" system, with the idea that we could interface between the external and internal sides of the wing.

Because we wanted to avoid drilling directly into the spar, we designed a shaft collar to which external pylons could attach. This part can be rapid prototyped and features a cutout where a nut can be inserted in the top part of the hole (Figure 5.17). The collar fits within the covering on the bottom of the wing. We designed clips to fit each of the three types of external stores used in mission three. These clips attach to the collars on the wing with a screw that is inserted vertically through the top of the clip.

Figure 5.17 External store attachment design

The clips used in the external attachments are similar to those for the internal stores: plastic clips with rubber linings and screw holes to clamp the stores. Mating alignment features on the collar and clip pieces prevent any twisting along the vertical axis, which keeps the stores

aligned in the direction of flight. The screws that close the circular clip put pressure on the body of the stores, preventing translation or rotation of the stores during flight.

5.4.3 Ballasting

Analysis of the store ballast requirements revealed that we would need a material with a density greater than 1.55 g/cm^2 to ballast the stores. While investigating materials, we found the main choice to be between a composite material (e.g. cement, compacted clay) and metal. Metals, particularly steel, easily met the weight requirements within our space constraints. They also allowed us to adjust the CG of the stores as desired by moving the ballast within the tube. The final choice of material was 1215 Carbon Steel, chosen for its high density, low price, and easy machinability. The metal rods could be cut, lathed, and grinded to precise sizes, as illustrated in Figures 5.18. The small cylindrical ballasts are secured in the stores with foam. For the internal stores, the ballast is placed near the nose to keep the CG of the stores as far forward in the aircraft as possible.
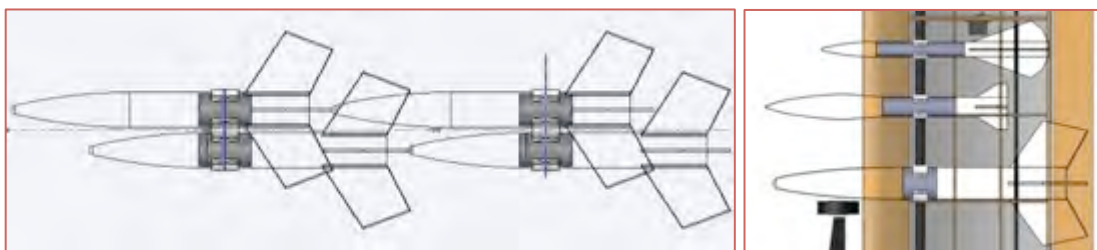
Figure 5.18 Internal ballasts (left), External ballasts (right)

5.4.4 External store attachment locations

External store attachment locations had to be chosen such that the aircraft's CG was well balanced. Since the different configurations of mission three are not all symmetric with weight, we sought to minimize the net rolling moment induced by the rockets while also minimizing the number of attachment points required. We created a tool in Excel to calculate the rolling moment for each configuration based on inputted store locations, as shown in Figure 5.19. We ultimately selected a mounting system in which there are three mounting points on each wing. This system results in a maximum rolling moment of 0.5 ft·lbf, which can be corrected with a small amount of aileron trim during flight.

Payloads		Mission	Left Wing			Fuselage				Right Wing			Rolling moment
			15.5	12.5	8.5	0.5625	0.5625	-0.5625	-0.5625	-8.5	-12.5	-15.5	
Mini Max	0.25												
mini honest jon	0.75	1											0
high flier	0.5	2											0
der red max	1	3											-0.25
		4											0
		5											0.5
		6											0.375

**Figure 5.19** Location of stores for each mission three configuration

5.5   Aircraft Component Weight and Balance

Figure 5.20 illustrates the component breakdown of aircraft's empty weight by system and subsystem. Approximately half of the aircraft's empty weight is contributed by the structural airframe, and the other half is contributed by the electronics used for propulsion and control.

Component		Qty.	Weight (lbf)	Moment bal. (ft·lbf)		Totals (lbf)
				X	Z	
Structures	Nose Cone	1	0.089	0	.013	2.19
	Tail	1	0.263	0	-.57	
	Fuselage	1	0.434	0	-.39	
	Wing	1	1.2	0	-.64	
	Landing Gear	1	0.205	0	.0016	
Controls	Receiver	1	0.009	-2.8e-4	-2.7e-4	0.12
	Receiver Battery	1	0.026	-2.8e-3	-.0013	
	Servos	4	0.02	0	-.096	
Propulsion	Motor Assembly	1	0.471	0	.070	2.06
	Propeller	1	0.021	0	.0064	
	Main Battery	2	0.741	0	-.16	
	Speed Controller	1	0.09	0	0	

Figure 5.20 Component weight breakdown for empty aircraft

The origin referenced on the aircraft in the calculation of moment balances is illustrated in Figure 5.21.
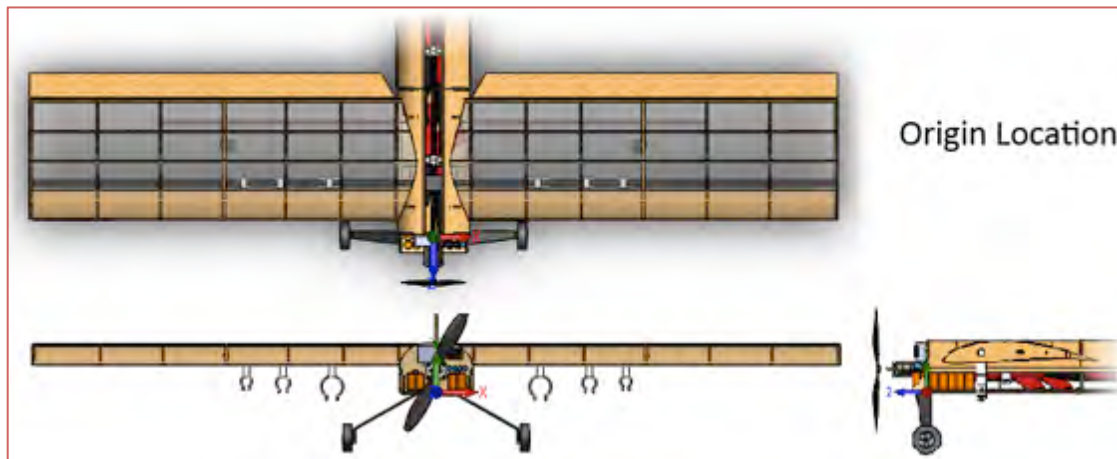
Figure 5.21 Aircraft origin used in moment calculations

Figure 5.22 lists the overall weight and balance for the aircraft broken down for each mission and external store configuration. The Z-moments reduce to zero when taken about the CG of the aircraft, which is located slightly behind the wing center of lift.

Mission	Mission 1	Mission 2	Mission 3					
			#1	#2	#3	#4	#5	#6
Weight (lbf)	4.37	5.37	7.39					
X (ft·lbf)	0	0	0	0	-0.25	0	0.5	0.38
Z (ft·lbf)	-3.54	-4.81	-4.23	-4.05	-4.35	-4.01	-4.27	-4.33

Figure 5.22 Weight and balance for each mission and configuration

5.6   Flight Performance Parameters

Figure 5.23 lists relevant flight performance parameters calculated by the mission model for each of the competition's three missions. The values shown reflect the final weight and geometry estimates developed during the detailed design phase. The mission three parameters listed correspond to configuration two, the highest drag configuration possible.

Parameter	Mission 1	Mission 2	Mission 3
C_{Lmax}	1.36	1.36	1.36
$C_{Ltakeoff}$	1.28	1.28	1.28
$C_{Lcruise}$	0.075	0.093	0.128
C_{D0}	0.058	0.058	0.065
$(L/D)_{takeoff}$	8.72	8.72	8.72
$(L/D)_{cruise}$	2.70	3.31	4.53
Stall speed (ft/s)	23.3	25.8	30.2
Takeoff speed (ft/s)	25.8	27.2	31.5
Takeoff distance (ft)	9.0	13.0	28.0
Takeoff angle (°)	9.0	9.0	9.0
Cruise speed (ft/s)	99.0	98.9	98.5
Cruise angle (°)	-6.24	-6.03	-5.59
Turn rate (°/s)	100	81.1	57.8
Max. load factor	5.0	4.1	3.0
Wing loading (lbf/ft^2)	0.87	1.07	1.48
Total flight time (s)	225	92	104
Gross weight (lbf)	4.37	5.37	7.39

Figure 5.23 Aircraft flight performance parameters

5.7   Mission Performance Summary

In Figure 5.24, we document the aircraft's performance for each of the three missions and for each of the phases of flight modeled. We generated these results using the mission model, again inputting the maximum-drag configuration for mission three.

Mission One Summary					
Flight phase	Qty.	Final speed (ft/s)	Distance (ft)	Time (s)	Capacity (mAh)
Takeoff	1	25.8	9	0.5	3.2
Climb	1	56.1	320	6.1	37.3
First leg	1	90.2	171	2.3	12.8
Cruise	7.68	99.0	1550	15.7	68.7
180 turn	16	90.5	-	1.6	8.7
360 turn	8	90.5	-	3.2	17.4
Accelerate	24	99.0	150	1.6	7.2
Mission One Totals			**16000**	**225**	**1030**
Mission Two Summary					
Flight phase	Qty.	Final speed (ft/s)	Distance (ft)	Time (s)	Capacity (mAh)
Takeoff	1	27.2	13	0.7	4.5
Climb	1	55.1	320	6.3	38.4
First leg	1	85.9	167	2.3	13.0
Cruise	2.66	98.9	1490	15.7	68.8
180 turn	6	84.3	-	2.2	10.7
360 turn	3	84.3	-	4.4	21.4
Accelerate	9	98.9	170	1.8	8.2
Mission Two Totals			**6000**	**92**	**433**
Mission Three Summary					
Flight phase	Qty.	Final speed (ft/s)	Distance (ft)	Time (s)	Capacity (mAh)
Takeoff	1	31.5	28	1.4	8.7
Climb	1	52.9	320	6.6	40.2
First leg	1	78.7	152	2.4	13.8
Cruise	2.65	98.5	1430	14.5	64.1
180 turn	6	90.2	-	3.1	15.0
360 turn	3	90.2	-	6.2	30.0
Accelerate	9	98.5	190	2.0	9.2
Mission Three Totals			**6000**	**104**	**494**

Figure 5.24 Aircraft mission performance summary

5.8   Drawing Package

In this section of the report, we present a comprehensive drawing package for the aircraft. The drawing package, generated using Solidworks, includes an annotated three view drawing of the aircraft, its structural arrangement, the layout and location of various subsystems, and the accommodation of payloads for different mission configurations.

16.0

3.0

6.3

2.0

12.0

66.0

6.0

Ø 12.0

15.0

5.6

11.2

42.2

8.9

2.9

6.5

8.8°
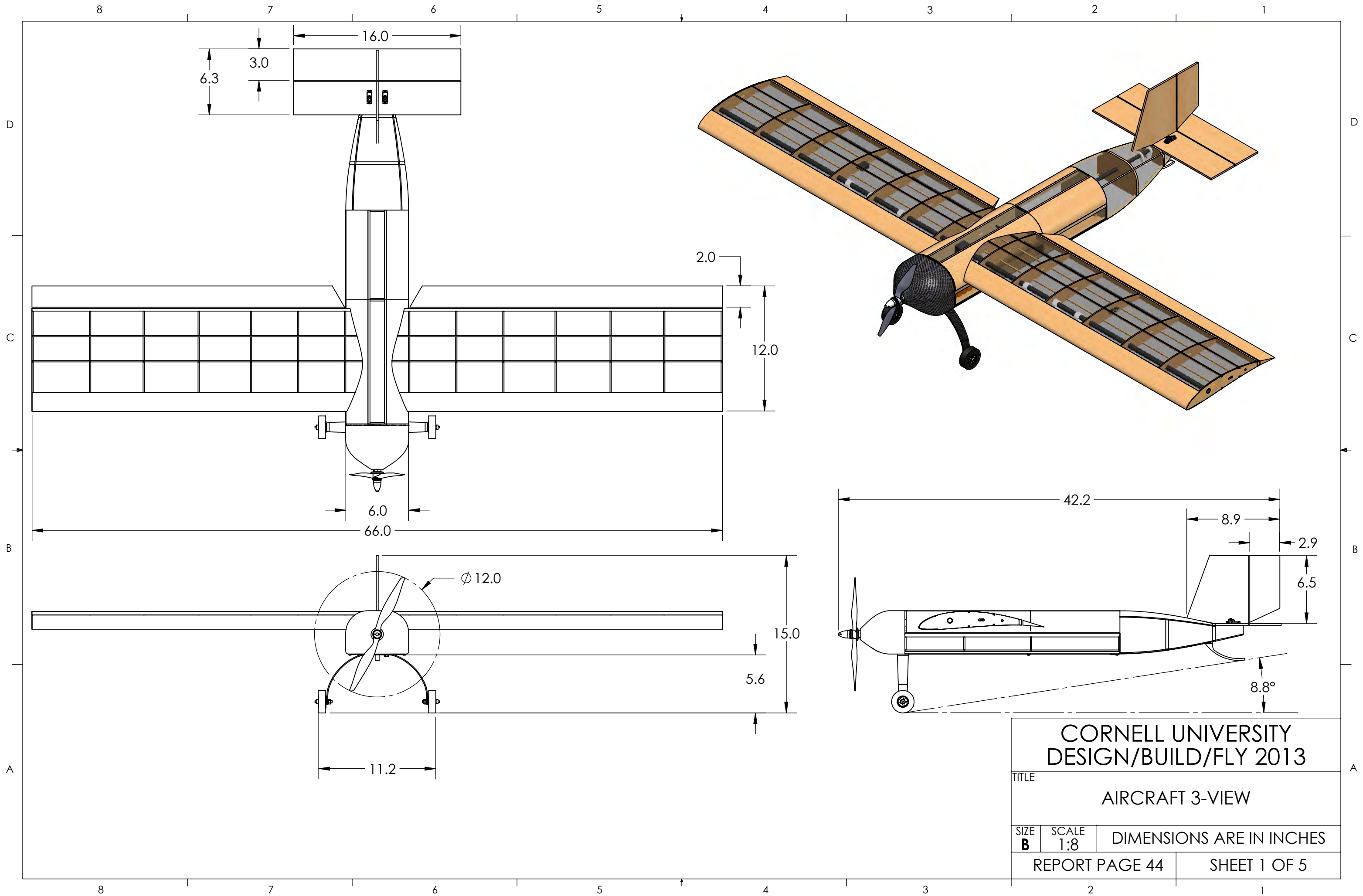
CORNELL UNIVERSITY
DESIGN/BUILD/FLY 2013

TITLE

AIRCRAFT 3-VIEW

SIZE B	SCALE 1:8	DIMENSIONS ARE IN INCHES
REPORT PAGE 44		SHEET 1 OF 5
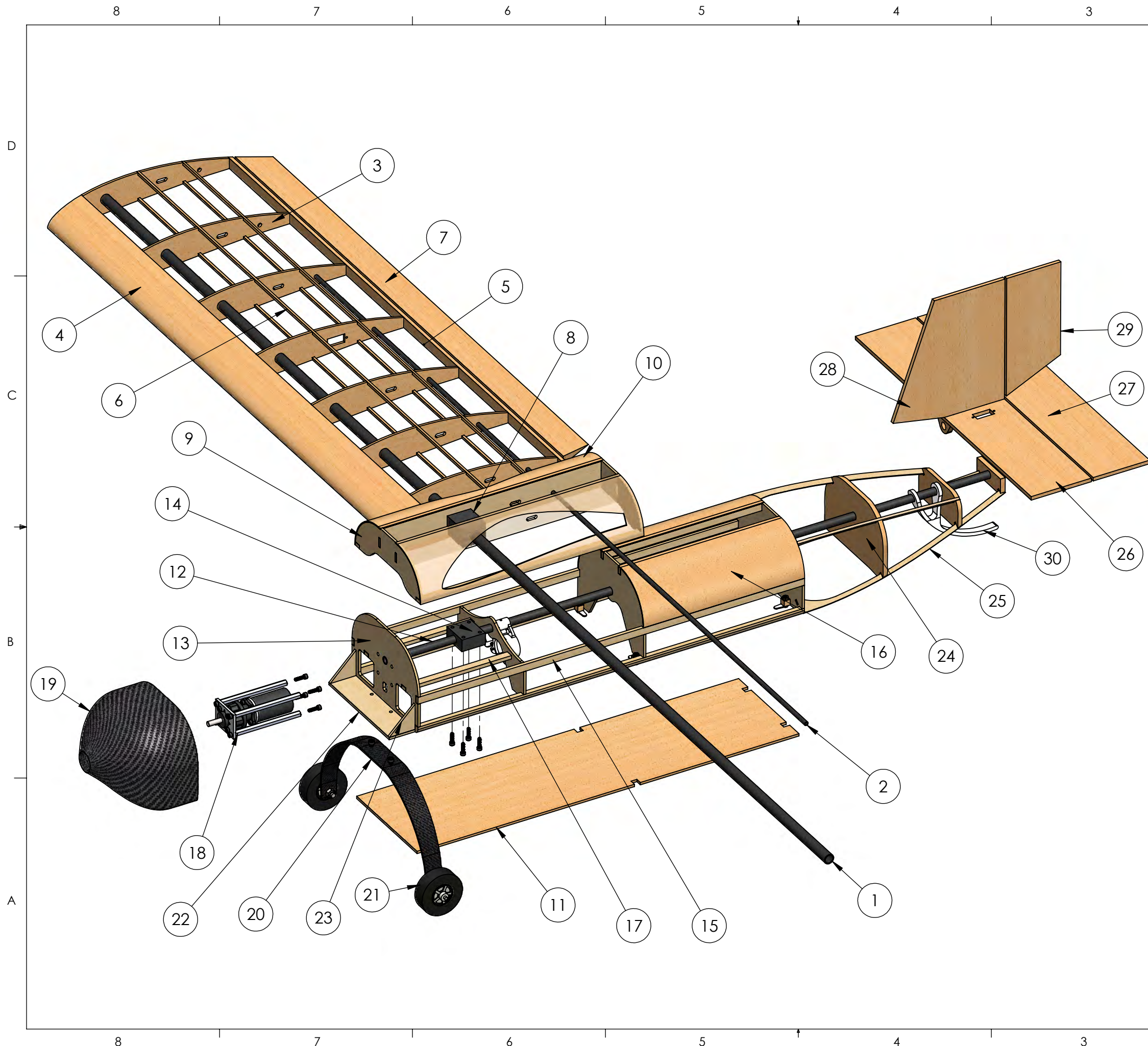
	PART	MATERIAL	QTY
1	WING MAIN SPAR	CARBON FIBER	1
2	WING REAR SPAR	CARBON FIBER	1
3	WING RIB	BALSA	16
4	WING LEADING EDGE	BALSA	2
5	WING TRAILING EDGE	BALSA	2
6	WING STRINGER	BALSA	8
7	AILERON	BALSA	2
8	WING BLOCK UPPER	POLYCARBONATE	1
9	WINGBOX BEAMS	SPRUCE	6
10	WING BLENDSHEET	BALSA	2
11	BAY DOOR	BALSA	1
12	FUSELAGE SPAR	CARBON FIBER	1
13	FUSELAGE BULKHEAD	SPRUCE	4
14	WING BLOCK LOWER	POLYCARBONATE	1
15	FUSELAGE STRINGERS	SPRUCE	6
16	FUSE. ROUND SHEETING	BALSA	2
17	BATTERY MOUNT BEAM	SPRUCE	2
18	MOTOR MOUNT ASSEM	ALUMINUM	1
19	NOSE CONE	CARBON FIBER	1
20	LANDING GEAR	CARBON FIBER	1
21	LG WHEELS	FOAM	2
22	LG MOUNT	SPRUCE	1
23	LG MONT GUSSET	SPRUCE	2
24	TAIL BULKHEAD	BALSA	3
25	TAIL STRINGERS	SPRUCE	4
26	HORIZ. STABLIZER	BALSA	1
27	ELEVATOR	BALSA	1
28	VERT. STABILIZER	BALSA	1
29	RUDDER	BALSA	1
30	REAR SKID	ABS PLASTIC	1

CORNELL UNIVERSITY
DESIGN/BUILD/FLY 2013

TITLE
STRUCTURAL ARRANGMENT

SIZE **B**
SCALE 1:4.5

DIMENSIONS ARE IN INCHES
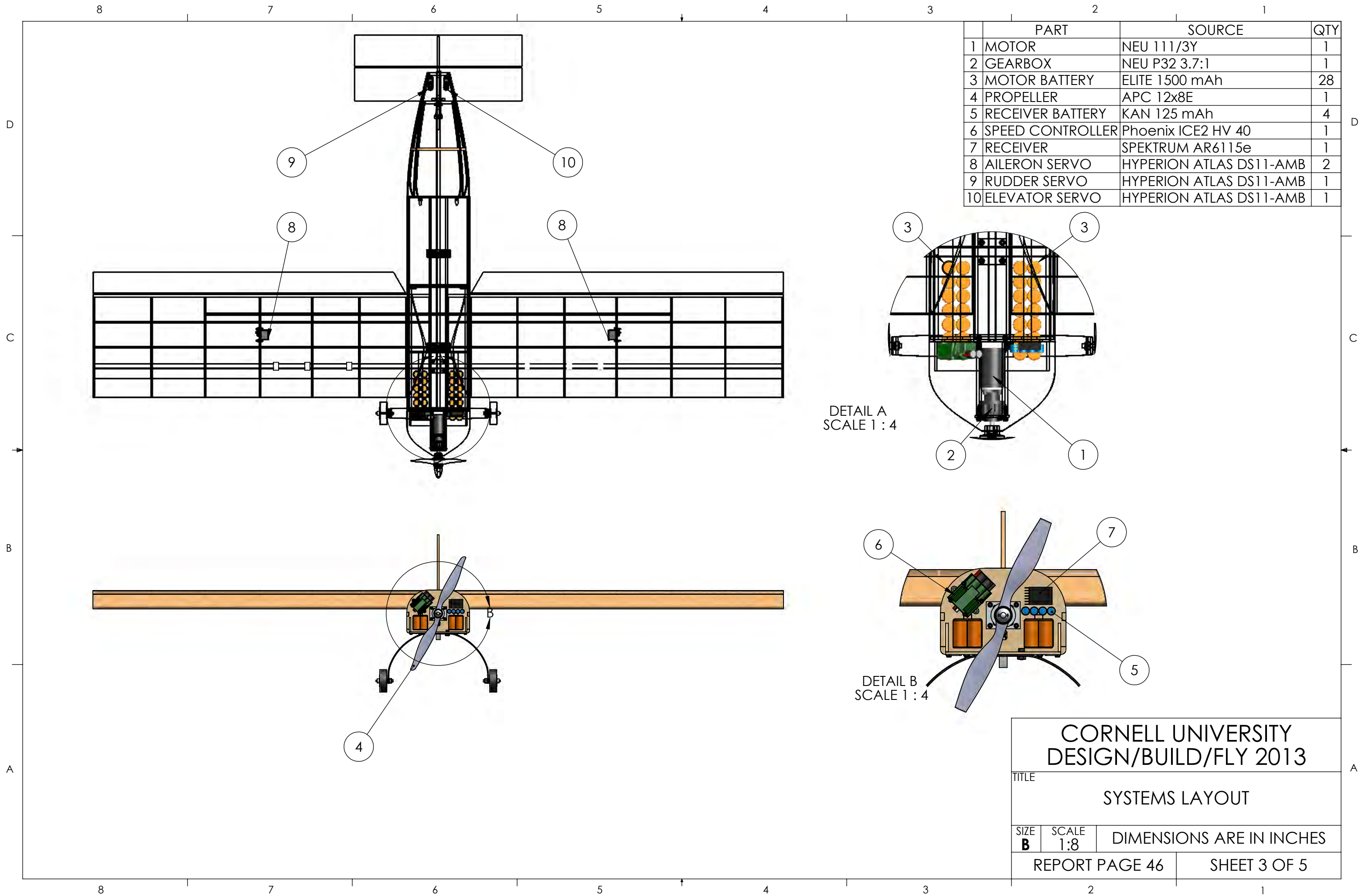
	PART	SOURCE	QTY
1	MOTOR	NEU 111/3Y	1
2	GEARBOX	NEU P32 3.7:1	1
3	MOTOR BATTERY	ELITE 1500 mAh	28
4	PROPELLER	APC 12x8E	1
5	RECEIVER BATTERY	KAN 125 mAh	4
6	SPEED CONTROLLER	Phoenix ICE2 HV 40	1
7	RECEIVER	SPEKTRUM AR6115e	1
8	AILERON SERVO	HYPERION ATLAS DS11-AMB	2
9	RUDDER SERVO	HYPERION ATLAS DS11-AMB	1
10	ELEVATOR SERVO	HYPERION ATLAS DS11-AMB	1

DETAIL A
SCALE 1 : 4

DETAIL B
SCALE 1 : 4

CORNELL UNIVERSITY
DESIGN/BUILD/FLY 2013

TITLE
SYSTEMS LAYOUT

SIZE **B**

SCALE 1:8

DIMENSIONS ARE IN INCHES

REPORT PAGE 46

SHEET 3 OF 5
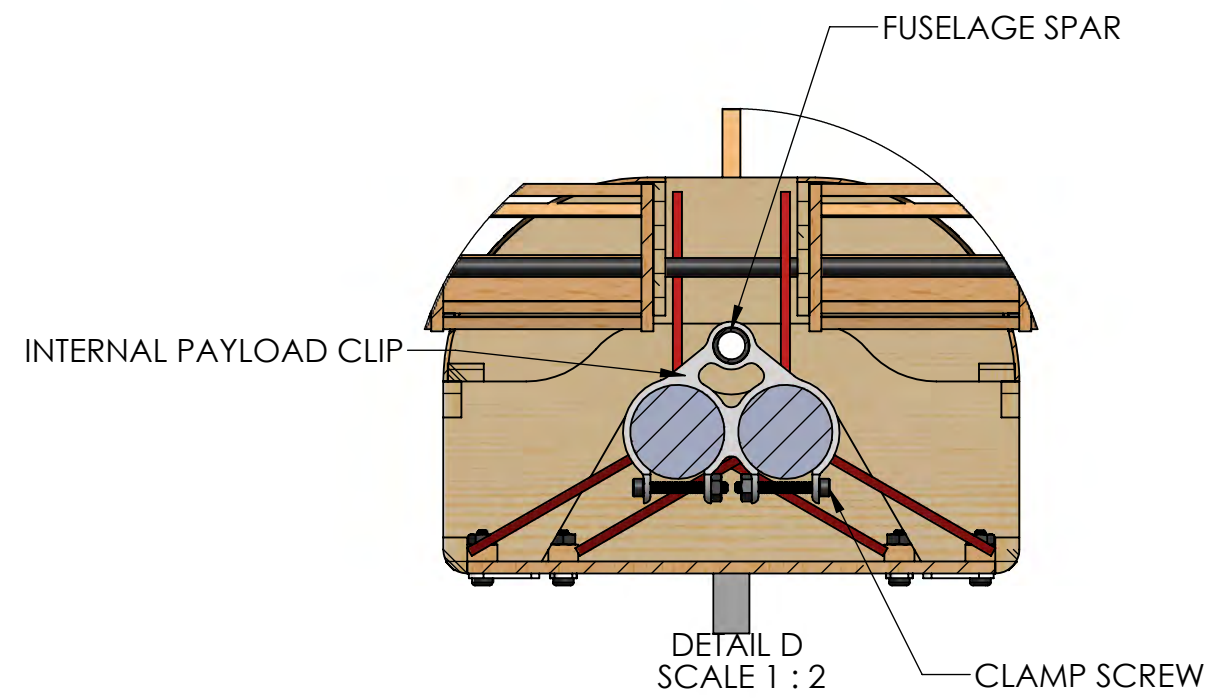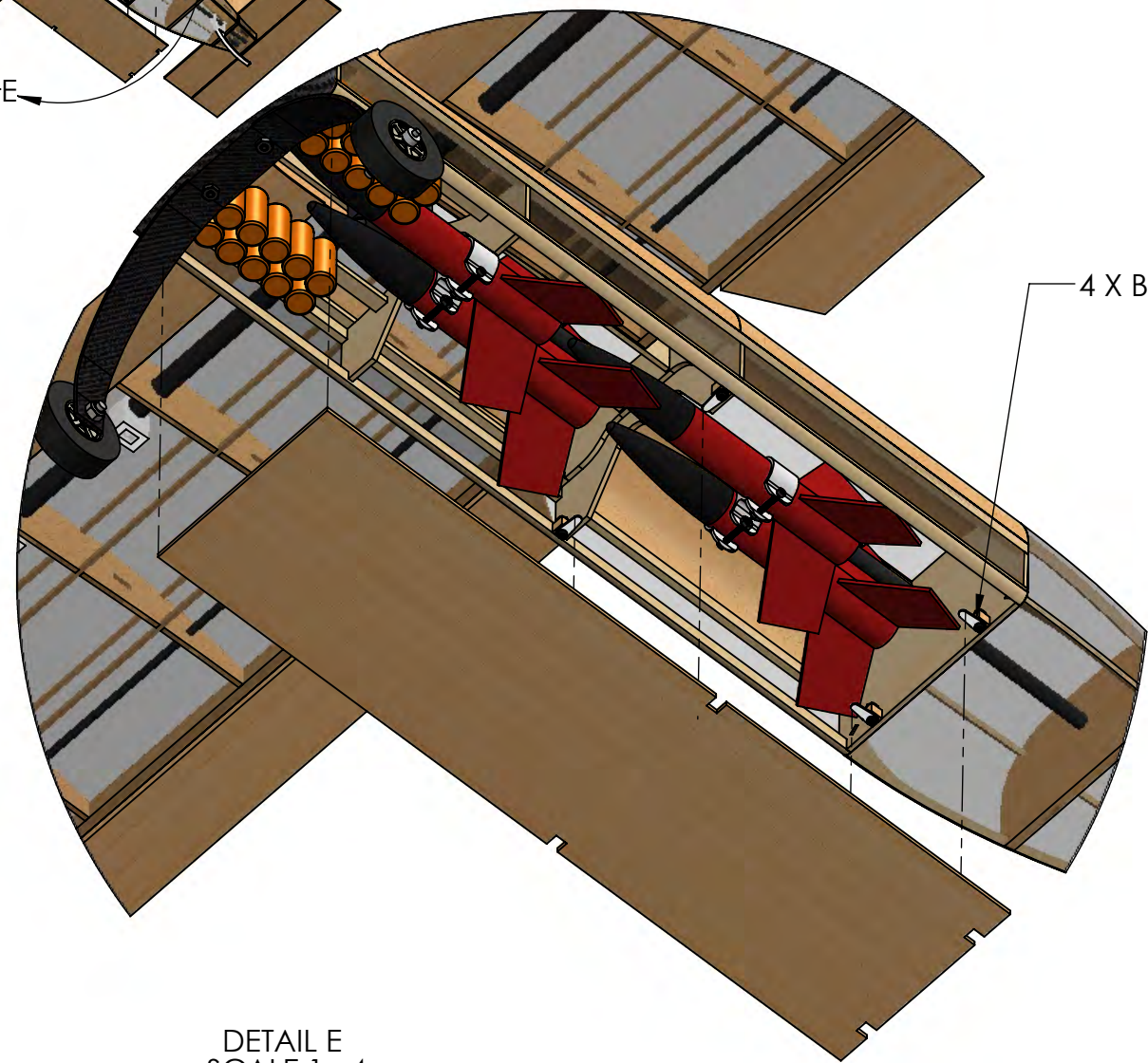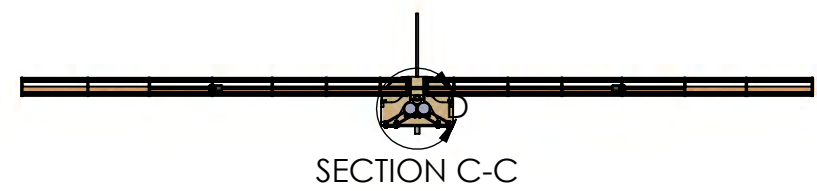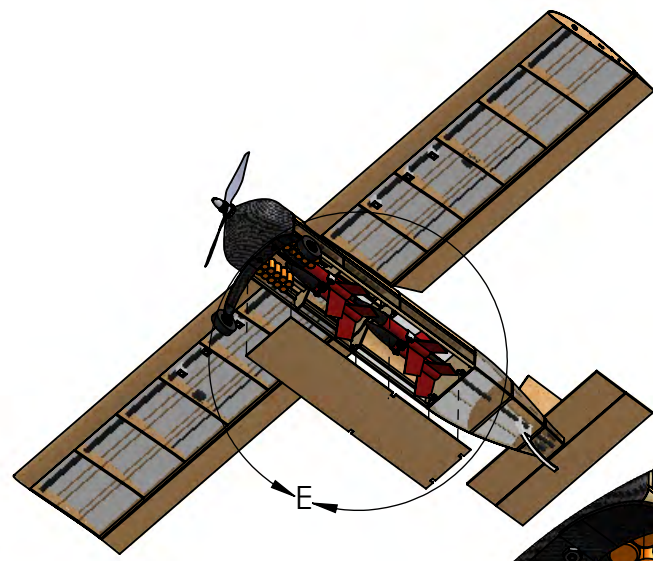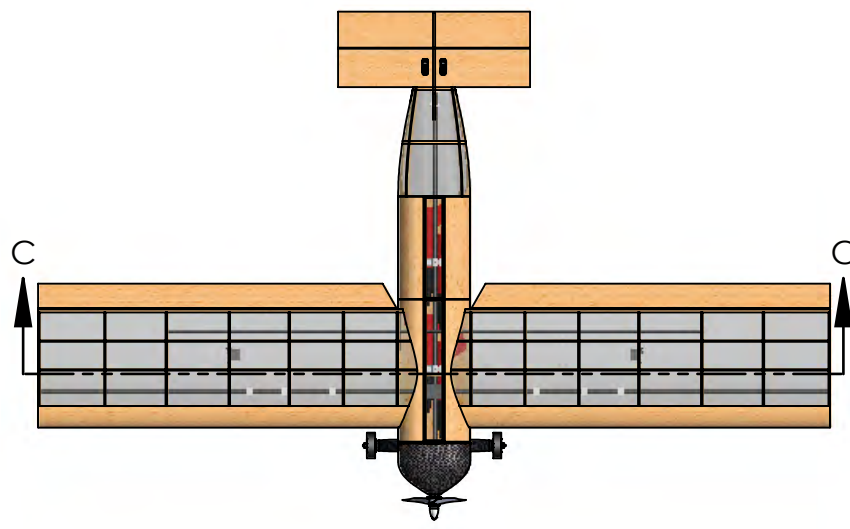
C

C

SECTION C-C

4 X BAY DOOR LATCH

FUSELAGE SPAR

INTERNAL PAYLOAD CLIP

CLAMP SCREW

DETAIL D
SCALE 1 : 2

DETAIL E
SCALE 1 : 4

E

**CORNELL UNIVERSITY
DESIGN/BUILD/FLY 2013**

TITLE

INTERNAL PAYLOAD
ACCOMODATION

SIZE	SCALE	DIMENSIONS ARE IN INCHES
B	1:16	

REPORT PAGE 47	SHEET 4 OF 5

SECTION F-F

MISSION 3 CONFIG 1

MISSION 3 CONFIG 2

MISSION 3 CONFIG 3

MISSION 3 CONFIG 4

MISSION 3 CONFIG 5

MISSION 3 CONFIG 6

DETAIL G
SCALE 1:2

CLIP TO SPAR
ATTACHMENT PIECE

CLAMP SCREW

EXTERNAL PAYLOAD CLIP

CLIP ATTACHMENT SCREW

EMBEDDED NUT
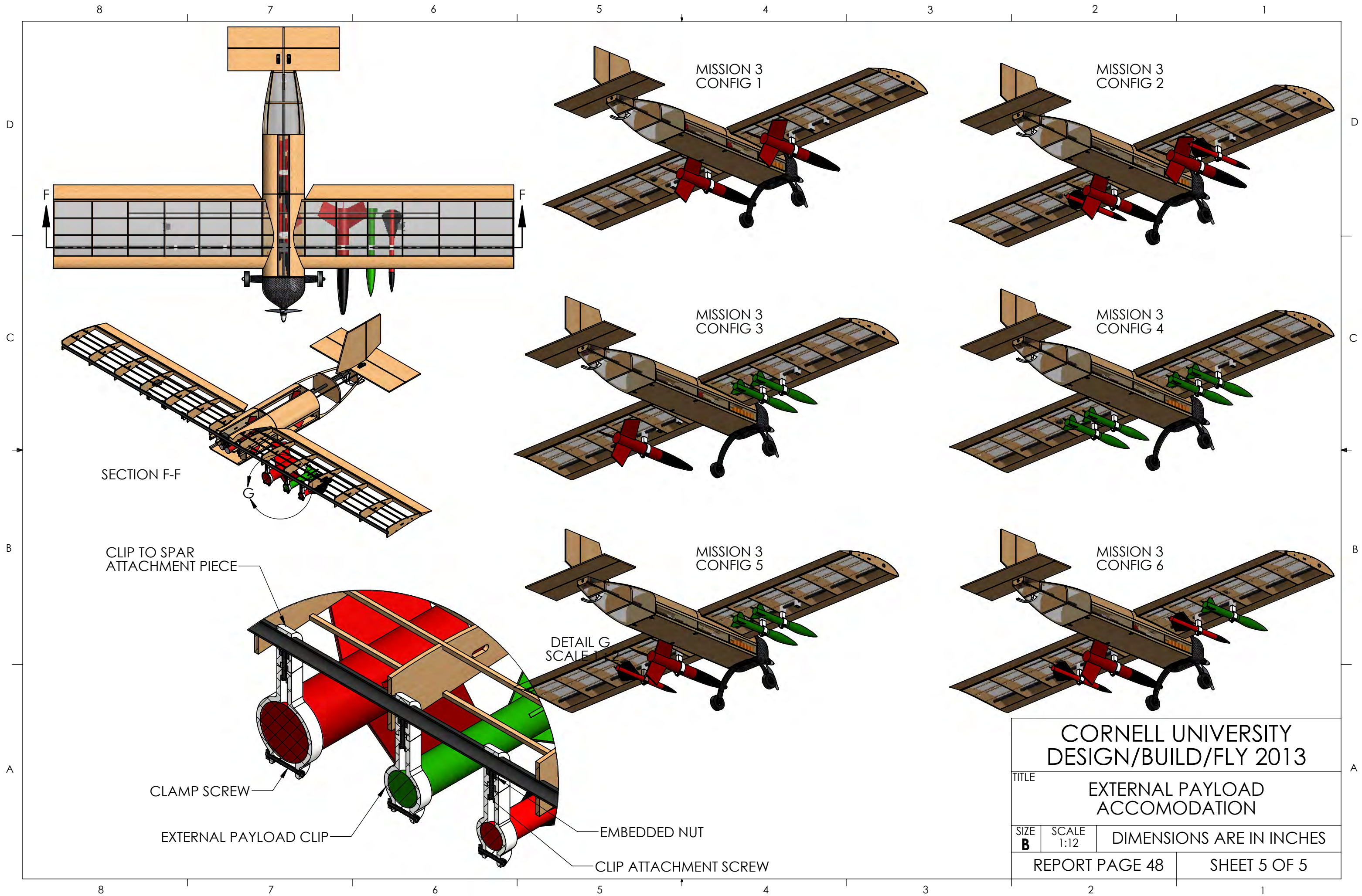
CORNELL UNIVERSITY
DESIGN/BUILD/FLY 2013

TITLE
EXTERNAL PAYLOAD
ACCOMODATION

SIZE B	SCALE 1:12	DIMENSIONS ARE IN INCHES
REPORT PAGE 48		SHEET 5 OF 5

6　Manufacturing Plan and Processes

Following completion of the aircraft's final design, we created a timeline for projected aircraft fabrication, determined the optimal process for manufacturing the aircraft's major components, and subsequently manufactured the aircraft's subsystems. The schedule for aircraft fabrication, shown in Figure 6.1, coincides with planned flight testing milestones. The plan dictates that we build and test three iterative prototypes in order to optimize the design such that actual performance results match our expectations from design and analysis.

Week of Phase	11/04	11/11	11/18	Winter break	01/28	02/04	02/11	02/18	02/25	03/04	03/11
First Aircraft Build											
Component fabrication										Planned	
Assembly										Actual	
Testing											
Second Aircraft Build											
Component fabrication											
Assembly											
Testing											
Third Aircraft Build											
Component fabrication											
Assembly											
Testing											
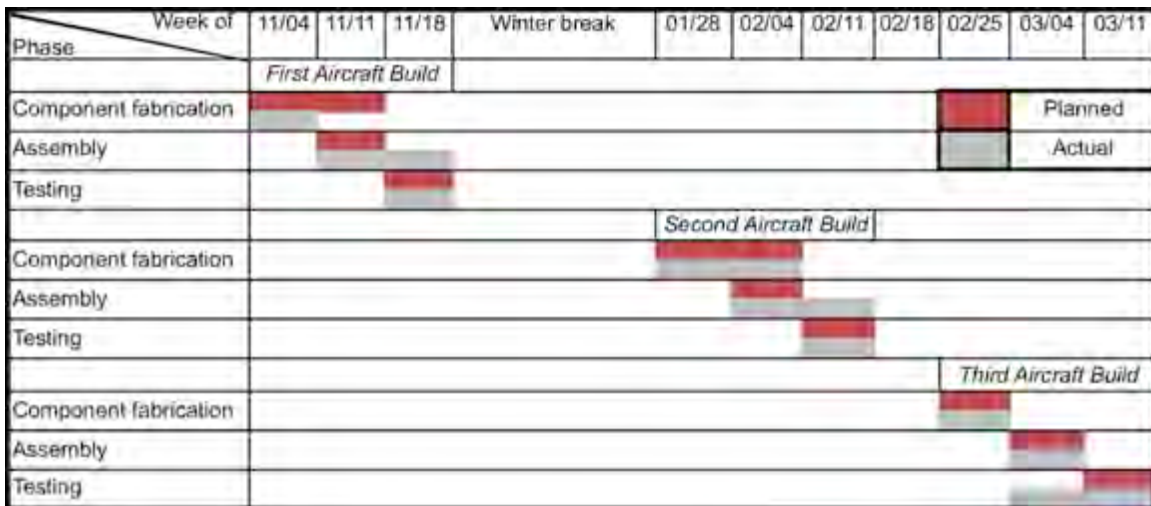
Figure 6.1 Manufacturing schedule

6.1　Manufacturing Process Selection

The overarching manufacturing process selected for fabrication plays a critical role in aircraft weight and overall flight score. Manufacturing methods for RC aircraft can be categorized into several primary groups:

- **Balsa Build-up** – With a great strength to weight ratio, this method offers a sturdy design at the cost of manufacturing time. The team has selected this method in the past and thus is more proficient at it than any other method.
- **Foam** – Although often heavier than a balsa build-up, foam construction can be built very quickly and easily because each part can be cut with a CNC machine. The team is not as experienced with creating foam parts.
- **Carbon Fiber** – Very rigid and heavier than balsa, carbon fiber can be laser cut in sheets, bought in a variety of plates and tubes, or laid up to create any shape. Although the team doesn't have much experience creating carbon fiber lay-ups, the addition of premade spars to either of the methods above can greatly strengthen the model and reduce the amount of other material needed.

We compared these methods based on aircraft weight, strength and manufacturability (Figure 6.2). We chose to pursue manufacturing methods combining the use of balsa build-up, carbon fiber, and other low-density woods. The airframe makes use of commercially available carbon fiber tubes sparingly to bear the primary structural loading, and carbon fiber cloth to lay up a lightweight nose cone. Laser cut balsa and spruce sheets, as well as balsa and spruce beams and stringers, form the rest of the aircraft's profile and structure.

Category	Weight	Balsa Build-up	Foam	Carbon Fiber
Weight	0.4	4	3	3
Strength	0.4	4	3	5
Manufacturability	0.2	3	3	3
Total	1	**3.8**	3	**3.8**

Figure 6.2 Manufacturing method decision matrix

6.2   Subsystems Manufacturing

In the following sections, we document the manufacturing process undergone to fabricate the wing, fuselage, empennage, payloads, nose cone, and propulsion subsystems.

6.2.1   Wing manufacturing (Figure 6.3)

The wing is composed of laser cut balsa ribs, two main spars, stringers, and a central wingbox structure. We aligned the wing components using the two spars and a wooden jig that supported the spars at the tips. We aligned the ribs spanwise using a printed drawing plan. Epoxy is used to glue all carbon fiber joints and CA glue for noncritical wood joints. Wetted balsa sheets fold over the outside of the wingbox, forming a profile that blends the fuselage and wing. Stringers and leading edge balsa sheeting provide attachment surfaces for Mylar covering.

Figure 6.3 Wing manufacturing

6.2.2   Fuselage manufacturing (Figure 6.4)

Fuselage manufacturing began by lining up the laser cut bulkheads and beams on a drawing plan, which were then glued together using the main fuselage spar as an alignment feature. We added balsa sheeting to the rear of the fuselage to retain its rounded profile. The bay door is cut from a single balsa piece. We laser cut bay door latches from spruce and mounted them with balsa blocks. The landing gear mounts to a thick plate with gussets to distribute loading into the fuselage front bulkhead. As with the wing, we used Mylar to cover the fuselage surfaces.

Figure 6.4 Fuselage manufacturing

6.2.3 Empennage manufacturing (Figure 6.5)

We fit and glued the vertical tail into a deep slot in the horizontal tail. We then bonded two wooden tail mount pieces to the bottom of the horizontal stabilizer using epoxy. These tail mounts allowed the tail to slide onto the carbon fiber fuselage spar. Before bonding the tail to the spar, a rig and level were used to maintain even height of the horizontal stabilizer with respect to the table while also insuring the tail was inline with the wing. To prevent the tail from sliding off, epoxy was again used to bond the tail to the spar via tail mounts.
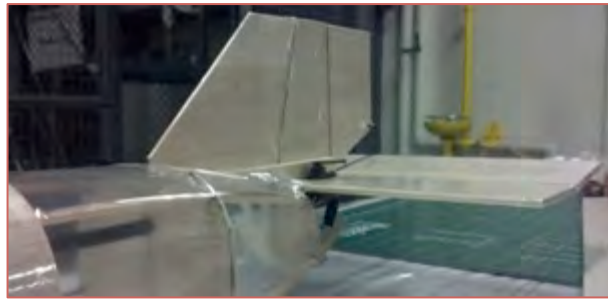
Figure 6.5 Empennage manufacturing

6.2.4 Payloads manufacturing (Figure 6.6)

We manufactured all payloads interfaces with a 3D-printer using ABS-plus plastic. To avoid stripping when screwing in the external pylons, we inserted nuts into the hole for the screw to thread into, rather than the plastic. Rubber bands were also added to the external clips using epoxy for extra motion constraint. We formed ballasts from steel rods of various diameters for each store. We then lathed down the rods and cut them to a length estimated to reach the required weight for each store based on density calculations.

Figure 6.6 Payloads manufacturing

6.2.5 Nose cone manufacturing (Figure 6.7)

The first step of nose cone manufacturing was to 3D print a mold, which we then sanded down to make smooth. After two layers of Duratec primer, we sanded again and waxed the part with mold release. Next, we sprayed the part with orange gel coat and laid 3-4 layers of fiberglass and vinyl resin. On the inside of the orange gel coat mold, we sanded and waxed before laying up epoxy resin and one layer of carbon fiber. We slid that into a vacuum back along with perforated release film, peel ply, and breather, and let it cure. Finally, we removed the hardened carbon fiber from the orange gel coat mold, and we had our nosecone.
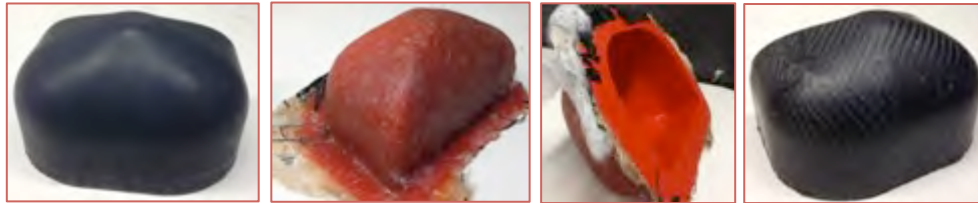
Figure 6.7 Nose cone manufacturing

6.2.6 Propulsion manufacturing (Figure 6.8)

The majority of the propulsion system components were commercially purchased as is mandated by the competition rules. One exception to this is the motor mounting plate, which we machined in-house using lightweight 6061-T6 Aluminum. The other main task of propulsion system manufacturing was the assembly of battery packs. We assembled each battery pack from loose cells. We formed connections using solder braid in order to ensure low resistance and weight. Lightweight Kapton tape provides insulation for the packs.
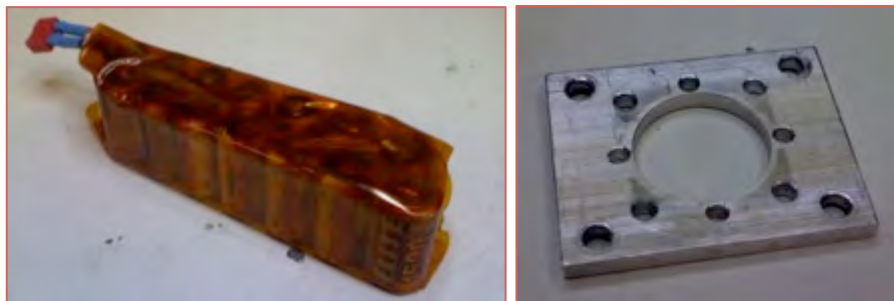
Figure 6.8 Propulsion manufacturing

7   Testing Plan

In this section of the report, we outline the planned subsystem and complete aircraft tests for our prototype aircraft. The purpose of these tests is to validate the estimated performance characteristics generated during the design process by comparing them with actual performance parameters. We provide a checklist of testing objectives in Figure 7.1, which summarizes what we wish to learn as a result of testing.

Structural Testing
☑ *Wing loading*: The wing must be able to sustain the loading applied during a 3g fully loaded turn without exhibiting failure or substantial fatigue. This will be simulated by a wing tip loading test.   ☑ *Landing gear strength*: The landing gear must be capable of absorbing and transmitting a shock during landing equivalent to a 4g load from the fully-loaded aircraft without failure.
Payloads Testing
☑ *Attachment strength*: The internal and external store attachments must prevent translation and rotation of the stores, and they must not break from the shock of landing.
Propulsion Testing
☑ *Receiver Battery*: The receiver battery must be able to power the receiver and all servos for a minimum of 5 minutes.   ☑ *Static Thrust Testing*: In order to validate theoretical calculations for current draw and thrust values, static thrust testing will be performed with all candidate propellers.
Flight (Complete Aircraft) Testing
☑ *Take-off distance*: We must takeoff fully loaded within a 30ft by 30ft square.   ☑ *Trim*: The aircraft must demonstrate adequate trim in both takeoff and cruise conditions.   ☑ *Directional/roll/pitch control*: Control surface sizing will be verified by observation of acceptable roll, bank, and climb rates.   ☑ *Stall recovery*: The aircraft must recover from a stall with minimal altitude loss   ☑ *Mission performance*: To validate our design predictions, we must perform each mission and configuration of mission three and record flight times.

Figure 7.1 Subsystem and complete aircraft testing checklist

Figure 7.2 displays the timing of planned and actual testing events leading up to competition. Note that flight testing continues after submission of the report.

Figure 7.2 Testing schedule

7.1   Propulsion Testing

The propulsion sub-team completed a series of tests on propulsion components in order to confirm theoretical predictions and optimize propeller selection. As a consideration of the takeoff distance constraint, the team also examined the effects of throttle advance rate on current draw. We developed a fixture to measure thrust that employed a 25-lb, S-band load cell (Figure 7.3). During thrust testing, we used a Castle Creations speed controller to log data of electrical parameters. We also tested the receiver battery's capacity by actuating all of the aircraft's servos simultaneously and timing the duration for which the receiver was powered.

Figure 7.3 Thrust testing setup

7.2   Structural Testing

Structural testing consisted of two main tests: a wingtip loading test and a landing gear test. For the wingtip-loading test, the objective was to simulate a 5g turn. Through stress analysis, we found this to be equivalent to a 2g wing tip test for the empty aircraft. We placed a prototype wing between two tables, secured it at the tips and loaded it centrally using steel weights. We recorded the weight added and the central wing deflection for several weights. For the landing gear test, the objective was to measure the amount of deflection for a given load; this was done both for structural integrity as well as to ensure that the external payloads would not come in contact with the ground during landing. For this test, we used a scaled down model of the landing gear. We secured the gear with plates to restrict any lateral motion. We then measured loading and deflection incrementally with increases in weight.
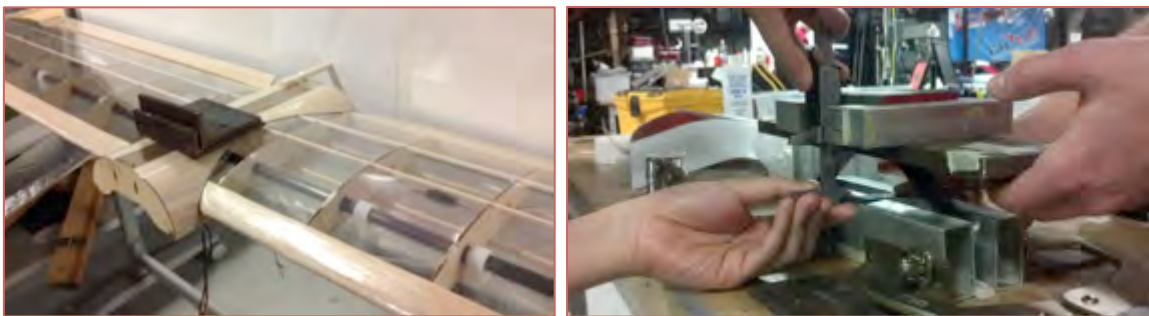
Figure 7.4 Structural testing: wing loading (left), landing gear loading (right)

7.3   Payloads Testing

The payloads sub-team tested the external payload attachments by creating a rig that simulated a section of the carbon fiber spar that they attach to on the wing (Figure 7.5). To test the readiness of the designs, they were subjected to drop tests simulating the shock of landing. We tested two variations of the 3D printed ABS plastic attachments. The first was a simple clip, while the second covered a greater amount of surface area (Figure 7.6). The latter is almost twice as long and is split down the middle to allow the hex key access to the internal screw.
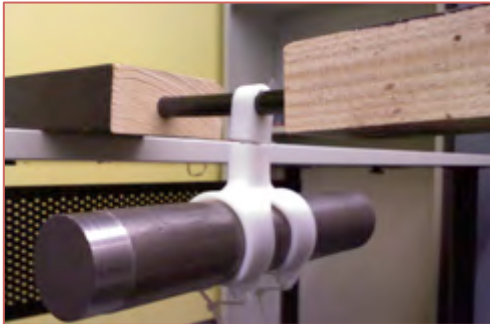
Figure 7.5 External payloads testing rig
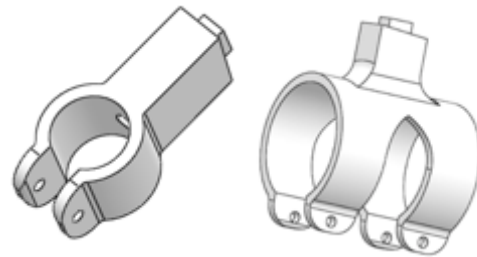
Figure 7.6 Payload clip types I and II

7.4   Flight Testing

Perhaps the most critical phase of design validation, flight testing enables us to evaluate aerodynamic, structural and performance characteristics for our complete aircraft solution. Through a myriad of individual flight tests (shown in Figure 7.7), we progress from validating basic stability and handling characteristics during the aircraft's maiden flight to determining precise flight times for each configuration of mission three. We allot a large portion of our testing schedule to flight testing in order to account for the often unpredictable weather conditions in Ithaca, NY, and to provide a buffer for unforeseen issues that arise during testing.

Flight	Aircraft	Testing description/goals
#1	#2	Maiden flight: Set empty aircraft trim, observe handling characteristics
#2	#2	Fly square patterns and figure eights; test stall and spin recovery
#3	#2	Fly mission one: record flight time and current draw
#4	#2	Fly mission two: record flight time and current draw
#5	#2	Fly each configuration of mission three: record flight time, current draw and takeoff distance; adjust rudder and aileron trim for each configuration
#6	#3	Maiden flight: Set empty aircraft trim, observe handling characteristics
#7	#3	Fly square patterns and figure eights; test stall and spin recovery
#8	#3	Fly mission one: record flight time and current draw
#9	#3	Fly mission two: record flight time and current draw
#10	#3	Fly each configuration of mission three: record flight time, current draw and takeoff distance; adjust rudder and aileron trim for each configuration

Figure 7.7 Flight testing plan for second and third aircraft prototypes

8 Performance Results

This section of the report outlines the performance results measured and recorded in the process of conducting the subsystem and complete aircraft testing described in the previous section. We use the results processed here in order to validate aerodynamic and performance predictions made in the design of the aircraft. We analyze discrepancies between predicted and actual performance and use them to optimize the aircraft for successive design iterations. Finally, we identify and correct any unexpected issues that arise from testing.

8.1 Propulsion Testing

Figure 8.1 shows a sample of the data collected for propulsion thrust testing using the Castle Creations speed controller. The output displays motor RPM, voltage and current draw versus time for a range of motor-propeller combinations.
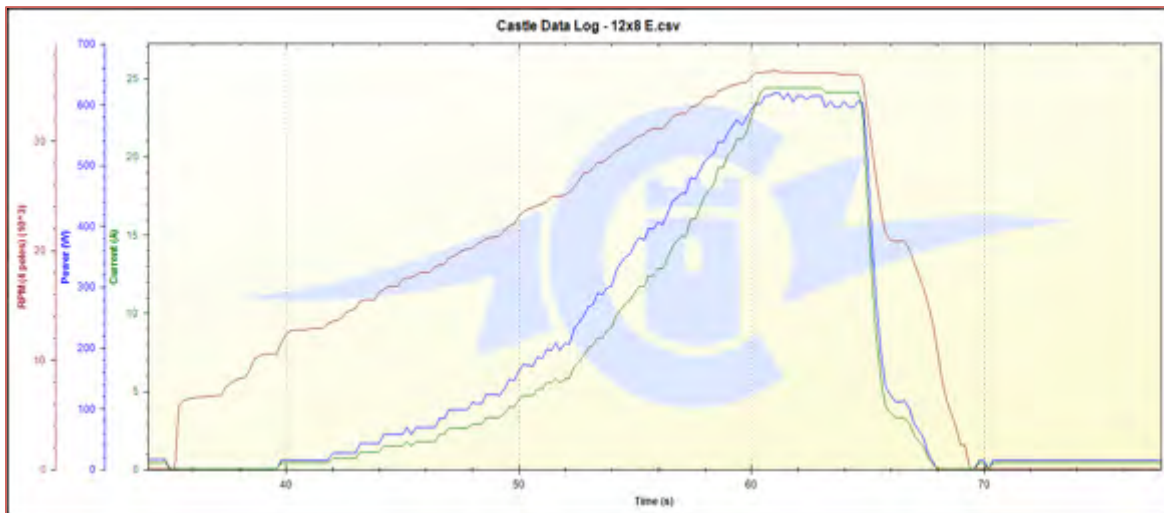
Figure 8.1 Sample data collected for propulsion thrust testing

The results of static thrust testing for the propellers of interest are summarized in Figure 8.2. These test results indicate that some of our calculations slightly underestimated the static current draw. This phenomenon will be closely examined during flight testing and, if necessary, propeller diameter and/or pitch will be reduced in order ensure safe operation within the current limit. In general, the results listed for thrust, power and RPM corroborate the performance predictions generated by the mission model with an accuracy of roughly ±20%.

Propeller	Thrust (lbf)	Current (A)	Power (lbf·ft/s)	Motor RPM
11x10 E	6.5	19.4	438	37590
12x8 E	7.1	24.4	446	36200
13x6.5 E	8.5	27.3	541	37809
12x7 SP	8.7	28.1	560	37949

Figure 8.2 Static performance parameters of propulsion system

Receiver battery testing indicated that the receiver was powered continuously for nine minutes. This testing will be validated in flight by measuring receiver battery current draw.

8.2   Structural Testing

The values recorded for wing loading and corresponding deflection are plotted in Figure 8.3. Deflection at the root of the wing was approximately linear with the load applied at the root of the wing. The wing exhibited perfectly elastic behavior in the testing regime and successfully withstood a loading equivalent to what it would experience in a 5g turn empty during flight. The trend between loading and deflection agrees well with results predicted from the structural model. Differences between predicted and actual structural characteristics can be attributed to the assumption made in analysis that the main spar bears all of the wing loading.
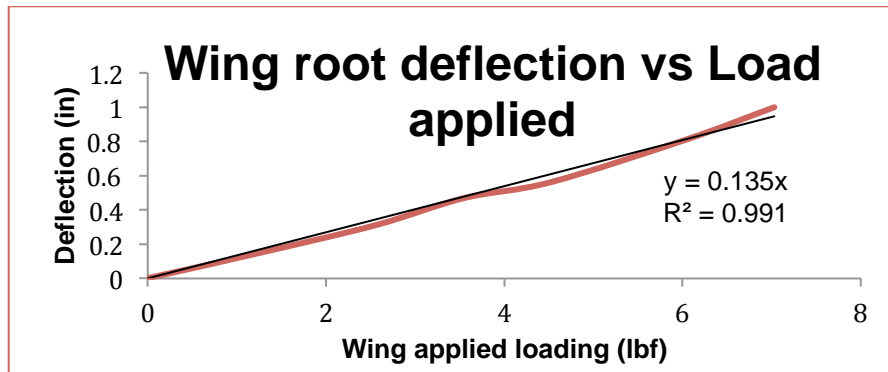
Figure 8.3 Wingtip testing results

Results recorded for the landing gear test outlined in 7.2 are displayed in Figure 8.4. The 2:3 scale, carbon fiber composite landing gear used behaves nonlinearly as the loading it experiences increases. We also found that the deflection became inelastic after a specified loading point, producing an approximate yield strength for the structure. Scaling the results appropriately for the full-size landing gear, we found that the equivalent loading experienced by the landing gear for the fully loaded aircraft fell within the allowable range of deflection.
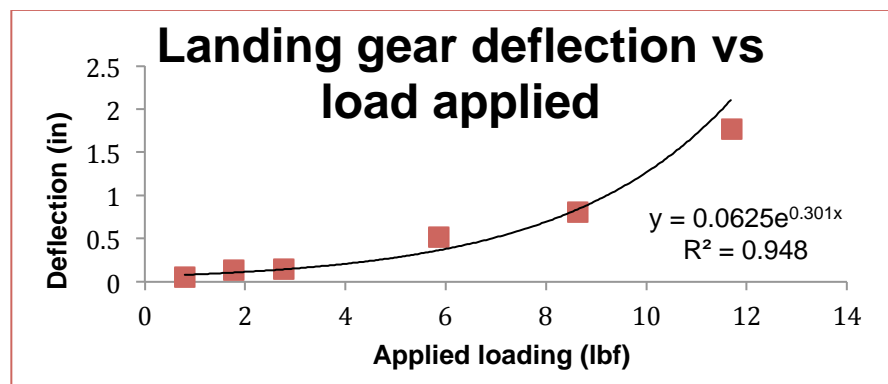
Figure 8.4 Landing gear testing results

8.3   Payloads Testing

Initial testing of the payloads systems revealed that the external attachment system would need to be redesigned for additional strength. Results for individual testing trials are listed in Figure 8.5. In tests simulating the shock of landing, the plastic screw used to attach the 3D printed attachments and collars would fail abruptly (Figure 8.6). For both attachment collars depicted in Figure 7.6, the plastic screw head securing the attachment ripped off for a simulated loading of between 3g and 4g. In light of this, the team decided to wait until after the attachments were redesigned before doing load tests and simulating all the various directions of motion under which the collars would have to support the payloads.

Trial	Clip type	Loading	Result
#1	Single	2g	Success
#2	Single	3g	Failure
#3	Double	2g	Success
#4	Double	3g	Success
#5	Double	4g	Failure

Figure 8.5 External payloads testing results   **Figure 8.6** Screw attachment failure

For future testing, the team will use aluminum screws to increase the tensile strength the attachments can handle. We also concluded that it would be useful to estimate momentum change by measuring velocity during testing and then collecting more data. This would provide a more quantitative understanding of the strengths and weaknesses of the attachments, as well as make it easier to compare test results with what might happen during flight. For manufacturability, the team will consider making the attachment screw more easily accessible, since it is slightly difficult to tighten using hex keys.

8.4   Flight Testing

The results presented here document the performance of the complete aircraft solution in flight tests leading up to the submission of the competition report. We conducted these tests using the second aircraft prototype. We uncovered several issues with flight handling and performance throughout the course of testing that will be fixed in the third aircraft design iteration by implementing the solutions listed (Figure 8.7).

Flight	Issue	Solution
#1	Pitch sensitivity due to small static margin	Move tail further aft & increase area
#2	Limited elevator authority in stalls and in cruise	Move tail further aft & increase area
#4	Landing gear plate broken during landing	Redesign landing gear mount
#5	External store mounts rotated during flight	Redesign mounts for increased rigidity
#5	42 foot takeoff distance	Cut weight & increase wing area

Figure 8.7 Flight performance issues and solutions

Using onboard telemetry, we were able to record approximate performance parameters throughout flight and compare them to our calculated performance predictions. Figure 8.8 displays measured average current draw from the receiver battery from three separate test flights, which we then average and multiply by the duration of flight to obtain an average required capacity for the receiver battery. We conducted test flights with an oversized receiver battery as a safety measure; the required capacity calculated validates our initial receiver battery selection.

Average current draw (A)	Required capacity (mAh)	Average required capacity (mAh)
0.17	11.3	
0.13	8.7	**11.6**
0.22	14.7	

Figure 8.8 Receiver battery current draw recorded during flight testing

Figure 8.9 displays recorded values for propulsion current draw and in-flight airspeed for several flight tests. The data recorded validated that we are meeting the current draw limitations and corroborates the predicted airspeeds for the cruise phase of flight. The takeoff current values recorded by the telemetry exceed the fuse limit of 20 amps, but testing has shown that the fuse does not blow at any time during flight. We plan on using these test results to optimize the third aircraft design iteration to best meet competition requirements. In particular, we will use the results presented here to adjust the wing size such that the aircraft takes off in the exact distance required. In addition to fixing the design issues listed in Figure 8.7, we plan on reducing the airframe weight significantly for the next iteration, which will lower the required wing and tail area. No other significant design changes are planned at this time.

Max takeoff current (A)	Average current (A)	Average speed (ft/s)	Max speed (ft/s)
27.4	15.1	66.0	105.6
23.5	11.9	53.2	95.3
24.1	14.9	62.4	98.3

Figure 8.9 Propulsion current draw and airspeed recorded during flight testing

Figure 8.10 Runway landing during flight #5

References

"2012/2013 Rules and Vehicle Design." *AIAA DBF*. Web. 31 Aug. 2012.
http://www.aiaadbf.org/2013_files/2013_rules.htm

"Airfoil Database Search." *Airfoil Tools*. Web. Nov. 2012. http://airfoiltools.com/search/index

Anderson, John. Introduction to Flight. 6th. New York: McGraw-Hill, 2005.

Etkin, B., & Reid, L. D. Dynamics of Flight Stability and Control Third Ed. Hoboken, New
Jersey: John Wiley and Sons, 1996

Drela, M., & Youngren, H. XFOIL. Retrieved Oct. 2012, from Subsonic Airfoil Development
System: http://web.mit.edu/drela/Public/web/xfoil/.

Drela, M., & Youngren, H. AVL. Retrieved Jan. 2013, from
http://web.mit.edu/drela/Public/web/avl/.

Gilruth, R. R., and M. D. White. "Analysis and Prediction of Longitudinal Stability of
Airplanes." *NASA Technical Reports* 711th ser. 1941.

Krauss, Tom. Airfoil Investigation Database. November, 2012. http://www.worldofkrauss.com

Muller, Marküs. "propCalc – Calculator for Propeller, Powered by Neu Motors". *Neu Motors*. Web.
Oct. 2012. http://www.ecalc.ch/motorcalc_e.asp?neumotors

Raymer, Daniel. Aircraft Design: A Conceptual Approach. 3rd. Washington, D.C.: American
Institute of Aeronautics and Astronautics, Inc., 1999.

Shevell, R. S., Fundamentals of Flight, 2th Prentice Hall, 1989.

UIUC Airfoil Coordinate Database. Web. Dec. 2012.
http://www.ae.uiuc.edu/mselig/ads/coord_database.html

SAN DIEGO STATE UNIVERSITY
AEROSPACE ENGINEERING

DESIGN BUILD FLY 2012-13

Table of Contents

- AR_{horiz} – Aspect Ratio- Horizontal
- AR_v – Aspect Ratio – Vertical
- AR_w –Aspect Ratio – Wing
- b_{horiz} – Horizontal Tail Span
- b_{vert} – Vertical Span
- b_w – Wing Span
- C_D – Coefficient of Drag
- C_{Do} – Coefficient of Parasitic Drag
- C.G. – Center of Gravity
- C_L – Coefficient of Lift
- C_{lmax} – Maximum Coefficient of Lift of Airfoil
- $C_{L_\alpha} = \frac{dC_L}{d\alpha}$ – Coefficient of Lift vs. Angle of Attack Slope
- C_{root} – Chord Length at Root
- C_{tip} – Chord Length at Tip
- D – Drag (lbs)
- EPS – Expanded Poly-Styrene
- F_{bats} – Bat Scoring Factor
- g – Gravity Constant
- H – Fuselage Height (in)
- K' – Induced Drag Factor
- K'' – Drag Due to Lift Factor
- L – Fuselage Length (in)
- L – Lift (lbs)
- L_h – Length of Horizontal Tail (in)
- m.a.c – Mean Aerodynamic Chord
- mAh – Milli-Amp Hours
- $N_{bats, ref}$ – Reference Number of Bats
- $N_{bats,team}$ – Team Number of Bats
- P – pressure (lb/ft²)
- PVA – Poly-Vinyl Alcohol
- ROC_{max} – Maximum Rate of Climb
- S – Planform Area of the Wing (in²)
- $S_{aileron}$ –Surface Area of Aileron (in²)
- $S_{elevator}$ –Surface Area of Elevator (in²)
- S_{horiz} – Surface Area of Horizontal Tail (in²)
- S_{rudder} – Surface Area of Rudder (in²)
- S_{vert} – Surface Area of the Vertical Tail (in²)
- TOFL – Take Off Field Length
- TOW – Take Off Weight
- T_{ref} —Reference Mission Time
- T_{team} —Team Mission Time
- T_x —Total Mission Time
- T/W – Thrust to Weight Ratio
- V – Velocity (ft/s)
- V_h – Horizontal Tail Volume (ft³)
- V_{max} – Maximum Flight Velocity (ft/s)
- V_{stall} – Stall Velocity (ft/s)
- V_{to} – Velocity at Take Off (ft/s)
- V_v – Vertical Tail Volume (ft³)
- W – Weight (lbs)
- W_{ref} – Reference System Weight
- W_{team} – Team System Weight
- W_v – Weight Score Factor
- W/S – Wing Loading (lb/ft²)
- ρ_{air} – Density of Air
- X_{cg} – C.G Location in X Dir.
- Y_{cg} – C.G Location in Y Dir.
- Z_{cg} – C.G Location in Z Dir.

1.0   EXECUTIVE SUMMARY

The American Institute of Aeronautics and Astronautics (AIAA) through the applied Aerodynamics, Aircraft Design, Design Engineering and Flight Test Technical Committees and the AIAA Foundation invited students from universities around the world to the Cessna/Raytheon Missile Systems Student Design Build Fly (DBF) competition. As an extra-curricular challenge, students from San Diego State University entered the competition with an aircraft that met all general and mission requirements. The design of the aircraft was analyzed and altered until optimal performance was reached to ensure it would be competitive. During the conceptual design phase, scoring analysis showed that in order to obtain the highest possible score the weight and wingspan must be minimized, flight times must be reduced, and the optimal payload of four rockets for mission two must be used. Therefore, the aircraft was designed to achieve optimal performance utilizing a bi-wing configuration, strong propulsion system, internal payload bay capable of carrying four Estes rockets, and external wing mounted pylons capable of handling all load cases as required by mission three.

The aircraft employs the use of two different airfoils (E210 and SD7032) to provide an ample amount of lift in order to get off the ground in the 30" x 30" runway. Designed with an aspect ratio of 0.96 per wing, a high overall C_L, and a low drag coefficient, the aircraft achieves optimal aerodynamic efficiency. The conventional empennage, low drag pylons, and streamlined fuselage create a fast and dynamically stable aircraft.

Material used consisted of both high density foam and carbon fiber ensuring a very lightweight, strong, and reliable aircraft. The team took advantage of the numerous manufacturing capabilities located on campus in constructing the aircraft. Airfoils were cut using a CNC hot wire foam cutter and then strengthened using a carbon fiber layup. The fuselage was constructed using a bladder molding process to ensure a rigid structure capable of handling required loadings.

Comprehensive finite element and fluid analysis in addition to extensive flight testing proved that the aircraft not only met all mission specifications but also excelled in performance capabilities. The pilot became highly familiar with the handling of the aircraft during rigorous the flight test schedule which was used to analyze and verify the design changes and performance predictions.   Unloaded, the aircraft weighs 3.50lbs and has a wingspan of 38.75 inches. Countless hours of work from disciplined and dedicated team members culminated to create a highly competitive, efficient, and lightweight aircraft destined to take the top prize in this year's competition.

2.0   MANAGEMENT SUMMARY

2.1   TEAM ORGANIZATION

In an effort to optimize the workforce, the team was broken down into three sections, Report, Design, and Manufacturing. Each team lead was in charge of their respective assignment and effectively distributing the workload to the assistants. The project manager, assistant project manager, and team leads formed the leadership of the group and thus were responsible for scheduling meetings, build dates, and ensuring clear communication for the team. Incorporating underclassmen is a pivotal element in the continuation of the SDSU DBF program. Whenever possible, underclassmen were tasked with activities that would both educate as well as assist in the design, analysis, and manufacturing of the competition aircraft.
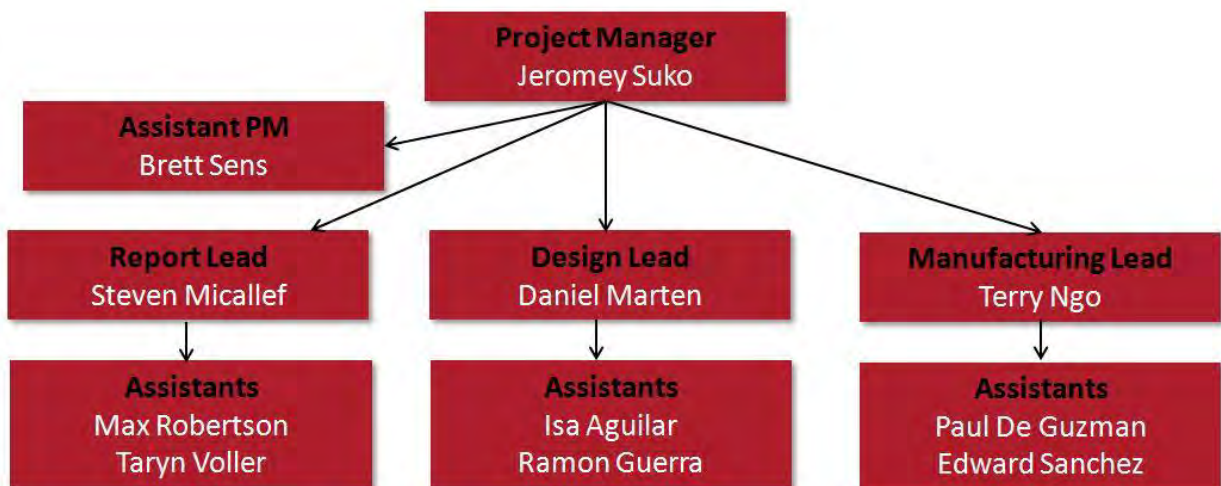
Figure 1 – Team Organization Chart

2.2   WORKING PLAN
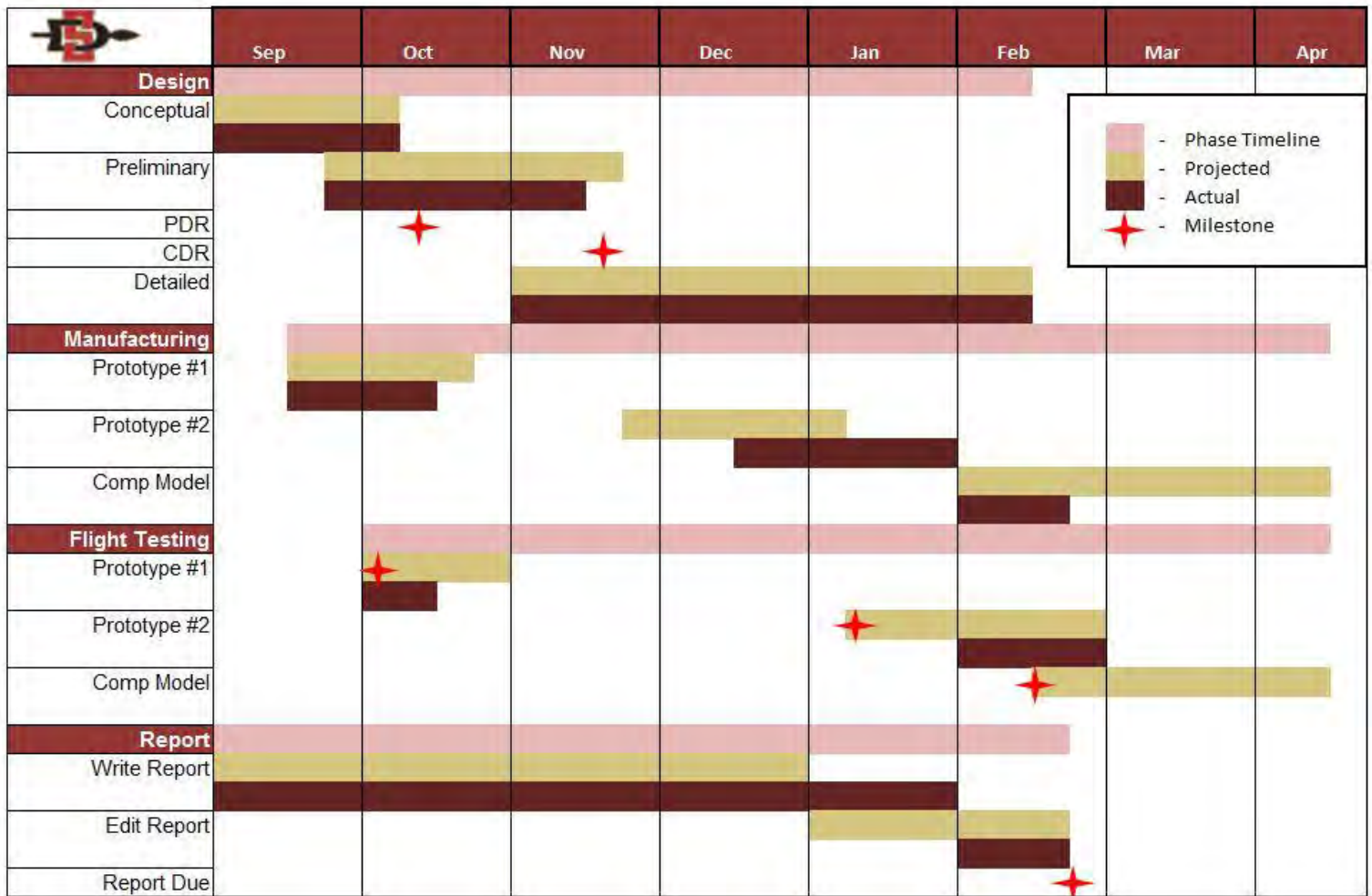
Figure 2 – Design Schedule

3.0 CONCEPTUAL DESIGN

The conceptual design phase of the project was driven by the rules and requirements of the competition as well as past SDSU DBF experience. In order to produce the highest scoring aircraft, a comprehensive set of design requirements was allocated to the competition rules constraints. A Figure of Merit (FOM) analysis was then carried out so to guide the development of the aircraft using the prior derived design requirements and constraints.

3.1 MISSION REQUIREMENTS

Each mission takes off from a simulated small austere field. The rules for the 2012-2013 AIAA DBF competition specify for all missions:

- o Ground rolling take-off and landing
- o Takeoff from inside a 30x30 ft. square marked on the runway
- o Complete a successful landing after each mission for a score
- o Have a latching lid stores case able to be opened on one side only

The competition is made up of three missions all of which take place on the course shown in the figure below.
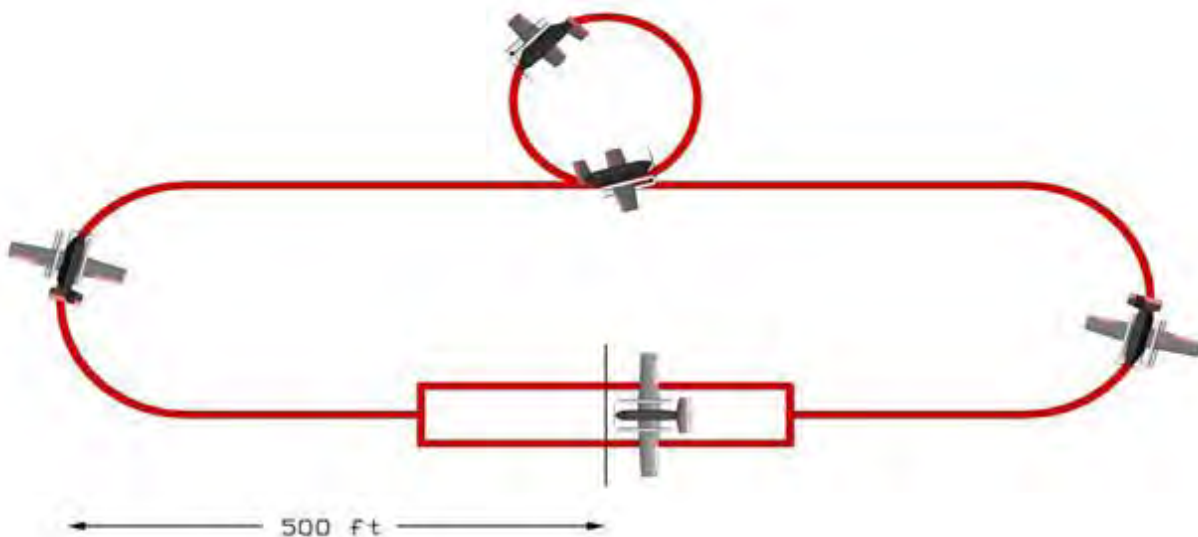
Figure 3 – Course Layout

3.1.1   Mission 1: Short Take-off

Mission 1 requires the aircraft to complete as many full laps as possible in four minutes without any payload. Teams will only be credited for the full laps completed, meaning that a team cannot receive points for completing a partial lap. The score for Mission 1 is given below:

$$M_1 = 2 \cdot \left(\frac{\#Laps}{\#Laps_{max}} \right)$$

Where, #Laps represents the number of laps our team completed and #Laps$_{max}$ represents the most number of laps completed by any team in the competition.

3.1.2   Mission 2: Stealth Mission

Mission 2 requires the aircraft to complete three laps with an internal stores payload consisting of Mini-Max model rockets ballasted to 4oz. The internal stores must be secured to a mounting rack that is a permanent part of the structure. All stores must be aligned in the direction of flight and not come in contact with anything other than the mounting rack on which they are secured. Scoring for this mission is given below:

$$M_2 = 4 \cdot \left(\frac{\#Rockets}{\#Rockets_{max}} \right)$$

Where, #Rockets represents the number of rockets carried by our team and #Rockets$_{max}$ represents the most rockets carried by any team in the competition.

Figure 4 – Mini-Max Rocket

3.1.3   Mission 3: Strike Mission

The third mission requires the aircraft to complete three laps carrying a payload of mixed rockets whose exact configuration is determined by the roll of a die when the team enters the assembly area. Internal stores must follow the requirements in mission two. External stores must be wing pylon mounted and completely external to the wing profile. The payload configuration possibilities are given in the table below:

Payload Configuration		1	2	3	4	5	6
Internal	Mini-Max	4	-	2	-	-	1
Left Wing	Mini Honest John	-	-	-	2	-	-
	High Flyer	-	1	-	-	1	1
	Der Red Max	1	1	1	-	1	1
Right Wing	Mini Honest John	-	-	2	2	2	1
	High Flyer	-	1	-	-	-	1
	Der Red Max	1	1	-	-	-	-

Figure 5 – Mission Three Payload Configurations

The score for mission three is determined using the equation given below:

$$M_3 = 6 \cdot \left(\frac{Time_{fastest}}{Time} \right)$$

Where Time$_{fastest}$ is the time of flight for the fastest team, and Time is the time of flight of our team.

Figure 6 – Mini-Honest John Rocket

Figure 7 – Der Red Max Rocket

Figure 8 – High Flyer Rocket

Rocket	Weight (lb)	Length (in)
Mini-Max	0.25	8.80
Mini Honest John	0.75	11.75
High Flyer	1.00	12.00
Der Red Max	0.50	16.00

Figure 9 – Payload Dimensions

3.1.4 Total Score

The total score is given as:

$$Score = \frac{Report\ Score \times (M_1 + M_2 + M_3)}{RAC}$$

Where,

$$Rac\ (Rated\ Aircraft\ Cost) = \frac{\sqrt{EW \times SF}}{10}$$

EW represents the empty weight of the aircraft measured after each successful scoring flight. If different configurations are used for each mission, the EW is the weight of the heaviest configuration with the payload removed.

SF represents the Size Factor of the aircraft:

$$SF = X_{max} + 2(Y_{Max})$$

Where,

- X_{max} is the longest possible dimension in the direction of flight (aircraft length).

- Y_{max} is the longest possible dimension perpendicular to the direction of flight (wingspan).

Since the entire score is divided through by the RAC, primary focus of design was to create an aircraft with the smallest possible RAC, while still being capable of completing each mission.

3.2 TRANSLATING MISSION REQUIREMENTS INTO DESIGN REQUIREMENTS

The mission requirements of this competition demand an aircraft to be designed for speed, versatility, and the ability to takeoff in a short distance.

o Lightweight: Lighter aircraft translates to lower RAC.

o Shorter wingspan: A shorter wingspan translates to lower RAC.

Weight and Wing Span vs RAC
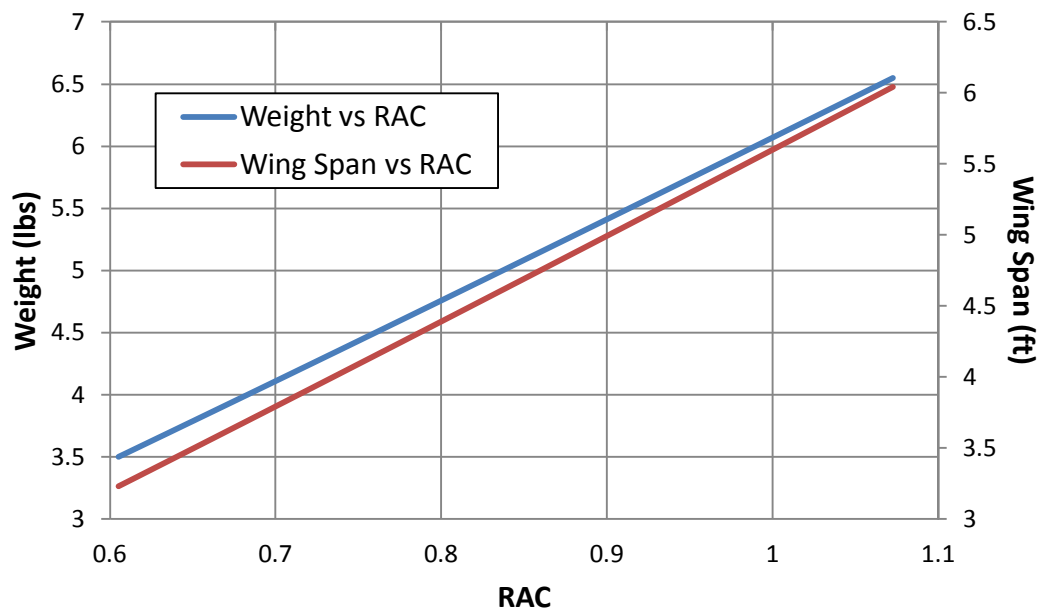
Figure 10 – Effect of Weight and Wingspan on Rated Aircraft Cost

o Speed: to score as high as possible in missions 1 and 3, the aircraft must be able to fly fast both empty, and with a heavy payload. In this case the aircraft must have high aerodynamic efficiency as well as a powerful propulsion system

o Ability to takeoff at short distance: A 30' x 30' runway means the aircraft must accelerate quickly and attain flying speed before the end of the runway is reached.

o Versatility for mission 3: Depending on the outcome of the roll of the die, the aircraft must be designed to handle all possible scenarios stated in the mission requirements.

- o Easy manufacturing so it can be repaired during the competition if need be. In the event of failure of any component of the plane, it must be able to be fixed in no more than 12 hours so as to carry on with the competition

Due to the impact of mission 2 in regards to the overall design of the aircraft (how many internal stores to be carried) it was necessary to determine how the number of internal stores affects the overall score in competition. The estimations, and calculations made were based on the fact that the more stores that are carried, the slower and heavier the aircraft will be. The aircraft will become progressively heavier with an increasing number of stores flown because an increasing number of stores mandate a larger structure to encase the stores. This will lead to an increase in wingspan, and or a large increase in the size of the fuselage, which would significantly impact the teams RAC. In principle, this would also make the aircraft slower due to the fact that it would lead to more drag. Because there is a limit on the watts available for the propulsion system based on max current, and max battery weight, higher drag cannot be overcome by adding more power. The speed of the aircraft will drastically affect the scores of both missions 1 and 3. Based on these estimations, the number of rockets the team decided to carry is four to maximize speed, and minimize weight. In the event that a team carries 14 or more internal stores, and gains advantage in mission 2, it can be demonstrated by the following chart that they can be beaten by attaining a much higher score in missions 1 and 3 while maintaining a lower RAC (Total Score does not include the report score, as it is a scalar value)
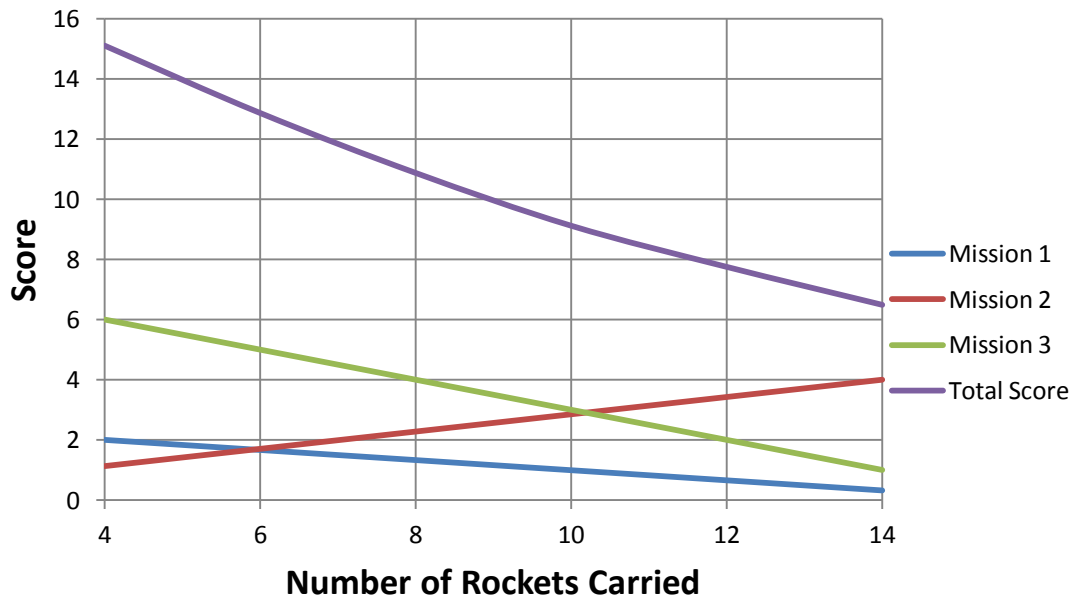
Figure 11 – Effect of Number of Rockets Carried on Overall Score

3.3 CONCEPTUAL DESIGN SELECTION

The conceptual design process considered four generic types of aircraft layout. Each configuration was analyzed and given a score of which the higher scores indicate a desired layout. Scores were awarded based upon how well the aircraft would theoretically perform for a given trait. The score was then multiplied by a weight factor due to conflicting importance of design specifications. This weight factor (located next to the FOM containing a decimal value) should not be confused for the "Weight" of the aircraft. For example a score of 5 for "Weight" does not mean the aircraft is heavier, in fact it means the aircraft is lighter as lightweight is a desirable trait. A score of 1 for "Weight" would indicate a heavy aircraft.

- ○ **Takeoff (30%)**: All of the selected configurations can be made to take off in 30 ft but, the consequences of this affect the other areas of performance, thus the normalization by making all an even number.

- ○ **Span (30%)**: The shorter the span the better for our score

- ○ **Multipurpose (15%)**: A design that can use structure in multiple ways, therefore saving weight, will score higher.

- ○ **In flight (15%)**: Certain configurations are naturally prone to perform worse in high wind situations thus reducing flight stability and receiving a lower score.

- ○ **Manufacturing (10%)**: A relatively simple fabrication process is desired because if the design is complex it can result in manufacturing errors that may cause failure of the aircraft and/or subsystems. A complicated fabrication process is also difficult to repeat should the aircraft require repairs during the competition.

Figure of Merit	Weight	Conventional	Biplane	Flying Wing	Canard
Takeoff	0.30	5	5	5	5
Span	0.30	3	5	4	3
Multi Purpose	0.15	5	4	3	3
In Flight	0.15	5	5	4	4
Manufacturing	0.10	5	4	3	5
Total	1.00	4.40	4.75	4.05	3.95

Figure 12 – Aircraft Configuration Figure of Merit Analysis

3.4 COMPONENT LAYOUT SECTION

The component layout selection process analyzed various elements of an aircraft in order to determine the overall conceptual design. Each element configuration of the aircraft was considered and given a score for certain traits as described in section 3.3.

3.4.1 Propeller Configuration and Location Selection

- **Weight (40%)**: Designs with multiple motors will weigh more due to the accompanying structure required as well as the weight of the propeller configuration itself.

- **Power (30%)**: Maximizing the power output of a propulsion system is critical in order to produce enough static thrust to take off in 30 ft.

- **Efficiency (20%)**: The efficiency of a propulsion system is the relation between power available, and the actual power output .

- **Takeoff (10%)**: The position of the motor with regards to the location of the wing will induce a moment around the CG that will help the aircraft to take-off.

Figure of Merit	Weight	Tractor	Pusher	Twin	Side by Side	Contra-rotate
Weight	0.40	5	5	3	3	4
Power	0.30	3	3	2.5	2.5	3.5
Efficiency	0.20	5	5	2	2	3
Take-off	0.10	5	4	3	3	4
Total	1.00	4.4	4.3	2.65	2.65	3.65

Figure 13 – Propeller Configuration Figure of Merit Analysis

3.4.2 Empennage Design

- o **Weight (40%)**: An increase in weight will result in a lower score.

- o **Manufacturing (25%)**: A relatively simple fabrication process is desired because if the design is complex it will result in errors therefore receiving a lower score.

- o **Stability (20%)**: A tail that provides adequate stability in flight is mandatory.

- o **Drag (15%)**: A design with too much drag will impact the speed and lower the score for mission one.

Figure of Merit	Weight	Conventional	Cruciform	V-Tail
Weight	0.40	5	3	4
Manufacturing	0.25	5	4	3.5
Stability	0.20	4	5	4
Drag	0.15	5	4	4
Total	1.00	4.8	3.8	3.875

Figure 14 – Empennage Configuration Figure of Merit Analysis

3.4.3 Control System Selection

- o **Weight (50%)**: A complex control system may provide better in flight stability however, it will raise the weight resulting in a lower score.

- o **Manufacturing (20%):** Certain control system configurations such as an Upper and Lower REA (Rudder, Elevator, Aileron) have proven difficult to manufacture and implement from prior SDSU DBF experience.

- o **Maneuverability (20%)**: Different control systems offer varying degrees of maneuverability.

- o **Drag (10%)**: A design with too much drag will impact the speed and lower the score for mission one.

Figure of Merit	Weight	Conventional REA Upper	Conventional REA Lower	Conventional REA Upper and Lower	Conventional EA	Conventional RE
Weight	0.50	4	4	2	3	5
Manufacturing	0.20	2	5	2	2	4
Maneuverability	0.20	4	4	5	4	2
Drag	0.10	4	4	3	3	4
Total	1.00	3.6	4.2	2.7	3	4.1

Figure 15 – Control System Figure of Merit Analysis

3.4.4 Landing Gear Design Selection

o **Weight (50%)**: The more structure required to hold the payload means more weight which results in a lower score

o **Strength (35%)**: The design must be able to handle a large impact loading upon landing without breaking to receive a score for the mission

o **Multipurpose (15%):** The possibility of wing mounted payloads factor in to the choice of landing gear because certain configurations could limit space on the wing for a pylon.

Figure of Merit	Weight	Strut	Double	Arc
Weight	0.50	5	3	5
Strength	0.35	3	5	5
Multipurpose	0.15	5	1	4
Total	1.00	4.30	3.40	4.85

Figure 16 – Landing Gear Configuration Figure of Merit Analysis

3.4.5   Payload Location Selection

- o **Aerodynamics (60%)**: Placing the payload in an optimal aerodynamic location will result in a better overall score because of the effects on overall lift and drag.

- o **Multipurpose (20%)**: Since the payload configuration for mission three can vary, the payload location must be arranged in a way that easily accommodates change. The fuselage may also house propulsion components, internal stores, and must not interfere with external loadings.

- o **Weight (20%)**: Multiple payload locations require more structure thus raising the weight and receiving a lower score.

Figure of Merit	Weight	Above	Between	Under	Behind	Multiple
Aerodynamics	0.60	1	3	4	4	3
Multipurpose	0.20	2	4	4	1	2
Weight	0.20	5	5	5	5	3
Total	1.00	2	3.6	4.2	3.6	2.8

Figure 17 – Payload Location Figure of Merit Analysis

3.5   SELECTED CONCEPTUAL DESIGN
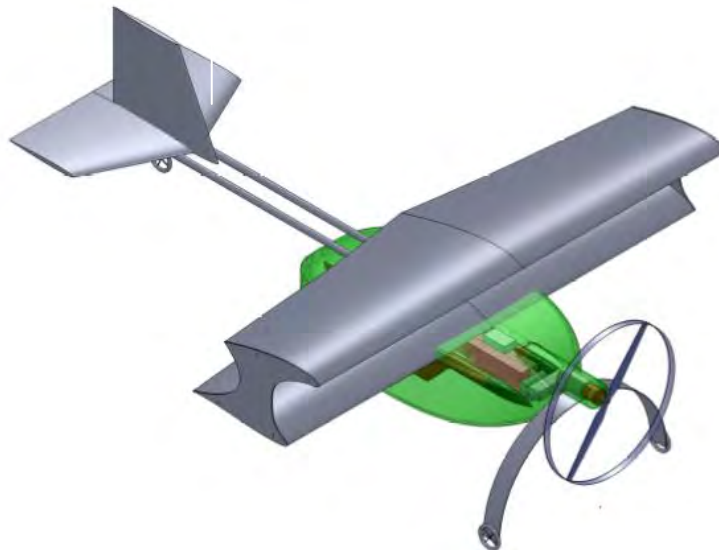
Figure 18 – Conceptual Aircraft

4.0   PRELIMINARY DESIGN

The preliminary design phase aimed to optimize design variables such as aerodynamics, stability and control, propulsion, and flight performance to achieve the highest possible flight score. From the scoring analysis in section 3, it was determined that weight and wingspan were the most crucial elements of the design. Preliminary design was carried out to satisfy weight and size requirements.

4.1   DESIGN AND ANALYSIS METHODOLOGY

The preliminary design phase began with an initial estimate of the size and weight of the aircraft. These parameters then determined necessary aerodynamic values for the lifting and propulsion systems. Aerodynamic calculations were then carried out to end the first iteration of deciding aircraft parameters. From these calculated values, the process was repeated using alterations to the size and geometry in order to further optimize the aircraft's performance. The iterative process was continued until an optimal design was obtained.

4.2   MISSION MODEL

In order to design a fully capable aircraft, preliminary designs had to be revamped to fit into the mission model. Each mission was modeled the same way.

- o **Take-off**: Due to a 30x30 ft. runway a large emphasis on getting off the ground in a short amount of time was made. If the aircraft could not reach a high enough speed or produce enough lift, the design must be altered.

- o **Acceleration**: After the aircraft has stopped changing altitude and is not in a turn, it must accelerate as quickly as possible to its maximum speed. This is especially important for mission one.

- o **Turning**: Each mission has a 180° turn and a 360° turn. The preliminary design must be able to handle a given wing-loading factor and complete the turn as fast as possible without tip-stalling.

4.3   INITIAL SIZING

To obtain the highest score possible, the aircraft should be able to carry four rockets. Fewer rockets allow a lighter fuselage and higher speed. The fuselage of the aircraft was then tailored to accommodate the least amount of rockets. Reducing the wingspan was also important in the initial sizing process. Using a biplane configuration, sizing efforts were made in order to optimize the lift/span ratio.

4.4   AERODYNAMICS

The aerodynamics group is responsible for airfoil selection, sizing, and configuration given the constraints of weight, size, and power. The design of the airfoil began by selecting an airfoil, performing aerodynamic simulations, and then altering both the size and configuration. Using [6]XFOIL and [6]XFLR-5, the group was able to narrow down the list of useable airfoils.

4.4.1   Airfoil Selection

Since the bi-plane has a stagger wing, the team decided to use two different airfoils. One would be set to a 0 AOA and the other at a 5 AOA. Lift, stall, and drag characteristics constituted the overall performance depending on the range of AOA.

- o **C_L (20%)**: A higher C_L means the plane can take-off faster.

- o **0-10 AOA (40%)**: For the lower wing, better performance in the 0-10 AOA range is desired.

- o **5-13 AOA (40%)**: For the upper wing, better performance in the 5-13 AOA range is desired.

Figure of Merit	Weight	E210	S8036	NACA 1209	SD7032
CL	0.20	4	2	3	4
0-10 AOA	0.40	5	3	3	4
5-13 AOA	0.40	2	3	2	5
Total	1.00	3.6	2.8	2.6	4.4

Figure 19 – Airfoil Selection Figure of Merit Analysis

The following plots represent preliminary data obtained using [6]XFLR-5 and [6]XFOIL to verify that the aircraft generate a large C_L at around 8 degree AOA, the expected AOA at take-off.
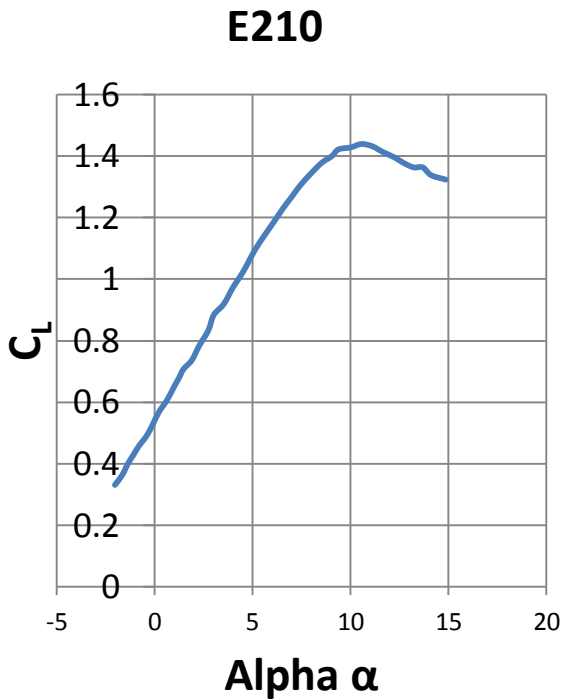
E210

SD7032

Figure 20 – Predicted Lift Curve (E210)
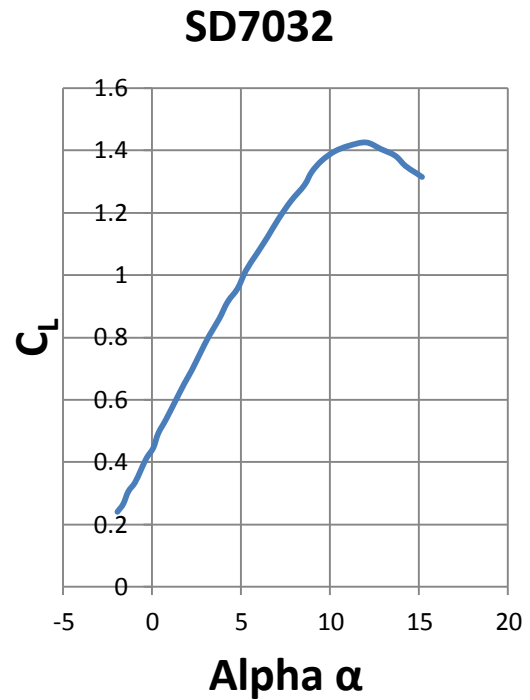
Figure 21 – Predicted Lift Curve (SD7032)
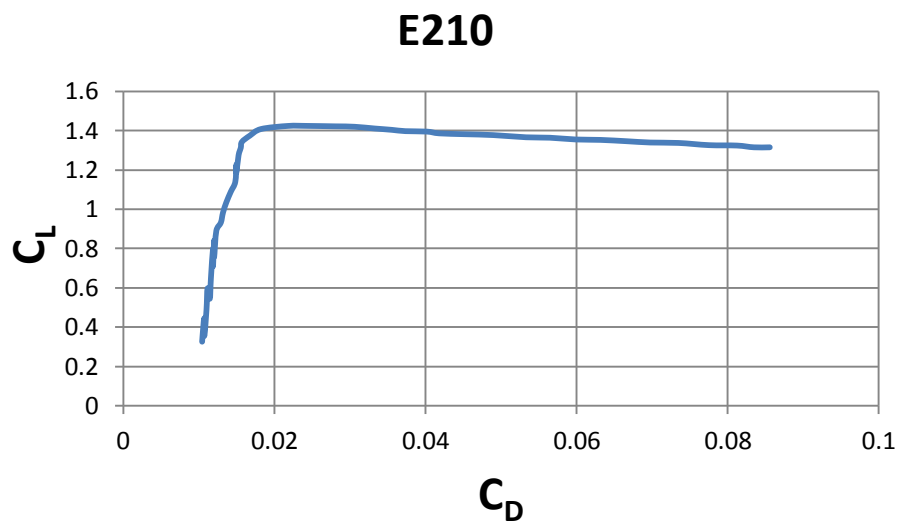
E210

Figure 22 – Predicted Drag Polar (E210)

SD7032
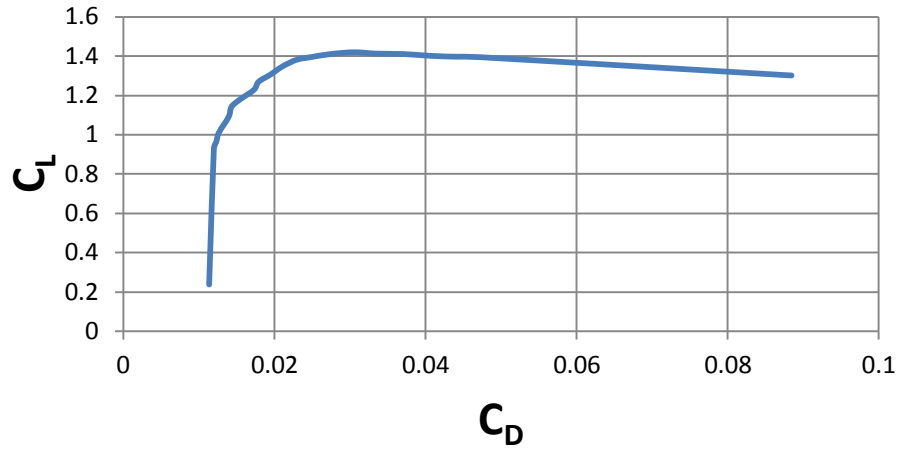
Figure 23 – Predicted Drag Polar (SD7032)

[6]XFLR-5 also allowed us to model the aircraft as a whole including a mock fuselage. The goal was to have a C_L of about 1.6 at an 8 degree AOA. Preliminary analysis using [6]XFLR-5 verified the aircraft is on track, as shown below.
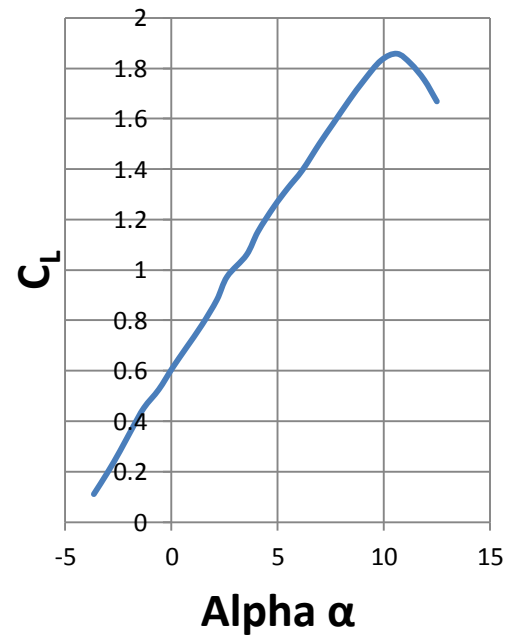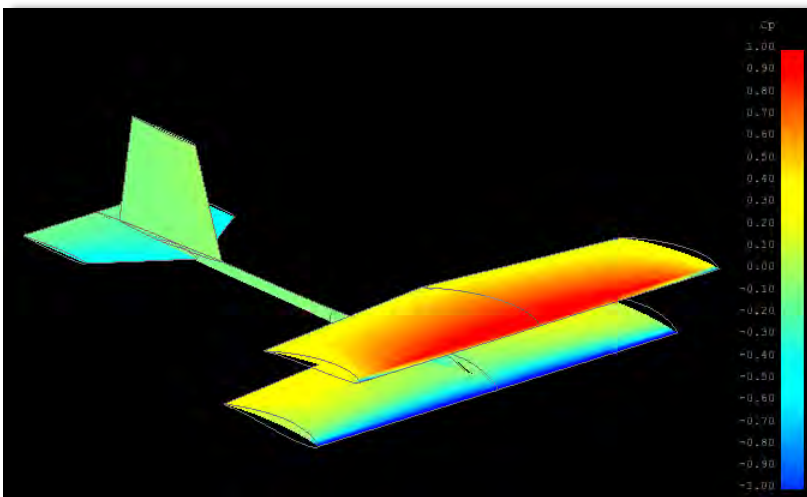
Figure 24 – XFLR-5 Analysis of Entire Aircraft and Corresponding Lift Curve

4.4.2   Aerodynamic Performance Predictions

Using [15]STAR-CCM + by CD Adapco, to perform computational fluid dynamics predictions could be carried out for the total drag build up. Simulation was at 0 angle of attack at 45 mph (estimated cruise speed). As shown below, around 70% of the total drag is due to the lifting and control systems.

Component	Drag (lbf)	% of total
Upper Wing	0.4501	37.11
Lower Wing	0.4094	33.75
Horizontal Stabilizer	0.0047	0.39
Vertical Stabilizer	0.0354	2.92
Fuselage	0.1042	8.59
Landing Gear	0.0891	7.35
Wing Support Brace	0.0293	2.42
Wing Tip Plates	0.0544	4.49
Tail Landing Gear	0.0213	1.76
Tail Spar	0.0057	0.47
Motor	0.0092	0.76
Total	1.2132	100

Drag Buildup

Figure 25 – Drag Build Up

4.5   STABILITY AND CONTROL

The main objective of stability and controls is to ensure that the aircraft is able to maintain controlled flight through all necessary maneuvers. Crucial stability and control characteristics are outlined below.

- o **Center of Gravity:** The center of gravity must be slightly ahead of the neutral point because this will create an aerodynamic moment that returns the aircraft to its initial AOA when wind disturbs it.

- o **Static Margin:** A large static margin will be overly stable but less responsive to pilot inputs while a small static margin is less stable but more responsive to pilot inputs. With the average static margin of stability being between 5%-15%, it was determined that the team would design the aircraft with a 10% static margin of stability in order to strike a balance between maneuverability and stability.

- o **Aircraft Analysis:** The weights of each component treated as a point loads distributed through various locations in the aircraft dictate the static margin of 10%. With a wing loading of 10.57 oz per ft^2 the total stability and responsiveness of our airplane was found to be 0.78 rad^{-1}. This small number determines how fast the plane responds to a control surface change or a wind perturbation.

4.5.1   Ailerons

Initially, both the upper and lower wing had ailerons but, there were negative aspects associated with having four ailerons that were determined to be unsuitable for the design. The primary concern was that there was a large increase in drag for a less than desirable increase maneuverability. After flight testing it was confirmed that a larger, single set of larger ailerons on the bottom wing was more efficient in terms of weight, maneuverability, and drag than two sets of ailerons. This allowed for a simplified control system as well as a reduction in weight. According to [10]*Aircraft Design* by Daniel p. Raymer, ailerons should be sized for 20% of the chord and 40% of the span of the wing. The selected sizing of the single aileron set was 23% of the chord and 61% of the span. Differences may lie in the fact that small radio controlled aircraft tend to not always match predictions of full scaled aircraft.

4.5.2   Horizontal Stabilizer

Typically small and lightweight aircraft use a symmetric airfoil for the horizontal stabilizer to provide stability and pitching moment for various AOA. A semi-symmetric airfoil could increase the total C_L, however that would require a larger airfoil thus increasing weight and moving the CG back of the entire aircraft backward. The chosen airfoil for the horizontal stabilizer is the NACA 0008, a thin, symmetric airfoil.

- o **Elevator:** Using the suggested values from [10]Raymer, the elevator should be approximately 40% of the horizontal stabilizer.

4.5.3   Vertical Stabilizer

The vertical stabilizer was chosen to be 50% of the size of the horizontal stabilizer based on values from [10]Raymer. The airfoil is the same as the horizontal stabilizer.

- o **Rudder:** Using the suggested values from [10]Raymer, the rudder should be approximately 40% of the vertical stabilizer.

4.6   PROPULSION

Given the mission objectives, the following propulsion requirements were determined:

- o **High Speed**: Mission one is dependent upon how fast the aircraft can fly. From a propulsion perspective this involves maximizing thrust. In order to do so, special attention must be given to storing the maximum amount of energy in the batteries and then efficiently converting it into usable power.

- o **High Static Thrust**: Due to the 30' x 30' runway, it is crucial to develop a high value of static thrust to accelerate quickly to achieve take-off velocity without blowing the safety fuse.

4.6.1   Propulsion Sizing

While having a lot of power is beneficial it requires more weight and its effect on the RAC would out-weigh any of these benefits. To optimize the propulsion system it was determined that various components would have the following weights:

Item	Name	Weight (lb)
Motor	Neu 1110-2.5Y	0.393
Batteries	Elite 1500A	1.5
Propeller	APC 13" x 10" (M2 and M3) APC 14" x 8.5" (M3 backup) APC 12" x 12" (M1)	0.05
Speed Controller	Castle Creations Pheonix ICE 2 HV40	0.0625

Figure 26 – Propulsion Component Weights

4.6.2 Propeller Analysis

The conceptual design phase established that the aircraft would have a single tractor propulsion system. Depending on the mission, different flight speeds are expected. Using different propellers for different missions will optimize overall performance. Missions 2 and 3 require payload thus require higher thrust at low airspeed. Mission 1 requires a propeller with higher pitch to provide enough thrust at high airspeeds.   It was important to use a propeller that would provide enough thrust without exceeding the current limit constrained by a 20A fuse.

The following charts were created using [12]Motocalc at simulated full throttle over increasing airspeed:
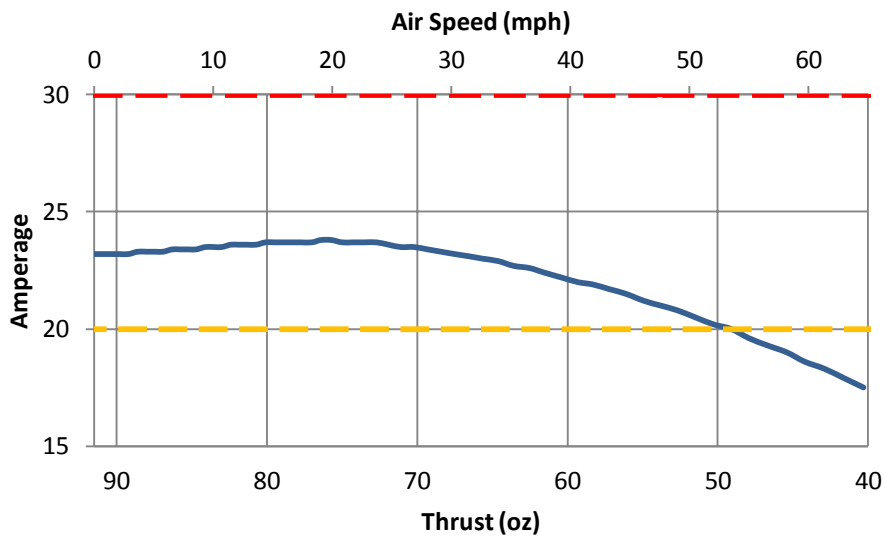
Figure 27 – 13' x 10' Propeller Thrust Analysis
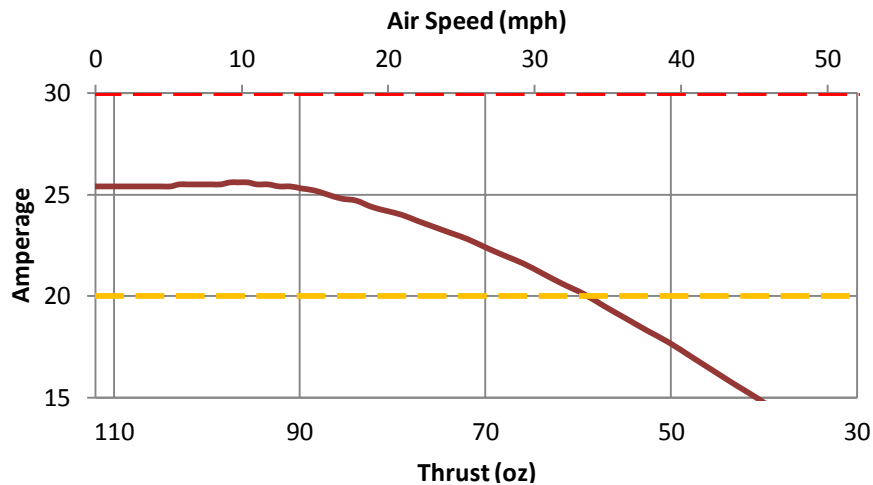
Figure 28 – 14' x 8.5' Propeller Thrust Analysis
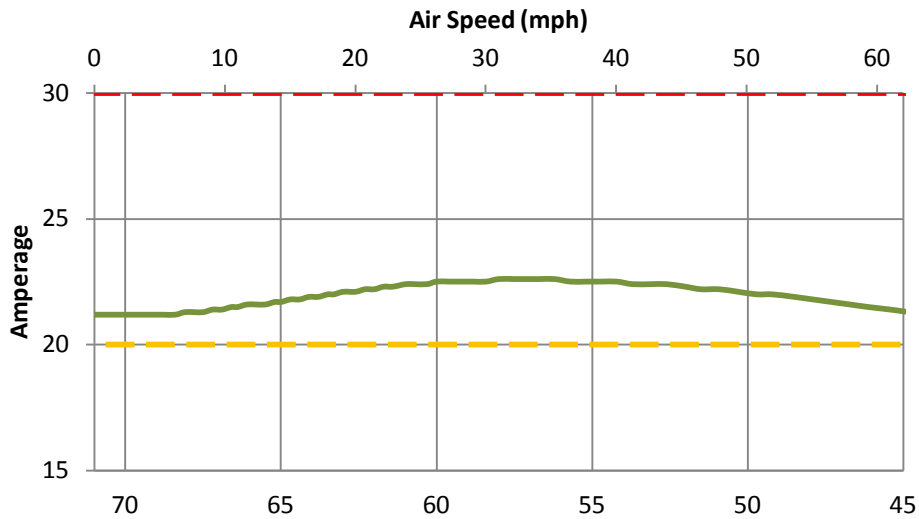
Figure 29 – 12' x 12' Propeller Thrust Analysis

4.6.3 Battery Analysis

An analysis of the type of batteries to be used was a critical step within the overall design. Ultimately, the deciding factors in selecting the type of cell to use were 4 minute power, and 4 minute average current. Average current was found by getting the cell capacity in terms of Amps per 60 minutes, then dividing through by 4 minutes:

$$4 \min Amps = \frac{Cell\ Capacity\ (A \cdot h) \times 60\ min}{4\ min}$$

The 4 minute power was simply calculated by multiplying 4 Minute current by Volts under load:

$$4 \min Watt = Pack\ Volts\ Under\ Load \times 4\ Min\ Amps$$

Based on the 4 minute performance, and the energy density of the various cells, the Elite1500A was selected as the type of battery due to the fact that as calculated, it would yield the best performance.

Battery Type	Capacity (mAh)	Cell Weight (oz)	# of Cells	Pack Volts Under Load	Energy Density (W-hrs/oz)	4 Minute Watts	4 Minute Average Amps
Elite 1500A	1500	0.81	28	26.10	1.67	587.25	22.50
Elite 1700AA	1700	1.00	23	20.70	1.53	527.85	25.50
Elite 2000AA	2000	0.68	33	18.00	1.55	540	30.00
Elite 2200	2200	1.46	15	13.5	1.29	445.5	33.00

Figure 30 – Battery Pack Configurations

San Diego State University   27

4.6.4 Motor Analysis

The initial motor selection process focused on choosing a motor that was lightweight yet efficient, at the desired continuous watts. Other factors for motor selection when paired with a given propeller, included thrust, and current draw. The 1110 series motors were chosen even though the continuous Watts were less than what was calculated for the chosen battery pack. This decision was made based on the fact that these motors yielded the best efficiency (85%-87%) using [12]Motocalc, and through the selected choice of propellers, they drew the correct amperage.

Motor	Continuous Watts	Kv (rpm/volt)	Weight (oz)
Neu 1105-6D	200	3050	2.30
Neu 1110-2.5Y	500	1814	4.00
Neu 1110-2Y	500	2250	4.00
Neu 1112-2Y	600	1750	4.70

Figure 31 – Motor Concepts

4.7 STRUCTURES

Structural analysis was performed on various elements of the aircraft to make sure it was able to withstand all applied loads. Sizing of the structures was done so as to provide the most amount of strength while keeping the overall weight at a minimum.

4.7.1 Fuselage Design

The main purpose of the fuselage for this aircraft is to carry the four rockets (using a 2x2 configuration) for mission two and one of two configurations for mission three. Due to the fact the motor was mounted on the exterior, the size of the fuselage could be reduced to be as small as possible.

4.7.2 Landing Gear Design

Typically, landing gear contributes a large portion of the overall weight to the aircraft. The landing gear consists of a carbon fiber double arc mounted to the wing. This design was intended to use the least amount of material and still have enough support to survive a hard landing. A simple tail dragger design was employed to support the aft end of the aircraft.

4.7.3 Weight Buildup

Component	Weight (oz)
Wing	10.00
Fuselage	7.00
Motor	5.00
Tail	3.00
Landing Gear	3.00
Propulsion/Electronics	4.00
Total	32.00

Figure 32 – Weight Build Up

4.8 AIRCRAFT MISSION PERFORMANCE

Parameter	Mission 1	Mission 2	Mission 3
C_L Cruise	0.19	0.22	0.26
C_L Takeoff	0.63	0.76	0.93
L/D Cruise	6.27	6.27	6.27
Cruise Speed (mph)	67.00	64.00	60.00
Takeoff Speed (mph)	19.70	21.52	25.00
Total Flight Time (s)	240.00	90.00	90.00
Empty Weight (oz)	56.58	56.58	56.58
Loaded Weight (oz)	56.58	72.58	112.58

Figure 33 – Aircraft Mission Performance

5.0 DETAIL DESIGN

The purpose of the detail design phase was to convert the proposed design into a physical structure. Once a physical structure was manufactured, changes could be made to bridge the gaps between the theoretical model and actual design. As always, reducing weight was the highest priority.

5.1 DIMENSIONAL PARAMETERS

Upper Wing	
Airfoil	SD7032
Root Chord (in)	11.00
Tip Chord (in)	9.00
Aspect Ratio	0.96
Area (in^2)	387.50
Span (in)	38.75

Lower Wing	
Airfoil	E210
Root Chord (in)	11.00
Tip Chord (in)	9.00
Aspect Ratio	0.96
Area (in^2)	387.50
Span (in)	38.750

Fuselage	
Length (in)	25.41
Width$_{max}$ (in)	7.74
Height$_{max}$ (in)	6.30
Overall Volume (in^3)	48.75

Aileron	
Span	12.00
% of avg. Chord	20.00

Elevator	
Span	18.00
% of avg. Chord	27.00

Rudder	
Span	9.00
% of avg. Chord	27.00

Horizontal Stabilizer	
Airfoil	NACA 0008
Root Chord (in)	8.00
Tip Chord (in)	7.00
Area (in^2)	135.00
Span (in)	18.00
Incidence (°)	0

Vertical Stabilizer	
Airfoil	NACA 0008
Root Chord (in)	8.00
Tip Chord (in)	7.00
Area (in^2)	67.50
Span (in)	9.00

Figure 34 – Dimensional Parameters

5.2 STRUCTURAL CHARACTERISTICS

In addition to being lightweight, the aircraft must also be able to sustain in-flight loads. With that in mind, the detail design process focused on removing extra material where possible. Where possible, a FEM analysis was conducted using [16]Abaqus. This not only allowed the team to understand the structural capabilities of the aircraft, but also allowed various load cases to be considered.

5.3 SYSTEM DESIGN, COMPONENT SELECTION AND INTEGRATION

5.3.1 Bi-Wing System

The purpose of choosing the bi-wing design was to produce adequate lift with a shorter wingspan. However, the structure to support the wings reduces aerodynamic efficiency so it was important to create a system that provided ample support without sacrificing too much lift.

Wing Tip Plates
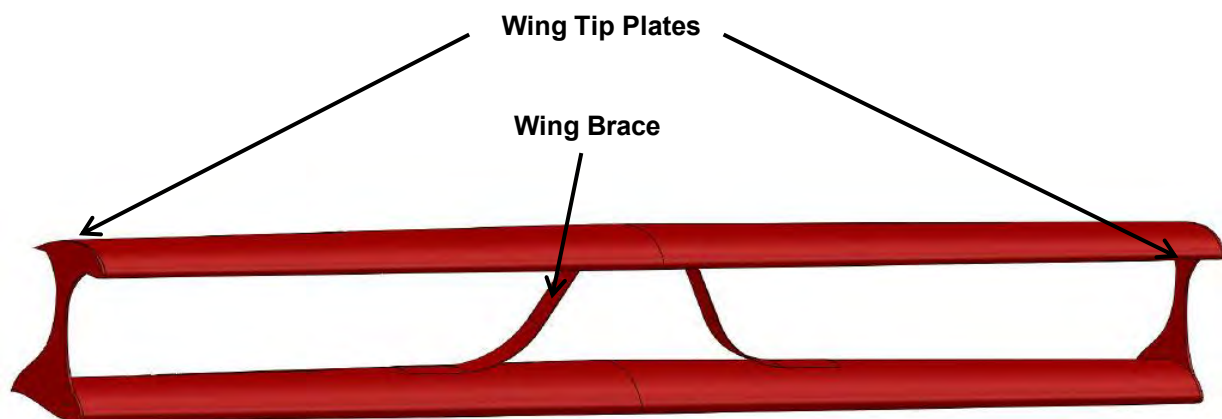
Wing Brace

Figure 35 – Bi-Wing System with Wing Tip Plates and Brace

In order to determine sustainable loads, a FEM analysis was performed. Only half of the wing was modeled due to symmetry. In particular, the team was evaluating brace structure ultimate loading. The load case consisted of two pressure loadings applied at the surface of the wing.
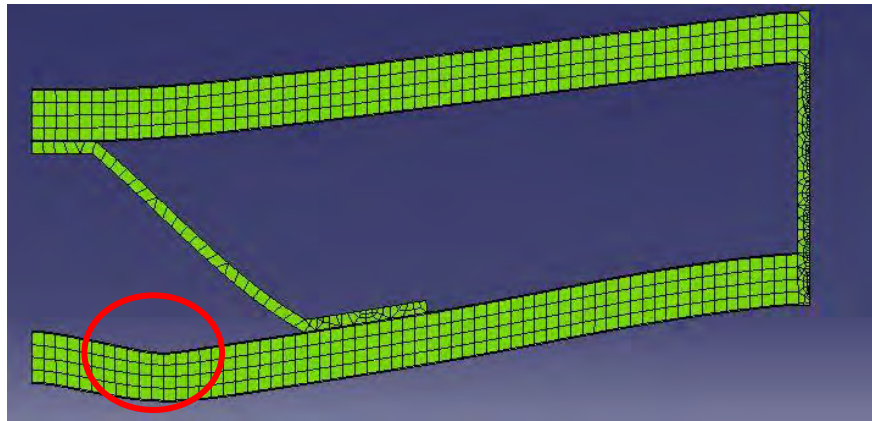
Figure 36 – FEM Model of Main Airfoils and Brace

It was determined that the bi-wing setup would be able to safely handle a wing loading of up to 25.6-lbs while in flight. Figure 36 shows the wing brace and wing tip plates could successfully handle the loads but local buckling occurs in the bottom wing on the inside of the support brace.

5.3.2   Payload Systems

Mission 2 requires internal payload stores while mission 3 requires wing-mounted payloads, therefore two different systems must be implemented.

For mission 2, the rules stipulate that:

Storage Requirements	Restraint Requirements
Stores must be completely internal as a part of the main fuselage or main wing	Stores must be secured to a mounting rack that is part of the permanent structure
Stores must be positioned in the direction of flight	The stores can only contact the mounting racks they cannot touch the fuselage
They must be capable of being released one at a time	Access to the stores must be through bay doors although the doors don't need to be mechanized

Figure 37 – Payload Storage and Restraint Requirements

To minimize weight, the pod will be as small as possible while following spacing requirements in the rules. Given the size of the rockets and the decision to carry four of them, the pod should have a volume of at least 405 in^3, the approximate volume of the selected design is 740 in^3.
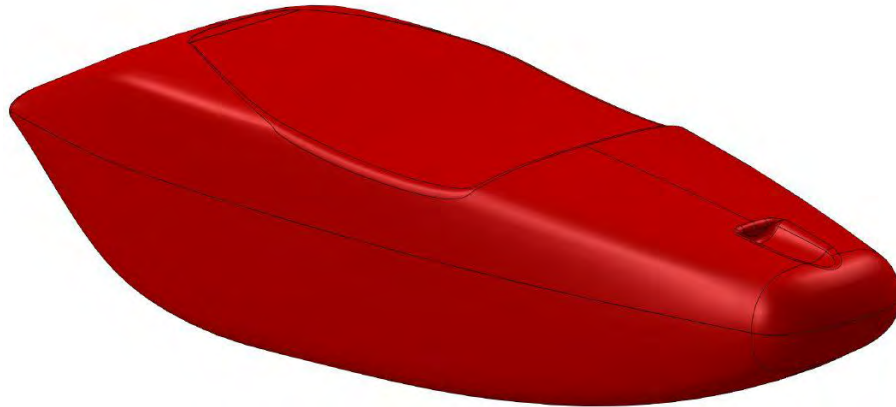
Figure 38 – Selected Fuselage Design

The shape was chosen so as to maximize aerodynamic efficiency. The structure is made up from balsa wood and carbon fiber.

As described earlier, the loading for mission three can vary. Nonetheless, a system to mount the stores to the wing must be implemented. The team decided to use a thin airfoil, NACA 0012, to serve as the pylon. Holes were drilled into the bottom wing at predetermined locations to accommodate various load conditions. Pins could then be inserted through the wing and into the pylon to hold it in place. Additional holes were drilled through the pylon and the actual stores were fastened using adjustable zip-ties as shown below.

Pins Securing Pylon to the Wing

Bottom Wing (E210)

NACA 0012 Airfoil used as Pylon
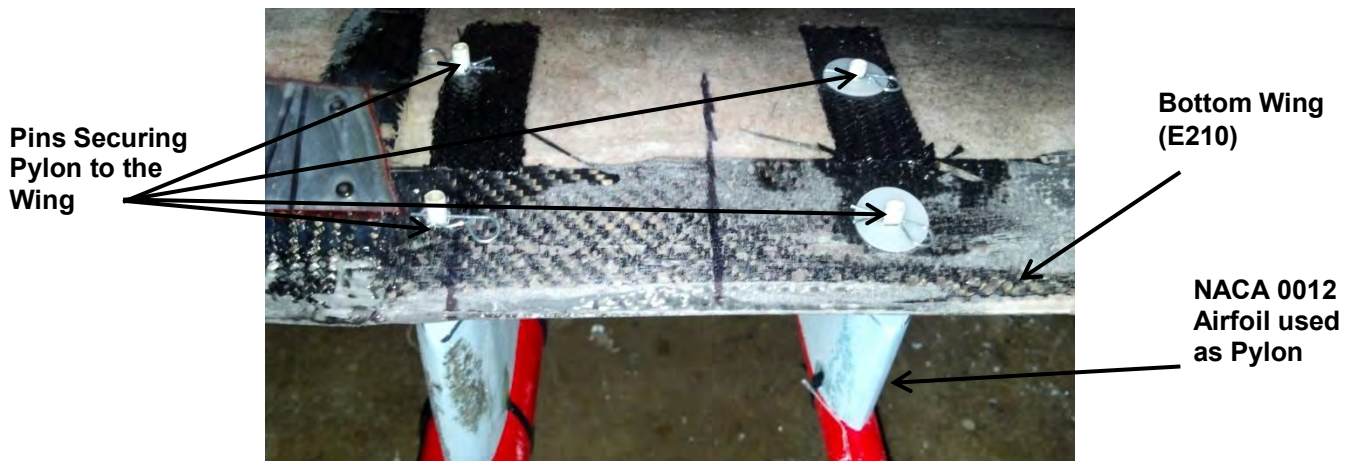
Figure 39 –Mission 3 Payload System and Pylon Attachment (Top View)

Figure 40 –Mission 3 Payload System and Pylon Attachment (Front View)

Rocket and Adjustable Zip-Tie Secured to Pylon

5.3.3   Landing Gear System

Typically landing gear accounts for a large portion of the overall weight of the aircraft. To reduce as much weight as possible and still be able to land safely, the team decided upon an arc design made of carbon fiber as shown below. Structurally sound landing gear is important because should it fail upon landing, the entire mission score will be lost. The arc design was intended to absorb impact loading and flex but not bend thus absorbing the forces instead of transmitting them throughout the structure.

Figure 41 –Selected Landing Gear Design

FEM analysis was carried out to determine what loads could be safely carried. In the figure below, the high stress in the horizontal direction is seen in the joining arch to the second arch. This location

of high stress is where the failure was predicted and expected. According to the FEM analysis, the landing gear made of carbon fiber will be able to withstand a 23.6-pound loading. Adding layers of carbon fiber during manufacturing can strengthen the structure further.
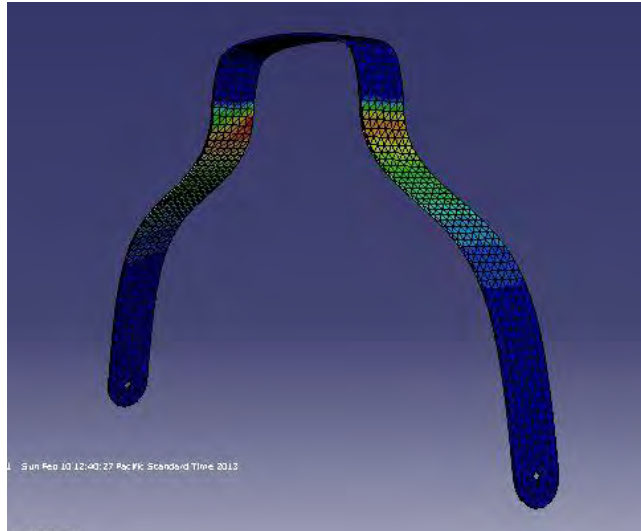
Figure 42 – FEM Model of Landing Gear Displaying High Stressed Areas

5.3.4 Power and Control Systems Integration

Although the preliminary design phase selected the Neu 1110-2.5Y motor, power system testing showed it did not draw enough amperage or produce enough acceleration. To compensate, the motor was replaced with the Neu 1110-2Y.

The selected power and control subsystem components are shown below.

Component	Description	Reason
HS-65MG Mighty Feather	Servos	Lightweight, sufficient torque and speed
Optima 9	Receiver	Long range, lightweight, 8 channel
Kan 700	Receiver Battery	Light, adequate power for one mission
Pheonix Ice2 HV 40	Speed Controller	Has a factor of safety of 2 for current and rated at 42 volts.

Figure 43 –Power Systems Integration and Capabilities

5.4 AIRCRAFT COMPONENT WEIGHT AND BALANCE

The target weight of the fully loaded aircraft was seven pounds.

Component	Weight (oz)	% of Total	X – Position (in)	Z – Position (in)
Top Wing	3	5.3	-12.97	6.00
Bottom Wing	3	5.3	-15.92	0.00
Motor	6.7	12.0	-3.12	0.00
Fuselage	5	9.0	0.00	-2.00
Landing Gear	2.5	4.4	-5.73	-5.00
Battery	24	42.4	-10.12	-.5.00
Spar	1.4	2.4	-28.65	0.00
Servos	1.68	3.0	-13.00	0.00
Speed Controller	1.44	2.5	-3.37	-.5.00
Receiver	0.8	1.4	-19.39	-.5.00
Receiver Battery	1.05	1.8	-16.67	-.5.00
Wing Tip Plates	1.4	2.4	-12.94	3.00
Wing Support Brace	1	1.7	-11.80	3.00
Tail	2	3.5	0.00	4.40
Propeller	1.6	2.9	-1.20	0.00
Total	56.58	100	-9.99	-9.60

Figure 44 –Weight Build Up and CG Location

5.5 FLIGHT PERFORMANCE SUMMARY

The table below shows applicable performance parameters for each mission. The missions were separated into phases; Take-off, climb, cruise, 180° Turn, 360° Turn, and Landing.

Parameter	Mission 1	Mission 2	Mission 3
C_L Cruise	0.198	0.221	0.257
C_L Takeoff	0.645	0.755	0.932
L/D Cruise	6.27	6.27	6.27
Cruise Speed (mph)	67.00	64.00	60.00
Takeoff Speed (mph)	19.70	21.52	25.00
Total Flight Time (s)	240.00	90.00	90.00
Empty Weight (oz)	56.58	56.58	56.58
Loaded Weight (oz)	56.58	72.58	112.58

Figure 45 –Flight Performance Parameters

5.6 MISSION PERFORMANCE SUMMARY

The course has been separated into different sections as shown below. Each section has its own optimal flight characteristics. For laps that do not involve take-off or landing, that portion of the track is considered to be cruise mode.

Cruise
Take-off
Climb
Landing Descent
360° Turn
180° Turn
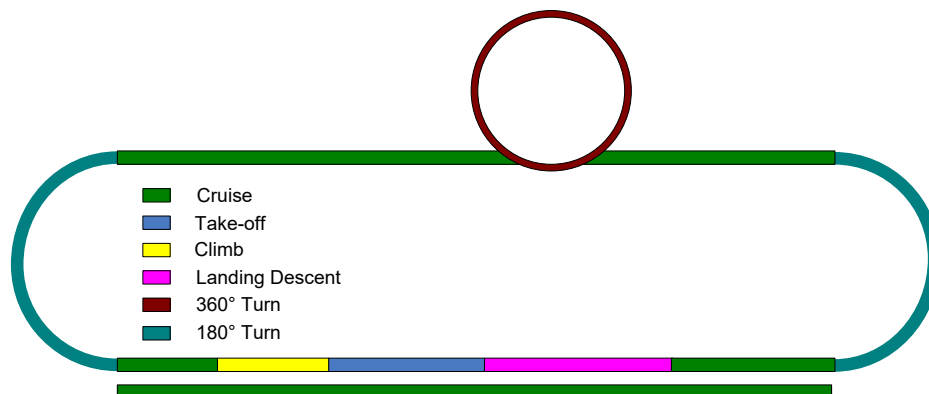
Figure 46 –Course Layout Broken Down Into Phases

Below is the performance summary for one lap of each mission:

Mission 1:

Phase	Distance (ft)	Time (s)	Current (A)	Capacity (mAh)
Take-off	21.00	1.20	23.00	7.30
Cruise	2000	23.70	21.5	141.50
180° Turn	157.00	1.59	19.20	8.48
360° Turn	314.00	4.16	18.70	21.61

Figure 47 –Mission 1 Performance Predictions

Mission 2:

Phase	Distance (ft)	Time (s)	Current (A)	Capacity (mAh)
Take-off	26.50	1.40	24.10	9.25
Cruise	2000.00	24.86	20.68	142.58
180° Turn	157.00	2.22	18.40	11.20
360° Turn	314.00	4.69	17.80	23.08

Figure 48 –Mission 2 Performance Predictions

Mission 3:

Phase	Distance (ft)	Time (s)	Current (A)	Capacity (mAh)
Take-off	32.00	1.60	25.20	11.20
Cruise	2000	26.03	19.87	143.67
180° Turn	157.00	2.85	17.60	13.93
360° Turn	314.00	5.23	16.90	24.55

Figure 49 –Mission 3 Performance Predictions

5.7   DRAWING PACKAGE

The following drawing package includes three main views of the aircraft, structural arrangement, component layout, and payload arrangement for the various missions. Drawings and parts were made using Solid Works.

2.00
7.00

C

A

B

11.00
9.00

9.00
11.00

D

C

38.96

6.00

12.58

E

47.477

7.00
2.00

11.83

5.64
38.53
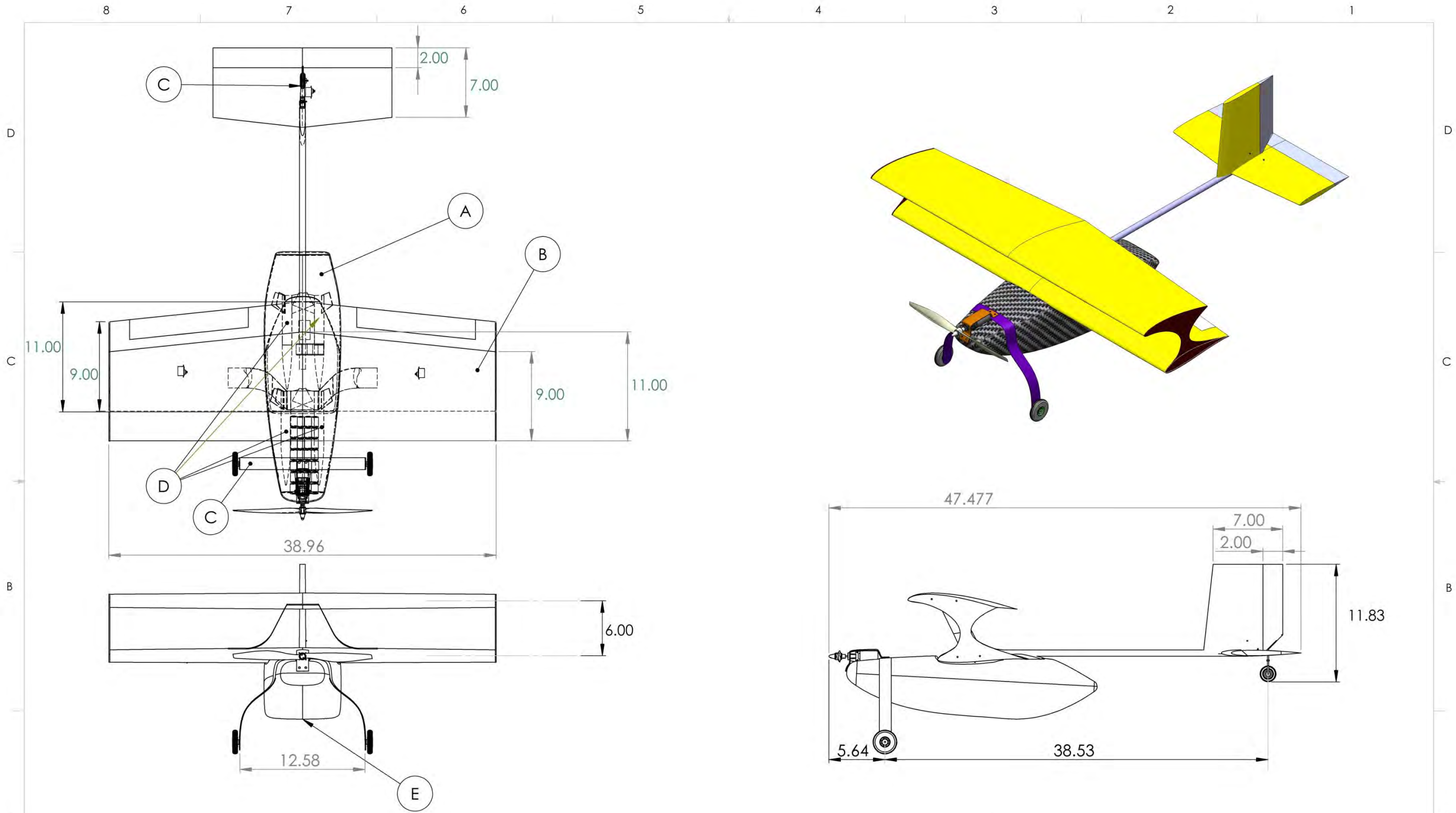
ITEM NO.	PART NUMBER	QTY.
A	Fuselage	1
B	Wings	1
C	Landing Gear	2
D	Internal Payload	1
E	Cargo Door	1

NOTE:
DIMENSIONS
ARE IN INCHES

SAN DIEGO STATE UNIVERSITY
AIAA DESIGN/BUILD/FLY 2013

DRAWN BY
DANIEL TAUGHINBAUGH

APPROVAL DATE:
2/23/13

CHIEF ENGINEER
JEROMEY SUKO

SIZE
B

DOCUMENT TITLE
AIRCRAFT 3_VIEW

REV
A

SCALE: 1:9

SHEET 1 OF 6
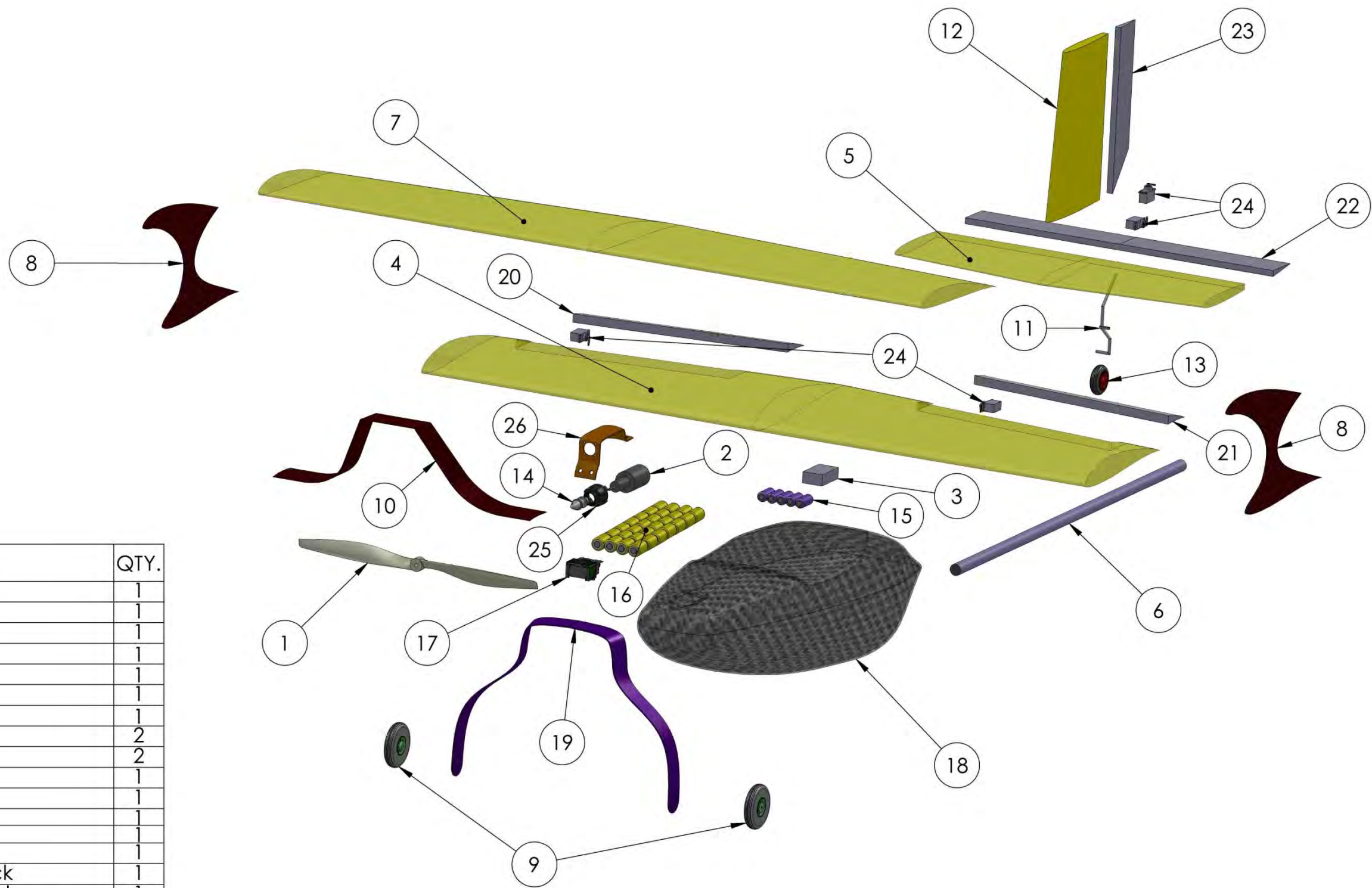
ITEM NO.	PART NUMBER	QTY.
1	Propeller	1
2	Neu 1110-2y Motor	1
3	Hi-Tech Optima 9 Receiver	1
4	E210	1
5	Horizontal Stabilizer	1
6	Tail Spar	1
7	SD7032	1
8	Wing Tip PLate	2
9	Main Landing Gear Wheel	2
10	Wing Support Brace	1
11	Tail landing gear	1
12	Vertical Stabilizer	1
13	Tail Wheel	1
14	Propeller Collet	1
15	Kan 700 Receiver battery pack	1
16	28 Cell Elite 1500A Battery Pack	1
17	Phoenix Ice 2 HV 40 Speed Controller	1
18	Fuselage	1
19	Main Landing Gear	1
20	Right Aileron	1
21	Left Aileron	1
22	Elevator	1
23	Rudder	1
24	Hi-Tech HS-65MG Servo	4
25	P-29 Motor Gearbox	1
26	Motor Mount Bracket	1

NOTE:
DIMENSIONS
ARE IN INCHES

SAN DIEGO STATE UNIVERSITY
AIAA DESIGN/BUILD/FLY 2013

DRAWN BY
DANIEL TAUGHINBAUGH

APPROVAL DATE:
2/23/13

CHIEF ENGINEER
JEROMEY SUKO

SIZE
B

DOCUMENT TITLE
Structural Arrangement

REV
A

SCALE: 1:9

SHEET 2 OF 6

DETAIL B
SCALE 1 : 4

DETAIL C
SCALE 1 : 2

DETAIL I
SCALE 1 : 4

DETAIL E
SCALE 1 : 1.5

DETAIL Q
SCALE 1 : 4
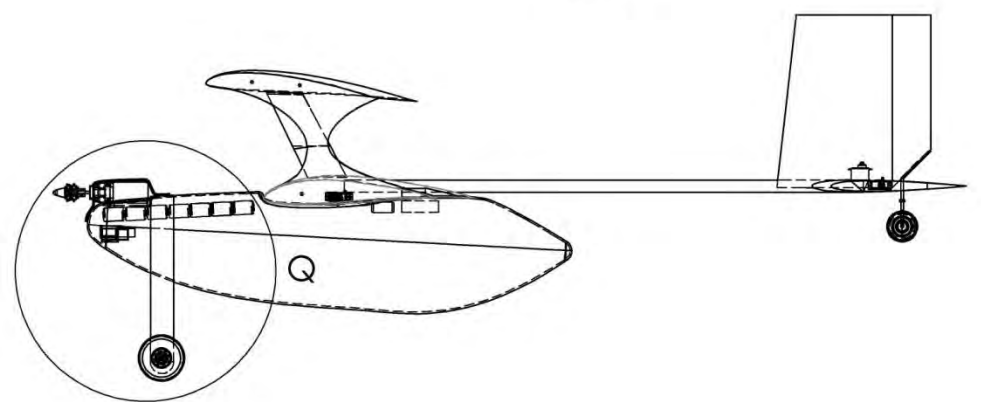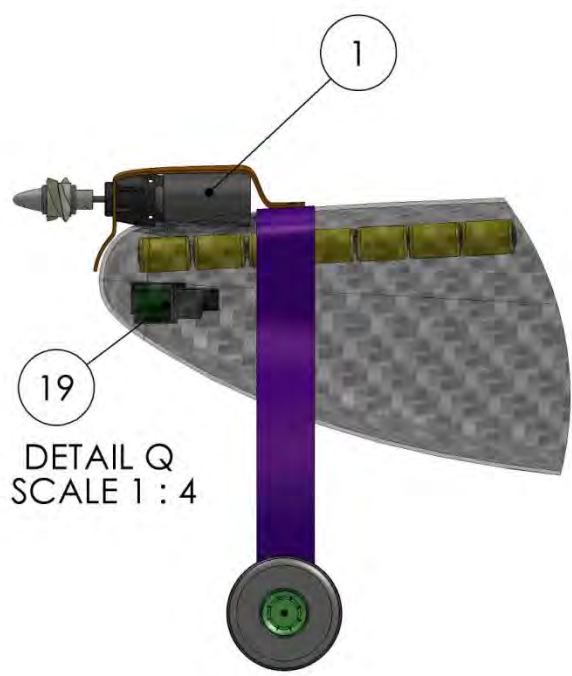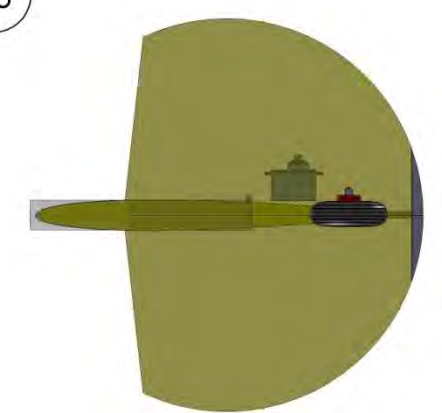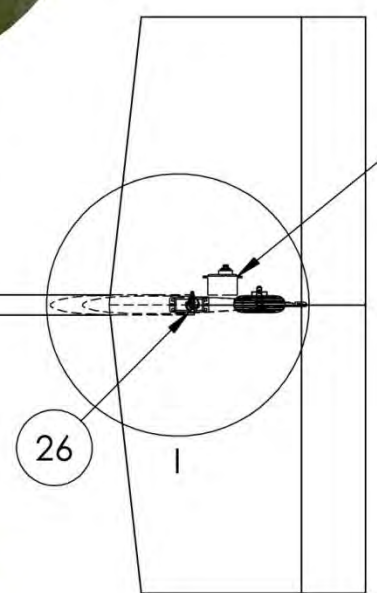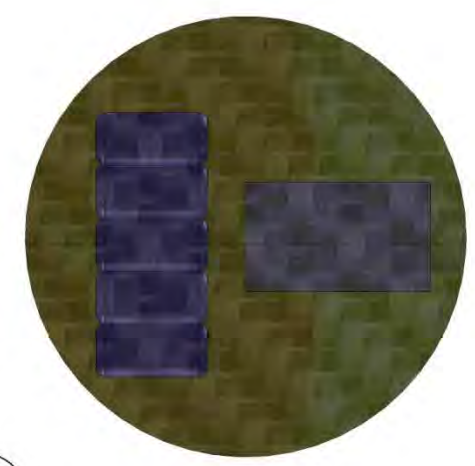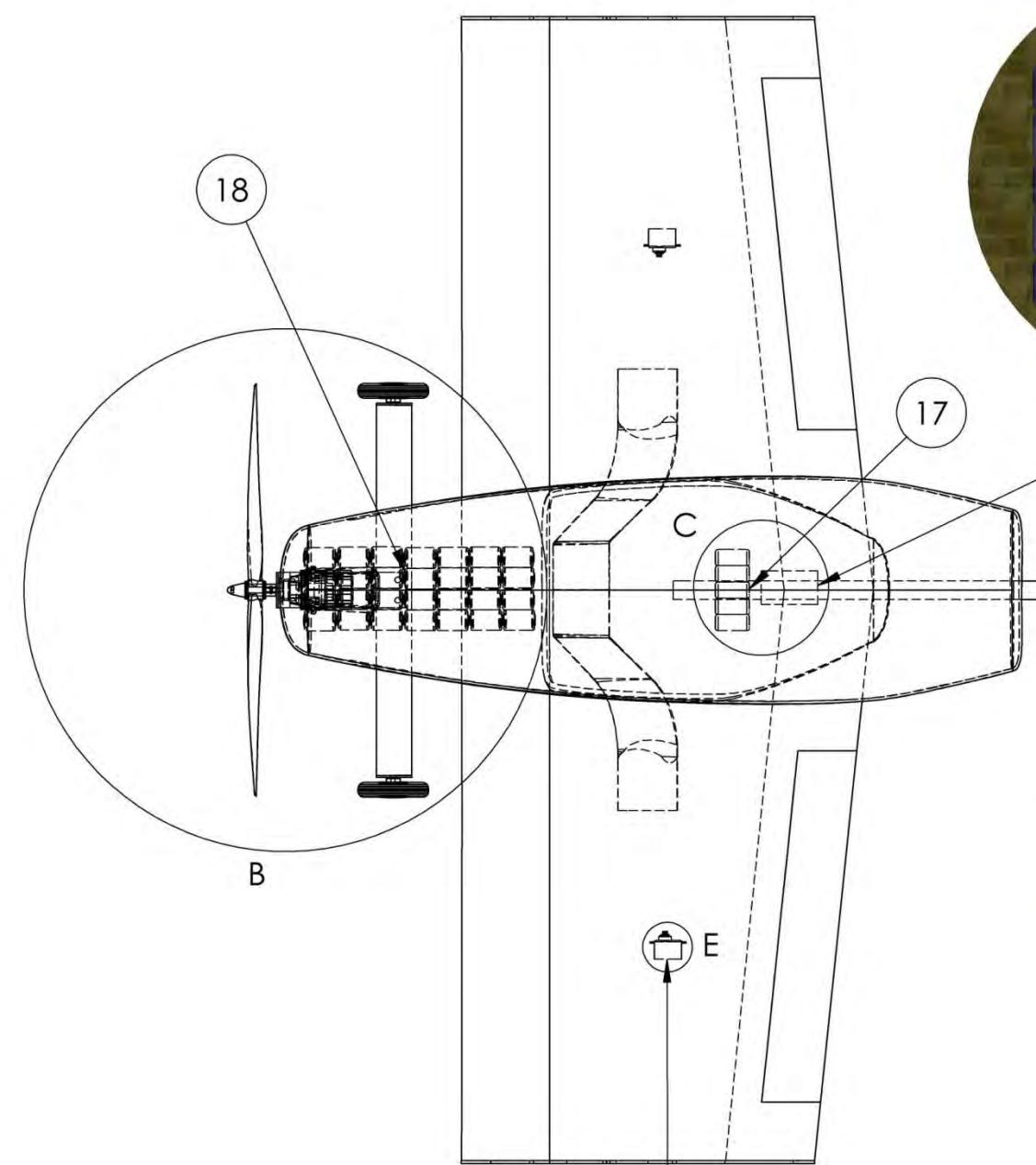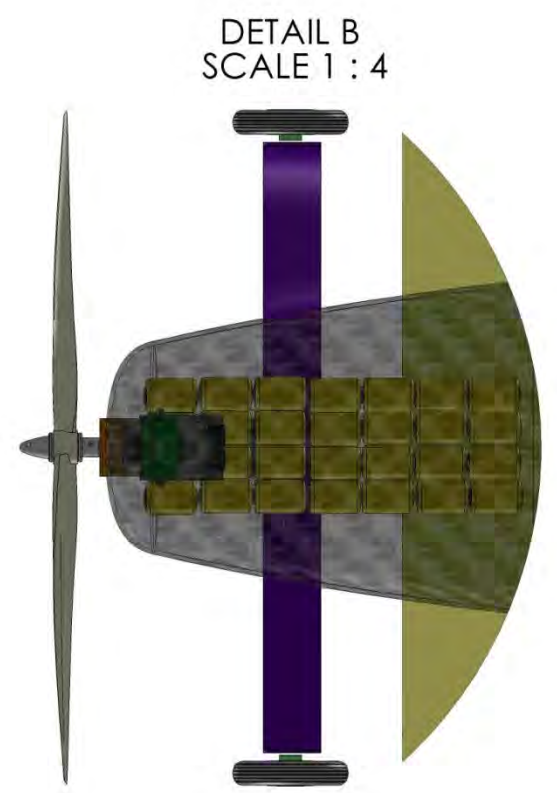
ITEM NO.	PART NUMBER	QTY.
1	Neu 1110-2y motor	1
2	Hi-Tech Optima 9 Receiver	
17	Kan 700 Receiver battery pack	1
18	Elite 1500A Battery PAck	1
19	Phoenix Ice 2 HV 40 Speed Controller	1
26	Hi-Tech HS-65MG Servo	4

NOTE:
DIMENSIONS
ARE IN INCHES

SAN DIEGO STATE UNIVERSITY
AIAA DESIGN/BUILD/FLY 2013

DRAWN BY
DANIEL TAUGHINBAUGH

APPROVAL DATE:
2/23/13

CHIEF ENGINEER
JEROMEY SUKO

SIZE
B

DOCUMENT TITLE
Systems Layout

REV
A

SCALE: 1:9

SHEET 3 OF 6

Configuration #1 Configuration #2 Configuration #3 Configuration #4 Configuration #5 Configuration #6
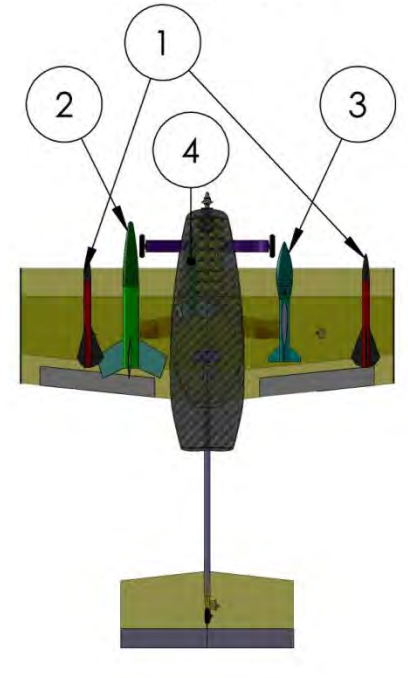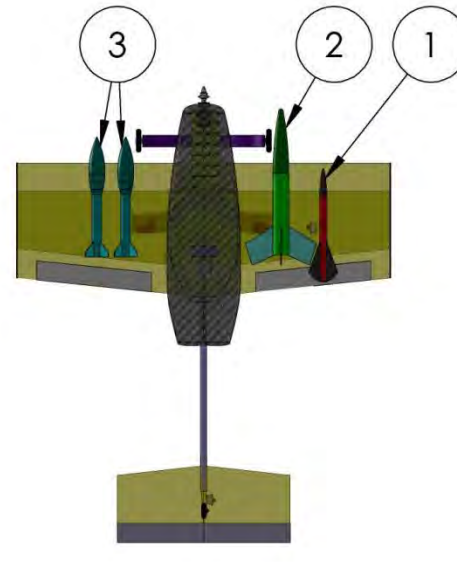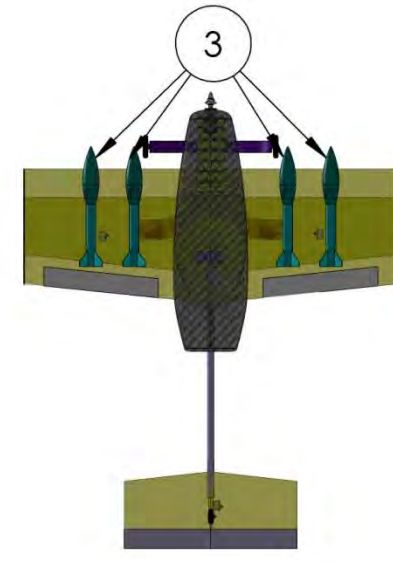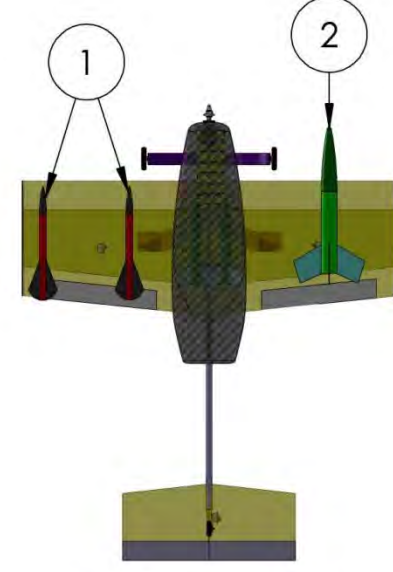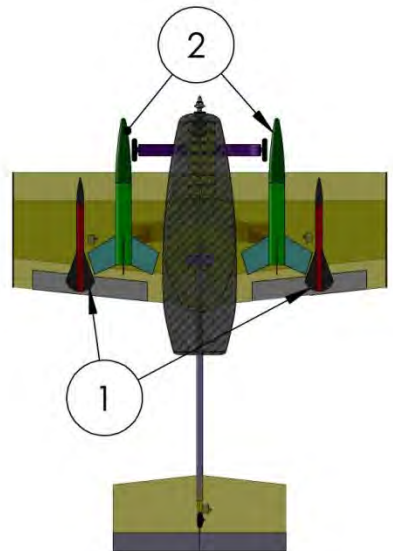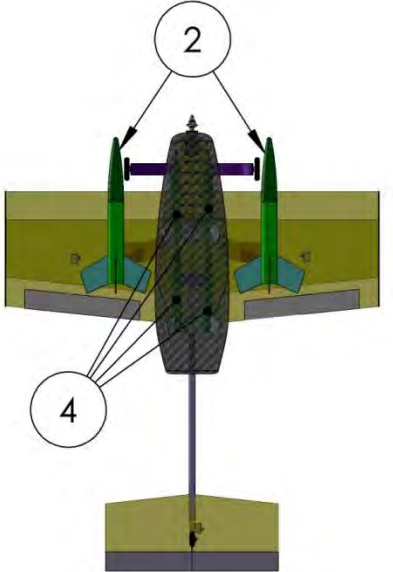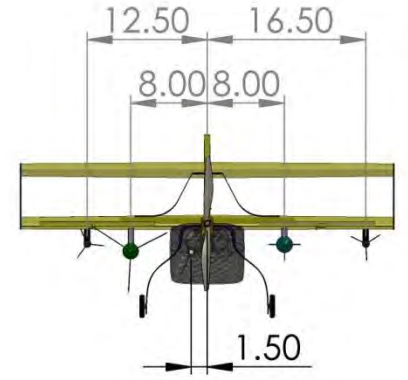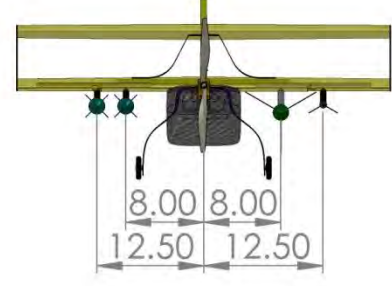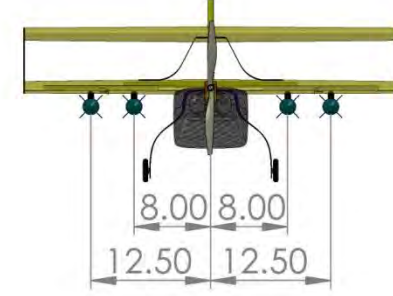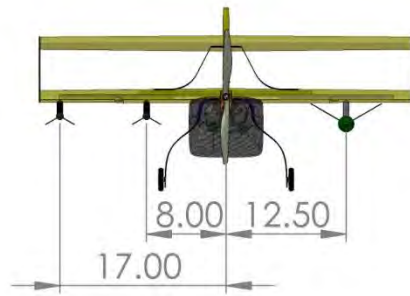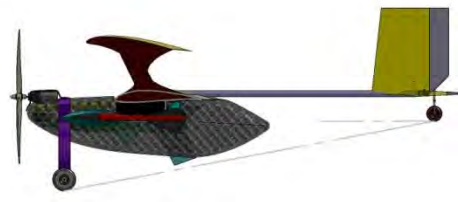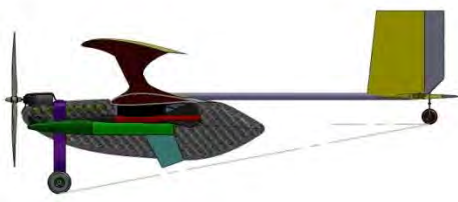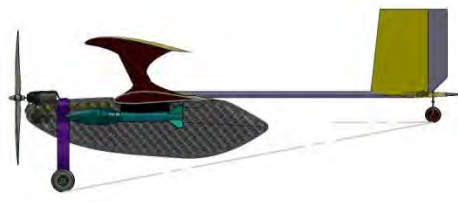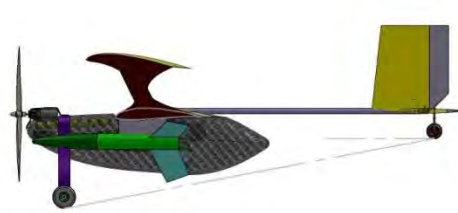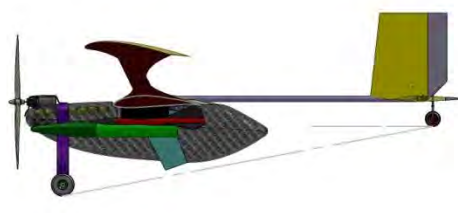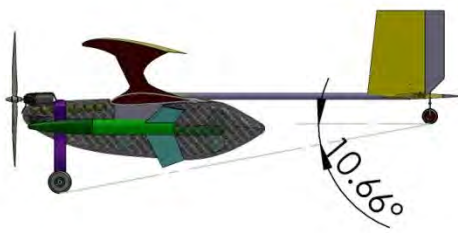
ITEM NO.	PART NUMBER	Wt.	QTY.
1	Hi-Flyer	0.5	2
2	Der Red Max	1	2
3	Mini Honest John	0.75	4
4	Mini Max	0.25	4

NOTE:
DIMENSIONS
ARE IN INCHES

SAN DIEGO STATE UNIVERSITY
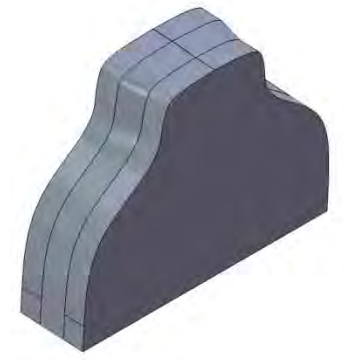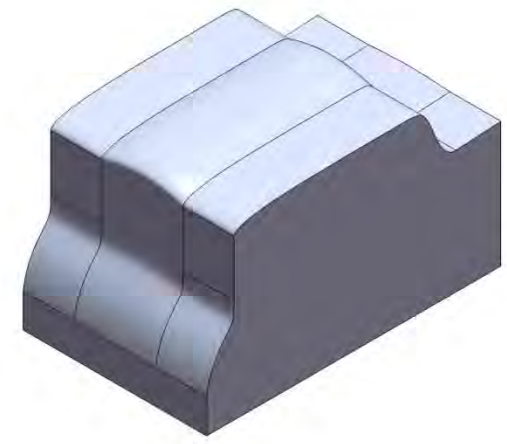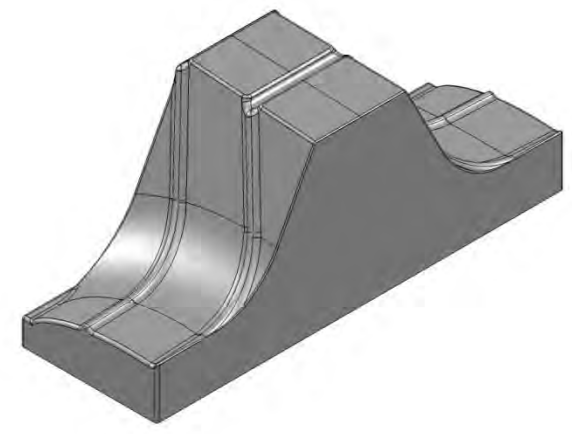AIAA DESIGN/BUILD/FLY 2013

DRAWN BY
DANIEL TAUGHINBAUGH

SIZE
B

DOCUMENT TITLE
Payload Configurations

REV
A

APPROVAL DATE:
2/23/13

CHIEF ENGINEER
JEROMEY SUKO

SCALE: 1:9   SHEET 4 OF 6

5.00

6.27 6.06

(A)

15.00

(B)

2.55

4.33

9.77

12.58

(C)
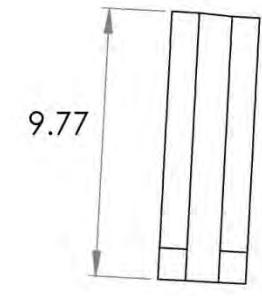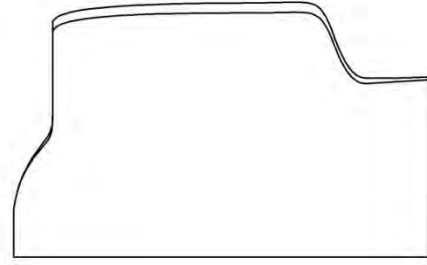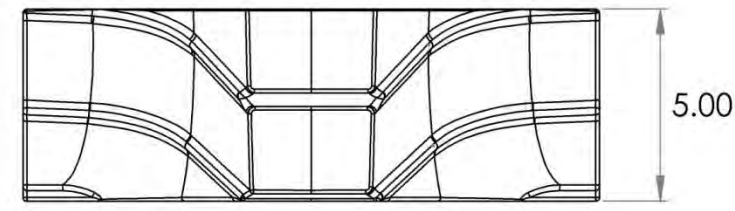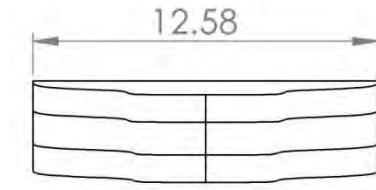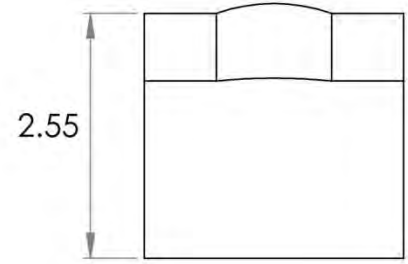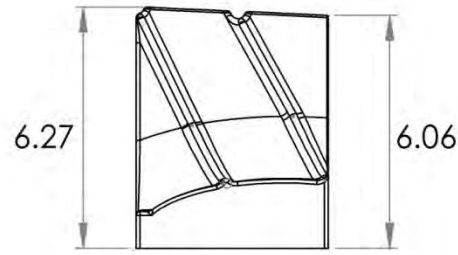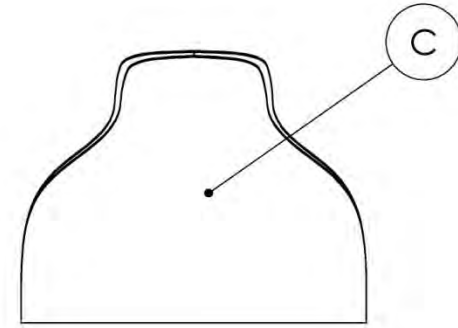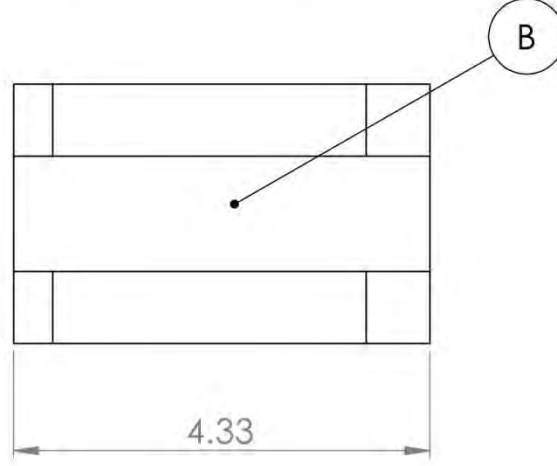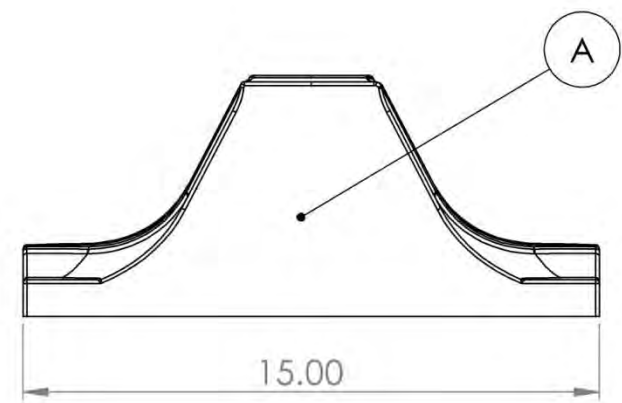
ITEM NO.	PART NUMBER	QTY.
A	Wing Support Mold	1
B	Motor Mount Mold	1
C	Landing Gear Mold	1

Top Mold

Bottom Mold

3.10

1.50

1.50

$\emptyset 0.75$

$\emptyset 0.63$

4.28

$\emptyset 0.25$

$\emptyset 1.63$

10.00

0.250

28.99

NOTE:
DIMENSIONS
ARE IN INCHES

SAN DIEGO STATE UNIVERSITY
AIAA DESIGN/BUILD/FLY 2013

DRAWN BY
DANIEL TAUGHINBAUGH

APPROVAL DATE:
2/23/13

CHIEF ENGINEER
JEROMEY SUKO

SIZE
B

DOCUMENT TITLE
Tooling

REV
A

SCALE: 1:9   SHEET 6 OF 6

6.0   MANUFACTURING PLAN AND PROCESSES

Manufacturing prototypes began as soon as possible in order to both test current design ideas as well as improve fabrication techniques.

6.1   MANUFACTURING AND MATERIAL SELECTION

The manufacturing process identified the following materials and subsequent fabrication techniques as potential candidates for the final design:

- o **Solid Foam**: EPS foam is considered extremely light. This material can be shaped using a CNC hot wire foam cutter and is available in large sections making it useful for the wing core. This material is weak in tension but strong in compression and bending.

- o **Balsa**: This material can be very light and easy to form to different contours. Depending on where it is used, balsa is a reinforcing material. Balsa wood increases shear strength as well as bending modes when combined to weak structures.

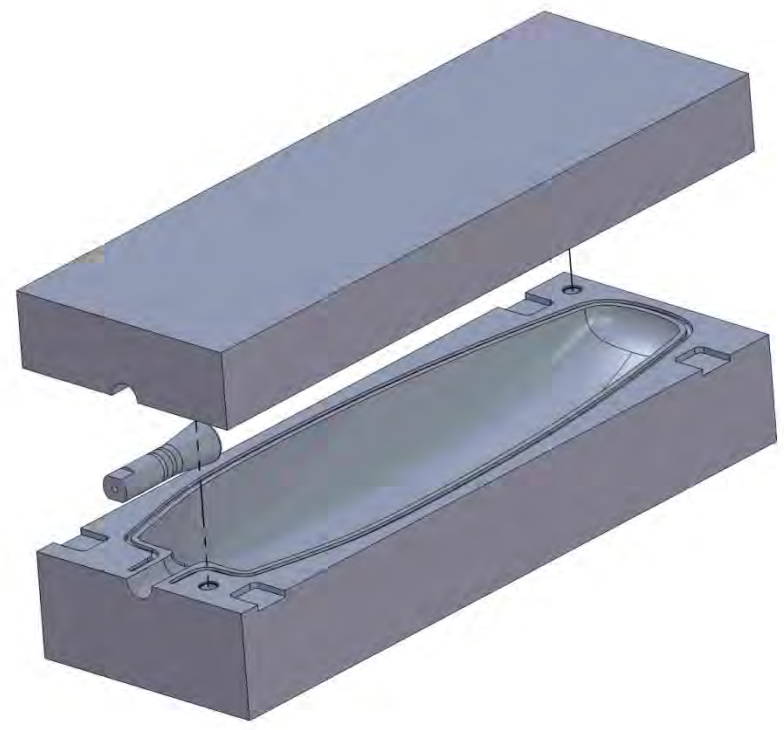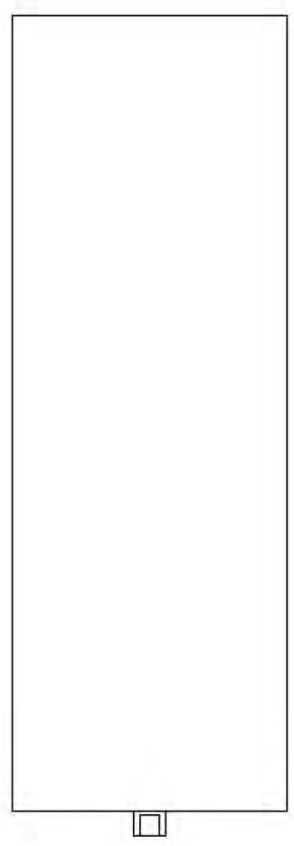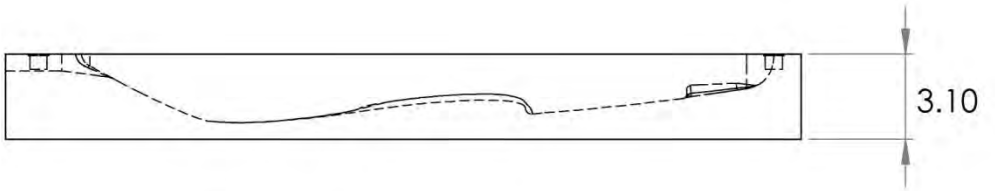- o **Carbon Fiber**: This material is manufactured by utilizing a wet layup process where carbon fiber cloth is placed over a mold with resin is distributed along the surface area, and then vacuum bagged and cured. Different orientations of weaving patterns will increase the shear strength and bending stiffness. If one direction is used (45°) the negative must be also used (-45°). If not the layup will introduce torsion stress within the component.

- o **Aluminum Sheet**: This material is a highly diverse element which can be molded or shaped to the team's specifications. Aluminum is strong in tension and compression, but if used too much it will add extra unnecessary weight.

- o **Hybrid**: This construction consists of a combination of one pound density foam, three ounce stitched carbon fiber and light-weight balsa. A carbon fiber-foam sandwich structure handles the bending loads while the carbon fiber-balsa structure focuses on tension as well as compression loading.

For each major section of the airplane a FOM analysis was carried out in order to select the ideal material. The FOM analysis for each section had the same parameters.

- **Weight**: As the most important element it was necessary to select a material that reduced as much weight as possible.

- **Strength**: Although weight is the highest priority, if the structure can't handle the loads the aircraft will fail. The selected material must have a balance of weight and strength.

- **Manufacturability**: A material that is quick and easy to manufacture is desired in case there is an unexpected failure of a part during the competition.

6.1.1 Airfoil Material Selection

Figure of Merit	Weight	Solid Foam	Balsa	Carbon Fiber	Hybrid
Weight	0.60	3	4	3	3
Strength	0.30	4	2	4	5
Manufacturability	0.10	4	3	3	3
Total	1.00	3.4	3.3	3.3	3.6

Figure 50 – Airfoil Material Selection Figure of Merit Analysis

6.1.2 Fuselage Material Selection

Figure of Merit	Weight	Solid Foam	Balsa	Carbon Fiber	Hybrid
Weight	0.60	3	4	3	3
Strength	0.30	4	2	4	5
Manufacturability	0.10	4	3	3	3
Total	1.00	3.4	3.3	3.3	3.6

Figure 51 – Fuselage Material Selection Figure of Merit Analysis

6.2 MANUFACTURING SCHEDULE
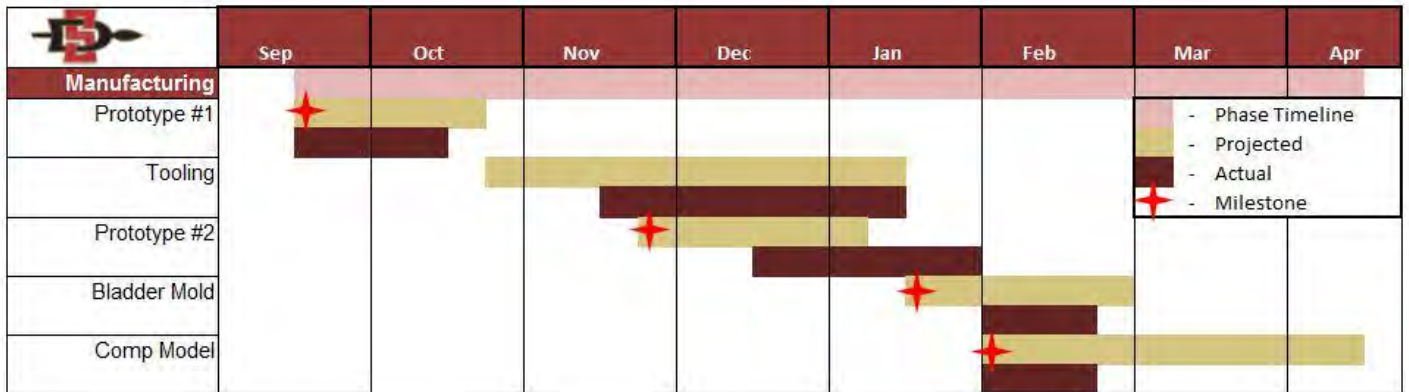
Figure 52 – Manufacturing Schedule

6.3 AIRCRAFT MANUFACTURING PROCESS

6.3.1 Wing/Empennage Manufacturing

The airfoil cores for the main wings, elevator, and stabilizer were all created the same way. A piece of foam was shaped using a CNC hot wire cutter, then a carbon fiber/ fiber glass/ epoxy layup was used to add strength and rigidity to the airfoils.

Figure 53 – Carbon Fiber Layup of the SD7032 Airfoil

To make the fuselage, the team decided to implement the bladder molding capabilities available at SDSU. First a mold of the fuselage must be machined, polished, and treated. It was decided that carbon fiber would be used, so patterns were cut and placed into the correct patterns. A bladder is then placed between the two molds and inflated to a pressure of 120 psi and 250°F, while a Platen Press maintains a load of 40 tons to keep the mold together and to cure the epoxy which is pre impregnated into the carbon fiber. The epoxy will cure in one hour with this method as opposed to overnight for a wet layup.

Figure 54 – Platen Press Machine (left) Bladder Mold (right) of Fuselage

6.3.3   Empennage and Second Wing Attachment

To connect the tail the main wing, a spar was inserted into the bottom wing by cutting a grove for the spar, and then placing a carbon fiber strip secured with epoxy for reinforcement, as shown in the picture below.

Figure 55 – Spar Connecting Empennage to Bottom Wing Using Carbon Fiber Strip Secured With Epoxy

CNC cut out of carbon fiber plates connected the wing tip plates. This allowed for high accuracy in placing the wings at the correct stagger, and decalage angle. A single center support was molded from Kevlar and carbon fiber that completed a truss like system used for the wing configuration.

Figure 56 – Final Wing Configuration and Assembly

7.0   TESTING PLAN

After all preliminary design, detail design, and initial manufacturing had been carried out, each system on the aircraft was tested to validate performance predictions. The experimental data provided allowed further changes to the design ultimately leading to a well-refined final product.
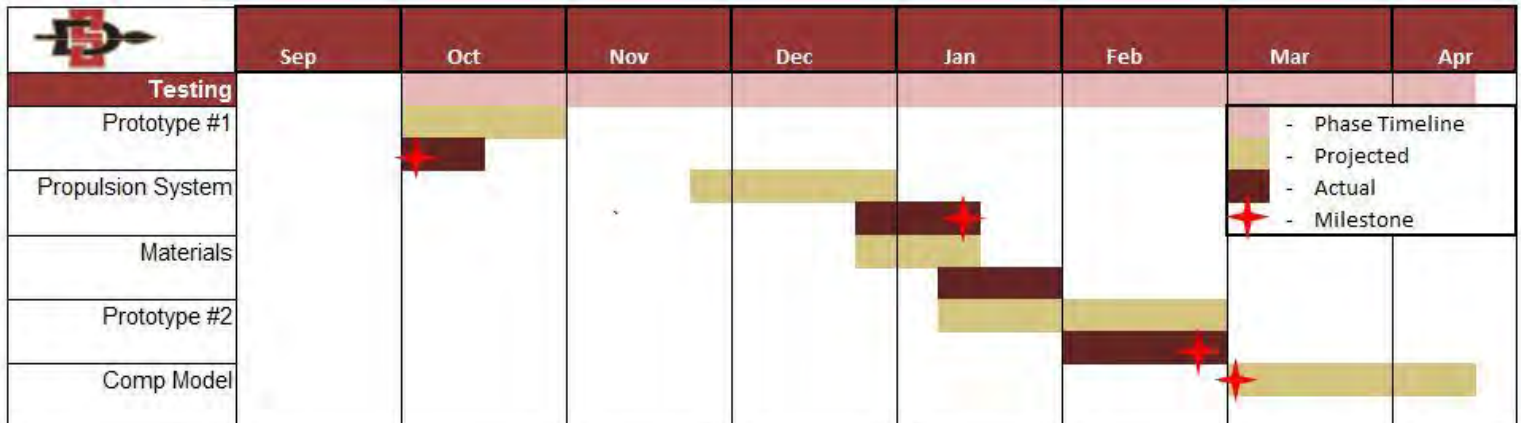
Figure 57 – Testing Schedule

7.1 PROPULSION SYSTEM TESTING

Acceleration sled testing was performed in order to confirm ground speed velocity for takeoff. Using the decided propulsion system configuration, the team ran multiple tests using the sled below.

Figure 58 – Acceleration Sled

7.2 STRUCTURAL TESTING

The purpose of structural testing was to ensure that various structures on the aircraft could successfully withstand expected loads. The testing also helped confirm the FEM analysis methods used previously were reliable.

7.2.1 Wing Tip Test

The aircraft is subjected to a wingtip test and loaded with more than double the maximum expected payload. The load was placed in the middle of the span and not loaded until failure.

Figure 59 – Wing Tip Test

7.2.2   Landing Gear Test

Much like the wing tip test, the landing gear was loaded in a similar fashion. To simulate maximum landing load, the falling force of the aircraft was calculated to be about 3g's which was applied at the point of connection between the fuselage and landing gear.

Figure 60 – Landing Gear Load Testing

7.3   FLIGHT TESTING

Flight testing was carried out to confirm that the aircraft and systems would perform as intended. Flight data including voltage and current was logged and upon review of the aircraft, used to further optimize the design. The pilot used these opportunities to become familiar with the aircraft and maneuvers required by the missions. Past SDSU DBF experience has relied heavily on pilot feedback. Using the feedback, the team was able to improve the design of the aircraft and subsystems. The team relied heavily on flight testing completing over 35 individual flights with 4 different configurations on 2 prototypes throughout the course of the design phase.

Figure 61 – Prototype One Before First Test Flight

Figure 62 – Prototype One Fully Loaded Configuration (left) Prototype two In Flight (right)

8.0 PERFORMANCE RESULTS

The performance results section is used to compare preliminary analysis data to actual performance data. The actual recorded data is then used to revise the final design of the aircraft.

8.1 PROPULSION TEST RESULTS

Initial testing using the acceleration sled showed that the 1110-2.5Y motor would not provide adequate acceleration in order to take-off from the 30' x 30' runway. The final velocity reached was 19.48 mph, significantly less than the required take-off velocity. This is due to the fact that the motor didn't draw enough amperage from the battery (10A-12A). To compensate, the team installed the 1110-2Y motor with a higher Kv rating (2250 Kv). Using the acceleration sled again with the new motor showed that at the end of a 30 foot runway, the aircraft could reach a velocity of 29.22 mph, and it was also verified that the new motor could draw the proper amperage (19A-24A). The determined take-off velocity was 25 mph and the testing proved that the aircraft could successfully reach the required take-off velocity within the allotted space.

8.2 WING TIP RESULTS

As described in section 7.2.1, the wing was loaded with a 7 lb. weight in the middle of the span. The maximum payload expected for the competition is 3.5 lbs. The airframe successfully handled the loading and showed no signs of permanent deformation or damage. The FEM analysis discussed in section 5.3 which showed the air frame could handle a load of up to 25.6lbs, compared the theoretical and experimental results. With this data, the team felt confident the airframe was structurally sound.

$$\#_{design} = \frac{\#_{\max}}{F.S.}$$

$$F.S. = \frac{7.75lb}{3.5lb} = 2.2$$

Since the wings weren't loaded to failure, Factor of Safety of 2.2 is conservative with respect to the failure loading of the wings.

8.3   LANDING GEAR RESULTS

As described in section 7.2.2, the landing was loaded with a 3g force to simulate impact loading upon landing. The double arc carbon fiber landing gear successfully handled the loading and showed no signs of fatigue or strain. FEM analysis showed the landing gear could handle a 23.6lb loading. Once again, comparing initial FEM analysis to the experimental results the following safety factor was determined.

$$\#_{design} = \frac{\#_{max}}{F.S.}$$

$$F.S. = \frac{21.0lb}{7.0lb} = 3.0$$

8.4   MATERIAL TESTING

In order to obtain accurate material input properties for both FEM analysis and overall aircraft design, the team carried out testing on the high density foam/carbon fiber sandwich representative of a wing section along with a solid carbon fiber plate to represent carbon fiber components. Testing these two materials yielded input values for FEM such as Young's Modulus and Poisson's ratio.
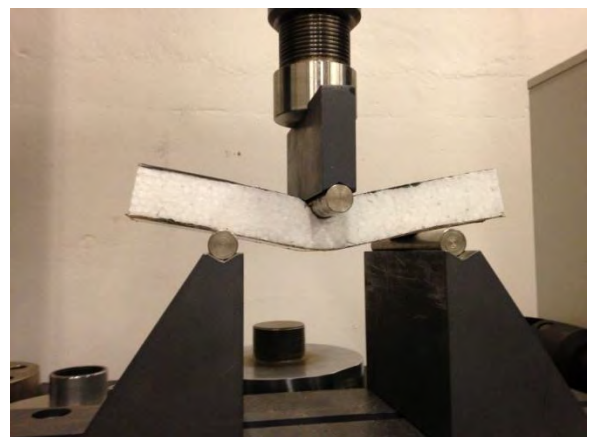
Figure 63 – Three Point Bend Test for Carbon Fiber (left) XPS Foam (right)

Throughout the development process, test flights were conducted to validate performance capabilities of the aircraft. Easy access to an airfield, high availability for the pilot and team members, and rather quick manufacturing for all parts of the aircraft allowed the team to carry out numerous flight tests whenever desired. Throughout the design phase of the competition, flight testing revealed the following problems.

Observation	Design Change
Tail boom was not stiff enough which caused the aircraft to suffer from aero-elastic effects.	Tail boom was then changed from two small spars to one spar with a larger diameter to increase stiffness.
The pilot felt the aircraft was top heavy due to the large amount of space between the top and bottom wing.	The stagger and offset was reduced because at lower Reynolds number interference between the two wings is not as high as anticipated.
Initial flight testing resulted in failure of the single arc landing gear.	A double arc design was used and aluminum was used to reinforce the curvature of the landing gear.
The 5° decalage between the two wings made it impossible to maintain flight trim at cruise speed. The lower wing could be flying at negative C_L during some trim conditions	The top wing initially at 5° was changed to now be at 0° angle of incidence. Two different airfoils were still utilized.
Uncertainty with preliminary analysis	Flight testing allowed the team to feel confident with the results produced by the CFD, FEM, and XFOIL analysis

Figure 64 – Flight Test Observations and Necessary Design Changes to be Implemented

Data was logged on the Castle Creations Phoenix Ice 2 HV40 speed controller. The sample rate was 5Hz and the following data was obtained for a 7 lap mission 1 exercise using the 12"x10" propeller. It can be seen that the maximum amperage is exceeded during the mid portion of the flight but, the slow blow fuse allowed us to slightly go over the 20A limit without blowing. The propulsion system hit a near 23A max. In addition, this flight was at nearly full throttle through the entire duration, so it was proven that the aircraft propulsion system was in fact maximized for 1.5lbs of batteries, and a 20A

fuse, and allowed for the completion 7 laps within 4 minutes. The team is confident that 8 laps can be completed in competition for mission 1, and fly a 90 second mission 3 at max payload with the competition model of the aircraft, and a well practiced pilot.
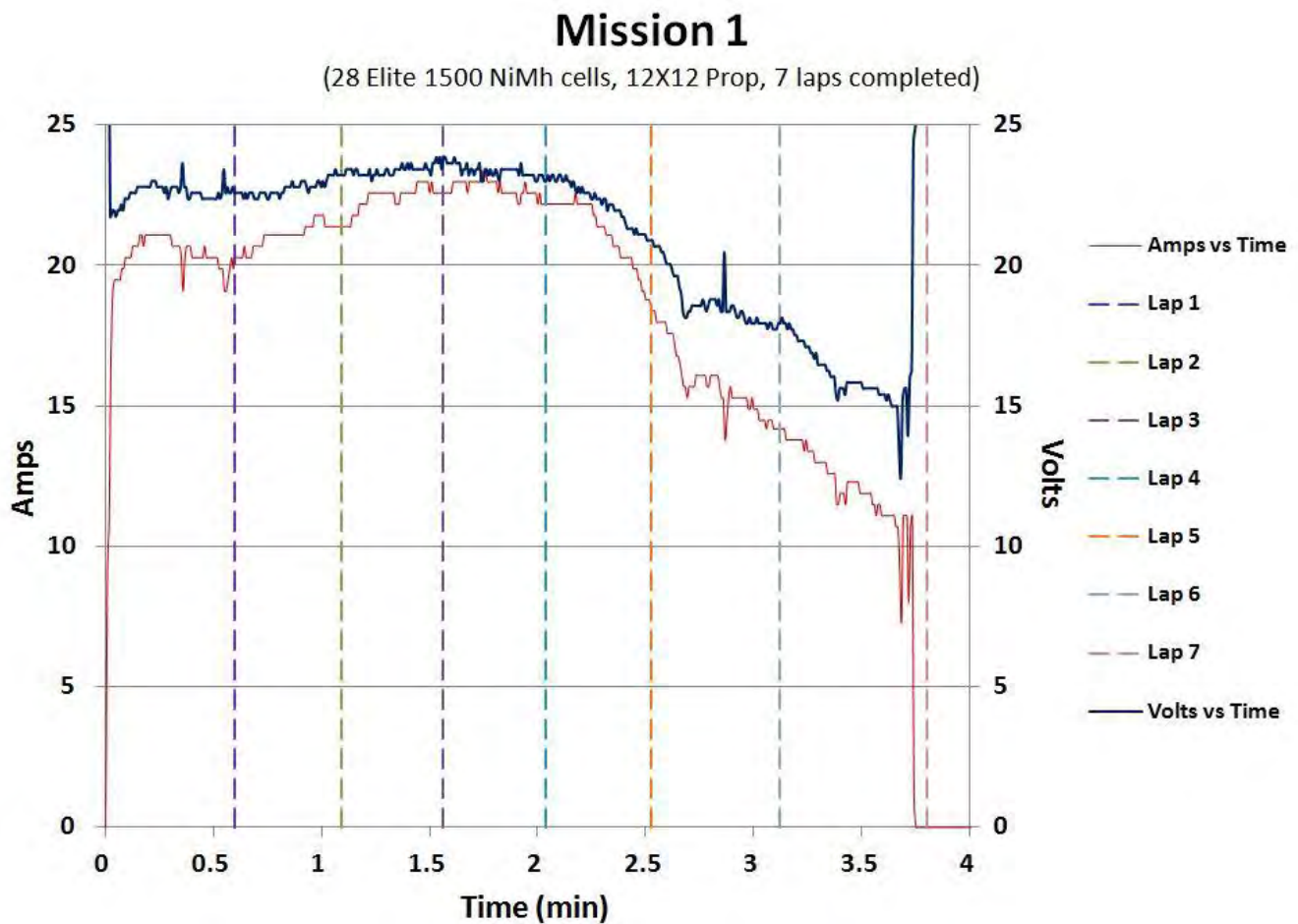
Figure 65 – Amperage vs. Time in Flight

8.6   AERODYNAMIC RESULTS

The aircraft as a whole was thoroughly analyzed using [15]Star-CCM+ (computational Fluid dynamics) to estimate maximum lift at takeoff and drag results from cruising speed. In total 3 different fuselage shapes and 3 different wing configurations were imported and analyzed totaling over 264 hours of simulations. Below is a graph showing the comparison between preliminary aerodynamic data from [6]XFOIL/XFLR-5 and refined data using [15]Star-CCM+. The [15]Star-CCM+ analysis allowed us to import an actual model of the aircraft whereas [6]XFOIL/XFLR-5 was very limiting in capabilities.

Cl vs. Alpha

Legend:
- CFD Complete Aircraft
- SD7032
- E210
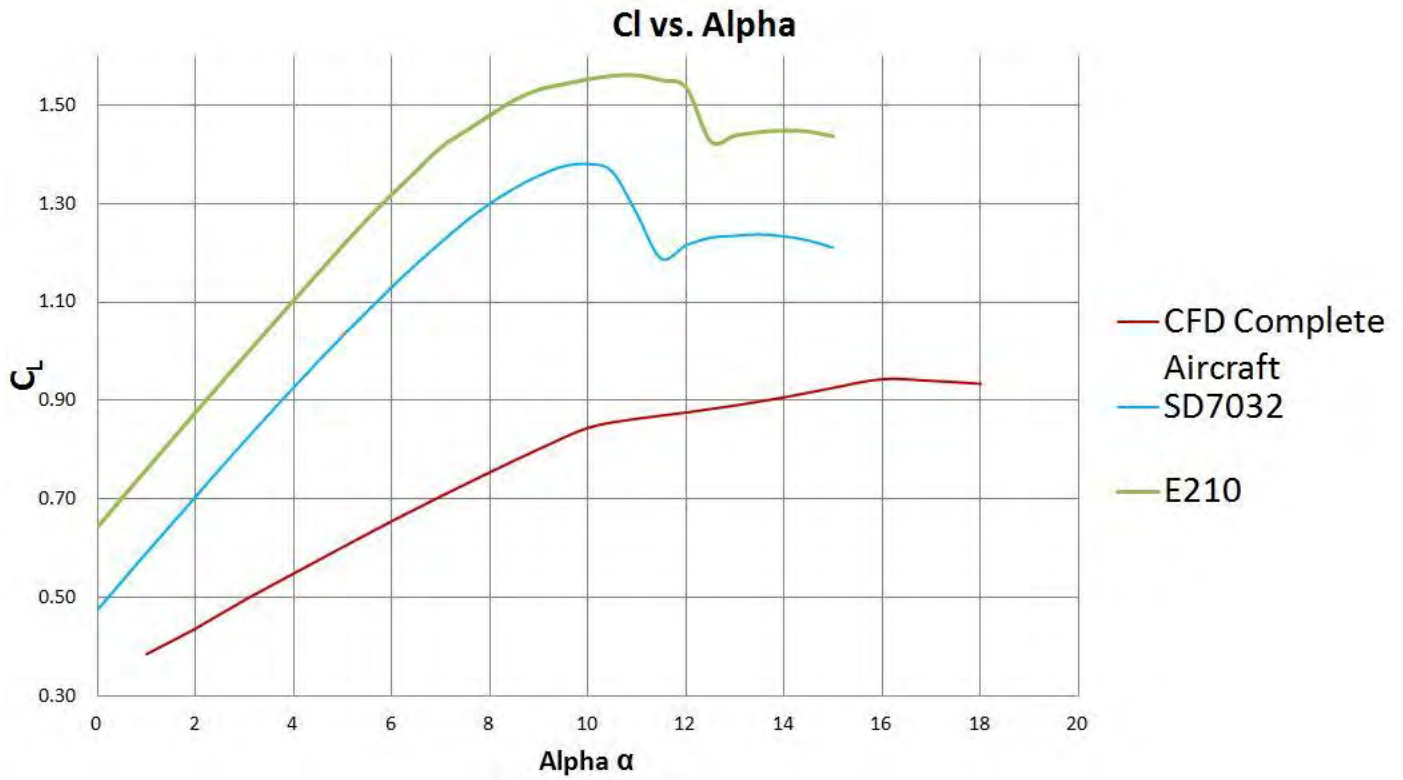
Figure 66 – Lift Curve Comparison Between Individual Wings and Entire Aircraft

As mentioned before, 3 different fuselage designs were analyzed using [15]CFD analysis. The goal of testing different fuselage shapes was to create a semi-lifting body that would increase the overall C_L and reduce as much drag as possible. The figure below depicts the selected fuselage design showing minimal flow separation at the trailing end of the fuselage thereby reducing drag caused by the geometry needed to carry four internal rockets.
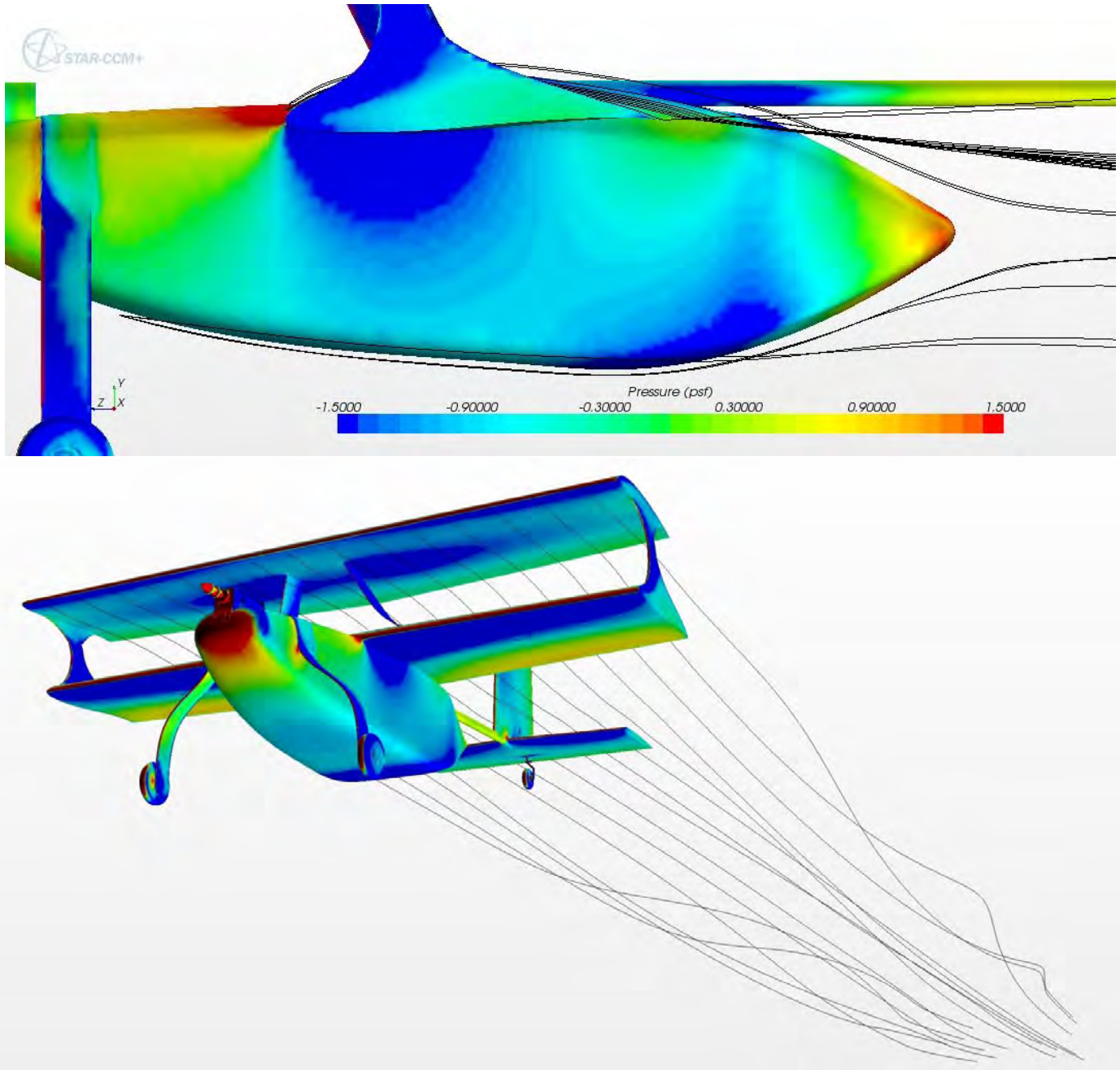
Figure 67 – CFD Analysis Displaying Minimal Flow Separation of Fuselage (top) and Streamlines of Aircraft in Flight (bottom)

Overall, three different wing configurations were analyzed, the initial wing configuration consisted of the preliminary design using two different airfoils having the top wing at a higher angle of incidence than the bottom. The next configuration was using two higher lifting airfoils both at 0° angle of incidence. The selected configuration uses the two different airfoils (as in the initial configuration) both at 0° angle of incidence where one airfoil was high lift (bottom) and one was low drag (top). The [15]CFD analysis results below show comparisons between the three configurations.

Component	E210 at 0° AOA and SD7032 at 5° AOA		2x E210 at 0° AOA		E210 at 0° AOA and SD7032 at 0° AOA	
	Net Drag(lbf)	% of Total Drag	Net Drag(lbf)	% of Total Drag	Net Drag(lbf)	% of Total Drag
Total AC	1.21	100.00%	1.24	100.00%	1.15	100.00%
Main Landing Gear	0.09	7.35%	0.10	7.80%	0.09	8.17%
Fuselage	0.10	8.59%	0.03	2.30%	0.11	9.89%
Top Wing	0.45	37.11%	0.46	37.19%	0.34	29.94%
Bottom Wing	0.41	33.75%	0.38	31.03%	0.33	29.04%
Wing Support Brace	0.03	2.42%	0.04	2.91%	0.03	2.22%
Wing Tip Plates	0.05	4.49%	0.07	5.33%	0.06	4.92%
Vertical Stabilizer	0.04	2.92%	0.04	3.21%	0.04	3.60%
Horizontal Stabilizer	0.04	0.39%	0.03	2.69%	0.05	4.08%
Tail Landing Gear	0.02	1.76%	0.02	1.96%	0.02	2.07%
Motor	0.01	0.76%	0.06	4.85%	0.06	5.47%
Tail Spar	0.01	0.47%	0.01	0.50%	0.01	0.52%
Servos	n/a	n/a	0.00	0.23%	0.00	0.08%

Figure 68 –CFD Analysis Comparison Between Proposed Wing Configurations

9.0 REFERENCES

[1]AIAA. (2012 04-September). 2012/13 Rules and Vehicle Design. Retrieved 2012 04-Sept. from AIAA DBF: [http://www.aiaadbf.org/2012_files/2012_rules.htm]

[2]Abbott and A.E. Von Doenhoff. *Theory of Wing Sections*, New York: Dover 1959

[3]Anderson, John D. *Introduction to Flight*. New York: McGraw-Hill, 1989

[4]Anderson, John D. *Fundamentals of Aerodynamics*. New York: McGraw-Hill, 1991

[5]Bandu N. Pamadi, *Performance, Stability, Dynamics and Control of Airplanes*. AIAA Education Series, 2004.

[6]Drela, Mark. XFOIL 6.96 user Guide. Boston MIT, 1986

[7]Etkin, Bernard. *Dynamics of Flight*. New York: John Wiley & Sons, 1996

[8]Kroo, Ilan *Aircraft Design: Synthesis and Analysis*, Version 0.9. http://adg.stanford.edu/aa241/AircraftDesign.html

[9]Nicolai, Leland. *Fundamentals of Aircraft Design.* San Jose: Mets, 1984

[10]Raymer, D. (2008). Aircraft Design: A Conceptual Approach. Reston, Virginia: American Institute of Aeronautics and Astronautics.

[11]Roskam, Jan. *Airplane Design: Part VI*. Lawrence: DARcorporation, 2000

[12]Motocalc 8. s.l. :Capable Computing inc. http://www.motocalc.com/index.html

[13]Muller, Markus. eCalc. http://wwww.ecalc.ch/motocalc_e.htm?ecalc

[14]UGS Corp., ComponentOne, DriveWorks Ltd., Geometric Ltd., Microsoft Corporation, Spatial Corp., Luxology, Inc., The University of Tennessee, Siemens industry Software Limited,   and Siemens Product Lifecycle Management Software inc. SolidWorks 2012. Vers.   Student. Waltham: Dassault Systemes, 1993. Computer Software.

[15]Star-CCM+. By CD-adapco. http://www.cd-adapco.com/products/star_ccm_plus/

[16]UGS Corp., ComponentOne, DriveWorks Ltd., Geometric Ltd., Microsoft Corporation, Spatial Corp., Luxology, Inc., The University of Tennessee, Siemens industry Software Limited,   and Siemens Product Lifecycle Management Software inc. Abaqus 2010. Vers. Waltham: Dassault Systemes, 1993. Computer Software.

RENSSELAER POLYTECHNIC INSTITUTE
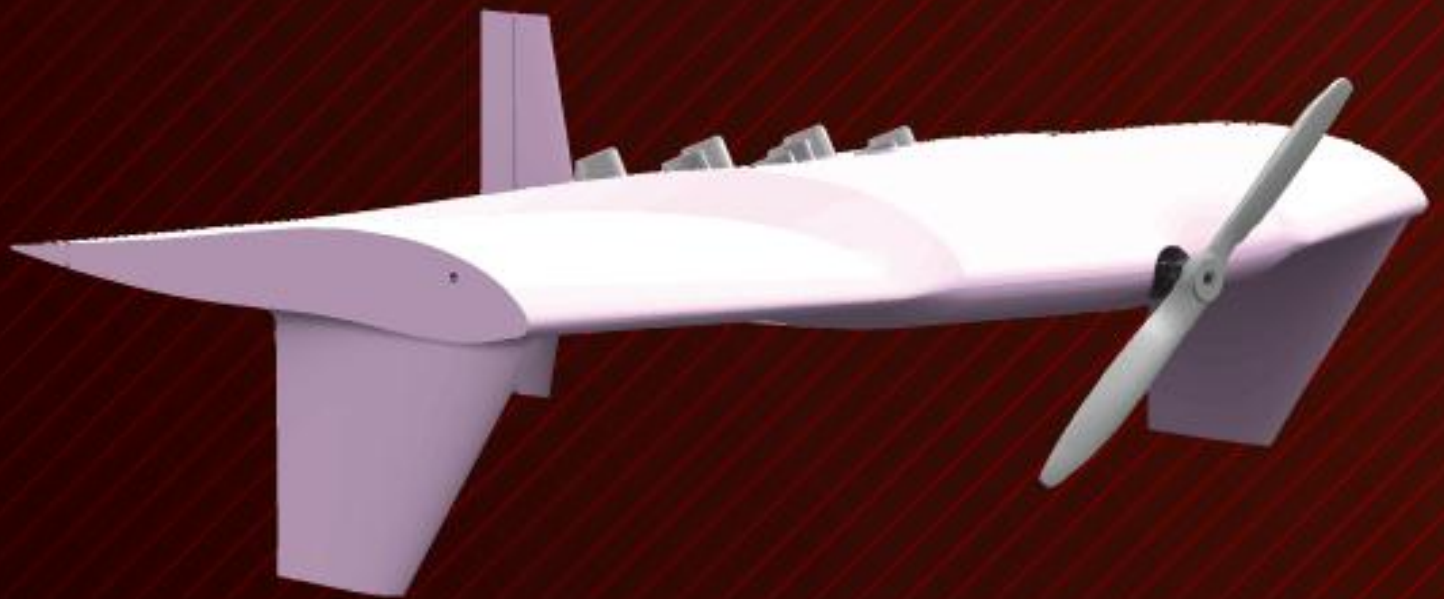
2013 - DESIGN BUILD FLY

Table of Contents

List of Symbols and Variables

α_{wing} = Angle of attack of wing

A_{thr} = Quadratic Thrust Coefficient

AR_{wing} = Wing aspect ratio

b = Wingspan

B_{thr} = Linear Thrust Coefficient

β = Crosswind angle of attack

$\bar{c}$ = Wing root chord

C_{thr} = Static Thrust

$C_{L_{\alpha,wing}}$ = Coefficient of lift slope (w.r.t. angle of attack) of the wing

$C_{L_{\alpha,htail}}$ = Coefficient of lift slope (w.r.t. angle of attack) of the horizontal tail

$C_{L_{\alpha,vtail}}$ = Coefficient of lift slope (w.r.t. crosswind angle of attack) of the horizontal tail

$C_{L_{To}}$ = Lift coefficient at takeoff

C_m = Pitching Moment coefficient for the airfoils

$C_{M_{AC,wing}}$ = Pitching Moment coeff. due to the wing about the aerodynamic center of the wing

$C_{M_{CG}}$ = Pitching moment coefficient at the center of gravity of the plane

$C_{N_{CG}}$ = Yawing moment coefficient at center of gravity of plane

D = Drag

$\dfrac{dh}{dt}$ = Rate of climb

δ_e = Elevator deflection

δ_R = Rudder deflection

e = Oswald's effiency factor

EW = Empty weight

f_{To} = Equivalent flat plate area (used for drag)

g = Acceleration due to gravity

i_{tail} = Angle of incidence on tail

i_{wing} = Angle of incidence on wing

k_n and k_{Re} = Fuselage yaw moment factors

l_t = Distance between tail aerodynamic center and center of gravity of plane

n = Load factor

η_t = Horizontal tail effiency factor

$\eta_v * \left(1 + \dfrac{d\sigma}{d\beta}\right)$ = Vertical tail efficiency factor

ρ_{To} = Density at takeoff

R = Turn radius

RAC = Rated Aircraft Cost (maximum empty weight)

S_t = Horizontal tail reference area

S_w = Wing reference area

t = Time

T = Thrust

τ_e = Elevator effectiveness factor

τ_R = Rudder effectiveness factor

V = Velocity

W_{To} = Takeoff weight

x_{cg} = Distance from the front of the wing to the center of gravity

x_{ac} = Distance from the front of the wing to the aerodynamic center of the wing

1.0 Executive Summary

This report documents the design, fabrication, and testing of the Rensselaer Polytechnic Institute Redhawks' aircraft for the 2012-2013 AIAA Design/Build/Fly competition. The team's goal was to maximize the overall score, which consisted of equally weighted flight and report scores. The flight score is dependent on the performance of the aircraft in the three flying missions as well as the Rated Aircraft Cost (RAC). In the first mission, the aircraft must fly as many laps as possible within four minutes. The second mission consists of the aircraft flying three laps while carrying as many internal stores as possible. The final mission is also comprised of flying three laps, but with a different payload. The payload is one of six internal and external store configurations determined by rolling a six-sided die. For all flying missions, the aircraft must takeoff within a 30 by 30 foot square. To achieve a maximum score the RAC must be minimized which is accomplished by creating a plane that is as light and small as possible. This is different from years past where only weight was considered in RAC.

The design phase began with conceptual design. The team considered and evaluated ideas for every aspect of the aircraft including the overall configuration, wing type, tail configuration, fuselage type, and payload storage. The conceptual design led to a blended body design with winglets constructed from foam. A vertical tail was attached to the rear section of the plane. The body section would contain the internal stores and a tricycle landing gear would be used. The team then moved on to preliminary design where the goal was to determine the plane configuration that would maximize the flight score. Using selected propulsion, airfoil, and structural data a scoring optimization routine was created and used to determine the optimal wing/body planform. From here, the vertical tail, control surfaces, and winglets were sized. The team finalized all the individual system configurations in the detail design. The wing structure was designed for minimal weight with sufficient strength. The internal store restraint system consists of a tight friction fit between foam slots and the stores with a Velcro securing system. The external stores were mounted to pylons with zip ties. The pylons were secured to the plane using clips that can securely snap into place. Finally, a CAD model was created using Solidworks to ensure full system integration and smooth assembly.

The final aircraft configuration features a 962 square inch wing constructed with foam and carbon spars. The span is 39.3 inches and tapers from a 26 inch chord at the root to a 21 inch chord at the tip to decrease the size factor (SF) which decreases RAC. The wing provides enough lift for the 30' takeoff distance while fully loaded. The aircraft is powered by a Neu 1112 2Y motor that spins a 17x10 propeller to provide 7 pounds of static thrust. A 23 cell Elite 2000 battery pack provides the necessary power and endurance to fly a predicted 6 laps for Mission one, carry eight internal stores for Mission two, and complete the Mission three climb in 131 seconds. The predicted score is 15.48. Overall, the power system and low drag allow the aircraft to complete a course lap in about 38 seconds. The aircraft's low RAC, powerful propulsion system, and simple design will allow it to be extremely competitive in this year's competition.

2.0 Management Summary

2.1 Team Organization

Shown in Figure 2.1, the organizational structure consists of administrative and technical leaders. The President and Vice President are administrative leaders whose duties include goal setting, running meetings, scheduling, and purchasing. The Chief Engineer oversees the technical design of the aircraft, ensures subsystem compatibility, and spearheads the optimization process. Under the chief engineer, additional technical leaders run the Aerodynamics, Propulsion, and Structure groups. The CAD Manager is responsible for collecting drawings from each individual subgroup and maintaining the master model of the aircraft. This organizational structure helps to encourage an interdisciplinary approach, maximizing team performance and ensuring knowledge is passed down to younger members.

Colin Lenhoff
President

Matt Oehlschlaeger
Faculty Advisor

Albert Le
Vice President

Jeff Mockleman
Chief Engineer

Kevin Housley
Treasurer

Andrew Trovato
Secretary

Mike Tuccio

Aerodynamics Lead

John Bartlett
Tanzim Imam
Wilfred Chan
Heidi Shellenberger
Chris Bertram
Dan Serino
Taiyang Ma

Jeremy Styborski

Propulsion Lead

Zach Smith
Brandon Small
Matt Dawson
Kevin Housley
Andrew Trovato
Albert Le

Peter Finigan

Structures Lead

Nicole Gagnon
Mike Beyar
Ian Curtis
Freddie Wang
Chris Bertram
Alex Austin
Zach Roebuck

Peter Finigan

CAD Manager

Figure 2.1: Team Organization Chart

2.2 Milestone Chart

		Sept	Oct	Nov	Dec	Jan	Feb	Mar	Apr
Design	167 days								
Conceptual Design	13 days								
Contest Overview	4 days								
Factor of Merit Charts	4 days								
Conceptual Design Review	1 day								
Preliminary Design	49 days								
Scoring Optimization	16 days								
Weight and Sizing	24 days								
Wing Sizing	24 days								
Airfoil Selection	24 days								
Motor Selection	16 days								
Prop Selection	19 days								
Battery Selection	19 days								
Rules Change Deadline	0 days			◆ 10/31					
Electronic Submission Deadline	0 days								
Preliminary Design Review	1 day								
Detailed Design	31 days								
CAD Model	22 days								
Static Thrust Testing	11 days								
Wind Tunnel Thrust Testing	9 days								
Prototype Component Structures Testing	18 days								
Design Review	3 days								
Build	104 days								
Prototype and Competition Plane Manufacturing	47 days								
Mill Main Components	1 day								
Mill Winglets	1 day								
Modify and Attach Main Components	6 days								
Construct and Install Door for Internal Stores	3 days								
Construct External Attachment Points and Pylons	1 day								
Install Propulsion System and Batteries	1 day								
Construct and Install Landing Gear	1 day								
Install Winglets	1 day								
Construct and Install Landing Tail	1 day								
Aircraft Structures Testing	1 day								
Build Review	1 day								
Fly	31 days								
Prototype and Competition Plane Flight Tests	7 days								
Taxi Testing	2 days								
Range Check	2 days								
M1 Competition Laps	1 day								
M2 Competition Payload	1 day								
M3 Competition Payload	1 day								
Competition Endurance	1 day								
Flight Review	1 day								
Report	181 days								
Sections Outlined	14 days								
Section Distribution	14 days								
Section Writing	85 days								
Compilation	22 days								
Editing	22 days								
Report Review	1 day								
Report Due	0 days						◆ 2/25		
Competition	2 days								4/19 ◆

Planned ▬▬▬ Actual ▬▬▬ (red) Summary ▭▭▭ Milestone ◆

Figure 2.2: Overall milestone chart.

3.0 Conceptual Design

For the 2012/2013 Design/Build/Fly Competition, there are three flying missions designed to replicate tasks that a joint strike fighter (JSF) might perform. Prior to designing the plane, it was necessary to understand each of the three missions completely to be able to formulate appropriate design requirements based on key mission elements. The scoring of each mission played a key role in determining which mission requirements were to be emphasized more in the design of the aircraft. A detailed score sensitivity analysis is outlined in Section 3.1.7. The following sections are an analysis of the competition rules coupled with the team's interpretation of these rules and subsequent translation into design requirements. These design requirements are then used to formulate conceptual designs for the aircraft. A summary of this analysis can be found in Table 3.1.

3.1 Detailed Mission Requirements

3.1.1 General Aircraft Requirements

The most important general aircraft requirement is the limitation to a 20 Amp current draw by means of a 20 Amp fuse. This significantly affects the power system requirements because less current results in less power. The plane must be of any configuration except rotary wing or lighter-than-air. The aircraft is required to be propeller-driven using an electric powered, over-the-counter motor along with unmodified, over-the-counter propellers. Batteries must be over-the-counter NiCad or NiMH cells with shrink wrap or other protection covering any and all electrical contact points. The maximum battery weight which is 1.5 pounds as specified in the mission requirements applies only to the propulsion battery pack. The radio receiver and servos must operate on a separate battery back than the propulsion system.

Both the aircraft and pilot have to be AMA legal, meaning that the max take-off gross weight of the aircraft must be less than 55 pounds. Unlike previous years, there is no limitation on the maximum size of the aircraft as enforced by a carrying case; however size is factored into the (RAC) this year. Size became the deciding factor in how large the aircraft was designed to be.

3.1.2 General Mission Requirements

The payload missions were designed to replicate duties a stealth bomber or fighter might encounter in flight. Payloads must be carried internal and external to the aircraft and secured sufficiently to assure a safe flight with no variation in the center of gravity. This indicates that internal mounts and storage area as well as external mounts must be present.

The aircraft ground roll during takeoff must be completed within a 30 X 30 foot square with no external assistance. Any take-off outside this area will count as a failed mission attempt. The landing must be a rolling landing, ruling out the possibility for a belly-lander. Flight attempt requirements include bringing the aircraft into the staging area with the payload uninstalled. Photographs of payload configurations #2 through #6 must be presented. The assembly crew member in the staging area with the aircraft is required to assemble and check the aircraft within 5 minutes. This time limit includes loading the

payload for the relevant mission. Assembling the aircraft in less than 5 minutes requires that the aircraft assemble easily and quickly, with as few tools as possible. Systems must fit together in such a way that one person could perform the task efficiently.

3.1.3 Scoring

Each team's overall competition score is a combination of the Written Report Score and the Total Flight Score. The formula governing this relationship is given in Equation 3.1 and the components of the score are shown in Equations 3.2, 3.3 and 3.4. X_{MAX} and Y_{MAX} are tip to tail and span, respectively. EW is the maximum of the empty weights measured after each successful scoring flight.

$$SCORE = \frac{Written\ Report\ Score * Total\ Flight\ Score}{RAC} \qquad \textbf{3.1}$$

$$Total\ Flight\ Score = M1 + M2 + M3 \qquad \textbf{3.2}$$

$$RAC = \frac{\sqrt{EW * SF}}{10} \qquad \textbf{3.3}$$

$$SF = X_{MAX} + 2 * Y_{MAX} \qquad \textbf{3.4}$$

The Total flight Score is the sum of the three mission scores. Based on these scoring formulas, it is extremely important to have a small, light aircraft, as this will yield a higher score. Each individual mission scoring formula will be outlined in the relevant section pertaining to that mission.

3.1.4 Mission 1: Short Takeoff

Mission 1 is designed to evaluate the speed and takeoff capabilities of the aircraft. Teams will be required to fly the competition loop for four minutes, with no payload, and will be scored on the maximum number of complete laps the plane flies normalized by the max laps flown by any plane. The flight time is measured from the moment the throttle is advanced for the first take-off to four minutes. The last completed lap is counted as the last time the aircraft passes over the start/finish line in the air under the four minutes. The scoring formula is given as Equation3.5.

$$M1 = 2 + \frac{N_{laps}}{MaxN_{laps}} \qquad \textbf{3.5}$$

Unlike previous years, the size of the takeoff area is limited this year to a 30 x 30 foot square. The mission implies a fast, powerful plane with high lift characteristics. For speed, drag must be minimized and thrust maximized. An aerodynamic design that minimizes protrusions (i.e. servos) along with a high power propulsion system can achieve this. For the short takeoff, high lift airfoils must be selected for the wing and body. These will produce more lift at the slow takeoff speeds ensuring liftoff is achieved within the prescribed area.

3.1.5 Mission 2: Stealth Mission

Mission 2 is designed to simulate a stealth aircraft carrying internal missiles. The mission consists of a three lap flight carrying as many internal stores as possible, with a minimum of four stores. Each

store is an Estes Mini-Max rocket. The rockets must each be ballasted to .25 lbs. The CG of each rocket is not specified and therefore can be set when each rocket is ballasted. The rockets measure 9 inches long and the tail fins are 1.875 inches from inboard to outboard edge. The stores must be oriented in the direction of flight. They are to be installed through the bottom of the aircraft such that they could be released down one at a time. This requires that the fuselage of the plane be at least 3.75 inches thick, making some aircraft configurations more appealing than others. The stores have to be mounted via a permanent structure and cannot be in contact with one another or with any part of the aircraft (except for the mounting structure). The stores must be mounted by the body of the rocket, which means they cannot be mounted by the fins. An external fairings or blisters must be a permanent part of the design; they cannot be specially added for this mission. The mission is scored based on the number of stores flown normalized by the maximum number of stores flown by any team. The relationship can be seen in Equation 3.6.

$$M2 = 4 * \frac{N_{stores}}{MaxN_{stores}}$$ **3.6**

In order to maximize the score for Mission 2, the plane must carry as many stores as possible. Due to the irregular shape of the rockets, their internal arrangement will be vital to minimizing the size of the aircraft. The mission is not timed so the speed of the aircraft does not play a role in the mission scoring.

3.1.6 Mission 3: Strike Mission

Mission 3 is designed to simulate a fighter that is carrying some random configuration of weapons. These weapons will be simulated by a random mix of internally and externally stored Estes rockets. When teams enter the assembly area, they will roll a 6-sided die to determine their configuration. The internal stores have the same requirements as from mission 2. The external stores must be mounted on wing pylons with no parts submerged in the plane. The rocket fins have to be below the trailing edge of the lower surface of the wing and the mounting points must secure the rocket by its body. Pylons can be removable and if so, their weight will not be included in empty weight. The external stores cannot block the deployment area of the internal stores. Spacing of the stores must be at minimum 3 inches store-to-store, measured from the centerline. Additionally, the innermost stores must be at least 3 inches from the aircraft centerline. These requirements require all external stores to be below the aircraft and offset from the center.

The scoring is calculated based on how quickly the team can fly when loaded in the given configuration normalized by the fastest time. Therefore, speed is important as is the ability to carry the maximum number of stores in any given configuration, that being two on each wing and 4 internally (as given in Mission 2). Being as there are 3 possible rockets to be carried externally, the mounts must be designed such that none of these rockets exceeds the set requirements above. The scoring relationship for Mission 3 is displayed in Equation 3.7.

$$M3 = 6 * \frac{FastestTime}{TeamTime}$$ **3.7**

Being as speed it the determining factor for the Mission 3 score, it will be imperative to design aerodynamic pylons with minimal size and weight. This will reduce drag increase speed.

3.1.7 Scoring Sensitivity Analysis

A sensitivity analysis was performed using the scoring equations from the competition rules to gain an understanding of how different aspects of the plane's performance affect its overall performance. Some of the results from this analysis are shown in Figure 3.1, where Ymax and Xmax are the plane's maximum dimensions in the span and flight directions, respectively.
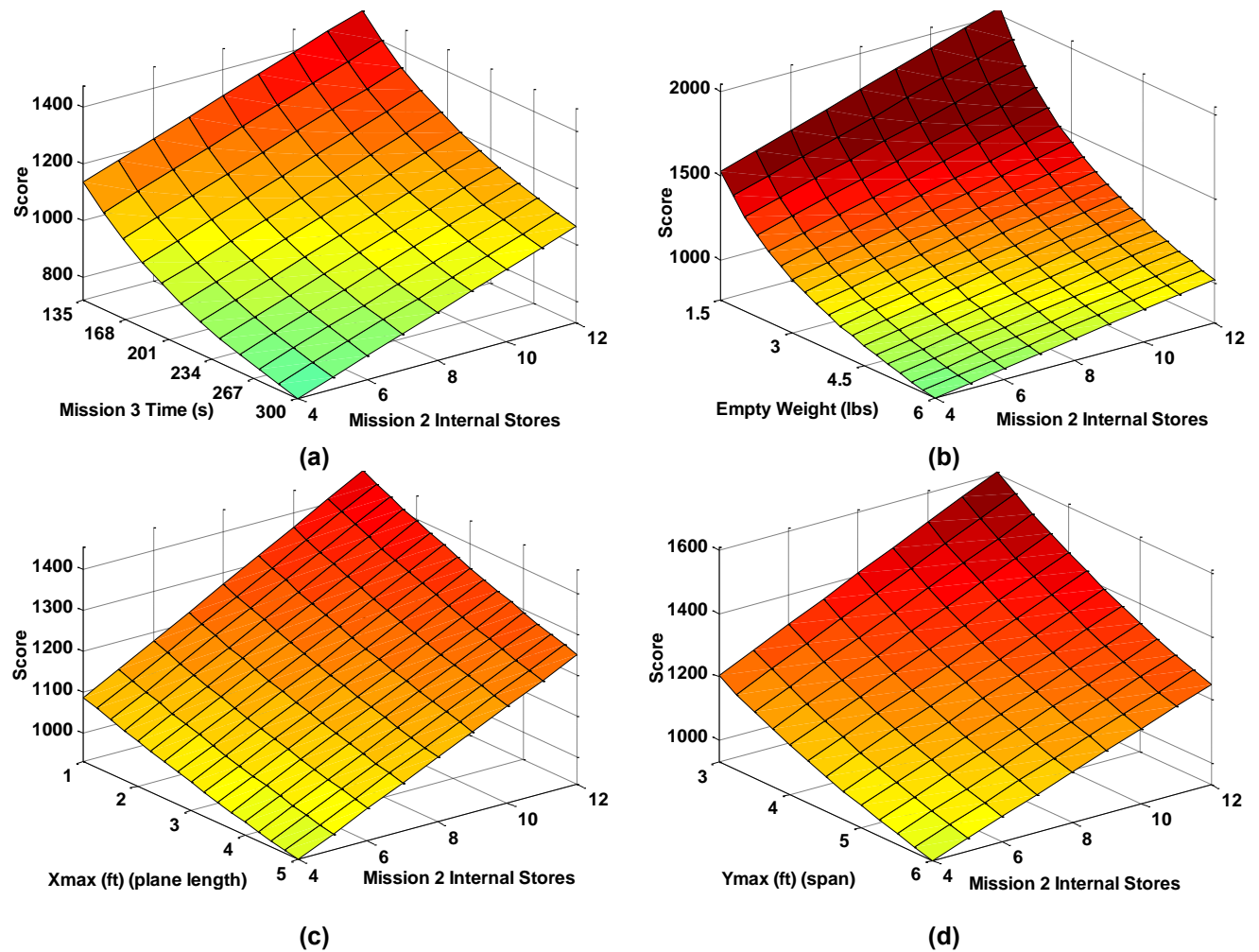

Figure 3.1: Scoring sensitivity with varying mission 2 internal stores and (a) mission 3 time, (b) empty weight, (c) Xmax, and (d) Ymax.

For the analysis, expected values were used for the max laps, internal stores, mission time, report score, and empty weight. The sensitivity plots show that there is a linear relationship between score and Xmax, Ymax, mission 2 internal stores, and mission 1 laps (not shown) and a quadratic relationship between empty weight and mission 3 time. The analysis showed that empty weight was the

most important factor with the second most important factor being shared between mission 2 internal stores, mission 3 time, and Ymax.

3.2 Design Requirements

Table 3.1: Summary of design requirements.

Mission Requirement	Effect on Plane Solution	Approach to Problem
General Aircraft Requirements		
Max battery weight 1.5 pounds	- Power system optimization	- Number of cells and size of pack(s) must be optimized to accommodate each mission
RAC is a function of empty weight, and size factor (wingspan & length)	- Weight minimized within payload constraints - Minimize aircraft footprint - Minimize wingspan and tip to tail length of plane	- Simplify and justify each component of aircraft. - Maximize lift produced for given length/span footprint - Low Aspect Ratio
Combination of internal and external payloads	- Must have payload storage area(s) and external hard points	- Package internal stores into aerodynamically functional body - Locate payloads to reduce spanwise loading.
All payloads must be secured	- Must have restraint systems for internal and external rockets	- Integrate restraint systems with plane structure to reduce weight and volume - Have removable pylons for external payloads
Aircraft will use ground rolling take-off and landing	- Plane must be able to reach take off velocity - Structural hard point required for landing gear	- Optimize the propulsion system and airfoil to take off quickly - Integrate structural hard point with pre-existing hard points, such as for landing gear
Aircraft must take-off within 30 ft x 30 ft square	- Critical wing area required - Powerful propulsion system	- Minimize the weight of the plane, and maximize the CL - Test the propulsion system for sufficient power
Assembly and loading in less than 5 minutes by 1 person	- Payload mount points must be easily accessible - Payload must be easy and efficient to load	- Use quick attachment methods for external payloads. - Design accessible payload area and restraint system which works quickly
Mission 1: Short Take-off		
4 minute flight	- Power system optimization	- Select & test batteries for 4 minutes at nearly full-power
Scored on number of complete laps	- Fast plane - Low drag - High power - High maneuverability for tight turning	- Aerodynamic design to reduce parasitic drag - Optimize propulsion system
Mission 2: Stealth Mission		

Fly 3 laps, untimed	- Propulsion system must handle weight of payload for 3 full laps - Take off within 30ft when loaded	- Optimize propulsion system and aerodynamics for loaded flight
Payload: Team selected quantity of De Estes Mini-Max rockets (.25lbs each), carried internally to plane, secured.	- Maximize payload to RAC ratio - Permanent internal restraints must be of optimal weight	- Dimension the fuselage to fit the payload without hindering aerodynamic performance - Balance the payload to keep CG centered - Use wingtip devices to reduce induced drag
Payload must be secured and positioned such that they "could" be released "down" one at a time.	- Access must be via underside of the aircraft - Restraints must conform to contest rules	- Space payloads to be independently releasable - Make flush doors continuous with underside of aircraft
<td colspan="3" align="center">**Mission 3: Strike Mission**</td>		
Fly 3 laps, untimed	- Propulsion system must handle weight of payload for 3 full laps - Take off within 30ft when loaded	- Optimize propulsion system and aerodynamics for loaded flight and short take-off
Random combination of internal and external, asymmetrical payload of rockets. All weigh 3 pounds.	- Additional roll and yaw stability concerns - External restraints must accept all types of rockets	- Simple, universal external mounts - Stability and control calculations take into account moments caused by payload - Use wingtip devices to reduce induced drag

3.3 Review of Conceptual Designs

After evaluating the competition rules and determining design requirements, the team began the process of conceptual design. Several brainstorming sessions were held to come up with the different possible configurations that the team wanted to evaluate for this aircraft. The team analyzed different aircraft types, materials, payload attachment methods, stabilizer configurations, and landing gear configurations. The different configurations were then evaluated using factor of merit charts to determine the final configuration for the aircraft. Each chart contains the different configurations considered, the factors for which they were evaluated, and the weights. The weights were determined by looking at how strongly each factor affected the mission score and RAC. Factors that had a stronger effect were weighted higher.

3.3.1 Aircraft Configuration

The overall aircraft configuration had to be flexible enough to allow for internal and external stores to be loaded quickly and securely. The configuration also needed to be stable and efficient enough to carry a relatively bulky load while maintaining a small planform. Finally, an aerodynamically efficient configuration would allow for fast lap times and short takeoff ability.

Configurations

- **Conventional:** An aircraft configuration with a wing, distinct fuselage, boom, and rear tail. This type of aircraft is easy to design and build and provides the most design flexibility.
- **Blended Body:** This configuration features a single wing/body and can have a rear tail. The blended body has less drag, added lift from the fuselage, and better aerodynamic performance.
- **Flying Wing:** A configuration that features a large, thick wing which also serves as a fuselage. It has no tail. This is the most aerodynamically efficient design.
- **Canard:** An aircraft configuration with a wing, fuselage, and forward canard surface. A canard design is flexible and provides some aerodynamic advantages.
- **Tandem Wing:** This aircraft configuration consists of a fuselage with two lifting surfaces. This design is similar to conventional and canard airplanes but may allow more lift for a smaller span.

Factors

- **Weight:** A light weight aircraft will takeoff quicker because there is a larger amount of excess lift and power that can be used for take-off (all Missions). Low system weight will also result in the ability to hold more stores (Mission 2) and a lower RAC, which increases the overall score. This was deemed the most important factor since it strongly affects both RAC and mission score.
- **Size:** A smaller aircraft has a lower RAC and it tied into reducing drag and weight. Those three things all make this a very important factor.
- **Drag:** An aircraft configuration with low drag will be able to take off sooner (all Missions) due to the excess power available fly faster (Missions 1 & 2). This can significantly increase flight score.
- **Stability:** The overall flight stability of the aircraft. A stable and easy-to-fly plane is essential for our pilot to complete the flight course.
- **Manufacturability:** The purpose of this factor to analyze how easy any given design is mainly to build, but also to repair.
- **Assembly:** This factor concerns the ease with which the payload can be stored and loaded into the fuselage and how quickly the aircraft can be put together on the flight line.

Table 3.2: Aircraft configuration.

Aircraft Configuration		Conventional	Blended Body	Flying Wing	Canard	Tandem
Factor	Weight	Scoring				
Weight	0.35	0	1	-1	0	0
Size	.25	-1	1	0	-1	0
Drag	0.1	0	1	1	0	-1
Stability	0.1	1	0	-1	0	0
Assembly	0.1	0	0	1	0	0
Manufacturability	0.1	0	-1	-1	0	0
Total	1	0.1	0.5	-0.35	-0.25	-0.1

The team selected the blended body configuration based on the results of the factor of merit analysis shown in Table 3.2. It was decided by the design team that the blended body would be able to carry internal payloads in the lightest manner possible since it didn't require a separate fuselage. Similarly, the blended body also scored high for size since even payload carrying components could be used to create lift. Finally, the blended body was assumed to cause minimal drag since there would be no fuselage or tail. While it was not thought to be the best for stability, assembly, or manufacturability, its exceling features in the more heavily weighted categories made it the strongest configuration.

3.3.2 Stabilizer Configuration

Although a blended body configuration doesn't require horizontal stabilizers, it could still have vertical stabilizers. The vertical stabilizer configuration serves to keep the airplane stable in yaw but should also be easily manufactured and aerodynamically efficient (low weight and drag). Feasible locations for vertical stabilizers included the wingtips and the center rearward section of the body.

Configurations

- **None:** A blended wing body with no vertical stabilizers would essentially be a wing and would leave the plane without effective yaw stability or control.

- **Winglets:** This configuration features two vertical stabilizers at the wingtips of the airplane. The main benefit of winglets would be induced drag reduction. The effectiveness of stabilizers far from the center of the airplane was uncertain.

- **Central Stabilizer:** Characterized by a relatively large 'plate' at the aft center of the body, a central vertical stabilizer would be effective at controlling the airplane's yaw.

- **Winglets and Central Stabilizer:** This configuration combines both positive effects of the winglets and the central stabilizer but implies additional weight.

Additional Factors

- **Effectiveness:** Effectiveness is concerned with how stable and controllable in yaw a vertical stabilizer (or lack thereof) would allow the airplane to be. Since an uncontrollable plane could not complete the missions, this was very important for score.

Table 3.3: Stabilizer Configuration.

Stabilizer Configuration		None	Winglets	Central Stabilizer	Central Stab. and Winglets
Factor	Weight	Scoring			
Effectiveness	0.5	-1	0	1	1
Weight	0.15	1	0	0	-1
Drag	0.15	0	1	-1	1
Assembly	0.1	1	0	0	0
Manufacturability	0.1	1	0	0	0
Total	1	-0.15	0.15	0.35	0.5

The team selected both a central stabilizer and winglets as revealed by Table 3.3. It was determined that a central stabilizer was necessary in order to have the greatest stability and control in yaw. Winglets were also favored since they would allow overall drag reduction. Additional weight was considered but was ultimately deemed a necessary cost.

3.3.3 Landing Gear Configuration

The aircraft must be able to make a successful, damage free landing on each mission. The landing gear must provide adequate ground maneuverability, ground clearance and damage protection while remaining lightweight. Three different landing gear configurations were considered.
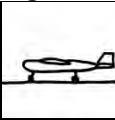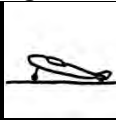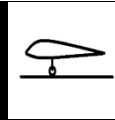
Configurations

- **Tricycle:** This configuration has a single long front wheel near the nose of the aircraft and a pair of rear wheels. It is a lightweight system and is easy to land the aircraft on.
- **Tail Dragger:** A set of two wheels is located near the front of the plane and a small wheel is attached at the back of the tail boom. The system is lightweight and easy to land on.
- **Central Wheel:** This configuration consists of a single central wheel embedded in the fuselage. The tread of the wheel would lie between 0.5" to 1" below the bottom of the fuselage and the plane would have to balance on this for takeoff and landing.

Additional Factors

- **Damage Protection:** This factor represents a measure of the ability of the system to protect it from damage on landing. Any damage taken during landing negates an otherwise successful flight attempt.
- **Ground Maneuverability:** The ease of handling the aircraft on the ground before takeoff and after landing.

Table 3.4: Landing Gear Configuration.

Landing Gear Configuration		Tricycle	Tail Dragger	Single Central Wheel
Factor	Weight	Scoring		
Weight	0.3	-1	0	1
Damage Protection	0.2	1	1	-1
Drag	0.1	-1	-1	1
Manufacturability	0.1	0	0	1
Ground Maneuverability	0.3	1	0	-1
Total	1	0.1	0.1	0

Both the tricycle gear and tail dragger configurations were chosen by the design team as shown in Table 3.4. The high clearance of both configurations was an attractive feature. Although both caused more drag than the central wheel, both allowed for safer landings and propeller clearance. It was at this point in the design process that the team decided that a prototype would be constructed as a preliminary

proof-of-concept. One main test point would be the landing gear configuration. Later on, the tail dragger configuration proved to be unpredictable and difficult to handle on the ground due to the relatively short distance between the front and tail wheels. This confirmed the tricycle landing gear as the configuration to be used in the final airplane.
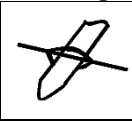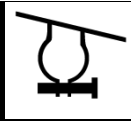
3.3.4 Payload Attachment

The rules dictate that the stores must be carried facing in the direction flight secured to a permanent mounting structure. They must not contact each other or any part of the aircraft except for the mount. The mount must hold the stores by their body. Finally, they have to be held such that they "could" be able to attach securely to the aircraft and be restrained as if they could "drop down." The attachment methods must be strong in order to endure take-offs and landings yet they must also be quick and easy to deal with so that stores may be loaded quickly and fluidly. 3 different attachment methods were considered.

Configurations

- **Rubber bands and Balsa:** A balsa spar across the internal section would have rubber bands hung on it that would wrap around the rocket bodies.
- **Velcro and foam slots**: The rockets would fit into tightly milled foam slots and be held in via Velcro.
- **Nut and bolt clamp:** Clamps would be glued to the foam and screws would be used to tighten them around the rockets

Table 3.5: Passenger configuration.

Passenger Configuration		Rubber bands	Velcro	Clamp
Factor	Weight	Scoring		
Weight	.5	0	0	-1
Assembly	.3	0	1	0
Size	.2	1	1	-1
Total	1	.2	.5	-.7

The Velcro and foam slots method was chosen to attach the internal payloads.

3.3.5 External Payload Attachment

The external stores must be held similar to the internal stores in that they have to be facing in the direction of flight. Additionally, the fins cannot be above the trailing edge of the wing and they must be spaced 3" apart center to center. Finally they must not block the "bay doors". This in mind, 3 different attachment methods were considered.

Configurations

Kenex mounts: Mounts would be made out of kenex that were a tight fit on the rocket bodies and attached to the foam.

Ethernet ports: Female ends of Ethernet ports would be permanently inserted into the bottom wing and the male ends could be attached to rocket mounts and click in.

Backpack Clips: Female ends of clips will be inserted into the bottom of the wing and male clips will be attached to pylons that will hold the body of the rocket.

Table 3.6: Passenger configuration.

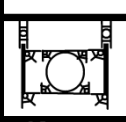| Passenger Configuration		Kenex	Ethernet	Clips
Factor	Weight	Scoring		
Weight	.5	0	0	1
Assembly	.3	-1	1	1
Drag	.2	0	1	0
Total	1	-.3	.5	.8

Backpack clips were chosen as the method.

3.3.6 Wing Structure

Since the chosen airframe is a blended body, the airplane lacks a need for structure to support connections between the wing, tail and fuselage. Therefore, most structural considerations centered on how to adequately support a thick central body section and the tapered wings attached to it. Similarly, space for an internal payload bay was also taken into account. The structure of the plane must be able to provide this space as well as support any external payloads. The airplane should also must be lightweight yet adequately withstand aerodynamic forces. Four construction methods and materials were considered.

Configurations

- **Balsa/Monokote:** This configuration consists of a laser-cut balsa wood skeleton covered in monokote skin.

- **Composite:** This construction method involves creating a fuselage mold and epoxying fiberglass or carbon fiber over the mold. The mold is then removed leaving a strong, lightweight exoskeleton.

- **Plastic:** In this configuration, plastic is heated, shaped and wrapped around a foam mold to create a shell. The mold is then dissolved away leaving a strong, shell.

- **Foam:** This construction method involves milling a sheet of residential insulation foam to the correct airframe shape and then cutting away sections for internal stores and infrastructure.

Table 3.7: Wing Material.

Fuselage Material		Balsa/Monokote	Composite	Plastic	Foam
Factor	Weight	Scoring			
Weight	0.25	1	1	1	0
Manufacturability	0.35	0	-1	-1	1
Assembly	0.15	-1	1	1	1
Durability	0.25	-1	1	1	0
Total	1	-0.15	0.3	0.3	0.5

The team chose foam, as shown by the results of Table 3.7. Since a foam plane could be constructed quickly and simply, it was easily the favorite. Weight was somewhat of a concern so the team resolved to cut out structurally insignificant portions as to lighten the airplane. The prototype built of foam in the fall semester proved to be durable and highly manufacturable.

3.4 Conceptual Aircraft Summary

The final conceptual configuration is a single-engine blended wing body to minimize the size factor. For manufacturability it is milled out of foam. Internal stores are held via foam restraints and arranged side by side, offset slightly to allow for tail fins to fit. There is vertical stabilizer as well as winglets. A tricycle landing gear is mounted under the fuselage. The motor configuration was determined in preliminary design based on the results of the scoring optimization.

4.0 Preliminary Design

During the preliminary design, the sizes of the plane's major aerodynamic components were optimized for the maximum flight score. An optimization routine was created that utilized given propulsion and airfoil characteristics to produce the sizes. This approach allowed airfoil and propulsion system choices to be checked by running the routine multiple times with varying inputs because the routine made performance and scoring predictions.

4.1 Design and Analysis Methodology

The goal of the preliminary design analyses was to achieve the highest possible score from the scoring formulas. To achieve this goal, the optimization routine was coded and used extensively. It was based on theoretical equations and the scoring formula. While the routine was being created, three major groups (Aerodynamics, Propulsion, and Structures) created the input needed for the routine. Inter-group communication was emphasized due to the interdependence of the different aspects of aircraft design. Individual group design methodologies are described in general below.

Propulsion

The requirement of a short takeoff and importance of lightweight, fast plane, as established in the sensitivity analysis, made propulsion a primary design point. A propulsion system allowing an estimated plane with the mission 3 payloads to takeoff in 30 feet and exhibiting a minimum mass was the goal. With the optimization routine, multiple configurations could be explored. This allowed the performance/weight trade-off to be accounted for.

Airfoils

The decision to vary the airfoil along the span was made for desired stability characteristics. The conceptual construction technique decision enabled this. The conceptual design configuration provided constraints for the types of airfoils needed. A survey of many airfoils eventually led to a list from which the final choices were selected based on the airfoils' lift, drag, pitching requirements, and zero lift angles.

Wing

The wing' design and sizing was heavily coupled with the propulsion system and airfoil selection. The wing sizing depended on the weight and power of the propulsion system, the airfoil drag and lift properties, and meeting the 30 foot takeoff requirement. Within structural constraints, the aerodynamic needs were balanced with scoring considerations to determine the final wing sizing of maximum score.

Fuselage

The fuselage comprised of thicker airfoil section of the wing and sized to the minimum size needed for the number of internal stores carried.

Tail and Control Surfaces

These were sized based on stability and control analysis and pilot preferences.

Winglets

Winglets were designed through an experimental approach by testing designs on a prototype.

4.2 Mission Model and Methodology

The mission model presented in this section was used in all optimization analysis and in the final performance estimates. The flight course layout (Figure 4.1) was broken into several different sections, each of which is presented below. Instantaneous acceleration was assumed for all parts except takeoff and landing. This assumption was validated because it was used for all plane configurations considered. Thus the optimization analysis still had a clear picture of better and worse designs.
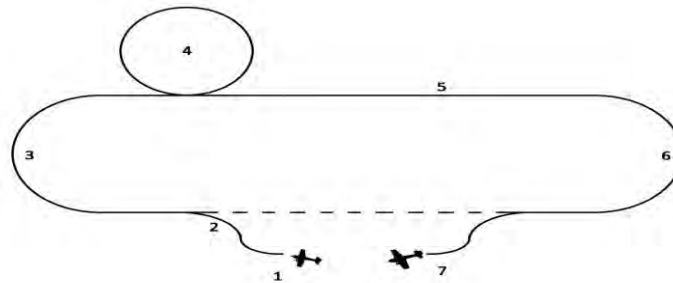
Figure 4.1: Flight course layout.

Takeoff (1)

The takeoff within the 30 foot square is one of the most difficult parts of the flight course. Several factors affect the ability of the aircraft to accomplish this requirement. High maximum lift coefficients allow the aircraft to produce more lift and takeoff sooner. More thrust production and less drag increases the acceleration of the aircraft. Additional weight increases the ground roll. These factors were combined into a differential equation (Equation 4.1) that was solved to determine the takeoff distance for a particular aircraft configuration. Lift and drag were calculated from airfoil data and empirical equations. Propulsion data was obtained through testing. Ground effect was neglected to create a small safety factor.

$$\frac{dV}{dt} = \frac{g}{W_{TO}} * \left(T(V) - .5\rho_{To}V^2 \left(f_{To} + S_{wing} \frac{C_{L_{To}}^2}{\pi * e * AR} - \mu_k S_{wing} C_{L_{To}} \right) - \mu_k W_{TO} \right) \tag{4.1}$$

Climb (2)

The initial climb out of the takeoff is based on the available excess power (Equation 4.2). The time to climb is calculated based on this rate and a cruise height of around 100 feet.

$$\frac{dh}{dt} = \frac{V(T - D)}{W_{TO}}$$

4.2

Turns (3,4,6)

An aircraft turning velocity of 60% of the cruise velocity was used because the aircraft's low aspect ratio causes it to lose a lot of speed in turns. The turning radius was based on a constant load factor (Equation 4.3). The turning radius and velocity are used to calculate the flight time through the turn.

$$R = \frac{V^2}{g\sqrt{n^2 - 1}}$$

4.3

Cruise (5,7)

Cruise analysis is based on straight, level, unaccelerated flight at a power setting less than full to ensure optimal battery performance. The mission time during cruise sections can be calculated from the aircraft velocity shown in Equation 4.4 and the distance traveled. The distance at Station 7 is shorter on the landing lap.

$$Cruise\ Velocity\ when\ Thrust = Drag$$

4.4

Landing (7)

A smooth, slow landing is required to ensure zero to minimal damage. The landing is modeled the same way as the takeoff, except the thrust values are set to zero.

4.3 Propulsion System Design and Analysis

Analysis of this year's rules unveiled propulsion system requirements. This placed an emphasis on a light system to decrease the plane's RAC. Requirements from specific missions are as follows:

- Mission 1 requires continuous high power for the duration of the 4 minute flight. As this is the longest of the 3 missions, a minimum battery capacity was dictated. A propeller efficient at high speeds is necessary to produce the maximum thrust out of a given battery and motor system. The propulsion system must also be powerful enough for the empty airplane to takeoff in 30 feet.

- Mission 2 requires the plane to complete three laps with no set time. A lighter propulsion system may help increase the score by allowing the plane to carry more internal stores. Lower power settings than the other missions can be used to reduce battery weight and achieve a better score.

- Mission 3 is based on flight time. Similar to mission 1, this requires continuous high power. Mission 3 includes payload, requiring a propeller with more thrust during takeoff than mission 1. However, this propeller must also produce a large amount of thrust at high speeds.

4.3.1 Fuse Analysis

The 20A fuses were optimized to operate at the maximum current that could be handled for the required 4 minutes of flight. Figure 4.2, from the manufacturer LittleFuse, Table 4.1 shows the blow times for blade fuses. Using an ammeter and a stopwatch, fuse blow time tests were done.
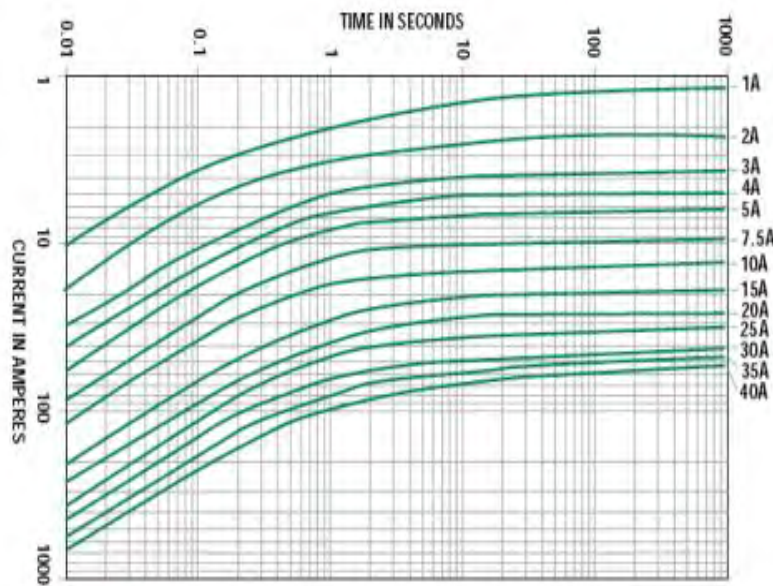
Figure 4.2: Fuse Blow Times

Table 4.1: Measured Fuse Blow Times

Trial	Amperage (A)	Blow Time (min:sec)
1	30	<0:01
2	28	0:03
3	28	0:02
4	27	2:35
5	27	1:58
6	26	8:50
7	26	9:32

The results showed that the 20A blade fuses can withstand 26 amps for the required 4 minute duration. This is within the limit in the manufacturer's data. The propulsion system was designed to draw a maximum current of 25A. All propulsion system components were chosen to have at least a 25A rating.

4.3.2 Battery and Motor Selection

Based on mission 1's 4 minute flight, the battery pack was required to have a minimum capacity of 1600 mAh. The batteries must handle 25 amps to be drawn without damaging the cells. A final consideration was the number of motors to be powered by the battery pack(s).

At first, a single motor configuration was assumed for the battery selection process because of the resulting simple design. Since the blended body aircraft has a swept leading edge, the dual motor configuration required extensions to hold the motors away from the plane to prevent the propeller from striking the plane. Although this would increase velocity, it adds weight, complexity, and drag. Therefore, the single motor configuration was chosen. Thus, the system could use a single battery pack and electronic speed control (ESC).

A goal of 100 Watts per pound was established to get the desired performance. Using a predicted plane weight of 7.5 lb, the goal became 750 watts. To supply this at 25A, 30 volts are required from the batteries. With most practical NiMH battery cells weighing roughly an ounce and supplying 1.2 Volts per cell, it was foreseeable that a battery pack weighing the maximum of 24 ounces could be necessary.

A table of practical batteries was compiled. Measurements on actual capacity and voltage per cell were taken for all cells purchased. In general, Tenergy cells tended to have a capacity and voltage equal to the advertised values. Elite Cells tended to have a starting voltage of 1.4 volts per cell and a capacity

roughly 112% of the advertised value. These values are shown in Table 4.2. The results for voltage were vindicated by a discharge curve found online and are shown below in Figure 4.3
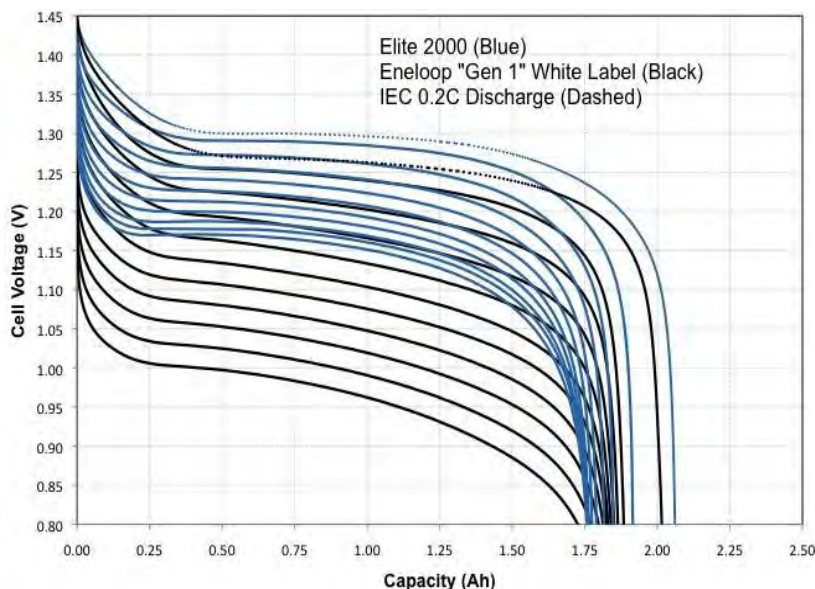
Figure 4.3: Elite 2000 Discharge Curves

Table 4.2: Battery Specifications

Battery	Advertised Capacity (mAh)	Actual Capacity (mAh)	Weight (oz)	Maximum Cells	Advertised Maximum Voltage (V)	Actual Maximum Voltage (V)	Ideal Maximum Power (W)
Elite 1500	1500	1680	0.81	29	34.8	40.6	1015
Tenergy 1600	1600	1670	0.71	32	38.4	38.4	960
Elite 2000	2000	2240	1.00	23	27.6	32.2	805
Elite 2200	2200	2464	1.55	15	18	21	525

All cells held a maximum current rating of 10C. However, cell testing determined that discharge rates of 12C did not impede on the overall voltage of the individual cells and barely lowered overall cell capacity (capacity was lowered by roughly 2 mAh per discharge at room temperature). Above 12C, the discharged batteries were damaged. A table of damaging currents was compiled for each cell type.

Table 4.3: Battery Current Rating

Battery	Advertised Maximum Current (A)	Actual Maximum Current (mAh)
Elite 1500	16.8	20.16
Tenergy 1600	16.7	20.04
Elite 2000	22.4	26.88
Elite 2200	24.6	29.57

A battery pack of 23 Elite 2000 cells wired in series was chosen. This allowed 32.2 volts at takeoff and could supply 25 amps continuously without cell damage. Ideally, this would achieve the target 750 watts per pound. Using three 23-cell packs (one per mission) of Elite 1500 batteries was considered since it could provide the same voltage and amperage while saving weight. However, irreparable battery damage would result from each flight. This consideration was rejected since it risked mission completion.

The decision on batteries meant that motor and ESC choices could be made. ESC's that could handle up to 34 volts are rare and therefore, choices were limited. The Castle Creations Phoenix Ice 50 High Voltage model was chosen. Although the amperage rating was unnecessarily high, it was the lowest that allowed voltages as high as 34 volts.

The battery pack affected the motor specifications. The motor needed a max voltage of about 34 volts and a designed power range between 600 Watts (expected output) and 800 Watts (ideal output). The motor's kV rating and gearing was chosen so the rpm at max voltage was less than 10,000 rpm.

Table 4.4: Motor Specifications

Motor	Weight (oz)	Continuous Power (W)	Max Power (W)	Maximum Voltage	kV (RPM/V)
Neu 1509 2Y w/ 6.7:1	7.5	750	1500	33	1820
Neu 1112 2Y w/ 6.7:1	4.7	600	1200	30	1750
Hacker B50 17S w/ 6.7:1	9.03	900	900	22	2124
Electrifly GPMG5225	5.9	425.5	830	18.1	1530

The Hacker was discounted due to its low maximum voltage and relatively high kV rating as seen in Table 4.4. The Electrifly's low maximum voltage made it undesirable. Both Neu's were purchased for testing. The Neu 1112 was chosen because the battery pack didn't provide ideal power. Section 8.1 further discusses the results of testing and the reasons that the Neu 1112 with the 6.7:1 gearbox was chosen.

4.3.3 Propeller Selection

To optimize the propulsion system for both take-off and cruise, propeller testing on a motor at speed was necessary. In the absence of a wind tunnel, a car-mounted test stand was constructed and tested each of a cache of 11 propellers. The selected propeller needed to draw a maximum current of about 25 amps to not strain the battery pack or blow the fuse. Propellers with higher thrusts at all speeds were desirable. A chart of 5 propellers is shown in Figure 4.4. Propellers were purchased from APC and tested on the Neu 1509-1820, the Castle Creations Phoenix Ice 50 ESC and a 23 cell pack of Elite 2000s.
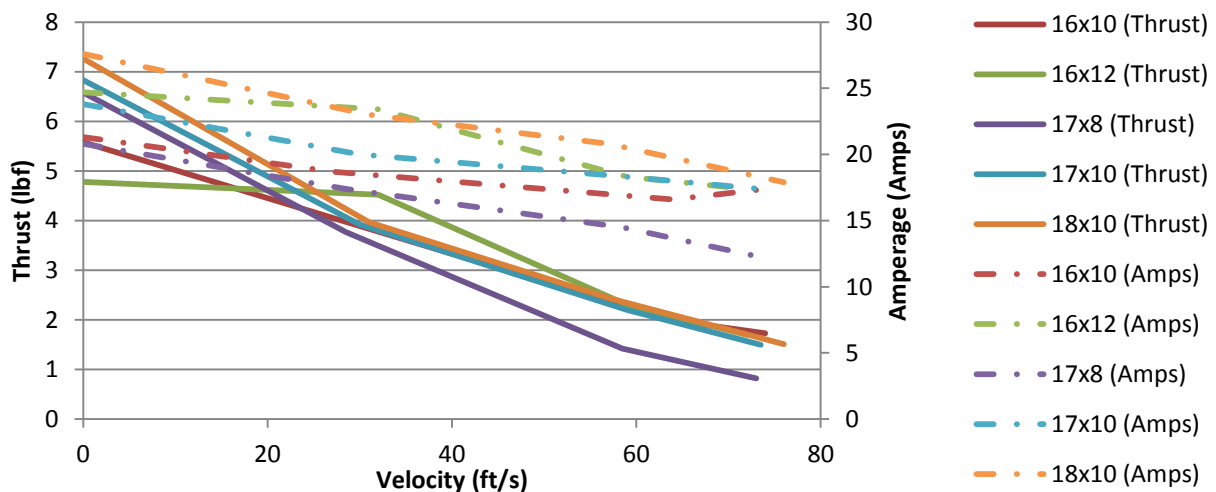
Figure 4.4: Thrust, Amperage vs. Velocity

From Figure 4.4, the 17x10 and 16x12 propellers were to be used in the competition. The 16x12 has higher thrust than all other propellers at high speeds, but lower thrust at low speeds. The 16x12 never draws more than 25 amps. It will be utilized for mission 1 where the airplane will be unloaded. Therefore, it will be able to take off quickly despite the lack of static thrust. This propeller allows the plane to achieve a higher cruise speed due to its high cruise thrust. The 17x10 offered the highest static thrust without drawing over 25 amps making it ideal for a quick takeoff with payload.

Testing the 32 Tenergy 1600 cells showed that too much current was drawn. This would blow the fuse and damage components. The test results can be seen in Table 8.1. The gear drive testing revealed that a higher gear ratio provided more thrust for takeoff and a lower gear ratio drew a current higher than the 25 amps.

4.3.4 Final Configuration

Table 4.5: Final Configuration

Component	Specification
Motor	Neu 1112 2Y w/ 6.7:1
ESC	Castle Creations Phoenix Ice 50
Batteries	(23) Elite 2000
Propeller	APC 17x10
Gear Ratio	6.7 : 1
Battery Voltage (nominal)	32.2 V
Motor Weight	4.70 oz.
ESC Weight	2.30 oz.
Battery Weight	23.45 oz.
Prop Weight	1.80 oz.
Receiver Weight	0.5 oz.
Total System Weight	32.9 oz.

4.4 Airfoil Selection

An initial airfoil downselect was completed based on specified criteria and desired performance for the wing and vertical stabilizer. An aerodynamic properties analysis was then performed for every airfoil considered and airfoil selections were made based on the importance of each factor considered.

The analysis was performed with Javafoil [2] which utilized a vortex panel method and an integral boundary layer method to generate airfoil performance data. The panel method recommended airfoils comprised of 50-100 X, Y data points. Some of the analyzed airfoils had 40-50 points which led to some anomalies in the results, most likely due to numerical errors.

Three airfoils were chosen for the wing/body; a thicker body airfoil to fit the internal stores, a thin tip airfoil to reduce the drag coefficient, and a transition airfoil to help create the desired characteristics.

Some of the desired properties for the three wing/body airfoils were a positive pitching moment coefficient (C_m), low drag, and high lift. The positive pitching moment was necessary for stability of the tailless design. Optimization analysis showed that a C_m of about .008 worked best. Additionally, washout

was desirable to obtain the best lift distribution and provide additional roll stability. Thus, the body and tip airfoil were chosen to have a zero lift angle of about -1 and 0 degrees, respectively.

4.4.1 Body Airfoil

To fit the stores and for manufacturability, a minimum thickness of 11% was chosen for the body airfoil. While also considering a high lift coefficient for a short takeoff and the positive C_m an initial pool of around 60 airfoils pulled from an online database [2] were evaluated. From the pool, three airfoils advanced: the Eppler 330, MH80, and Fauvel 14% flying wing airfoil. Using Javafoil, the team also designed a custom airfoil with 17% thickness and 2.5% camber using the Horten Brothers airfoil family.

For the angle of attack range of -5 to 20 degrees and Reynolds' number of 500,000, Javafoil generated data. The lift coefficient, thickness, and pitching moment coefficients were considered.

(a) Eppler 330
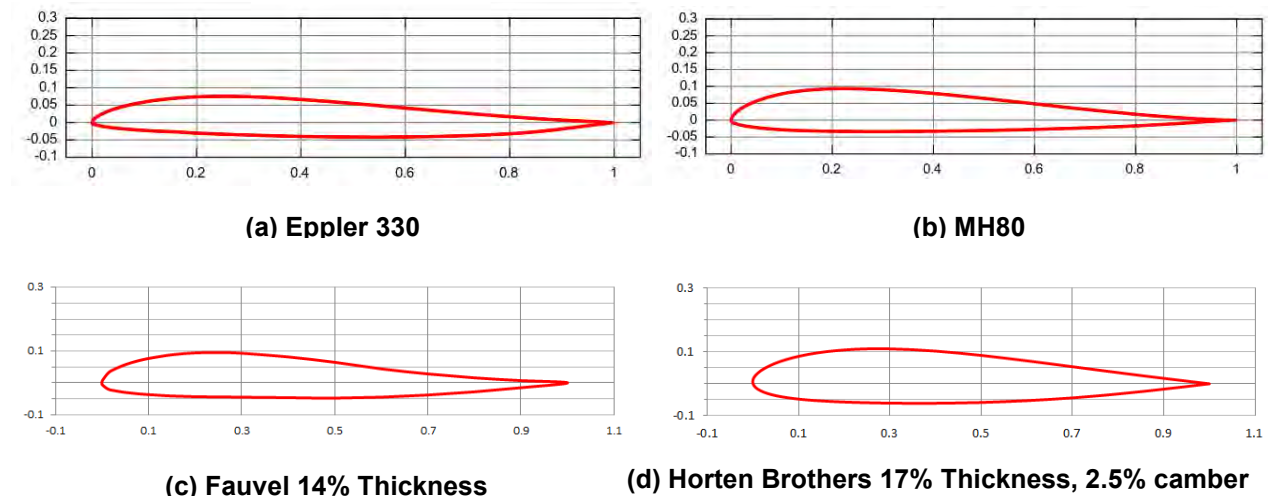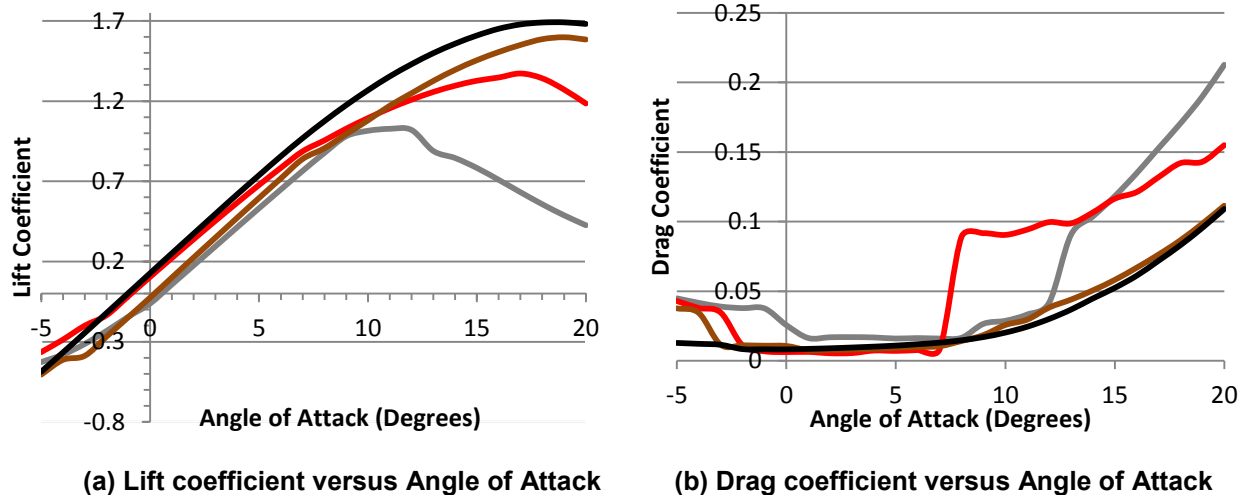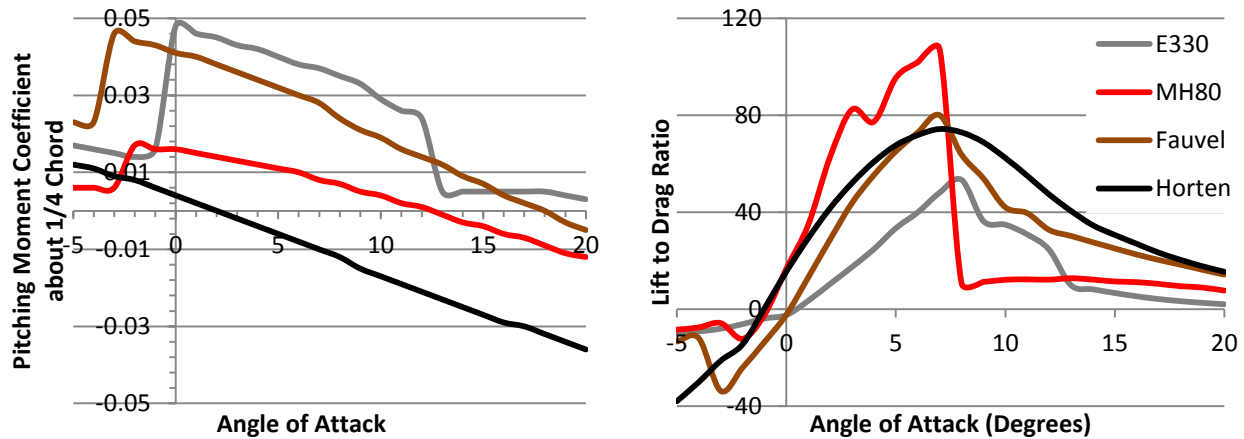
(b) MH80

(c) Fauvel 14% Thickness

(d) Horten Brothers 17% Thickness, 2.5% camber

Figure 4.5: Geometry of Considered Body Airfoils

(a) Lift coefficient versus Angle of Attack

(b) Drag coefficient versus Angle of Attack

(c) Pitching moment coefficient versus Angle of Attack   (d) Lift to drag ration versus Angle of Attack
Figure 4.6: Body Airfoil Candidate Polars

Table 4.6: Body Airfoil Candidate Properties

Body Airfoils	Thickness	Max C_L	Zero-lift angle	C_{MAC}	X_{AC}
E330	11.0%	1.03	0.5˚	.047	.264
Horten	17.0%	1.69	-1.0˚	.006	.267
MH80	12.7%	1.12	-0.5˚	.017	.259
Fauvel	14.0%	1.60	0.1˚	.033	.265

After considering aerodynamic coefficients, the Eppler 330 was eliminated because it had the lowest max lift coefficient and thinnest geometry, making it undesirable for aerodynamics and structures. From the remaining airfoils, the Horten was chosen for the body airfoil because it had the highest maximum lift coefficient of 1.69, greatest thickness of 17%, lowest drag, and the desired zero-lift angle. It's higher than desired pitching moment could be compensated for with the other airfoils. The high lift and thickness was desirable to aid in the short takeoff and fitting the internal stores, respectively.

4.4.2 Tip Airfoil

Airfoils with high maximum lift coefficients, high stall angles to avoid tip stalls, zero lift angles close to 1 degree to provide aerodynamic washout, low positive pitching moment for stability, and low drag for a fast cruise speed were gathered from an online database [2] to be considered for the tip airfoil. An airfoil with low drag and high lift would allow a smaller wing to takeoff within the prescribe area, increasing the score.

A tip zero lift angle of about zero compared to the zero lift angle of about -1 for the body airfoil would create the aerodynamic washout which is desired for an elliptical lift distribution and stability. This lift distribution results in minimal downwash and consequently induced drag. Low drag allows faster flight speeds which is important since 2 of the three missions are scored based upon speed. The desired pitching moment was now slightly lower than .008 because the body airfoil's pitching moment was higher than .008. A small thickness ratio was also a major concern because the tip chord would be large. Structurally, an unnecessarily thick wingtip was not desired.

Two airfoils fit these criteria well, the HS3412b and HS3512. A third airfoil was added as a possible structural compromise, a version of the HS3412b, but only 85% as thick as the original, creating thinner wingtips. The airfoil geometries can be seen in Figure 4.7 and the polars below in Figure 4.8.

(a) HS3512   **(b) HS3412b**   **(c) HS3412b 85%**
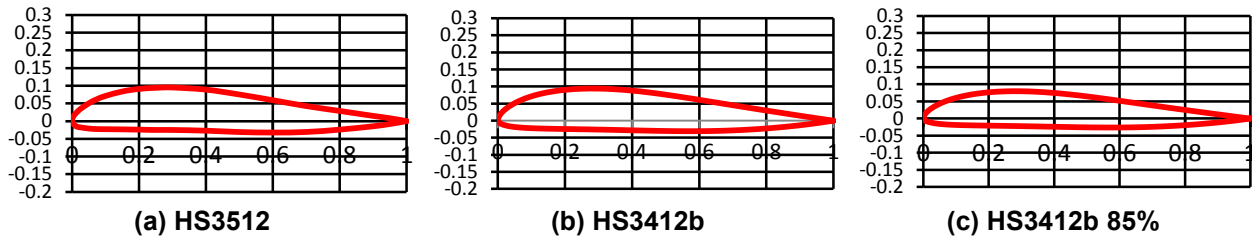
Figure 4.7: Geometry of Considered Tip Airfoils
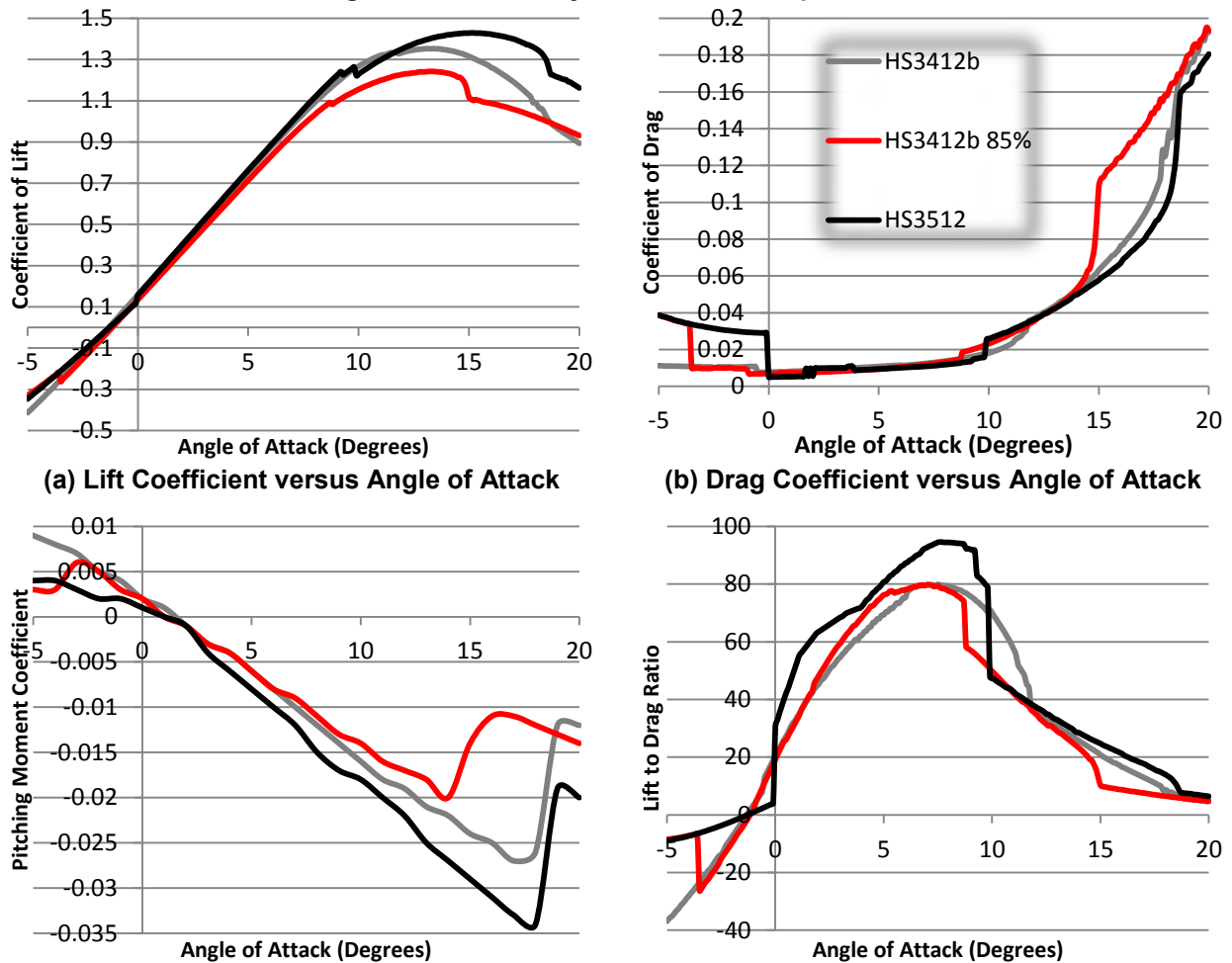
(a) Lift Coefficient versus Angle of Attack   **(b) Drag Coefficient versus Angle of Attack**

(c) Pitching Moment Coefficient versus Angle of Attack   **(d) Lift to Drag Ratio versus Angle of Attack**

Figure 4.8: Tip Airfoil Candidate Polars

Table 4.7: Tip Airfoil Candidate Properties

Tip Airfoils	Thickness	Max C_L	Zero-lift angle	C_{MAC}	X_{AC}
HS3512	12.0%	1.43	-1.29°	.004	.266
HS3412b	12.0%	1.35	-1.33°	.005	.265
HS3412b 85%	10.2%	1.24	-1.16°	.004	.264

Although the C_{mAC} of the HS3412b was closest to the desired .008 it was discarded because it produced less lift and more drag than the HS3512. Although the thinnest, the thinner HS3412b was deemed a poor airfoil because it ranked worst in lift, drag, and C_{mAC}. Thus, the HS3512 was chosen for the tip airfoil. It has a high lift to drag, but its C_{mAC} is a bit lower than desired (.004).

4.4.3 Transition Airfoil

The transition airfoil was used to connect the thick body to the thin wingtip sections. The selection process was very similar to that of the body airfoil.

A transition airfoil thinner than the body airfoil was desired because this section would not house internal stores and to help decrease thickness along the aircraft's span. Since washout is incorporated into the wing, this airfoil needed a zero lift angle between zero and negative one. For stability a C_{mAC} of .008 was again a priority.

The same airfoil pool as before was narrowed to two selections. These airfoils have a similar C_l and C_{mAC}. They both have zero lift angles in the right region. The S5020 produces slightly more lift, but at a significant increase in drag, making its lift to drag ratio inferior to the MH45. Low drag was imperative for speed. The MH45's C_{mAC} is only one thousandth lower than that of the S5020. The MH45 was chosen because it was slightly thicker, which worked better structurally with the chosen tip airfoil.

(a) Lift Coefficient versus Angle of Attack | **(b) Drag Coefficient versus Angle of Attack**

(c) Pitching Moment Coefficient vs Angle of Attack | **(d) Lift to Drag Ratio versus Angle of Attack**
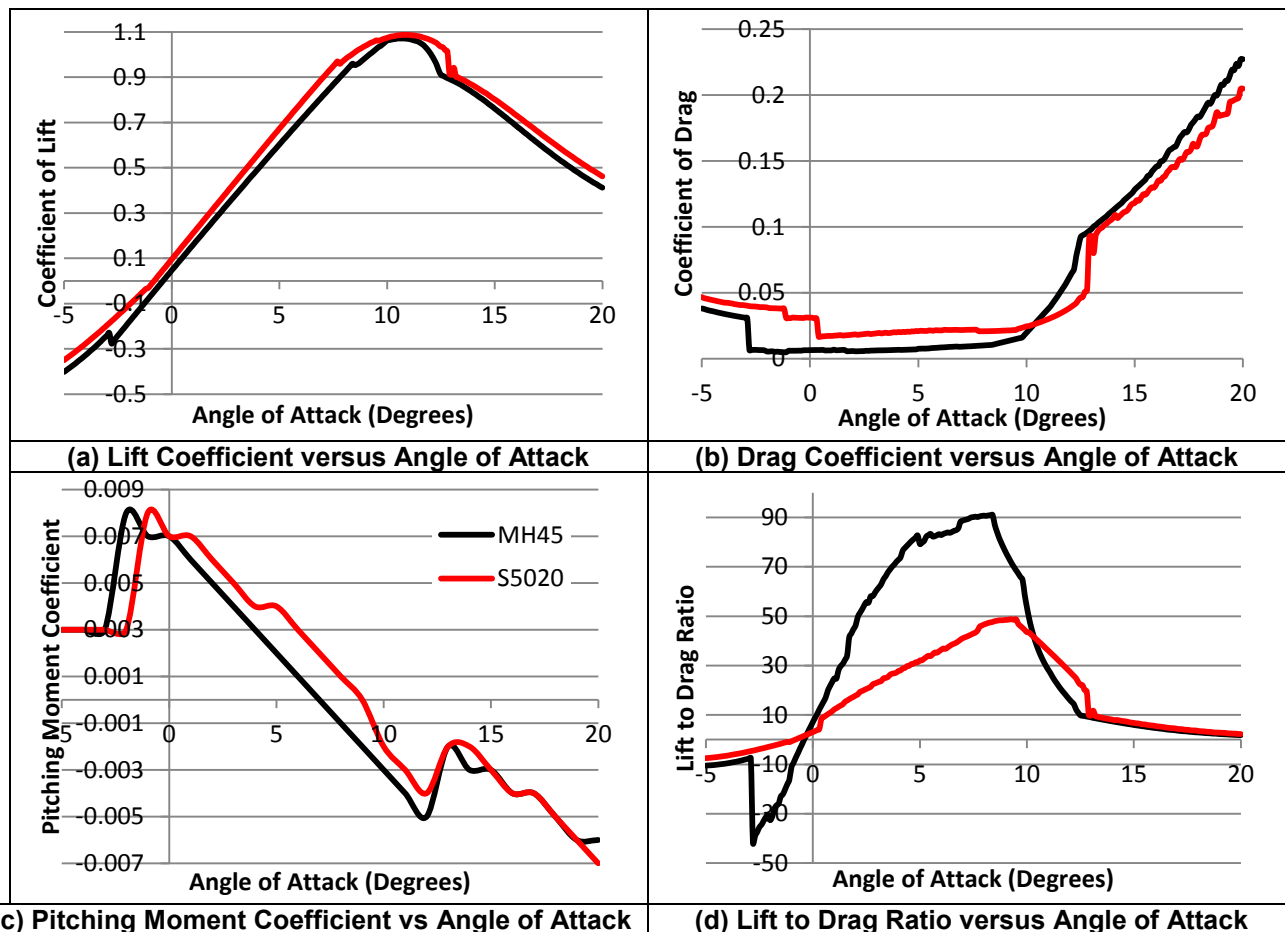
Figure 4.9: Transition Airfoil Candidate Polars

(a) S5020   (b) MH45
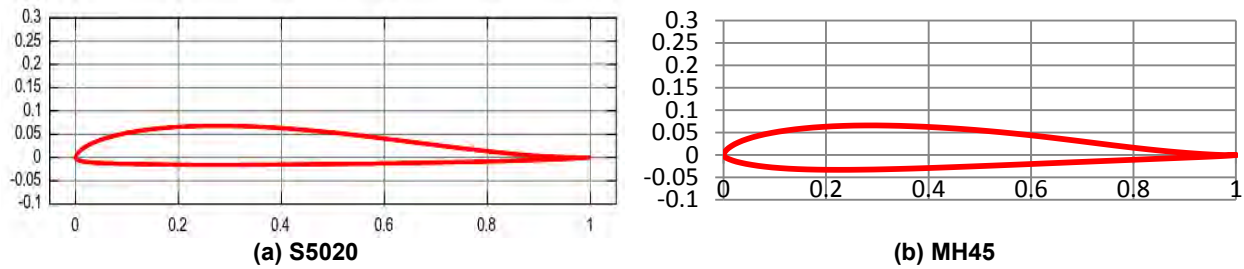
Figure 4.10: Geometry of Considered Transition Airfoils

Table 4.8: Transition Airfoil Candidate Properties

Transition Airfoil	Thickness	Max C_L	Zero-lift angle	C_{MAC}	X_{AC}
S5020	8.4%	1.087	-0.8°	.008	.257
MH45	9.9%	1.071	-0.4°	.007	.258

4.4.4 Vertical Stabilizer Airfoil

High lift, low drag and a thickness of about 10% were desired for the vertical stabilizer's airfoil. The desired thickness was an aerodynamic and structural compromise because thicker airfoils produce more drag while thinner airfoils are difficult to make strong and light. Only symmetric airfoils were considered so the vertical stabilizer provides an equal response to crosswinds from opposite directions. With these considerations, three top airfoils were selected and shown in Figure 4.12. The FX 76-100 airfoil was selected for the vertical stabilizer because it had the highest maximum lift and lowest drag.

(a) FX 76-100   (b) LWK 80-080   (c) LWK 80-100
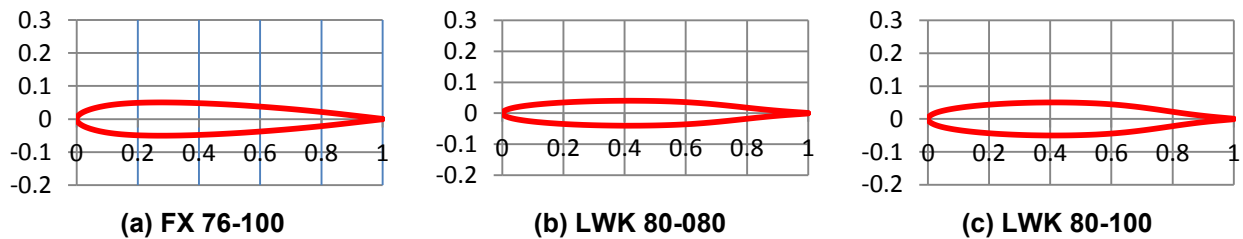
Figure 4.11: Vertical Stabilizer Airfoil Geometry
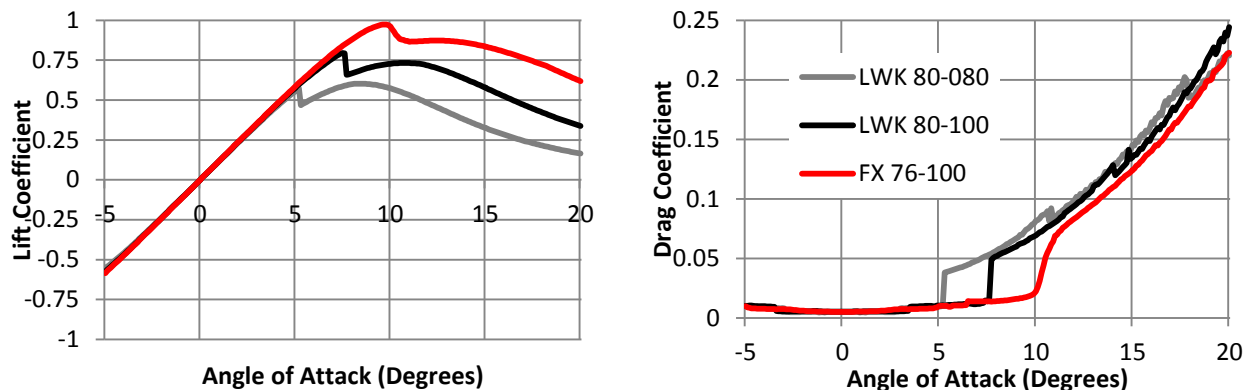
(a) Lift Coefficient versus Angle of Attack   (b) Drag Coefficient versus Angle of Attack

Figure 4.12: Vertical Stabilizer Airfoil Polars

28

4.5 Body Estimations

Required body size estimations were created for each number of internal stores considered. The estimations consisted of the length and width required to fit the internal stores within the body section's airfoil. Using 0.192 pounds per square foot and 0.018 pounds per internal store attachment, empty weight estimations were created for each number of internal stores. Table 4.9 shows selected results.

Table 4.9: Selected results of body estimations.

Internal Stores	Fuselage Empty Weight (Pounds)	Fuselage Length (Feet)	Fuselage Width (Feet)
6	0.577	1.5	0.958
7	0.636	1.5	1.042
8	0.715	1.5	1.167

4.6 Scoring Optimization

To ensure the creation of the highest scoring plane possible, a scoring optimization routine was created and implemented via MATLAB. The routine used the following input from the three major design groups; propulsion configuration, airfoil selections, and body estimations. The routine was also used to check alternative configurations from the design groups to insure the configurations used resulted in a maximum score. Figure 4.13 shows the main step in the optimization routine.
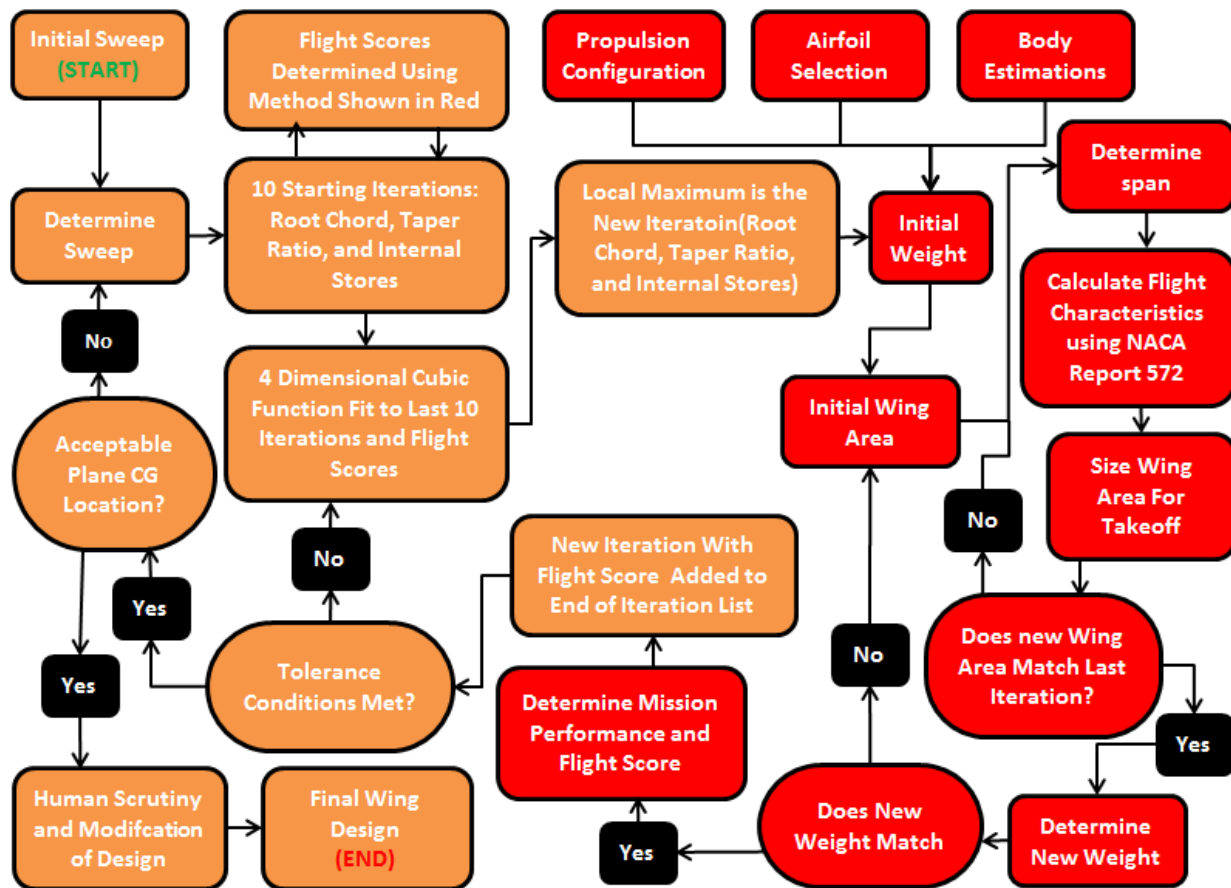
Figure 4.13: Scoring Optimization Routine. Red Boxes: Plane Design. Orange Boxes: Optimization

The optimization routine had two parts, optimization and plane design. The plane design portion used a given root chord, taper ratio, sweep, internal stores, propulsion, airfoil, and body configurations to create a plane that could take off in less than 30 feet. It utilized a lifting line theory from NACA report 572 [1] and additional information from McCormick's Aerodynamics, Aeronautics, and Flight Mechanics [2]. Then the flight score estimation was made. The optimization portion optimized the root chord, taper ratio, sweep, and internal stores to give the maximum flight score, as determined through the plane design portion. Because the optimization portion had no concept of stability, sweep was not optimized in the same loop as the other 3 variables. Instead, an initial sweep was used, the 3 variables were optimized, sweep was adjusted for more or less stability, and this was repeated until the plane's CG was in a location that could be manufactured. The optimization loop for the root chord, taper ratio, and number of internal stores fit a 4 dimensional cubic function to 10 plane configurations and their flight scores. The local maximum of this function was taken as the next iteration configuration. Once the flight score for the new configuration was estimated, a new 4 dimensional cubic function was fit as the process repeated.

The final wing configuration's span was 39.3 inches, area was 6.68 square feet, quarter chord sweep was 14 degrees, carried 8 internal stores, taper ratio was .8, and an aspect ratio of 1.6. A more detailed description of the wing and plane is given in section 5.1.

4.7 Aircraft Lift, Drag, and Stability Characteristics

The stability analysis performed below utilized Nelson's Flight Stability and Automatic Control [3].

4.7.1 Vertical Tail and Rudder Sizing

The vertical tail and rudder were sized to provide adequate directional stability and control at all flight stages. To ensure this, components were analyzed at the most intensive stage of flight: direct crosswinds at takeoff. Using Equation 4.5, the sizes of the vertical tail and rudder were determined.

In Figure 4.14 (a) the vertical tail surface was varied from 20 to 60 sq. inches to examine the effects on yawing moment. A small tail size is preferable to decrease weight and drag, but a small vertical tail will not provide enough damping to eliminate the disturbances that occur during flight. An area of 40 sq. inches was chosen. Figure 4.14 (b) examines the effect of different ratios of rudder to total tail areas on the required deflection to trim out the plane in a crosswind. Using historical data, the ratio .45 was chosen. Later, the tail area was increased to 40.5 sq. inches for structural reasons. The rudder area ratio was decreased to .42 as a structural compromise. Details on the selected design and a stability graph are in Figure 4.14 (c) and (d), respectively. At takeoff, the plane can handle a 10 mph hour crosswind.

$$C_{N_{CG}} = \left(\eta_V \left(1 + \frac{d\sigma}{dB} \right) \frac{S_V l_V}{S_{wing} b} C_{L_{\alpha,v}} \right) B - \left(\eta_V \frac{S_V l_V}{S_{wing} b} C_{L_{\alpha,v}} \tau_r \right) \delta_r \qquad \textbf{4.5}$$
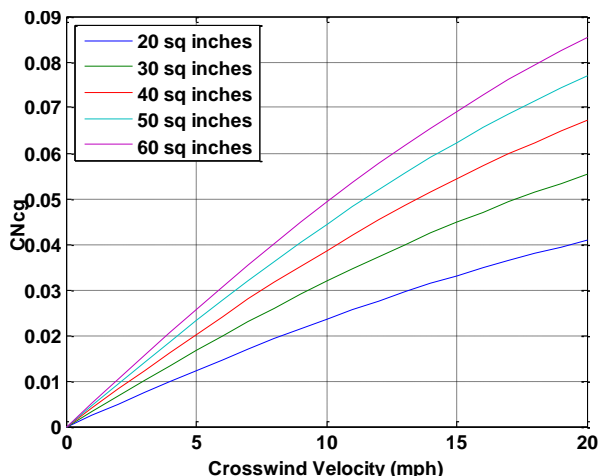
(a) Yawing Moment about CG vs. Crosswind

(b) Rudder Trim vs. Crosswind (using 30 sq. inch tail)

- **Vertical tail span: 12 inches**
- **Vertical tail is symmetric on the top and bottom of fuselage (6 inches on top and bottom).**
- **Vertical tail area: 40.5 sq. inches**
- **Rudder size: 1.5 inches running full span**
- **Root chord: 4 inches**
  Tip chord: 2.75 inches

(c) Selected Design
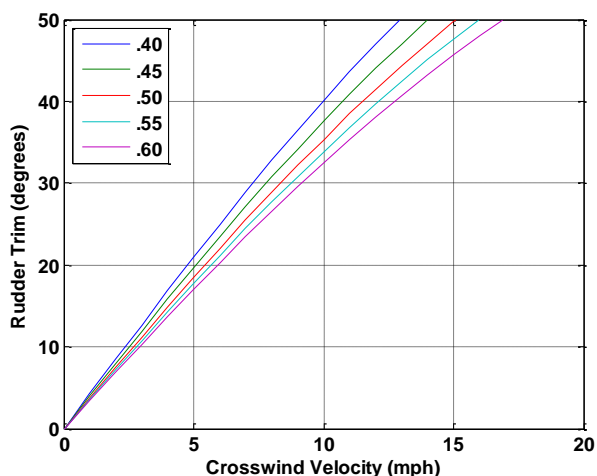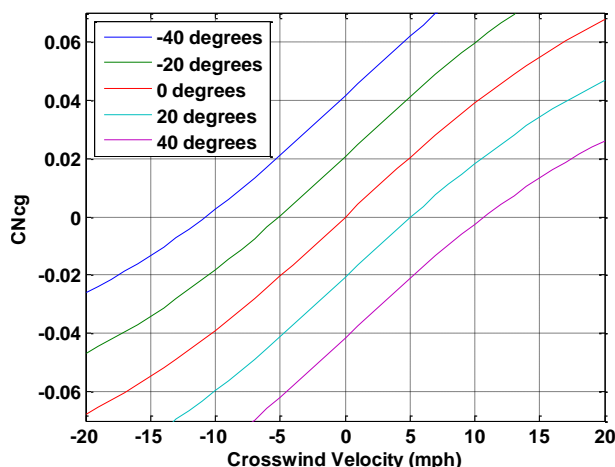
(d) Yawing moment vs. Crosswind for Selected Design

Figure 4.14: Directional Stability with (a) varying tail area, (b) varying rudder size (d) selected design

4.7.2 Elevon Sizing

Because the scoring optimization produced a plane that was already stable in pitch, the main concern of designing the elevons was roll and pitch control. For elevons, symmetric and differential deflections represent the same controls as conventional elevators and ailerons, respectively. This allowed the use of historical data and pilot preference to determine how much roll and pitch control was sufficient. To account for changes in the plane's CG, an elevon size was chosen to provide more than sufficient roll and pitch control. The elevons were sized at takeoff velocity the most demanding flight segment. Below, Equations 4.6 and 4.7 are the pitch and roll moment equations, respectively.

$$C_{M_{CG}} = \left(C_{L_{\alpha,wing}} \left(\frac{x_{cg} - x_{ac}}{\bar{c}} \right) \right) \left(\alpha_{wing} - \alpha_{0L,wing} \right) + C_{M_{AC,wing}} + \left(\frac{2}{S_{wing}} C_{L_{\alpha,wing}} \tau_e \left(\int_{y_1}^{y_2} c(y) dy \right) \left(\frac{x_{cg} - x_{ac}}{\bar{c}} \right) \right) \delta_e \qquad \textbf{4.6}$$

$$C_{LL_{CG}} = \left(-\frac{C_L}{4} \tan \left(\Lambda_{c/4_{wing}} \right) - \eta_v \left(1 + \frac{d\sigma}{dB} \right) \frac{S_v}{S_w} \frac{z_{ac_v}}{b} C_{L_{\alpha,v}} \right) B + \left(\frac{2C_{L_{\alpha,wing}} \tau_a}{S_{wing} b} \left(\int_{y_1}^{y_2} c(y) y \, dy \right) \right) \delta_a + \eta_V \frac{S_V}{S_w} \frac{z_{ac_v}}{b} C_{L_{\alpha,v}} \tau_r \qquad \textbf{4.7}$$

31
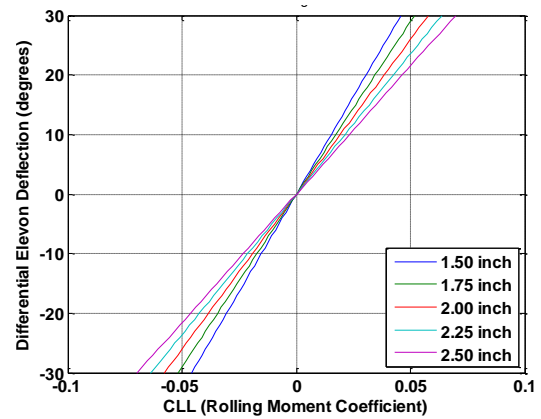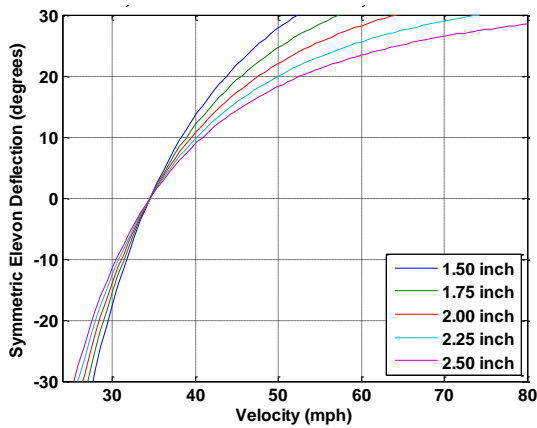
(a) **Required Symmetric deflection vs. cruise velocity**
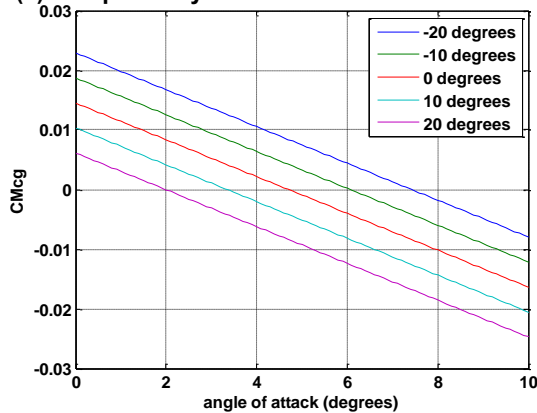
(b) **Rolling moment vs. differential deflection**
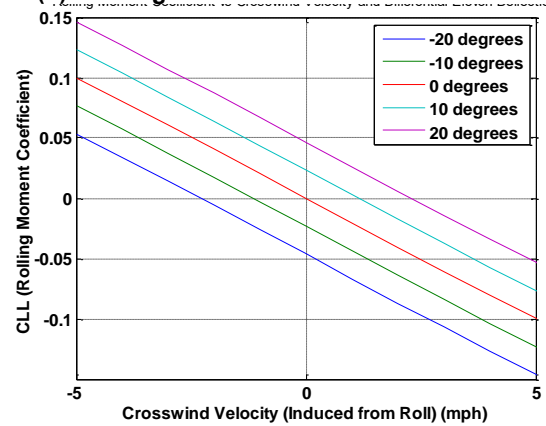
(c) **Pitch moment vs. angle of attack and symmetric deflections**

(d) **Roll moment vs. crosswind and differential deflection**

Figure 4.15: (a) and (b) Control variations vs. elevon sizes, (c) and (d) Control characteristics with 2.5" elevons

Figure 4.15 (a) shows an elevon span of 2 inches gives sufficient pitch control. While 30 degrees deflection is not the elevon's limit, the elevon must control both pitch and roll. Thus, 30 degrees is a good estimate of what can go entirely towards either pitch or roll. Figure 4.15 (b) shows the rolling moment coefficients obtained from differential deflections of the control surface sizes. A span of 2.5 inches was chosen to allow the plane to compensate for any variations in the CG. Figures # (c) and (d) show the pitch and roll stability while varying the deflection of the selected elevon symmetrically and differentially, respectively,

The pitching moment about the CG is positive at a 0 angle of attack for the range of deflections, and has a negative slope as the angle of attack increases. These are the conditions for pitch stability. The conditions for roll stability are also met.

4.7.3 Final Characteristics

Figure 4.16 shows the lift, drag, and lift to drag ratio for the final plane design. The lowest drag occurs at an angle of attack of about 1 degree. Thus, the landing gear was set at this angle. Additionally, l/d max occurs at about 6 degrees angle of attack. The maximum lift coefficient was estimated to be 1.23.
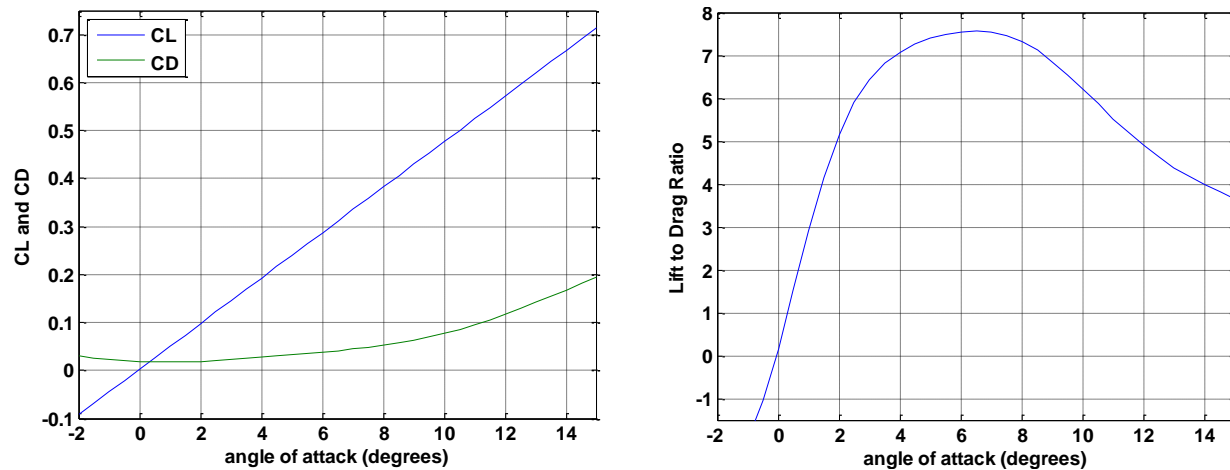
Figure 4.16: (Left) CL and CD vs. angle of attack, (Right) Lift to drag ratio vs. angle of attack

Table 4.10: Aircraft stability characteristics.

Modes of Motion	Unloaded Takeoff	Loaded Takeoff	Unloaded Cruise	Loaded Cruise
Long Period Motion Frequency	.0427	.0283	.0427	.0283
Long Period Motion Damping	.019	.019	.0676	.0444
$t_{1/2}$ Long Period (s)	852.8	1286.5	239.3	550.0
Short Period Motion Frequency	1.1781	1.4009	4.5070	3.4409
Short Period Damping	.0611	.0341	.0569	.0324
T_{roll}	.0134	.0099	.0038	.0042
Dutch Roll Frequency	7.8503	10.5261	27.9685	24.6178
Dutch Roll Dampening	.2343	.2078	.2343	.2078
Spiral Mode Stability	-104.78	-124.89	33.79	147.84

4.8 Winglet Design

Due to the low aspect ratio of this year's design, research was performed into the benefit of using wingtip devices to reduce induced drag. Induced drag would typically be insignificant compared to viscous and form drag at the low Reynolds's number flight of a DBF plane. Equation 4.8 shows induced drag will be significant during high C_L flight for a low aspect ratio aircraft. This includes low speed, heavy payload flight, high load maneuvers, and short distance takeoff, all of which are included in this year's missions.

$$C_{Di} = \frac{C_L{}^2}{\pi * e * AR}$$ **4.8**

Winglets add viscous drag and reduce induced drag. This change in drag is dependent on winglet size, flight weight, and flight velocity. Assuming steady level flight, C_L was calculated for a given weight and range of velocities. Extracted from Hoerner's "Fluid-Dynamic Drag," the change in effective aspect ratio is given by Equation 4.9, where S_{wl} is the planform area of one winglet. These two equations were used to compute a change in C_{Di}. The viscous drag was calculated using flat plate skin friction formulas. The summation of the change in induced and friction drag is shown Figure 4.17.

$$\Delta AR = 1.1 * \frac{2 * S_{wl}}{S} * AR$$ **4.9**
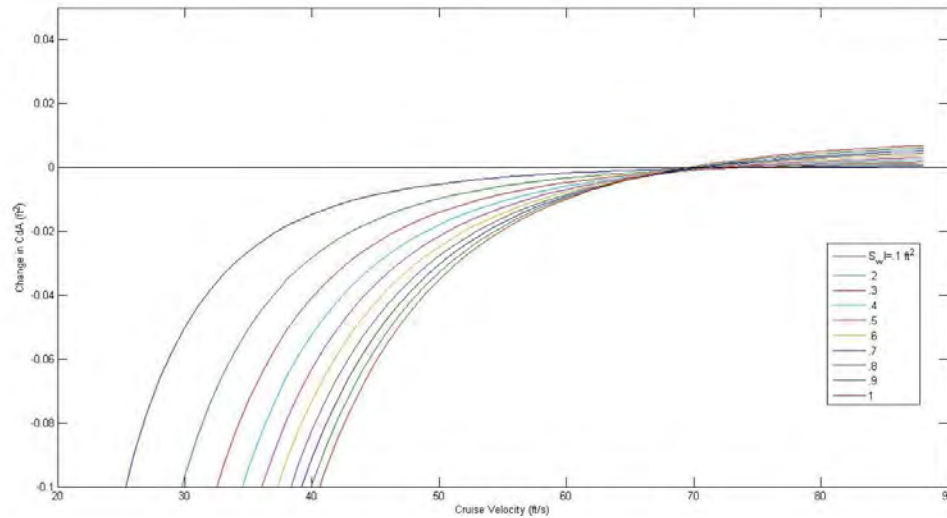
Figure 4.17: Change in Drag vs. Cruise Velocity vs. S_w at 7lbs Flight Weight

From these formulas, the breakeven velocity was calculated, the speed at which winglets transition from providing a drag reduction to a drag increase. The breakeven velocity is a strong function of flight weight. At 4 and 7 pounds the addition of winglets yielded a breakeven velocity of 45 ft/s and 70 ft/s, respectively. The breakeven velocity is also affected by winglet size. Large winglets break even at lower speeds, but provide more drag reduction below the breakeven velocity. Above the breakeven velocity, larger winglets create more viscous drag. A winglet area of 60 in^2 was selected because it provided a balance between skin friction and induced drag. Figure 4.18 shows the breakeven velocities.
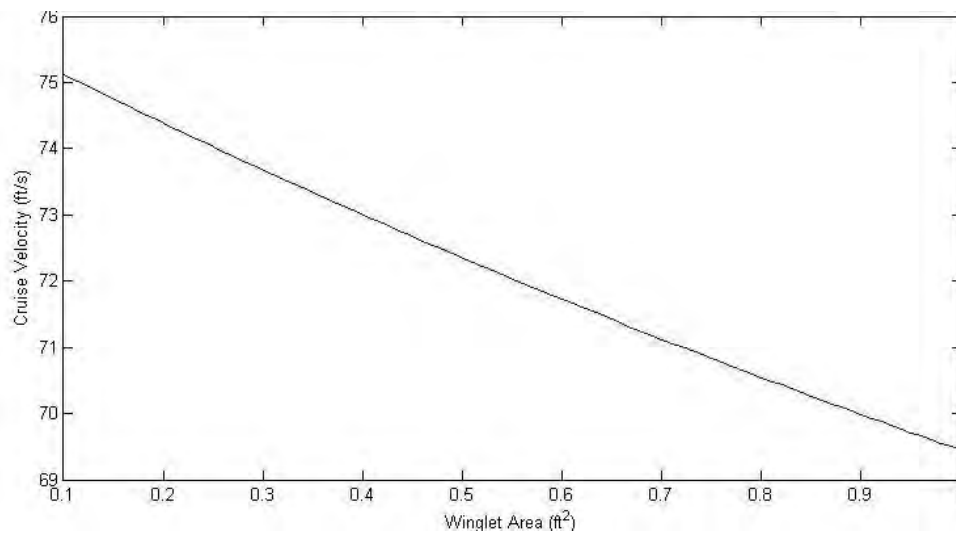
Figure 4.18: Breakeven Velocity vs. Winglet Size at 7lbs Flight Weight

Research was performed with XFLR5 [4] to identify the optimal aspect ratio, placement, and airfoil for the winglets. PSU-94-097, a custom designed airfoil for sailplane winglets, initially was selected for its superior lift to drag ratio across a wide range of angles of attack at low Reynolds's numbers. However, when the full wing and winglet system was modeled in XFLR [4], the cambered PSU-94-097 airfoil was proven inferior to a symmetrical winglet airfoil at all considered velocities. A series of

symmetrical airfoils were researched at Re=150,000 and FX-76-120 was selected for maintaining a superior lift to drag ratio over the widest range of angles of attack.

The XFLR5 [4] analysis revealed that while holding planform area constant, higher AR winglets provide greater induced drag reduction. This agreed with the theory that winglets do not simply reduce the strength of wingtip vortices, they create lift as a result of the induced angle of attack due to the vortices. That lift is directed partially in the forward direction of flight. Just as a high AR wing is more efficient, a high AR winglet is also more efficient.

From these findings, the winglets were designed with a root chord of half the wing tip chord (10.5 inches) tapering to 5 inches. The extreme taper ratio should not lead to tip stall problems since the induced angle of attack should decrease as one moves up the winglet (away from the theoretical center of the wingtip vortex). The winglets were set to avoid extending the length and span dimensions of the aircraft. The trailing edge of the winglet was kept vertical to keep the winglets as far aft as possible. The leading edge has a sweep angle of 34.5 degrees. A height of 8 inches yields the appropriate planform area and an aspect ratio of 1.07. While this AR is low by common standards, it has a higher aspect ratio than many of the other designs that were considered, including some with heights as low as 3 inches. Additionally, due to stability and weight considerations, the winglets were placed forward on the wingtips.

4.9 Structure Design

To gain insight into the lightest structural configuration, structures of previous years' competitions planes were used heavily in the preliminary structure design. In addition, prototyping was used when available to test the weight and strength of structural configurations.

The conceptual wing structure called for a completely foam wing. One of the uses of the first prototype, constructed during the fall semester, was to verify that a completely foam wing was feasible from the manufacturing, structural, and the flight performance aspects. As seen in Figure 4.19, the first prototype had a purely foam wing. After flight tests, the wing proved a foam wing could be manufactured, could be structurally sound, and exhibited the desired aerodynamic performance. Thus, a foam wing's feasibility was verified.

Figure 4.19: First prototype, constructed during the Fall semester

During the preliminary design it was decided to put wheels at the wingtips to reduce the drag by placing a portion of the landing gear inside the winglets. This landing gear configuration could result in

large stresses in the wing in the event of a hard landing on a single wheel. In addition, the large empty space in the center of the wing for the internal stores would not maintain enough rigidity for a sound structure. To alleviate these problems, historical aircraft structures were examined. The lightest structure found was from the 2011-2012 competition plane. It utilized 2 carbon spars, one running the entire span and one running about two-thirds of the span. Thus 2 carbon spars were added to the foam wing design to strengthen the fuselage section and allow hard landings. Only one spar would run the full span.

Previous aircraft provided vertical surfaces of various structural configurations and materials. By a direct comparison of weighing similar sized surfaces, the lightest configuration was determined to be foam. The first prototype showed sufficiently thick foam vertical surfaces maintain enough rigidity for desired aerodynamic performances. Foam vertical surfaces could also result in a lighter connection to the foam wing. Thus, completely foam vertical surfaces were selected because it provided a light solution with sufficient rigidity that could easily be connected to the wing. Deviation from completely foam configuration would be allowed in the detailed design if it was necessary to maintain sufficient rigidity.

4.10 Mission Performance Estimates

4.10.1 Weight Build Up

The weight of the aircraft was estimated by weighing similar parts on previous competition aircraft. When physical parts weren't available, estimations were made based off of the densities of the materials the parts consisted of. Figure 4.20 shows the estimates of the major components.

Component	Weight (lb)
Wing	1.3
Winglets	.1
Store Mounts	.15
Vertical Tail	.05
Landing Gear	.1
Propulsion System	.6
Batteries	1.5
Miscellaneous	.1
Total Empty Weight	4
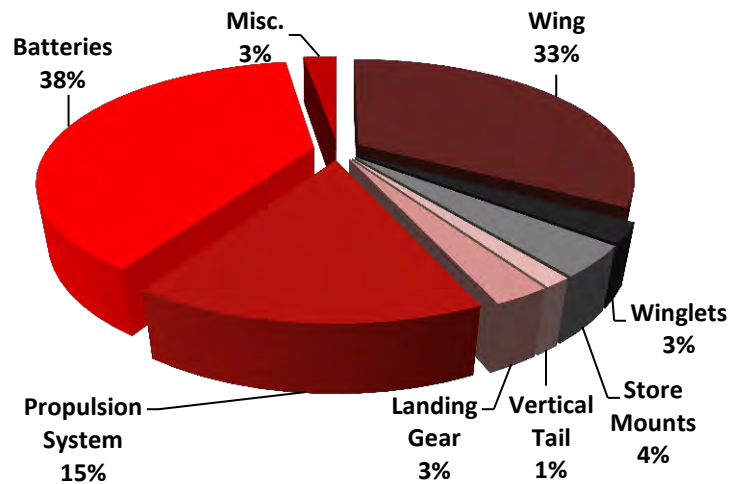
Figure 4.20: Weight Build Up

4.10.2 Drag Build Up

A drag buildup of the plane's main parts with no stores is shown in Figure 4.21. The integrated design limits the number of components. In flight, a large portion of drag will be from lift induced drag.

Component	C_{D0}
Wing	.015
Tail	.003
Winglets	.006
Landing Gear	.007
Total	**.031**
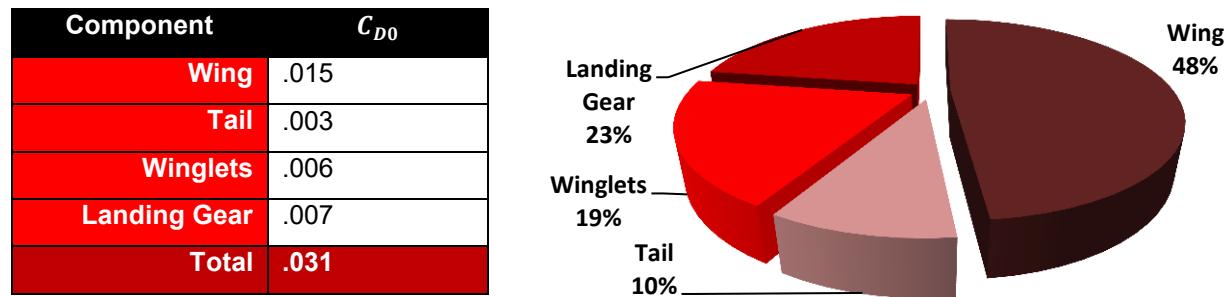
Figure 4.21: Drag Build Up

4.10.3 Mission Performance Estimates

Using information from the aerodynamic performance and propulsion configuration, mission performance estimations were created. Max velocity and turn time was determined using the methods discussed in section 4.2. To give results descriptive of all mission 3 possibilities, performance estimates were made for each configuration and averaged. Although the individual mission scores are low, the RAC is also low, resulting in a good flight score. Table 4.11 shows selected mission performance results.

Table 4.11: Estimate Mission Performance

Mission 1		Mission 2		Mission 3 Averages	
Max. Velocity	50 mph	Max. Velocity	47 mph	Max. Velocity	42 mph
180 deg Turn Time	3.1 sec	180 deg Turn Time	3.3 sec	180 deg Turn Time	3.3 sec
Lap Time	38 sec	Flight Time	125 sec	Flight Time	135 sec
Laps	6	Internal Stores	8	Max. Takeoff Dist.	28 ft
Score	1.71	Score	2.28	Score	5.11
Max. Empty Weight: 4 lb.		Xmax: 2.32 ft		Ymax: 3.28 ft	
RAC: .598			Total Flight Score: 15.21		

5.0 Detail Design

The goal of the detail design was to complete the individual design of each system not finalized in the preliminary design and to integrate them into the final aircraft configuration. The design of the wing/body structure, vertical stabilizer structure, winglets, payload restraints and landing gear were all finalized. Based on these designs, the mission and flight performance could be predicted.

5.1 Final Design Parameters

Table 5.1: Final design parameters.

Wing				Vertical Stabilizer	
Area	962 in^2	**Aspect Ratio**	1.6	**Area**	40.5 in^2
Span	39.3 in	**Sweep**	14°	**Span**	12 in
Body Chord	26.2 in	**Body Airfoil**	MHt17C2.5	**Airfoil**	4 in
Trans. Chord	25.8 in	**Trans. Airfoil**	MH45	**Tip Chord**	2.75 in
Tip Chord	21 in	**Tip Airfoil**	HS3512	**Sweep**	8.88°
Body Incidence	0°	**Trans Incidence**	0°	**Rudder Area**	18 in^2
Tip Incidence	-1.15°	**Elevon Area**	63 in^2	**Airfoil**	FX76-100
Winglet			Propulsion		
Root Chord	10.5 in	**Motors**	Neu 1112-1750		
Tip Chord	5 in	**Propeller**	APC 17x10		
Height	8 in	**Batteries**	Elite 2000		

5.2 Wing/Body Structure and Design

Milling foam was chosen as the main construction method for the plane. The external geometry was determined from the optimization code and the internal structure was designed for high strength and weight minimization. Two carbon rods were installed to provide the strength in bending and torsion necessary to handle the aerodynamic forces. The larger rod was placed close to the center of gravity. It was sized to handle a hard landing on one main wheel. A second smaller rod was placed further rearward to provide extra strength in the body section where there is less foam. The wing/body and spars can be seen in Figure 5.1.

While the specific dimensions can be seen in Table 5.1, the wing/body has an aspect ratio of 1.6. The root chord is 26.2" and the tip chord is 21 inches. Of the 39.3" span, the body section takes up 14" of this. Outboard of this is a two inch blended area between the body area and the transition airfoil. Finally, the remaining 10.65" of the wing are transition between the transition airfoil and the tip airfoil. In this region, the -1.15° degrees of washout also twist in.
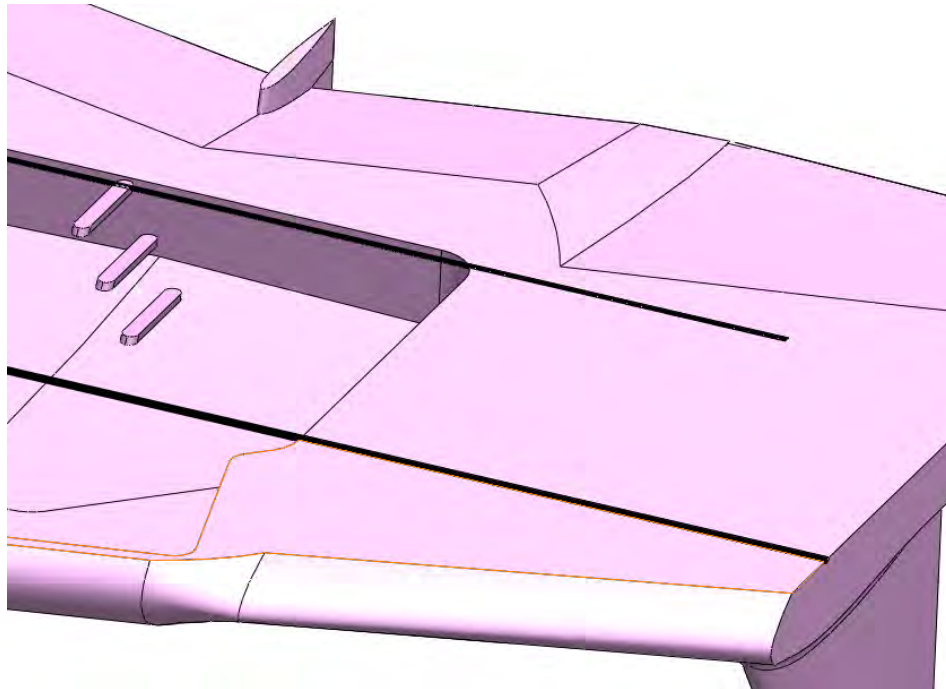
Figure 5.1: Spars in the foam wing/body

A two-inch deep cavity was machined out of the bottom of the body section for the internal stores to be carried in. As discussed in Section 5.3.1, the internal store mounting system is carved into the upper wall of this cavity. The rectangular cavity has a tapered front section with shelves that house the batteries. The cavity has space for the ESC, receiver, and receiver battery. This internal storage area eliminates drag from protruding system components. Additionally, it does not interfere with the external shape of the design in any way. This cavity can be seen in Figure 5.2.
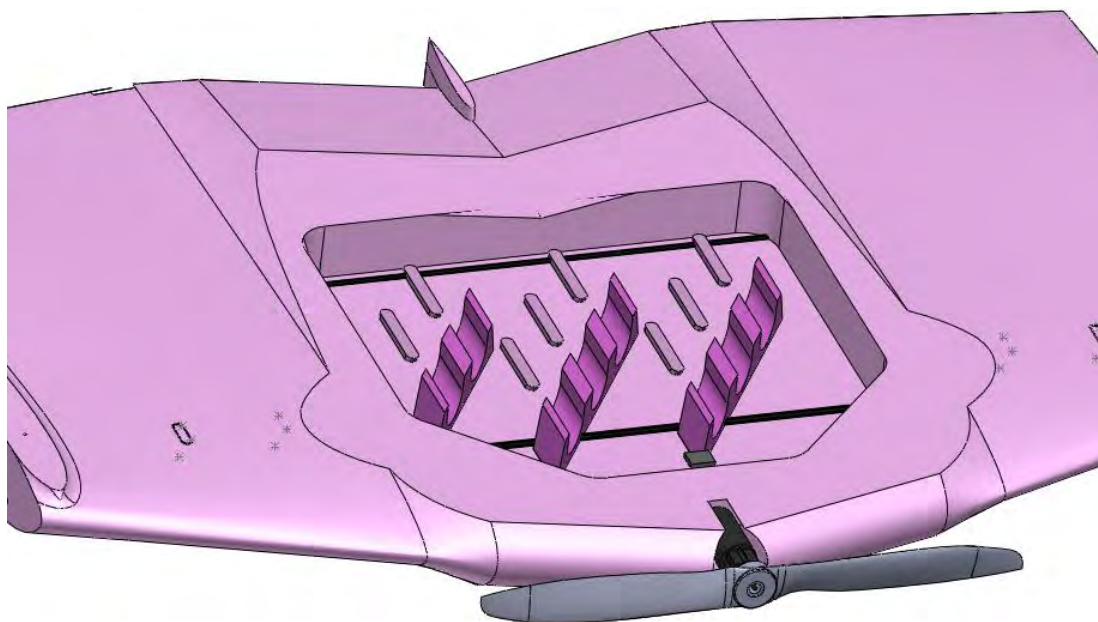
Figure 5.2: Internal store cavity

The upper fins of the internal stores do not fit in the cavity. They extend out through the upper wall of the aircraft. To keep them enclosed, fairings were installed over the protruding fins. While these create drag, they were the only way to keep the rockets entirely internal.

The motor was attached to a mount at the very front of the plane. The mount was constructed from laser-cut balsa and fiber-glassed for structural reinforcement. It was epoxied to the front of the plane. The motor and propeller were then attached to the mount.

5.3 Payload System Design

The irregular geometry of this year's payloads along with the addition of aircraft size affecting score resulted in the need for an innovative, efficient design for the internal stores. Additionally, a lightweight design that added minimal drag was key in obtaining the highest flight score possible.
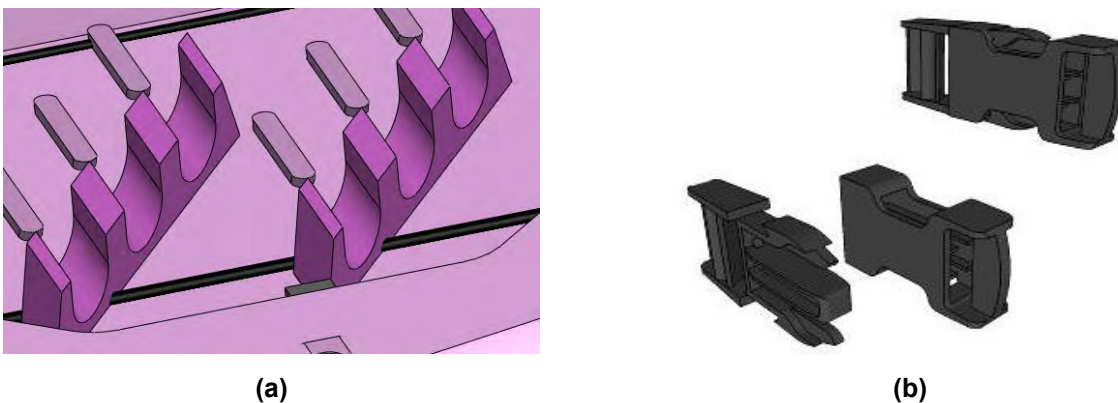
(a)   **(b)**
Figure 5.3: Payload restraints for (a) internal and (b) external stores.

5.3.1 Internal Stores

Internally the plane must hold Mini-Max internal rockets facing in the direction of flight without touching each other. The optimization code said eight was the optimal number of stores. A foam restraint was designed to make use of the fuselage material. Extending down from the top of the storage cavity are eight notches which the rocket bodies fit in snugly. The notches are arranged diagonally as seen in Figure 5.3 (a) in order to offset the rockets so that the fins fit. The rockets are held in two groups of three and a group of two. The large foam restraints are 8.9 inches in length to hold three rockets.

The central axis-to-axis distance between the individual rockets is 1.5 inches for fin spacing and to maintain enough stiffness in the walls of the foam notches. The foam restraint spans 1.15" of the rocket body. So that the rockets do not fall out of the restraints, they will be held in place by foam plates that cover all of the cutouts. The plates are held in place with Velcro that can hold the weight of all of the rockets. The internal cavity will be closed by a piece of foam to act as a bomb bay door. This system allows for simple access to the stores allowing for easy loading and unloading. Furthermore, it is effective and light weight at .3 oz.

5.3.2 External Stores

Each side of the wing must be able to hold at least 2 external stores. There centerlines must be at least 3 inches from each other and the center of the plane and they cannot prevent the opening of the fuselage door. The heaviest internal store weighs 1 lb. The stores themselves are mounted directly to a balsa wood pylon. These pylons hold the external stores far enough below the wings that the fins on the stores do not contact the underside of the wing. The rockets are zip tied to the pylons. Zip ties are a light and strong solution that can be removed and reused with some care. The rapid installation of the rocket into the ties is a benefit during the timed assembly period.

In order to save weight and reduce aerodynamic drag, the external store pylons are designed to be removable when external stores are not present. The pylons lock into the wing using a modified side-release buckle. These types of buckles are often found on backpacks and are durable, easy to install, and relatively light weight. Each pylon will have the male end of the buckle mounted to the top. The female part of the buckle is mounted inside the wing, so that it is flush with the bottom surface. Installation of the pylons is a simple as inserting the male part of the buckle until it snaps together. Since the buckle is embedded in the wing, a small hole will be drilled by the buckle to allow the insertion of a small wire to depress the release tab.

5.4 Tail and Winglet Structure and Design

The structural design of the vertical stabilizer and winglet was dictated by the information provided by the aerodynamics team during preliminary design. The primary goal of the design of these structures was to devise an extremely lightweight solution that would be rigid enough to maintain aerodynamic performance.

For both parts, the devised structural solution consisted completely of foam, a method that the first prototype showed would work. The foam would be milled into the desired shape when the wing is milled. As much of the tail and winglets as the foam sheets allow would be part of the same piece as the wing. This allowed the interface between the wing, tail, and winglets to be rounded, reducing interference drag. In addition, this provided a secure connection to the wing. The rest of the tail and winglets would be milled and attached with adhesive.
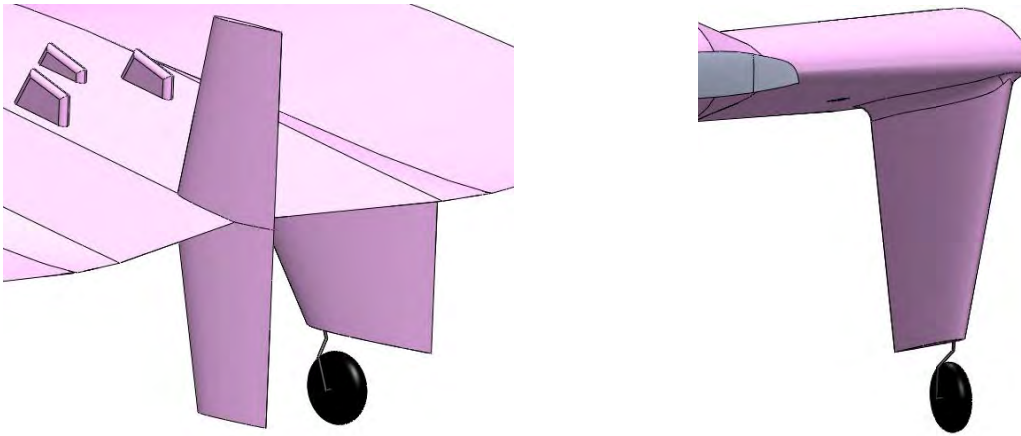
Figure 5.4: Vertical Stabilizer and winglet.

5.5 Landing Gear

The landing gear was designed to be lightweight and strong enough to support the aircraft in the event of a hard landing. Piano wire was selected because it is a lightweight and strong material that can be easily assembled into the required shape. The struts for each part of the tricycle landing gear configuration were hand bent from 1/8 inch piano wire. Figure 5.5 shows how the landing gear is shaped. The landing gear sets the plane at a one degree angle of attack, the minimum drag angle, and it provides 9 inches of clearance, sufficient clearance for the prop and external stores. The front gear is located directly behind the propeller. The back landing gear is partially inside the winglets to reduce drag and attaches to the carbon spar. Each part of the landing gear consists of a single strut with a wheel attached.
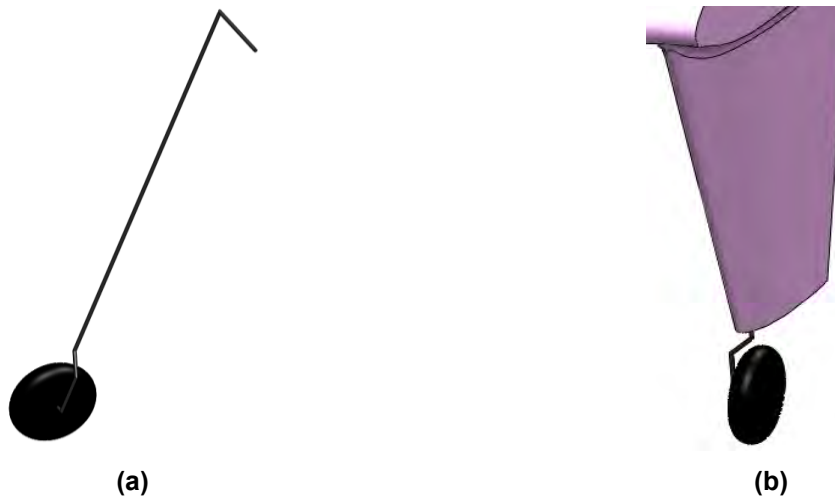
(a)   **(b)**
Figure 5.5: (a) Front and (b) side landing gear struts and wheels.

5.6 Weight and Balance

The center of gravity (CG) of the aircraft was found by adapting and enhancing a base chart. To begin estimating the CG as early as possible, the chart was populated with frequently-used aircraft components from earlier planes. As a result of the iterative design process, the chart was constantly refined. Components were added, removed or moved as soon as the team had a better vision of the final

product. The chart (Table 5.2) allowed the team to accurately track changes in the CG whenever it adjusted the aircraft's specifications and components' placement; consequently, an optimal performance was gradually established. The overall goal was to have the CG close to the quarter-chord of the wing to ensure for aircraft stability. This goal was met as the estimated CG is between 4.74 to 5.66 inches from the front rib.

Table 5.2: Weight and balance chart for aircraft.

Part	Weight (ounces)	Motor Front Face to Part CG (Inches)	Moment about Front Face of Motor (Ounce-Inches)
Aileron Servos	0.66	17.43	11.5038
Aileron Servo Push Arms	0.2	18.23	3.646
Electronic Speed Control	2	1.25	2.5
Front Batteries	23.68	3.56	84.3008
Wing/Body and Vertical Surfaces	28.65	13.32	381.618
Landing Gear	4.02	6.97	28.0194
Motor and Mount	6.24	1.1	6.864
Carbon Spars	0.9968	10.32	10.286976
Rocket Fin Caps	1.43	14.35	20.5205
Wires	1.03	3.23	3.3269
Prop	1.65	-0.089	-0.14685
Receiver	0.16	2.21	0.3536
Receiver Battery	1.53	2.34	3.5802
Rudder Servo	0.2	5.34	1.068
Rudder Servo Push Arm	0.1	18.22	1.822
Mission 2 Payload	32	7.93	253.76
Mission 3 Configuration 1	48	8.21	394.08
Mission 3 Configuration 2	48	8.24	395.52
Mission 3 Configuration 3	48	8.92	428.16
Mission 3 Configuration 4	48	7.78	373.44
Mission 3 Configuration 5	48	8.86	425.28
Mission 3 Configuration 6	44	8.48	373.12
Totals			
	Mass Total (Ounces)	Moment Total (Ounce-Inches)	CG (Inches)
Mission 1	72.5468	559.263326	7.709000618
Mission 2	104.5468	813.023326	7.776644775
Mission 3 Configuration 1	120.5468	953.343326	7.908491358
Mission 3 Configuration 2	120.5468	954.783326	7.920436926
Mission 3 Configuration 3	120.5468	987.423326	8.191203134
Mission 3 Configuration 4	120.5468	932.703326	7.737271549
Mission 3 Configuration 5	120.5468	984.543326	8.167311998
Mission 3 Configuration 6	116.5468	932.383326	8.000076587

5.7 Flight and Mission Performance

Table 5.3 lists performance parameters that are applicable to the missions. The wing's unusually high efficiency factor of 1.4 is due to the addition of the winglets. As confirmed via XFLR5 [4] and the use of NACA report 572 [1] in the design code, without the winglets, the lift distribution is nearly elliptic. This gave an efficiency factor of about 1. XFLR5 [4] showed the addition of the winglets increased the efficiency factor to the given value of 1.4. Table 5.4 lists the mission performance broken down for each step of the mission. The most demanding mission uses 1200 mAh, well under the batteries' 2000 mAh

advertised capacity. Most demanding flight stage draws 25 amps, below both the battery and fuse thresholds. Table 5.5 assumes the maximum laps flown is 7, maximum internal stores is 14, and a minimum flight time of 115 seconds. This gives a score of 14.91.

Table 5.3: Flight Performance Characteristics.

Characteristic	M 1	M 2	M 3.1	M 3.2	M 3.3	M 3.4	M 3.5	M 3.6
$C_{L.Max}$	1.23	1.23	1.23	1.23	1.23	1.23	1.23	1.23
$C_{D.0}$	.031	.031	.035	.036	.035	.037	.037	.036
Efficiency Factor	1.4	1.4	1.4	1.4	1.4	1.4	1.4	1.4
$(L/D)_{Max}$	7.6	7.6	7.1	6.9	7.0	6.9	6.9	7.0
Flight Weight (lb)	4	6	7	7	7	7	7	6.75
Thrust/Weight	1.75	1.17	1	1	1	1	1	1.04
Weight/Wing Area (lb/ft^2)	.598	.898	1.05	1.05	1.05	1.05	1.05	1.01
Max Speed (mph)	50	47	42	41	42	41	41	42
Stall Speed (mph)	15	18	20	20	20	20	20	19
Flight Time (sec)	231	125	134	136	135	136	136	134

Table 5.4: Mission Performance

M1	Segments	Velocity (ft/s)	Distance (ft)	Time (sec)	Current (A)	Battery Used (mAh)
Takeoff	1	41	27	1.2	25	8
Climb	1	38	101	3.7	24	25
Cruise	1	73	372	5.1	21	30
Cruise	23	73	500	6.8	21	912
Half Turn	12	43	48	3.1	14	145
Full Turn	6	43	96	4.2	14	98
Total	(6 Laps)			231		1218
M2	**Segments**	**Velocity (ft/s)**	**Distance (ft)**	**Time (sec)**	**Current (A)**	**Battery Used (mAh)**
Takeoff	1	35	27	1.4	25	10
Climb	1	40	239	6.5	21	38
Cruise	1	69	261	3.8	19	20
Cruise	11	69	500	7.2	19	418
Half Turn	6	41	55	3.3	14	77
Full Turn	3	41	110	4.6	14	54
Total	(3 Laps)			125		617
M3 (Ave.)	**Segments**	**Velocity (ft/s)**	**Distance (ft)**	**Time (sec)**	**Current (A)**	**Battery Used (mAh)**
Takeoff	1	33	27	1.5	25	10
Climb	1	40	331	8.6	19	45
Cruise	1	62	269	4.3	18	22
Cruise	11	62	500	8.0	18	440
Half Turn	6	37	47	3.3	12	66
Full Turn	3	37	94	4.5	12	45
Total	(3 Laps)			135		628

Table 5.5: Total Flight Score

Mission 1	Mission 2	Mission 3	RAC	Report Score	Final Score
1.71	2.29	5.11	.598	.98	14.91

5.8 Drawing Package
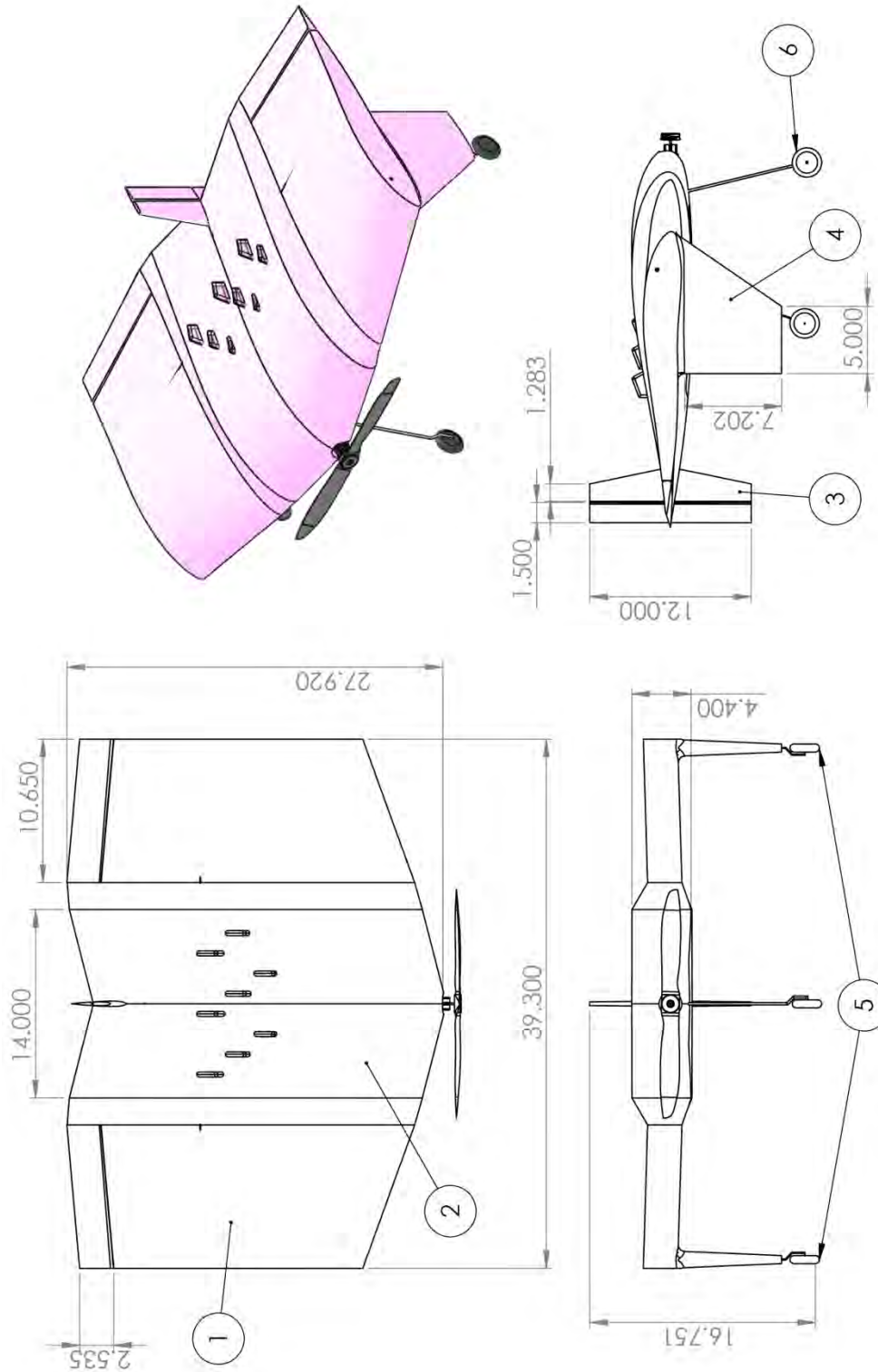
Item #	Item Description
1	Wing
2	Fuselage
3	Vertical Stabilizer
4	Winglet
5	Landing Gear
6	Front Landing Gear

RENSSELAER POLYTECHNIC INSTITUTE
CESSNA - RAYTHEON - AIAA DESIGN/BUILD/FLY 2013

AIRCRAFT THREE-VIEW

DRAWING PACKAGE

DRAWN BY: PETER FINIGAN

CHIEF ENGINEER: JEFF MOCKELMAN

APPROVED: 21 FEB 2013

ALL DIMENSIONS IN INCHES | SCALE 1:10 | SHEET 1 OF 5
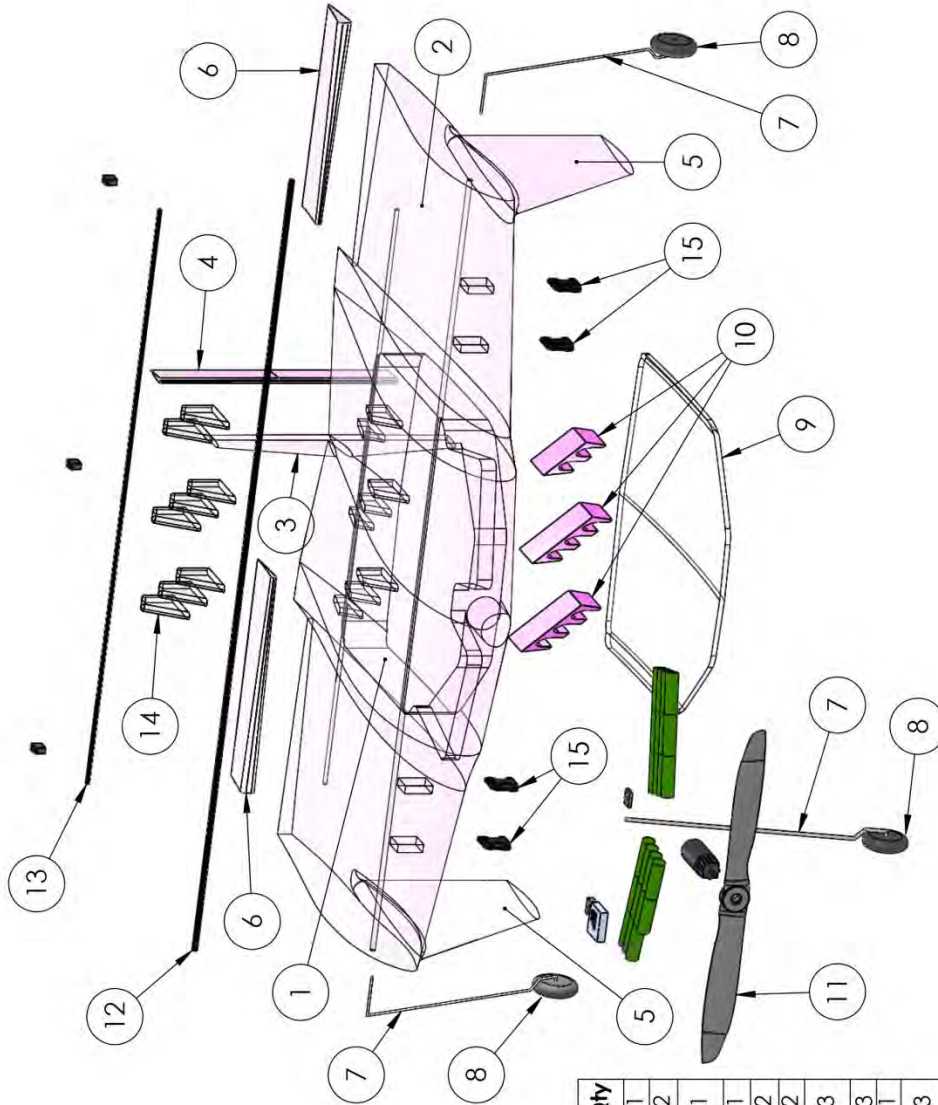
Item #	Part Description	Material	Qty
1	Fuselage	Polystyrene Foam	1
2	Wing	Polystyrene Foam	2
3	Vertical Stabilizer	Polystyrene Foam	1
4	Rudder	Polystyrene Foam	1
5	Winglet	Polystyrene Foam	2
6	Elevon	Polystyrene Foam	2
7	Landing Gear Strut	Stainless Steel	3
8	Wheel	Foam	3
9	Cargo Door	Plastic	1
10	Internal Store Rack	Polystyrene Foam	3
11	Propeller	Plastic	1
12	Main Spar	Carbon Fiber	1
13	Rear Spar	Carbon Fiber	1
14	Store Fin Cap	Plastic	8
15	External Store Mount	Plastic	4

RENSSELAER POLYTECHNIC INSTITUTE
CESSNA - RAYTHEON - AIAA DESIGN/BUILD/FLY 2013

STRUCTURAL ARRANGMENT

DRAWN BY:
PETER FINIGAN

DRAWING PACKAGE

CHIEF ENGINEER:
JEFF MOCKELMAN

ALL DIMENSIONS IN INCHES | SCALE 1:7 | SHEET 2 OF 5

APPROVED:
21 FEB 2013

46
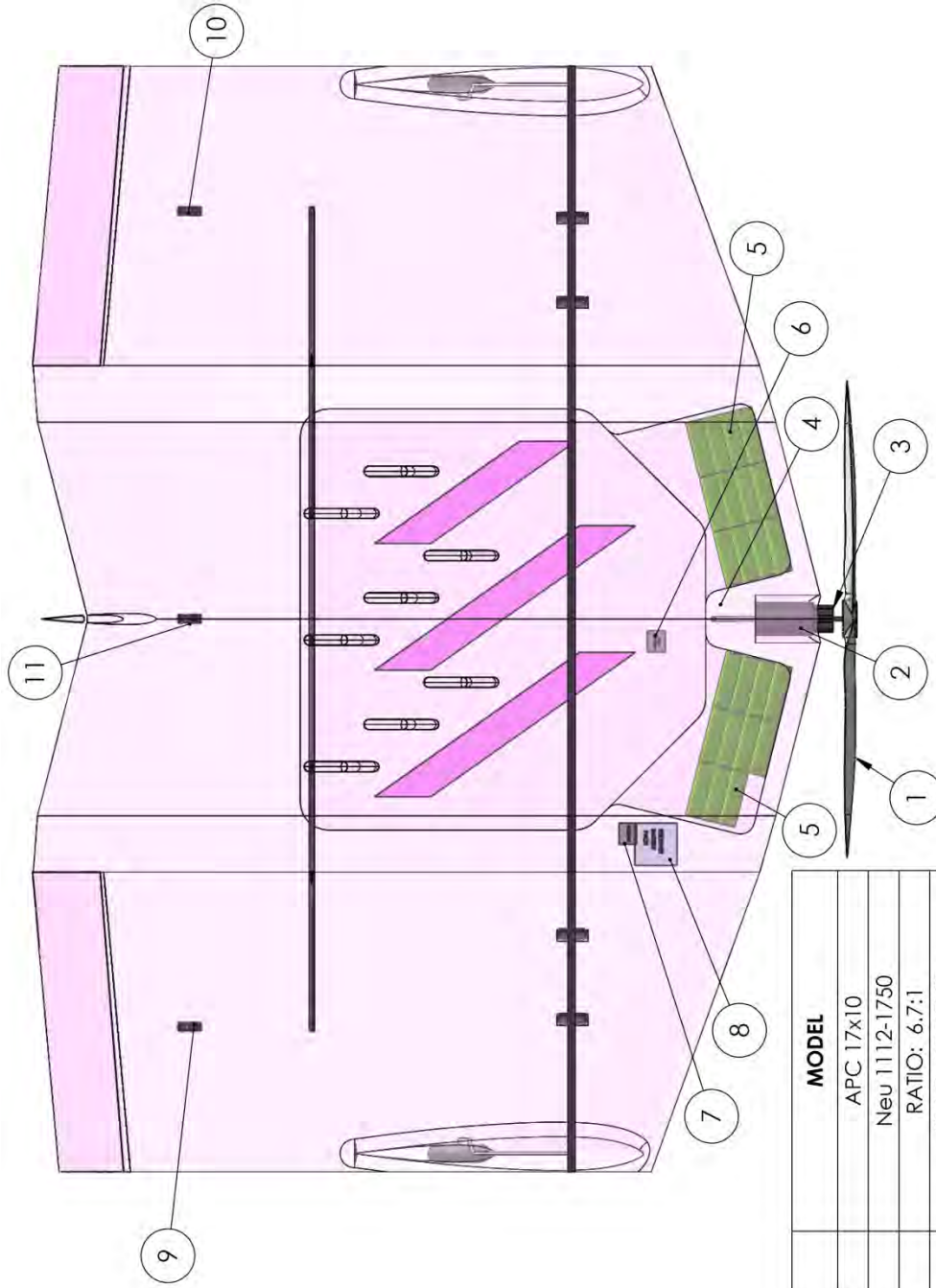
ITEM #	PART	MODEL
1	PROPELLER	APC 17x10
2	MOTOR	Neu 1112-1750
3	GEARBOX	RATIO: 6.7:1
4	FUSE	20A BLADE FUSE
5	BATTERY PACK	23 ELITE 2000s NIMH IN SERIES
6	SPEED CONTROLLER	CASTLE CREATIONS PHOENIX ICE 50
7	RECEIVER	FRSKY TFR4 4CH 2.4GHZ
8	RECEIVER BATTERY	KAN400AAA DOUBLE STICK, 16 AWG
9	RIGHT ELEVON SERVO	MKS PROPO DS 4X0
10	LEFT EVELON SERVO	MKS PROPO DS 4X0
11	RUDDER SERVO	FUTABA S3114

RENSSELAER POLYTECHNIC INSTITUTE
CESSNA - RAYTHEON - AIAA DESIGN/BUILD/FLY 2013

SYSTEMS LAYOUT

DRAWN BY:
PETER FINIGAN

DRAWING PACKAGE

CHIEF ENGINEER:
JEFF MOCKELMAN

APPROVED:
21 FEB 2013

ALL DIMENSIONS IN INCHES | SCALE 1:5 | SHEET 3 OF 5

47
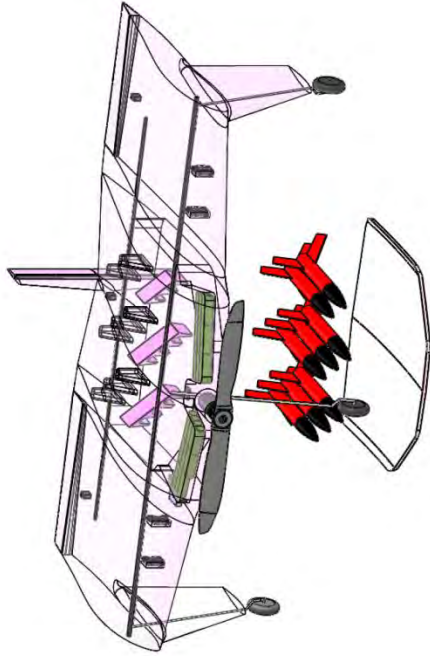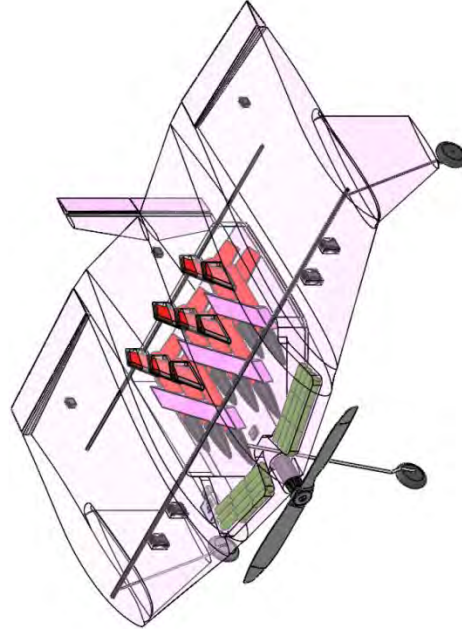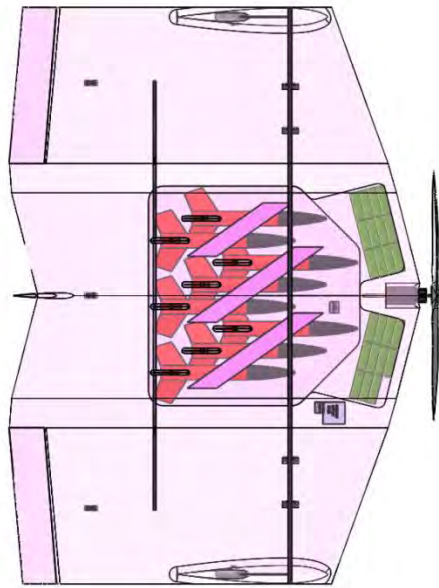
BOTTOM-LOADING STORE ACCESS

RENSSELAER POLYTECHNIC INSTITUTE		
CESSNA - RAYTHEON - AIAA DESIGN/BUILD/FLY 2013		
	MISSION 2: INTERNAL STORE CONFIGURATION	
DRAWN BY: PETER FINIGAN		APPROVED: 21 FEB 2013
CHIEF ENGINEER: JEFF MOCKELMAN	DRAWING PACKAGE	
	ALL DIMENSIONS IN INCHES	SCALE 1:10	SHEET 4 OF 5

DETAIL B
SCALE 1 : 2

3.00

3.00
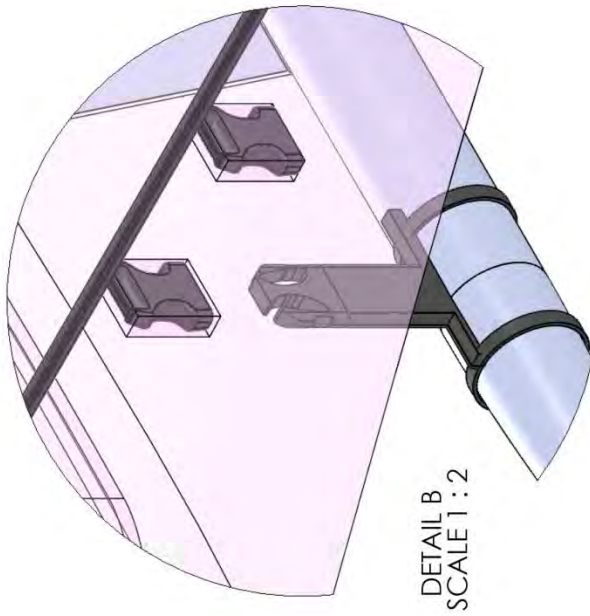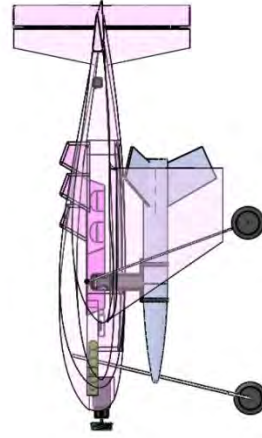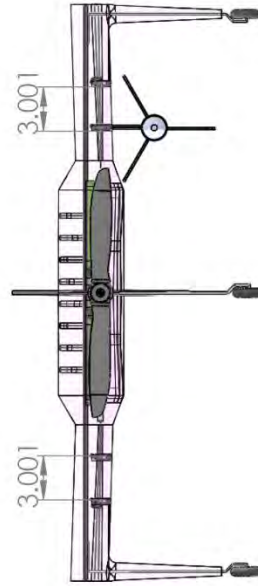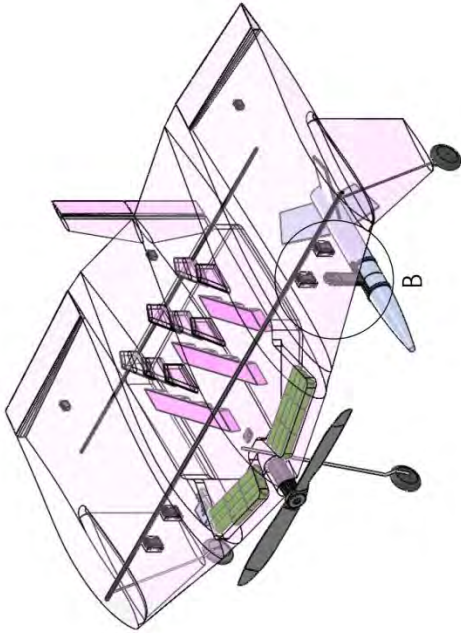
NOTE: ATTACHMENT METHOD FOR EACH EXTERNAL STORE
IS IDENTICAL. PYLON LENGTH IS ONLY DIFFERENCE BETWEEN
EACH STORE.

RENSSELAER POLYTECHNIC INSTITUTE		
CESSNA - RAYTHEON - AIAA DESIGN/BUILD/FLY 2013		
DRAWN BY: PETER FINIGAN	MISSION 3: EXTERNAL STORE ATTACHMENT METHOD	
CHIEF ENGINEER: JEFF MOCKELMAN	DRAWING PACKAGE	APPROVED: 21 FEB 2013
ALL DIMENSIONS IN INCHES	SCALE 1:10	SHEET 5 OF 5

6.0 Manufacturing Plan and Processes

This section describes the methods and materials used for fabricating the aircraft. Since this aircraft was designed as a flying wing, all of the typical aircraft fuselage components were integrated within the construction of the wing itself. The aircraft needed to be strong enough and stiff enough to retain dimensional accuracy over the entire airframe, while also having a large portion of the interior free to store internal cargo and flight systems. Lightweight construction methods were chosen for the main fuselage and the vertical stabilizers through empirical evaluation and prototype testing.

6.1 Wing/Body

Several different manufacturing methods were considered for the construction of the wing/body. Since it serves as the only lifting body it is important that it keep the shape of the airfoil. It must retain its shape in flight. As such, three different construction techniques were considered: a balsa-ribbed structure with full external balsa sheeting, a balsa-ribbed structure with plastic covering, a foam wing with external fiberglass sheeting and a foam wing with an internal spar and no external surface treatment. Table 6.1 below shows the factor of merit associated with each type of construction.

Table 6.1: Fabrication Factor of Merit Chart

Manufacturing Methods	Weight	Balsa Ribs W/ Plastic Covering	Balsa Ribs W/ Balsa Sheeting	Foam Core W/ Fiberglass	Foam Core W/ Carbon Rod
Factor	Weight	Scoring			
Dimensional Accuracy	0.2	0	1	1	1
Strength	0.2	0	1	1	1
Design Freedom	0.2	0	-1	1	1
Skill	0.2	0	-1	-1	1
Weight	0.2	0	-1	-1	1
Total	1	0	-0.2	0	1

It was evident that a ribbed balsa structure with plastic covering would not adequately hold the dimensional accuracy of the airfoil due to sagging between rims along the large wing chord. A fully sheeted balsa structure would adequately hold the required shape, but simply weighed too much. A foam wing with fiberglass sheeting would be unnecessarily strong at the cost of extra weight. A foam wing with an internal carbon fiber support rod was selected as the method of manufacture for the fuselage.

The fuselage was built up from two halves of CNC cut rigid insulation foam which were glued together around a carbon fiber spar. The cut foam provided high dimensional accuracy of the airfoils while still remaining light enough to be competitive. Splitting the fuselage into an upper and lower half allowed cavities and channels to be machined in the center of the fuselage before the halves were bonded together. These hollow areas were used to provide space for internal payloads and flight components such as servo wiring and radio hardware. The surface of the foam was hand sanded to remove machining tool marks and create a smooth finish for minimal drag. This method ensured a dimensionally accurate result. This construction had the added benefit of reducing the cost of materials and need for manual skill to fabricate the wing components.

A central carbon fiber spar reinforced the fuselage and connected to each of the main load points on the aircraft, such as the batteries, internal stores, external stores, and the landing gear. A prefabricated unidirectional carbon fiber tube was used due to its high rigidity. It was cut to length and glued in between the machined foam fuselage halves to create a single bonded structure. This combination of materials provided sufficient airframe strength and dimensional rigidity, while still allowing sufficient internal storage space.

6.2 Vertical Surfaces

The vertical stabilizing surfaces in this design were the centrally located tail and the outboard winglets. The goal of manufacturing these parts was to keep them as light as possible while still maintaining the necessary strength for aerodynamic forces during flight maneuvers. Two different fabrication methods were proposed; balsa ribbed structure with plastic covering or a CNC cut solid foam structure with central strengthening spar.

The aerodynamic and mechanical forces on these parts are not exceptionally large, thus high mechanical strength was not a major concern with these components. The two proposed construction methods were evaluated based on their dimensional accuracy and total weight.

The approximate weight of a balsa ribbed structure with plastic covering was estimated by weighing samples of tail structure from previous years' competition planes. Similarly, a similar sized tail surface was prototyped out of rigid insulation foam and weighed in comparison to the balsa structure. The results are shown in Table 6.2.

Table 6.2: Vertical Surface Material Weight Evaluation

Material	Foam	Plastic Covered Balsa
Weight (g)	5	15
Area (in^2)	36.5	53
Weight Factor (Surface Area/ Unit Cell)	0.1	0.3

Figure 6.1: Weighing of Vertical Surface Samples

The winglets and vertical tail were made out of CNC cut rigid insulation foam with fiberglass cloth to reinforce their attachment points. The foam insulation is very light and retains its machined dimensions accurately. The tail and winglet components had both sides milled on a CNC router to create the desired airfoil shape. A small carbon reinforcing spar was bonded to the vertical tail to add strength and reduce flexibility. The vertical stabilizers were bonded with adhesives to the aircraft fuselage.

The strength of the foam winglets was verified by fabricating prototype foam winglets and mounting them on the prototype airframe. Various flight maneuvers were conducted with the winglets installed to verify that they were a durable solution.

6.3 Schedule

The manufacturing process consists of six main stages that were followed in succession during the aircraft build. The milestone chart presented in Figure 2.2 was used to track the build progress.

- **Stage 1: Gathering –** The materials and tools necessary for the build were purchased and gathered in the workspace. The parts list for each aircraft system was checked and the tools were prepared for use.
- **Stage 2: Cut Parts –** Both automated and hand-cutting methods were used to cut parts from each material based on dimensions specified in the drawings.
- **Stage 5**: **Wire Propulsion and Electronics** – Before assembling the aircraft, the electronics were installed internally and the propulsion system was mounted on the front of the body.
- **Stage 3: Assemble Parts** – The body and each system were assembled according to drawing plans from the various parts and then inspected for quality during and after assembly.
- **Stage 4**: **System Integration** – Each of the main aircraft systems were integrated to complete the central structure. Assembly and structural integrity were tested and checked.
- **Stage 6**: **Finishing Touches** – The final stages of aircraft manufacturing were completed. The aircraft systems were sanded smooth and finished, and all flight systems were calibrated.

7.0 Testing Plan

Testing was utilized to aid in the design of systems and also to analyze system performance to validate theoretical equations used in design. Prior to building, structure and aerodynamics testing occurred with a prototype. Propulsions testing also occurred with static and dynamic thrust tests to validate chosen design paths. After building, further strength testing and flight testing was conducted.

Table 7.1: Testing Schedule

Test	Start Date	End Date
Thrust Testing	11/28	12/8
Assembly	2/16	2/16
Prototype Flights	2/17	2/17
Strength Testing	2/24	2/24
Flight Testing	3/8	3/11

7.1 Pre-Assembly Propulsion Testing

Propulsion testing included blade fuse current testing, battery discharge testing, and car-mounted thrust tests. In fuse testing, a variable AC power supply was connected to 2 step-down transformers

which were wired to a single 20A blade fuse. Amperages and fuse blow times were observed. The current was kept constant by increasing the voltage to account for rising resistivity due to rising temperatures.

Analysis of available data resulted in the selection of Elite 2000 battery pack with a 6.7:1 gear drive. After these selections were made, testing on lower gear ratios and different batteries insured that the 6.7:1 gear drive and Elite 2000 battery pack were the optimal components. Two alternate components were tested on the selected 17X10 and 16X12 propellers: the use of 32 cells of Tenergy 1600s wired in series and a 5.2:1 gear drive. Again, the Neu 1509-1820 motor and the Castle Creations Phoenix Ice 50 ESC were used.

Battery voltage and discharge tests were performed using a Thunder AC6 programmable battery charger/discharger and the data logging Phoenix Ice 50 ESC. The Thunder AC6 could charge, discharge and display the fully charge capacity of battery. Capacity was checked before and after each thrust test, described below. If the capacity dropped significantly, the batteries had been damaged in testing.

Thrust testing and amperage testing was performed with car-mounted thrust test stand. A strain gauge and pitot tube provided thrust and wind speed data, respectively. The data logging ESC provided data on voltage and amperage. A single test consisted of attaching a propeller to the Neu 1509-1820 and collecting data at a constant speed, read from the car's speedometer.

7.2 Post-Assembly Testing

A crucial part of the design process for this year's competition plane is the prototype test-flying phase. Since the foam construction of the aircraft lends itself to a rapid production cycle, the decision was made to fabricate two prototype aircrafts.

7.2.1 Prototype 1

The first prototype was built in the fall semester and was intended to verify many aspects of the conceptual and preliminary designs. Most importantly, this prototype would verify that a stable wing/body design could be built and manufactured. No member had ever designed any kind of flying wing before, so this prototype was important in verifying the wing/body concept could be designed before getting too far into the design process. This prototype was designed from the same code that would design the final plane. Thus, this prototype also verified the final plane's design code.

The verification of the structure was another important role of the first prototype. The manufacturing process and strength of the foam wing and vertical surfaces were verified through this prototype during the fall. This allowed time for any revisions to the structure and manufacturing process to be made.

This prototype was also to be used to for gathering any information that can be used to improve the overall competition score. Anything from reducing favorable flight characteristics to increasing the wing size were to be considered.

This prototype plane was designed in CAD and cut from foam on a large CNC router. It was outfitted with an inexpensive motor and battery selection for initial testing. This motor and battery

combination was selected to output approximately the same amount of power that the final chosen power system would. The low cost of this initial system would be beneficial if the prototype were to crash and destroy these components.

After initial ground testing, the prototype was allowed to fly. The first flight was unloaded. Subsequent test flights were devoted to seeing how well the plane flew with additional cargo weight. Practice competition laps were flown with an increasing number of aluminum bars added to the aircraft to simulate the weight of the rocket cargo. The aircraft was loaded to a maximum of 3.5lbs of additional cargo weight.

Stability was also tested by trying to induce instabilities at high altitudes. Various flight speeds and maneuvers were attempted.

7.2.2 Prototype 2

The second prototype was to perform initial flight testing of the final design. This final design utilized the design code verified with the first prototype. However, the design code was passed through an optimization routine, so the flight characteristics needed to be reevaluated. Thus, the second prototype was designed to be a close approximation of the final design and was intended to be used to verify that all of the aerodynamic calculations and considerations were valid. The goals of the prototype flight testing were to make sure that the aircraft was capable of flying a mock mission lap with full payload. Validating the final structural design was another goal for this prototype. Based on the results of the test flight, modifications could be made to the design of the final aircraft.

This prototype plane was also designed in CAD and cut from foam on a large CNC router. This aircraft was outfitted with the motor and battery selection for the competition plane.

Initial high speed ground handling tests were performed to make sure that the landing gear had straight and stable ground handling. Some initial trimming of the steerable nose wheel was required to get the aircraft to taxi straight down the runway. Once this was complete, the aircraft was brought up to full speed and flown for the first time.

Subsequent test flights were devoted to seeing how well the plane each of the competitions missions. Practice competition missions were flown with the proper payload. In addition, the aircraft was flown with payload than any mission called for. This ensured a reasonable factor of safety existed.

To test stability characteristics, the prototype aircraft was repeatedly flown in low speed, high angle of attack and high altitude landing approach patterns. Performing these maneuvers at a high altitude ensured that there would be time to recover the aircraft if it became unstable. During these maneuvers, the aircraft's rudder was shaken back and forth to try to induce instability.

Table 7.2: Pre-flight checklist for testing and competition.

	Pre-Flight Checklist	
1	Check exterior for damage.	
2	Check all assembly joins for secure attachment.	
3	Check all pushrods and control linkages.	
4	Check all electrical connections.	
5	Check props for damage and ensure collets are tightened.	
6	Check that any and all payload is secure.	
	Attach batteries and check connection.	
8	Clear prop.	
9	Activate receiver.	
10	Plug in fuses.	
11	Range check and verify control surface deflection.	
12	Check surroundings for obstacles or bystanders.	
13	Static motor run-up.	

Table 7.3: Flight test plan sequence for prototype 2.

		Flight test plan	
Flight Number	Designation	Setup	Objectives
1	Maiden Flight	No payload	Successful take-off, trim aircraft
2	Internal Payload	2 store payload	Successful take-off, fly one lap
3		4 store payload	Successful take-off, fly one lap
4		6 store payload	Successful take-off, fly one lap
5		8 store payload	Successful take-off, fly one lap
6-11	External Payload	M3 Configuration 1-6	Successful take-off, fly one lap
12	Mission 1	Exact specifications in Mission 1 profile.	Successful take-off, complete as many laps as possible
13	Mission 2	Exact specifications in Mission 2 profile.	Successful take-off, complete 3 laps
14-19	Mission 3	Exact specifications in Mission 3 profile.	Successful take-off, complete 3 laps

8.0 Test Results

The flight and non-flight tests were all completed successfully. This allowed the review of the overall aircraft design and changes to be implemented for the next aircraft iteration.

## 8.1 Non-Flight Test Results

8.1.1 Propulsion

Battery tests showed that roughly 22-24 NiMH cells provided the desirable amperage of about 25 amps and any number above this drew too much current. The gear drive tests revealed that a higher gear ratio provided more thrust for take-off. However, a lower gear ratio drew too much.

Table 8.1: Battery Discharge Tests

Trial	Battery	# of Cells	Maximum Voltage (V)	Voltage per Cell (V)	Maximum Amperage (A)	Capacity Before (mAh)	Capacity After (mAh)
1	Elite 2000	23	32.5	1.41	17.4	2256	2254
2	Elite 2000	23	32.2	1.4	21.3	2254	2261
3	Elite 2000	23	32.1	1.4	24.7	2261	2256
4	Elite 2000	23	32.2	1.4	27.6	2256	2248
5	Tenergy 1600	32	38.8	1.21	35.7	1656	1579
6	Tenergy 1600	22	26.2	1.19	25.4	1579	1539

The results in Table 8.1 show that the Tenergy 1600 mAh cells damage even at currents that the Elite 2000s can handle. The initial use of Tenergy 1600s in trial 5 contributed to damaging the cells. Trial 6 showed damage to the cells. Testing conditions included 30 degree (Fahrenheit) weather. In the heat of Tucson, the damage would be expected to be much greater.

Most results for propeller and motor testing can be seen in Figure 8.1.

**(a) Thrust vs. Velocity**   **(b) Amperage vs. Velocity**
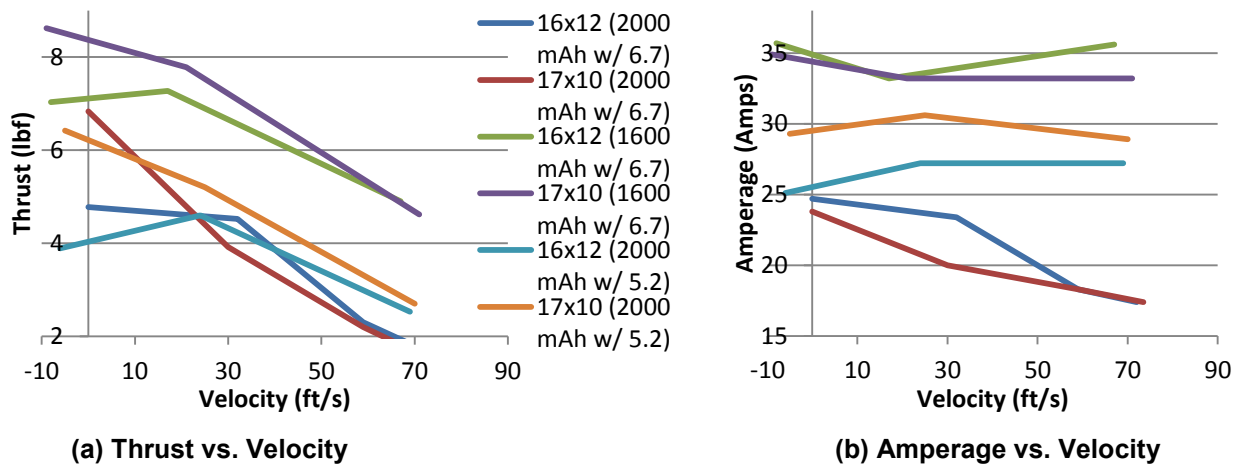
Figure 8.1: Thrust and Amperage vs. Velocity

Although the Neu 1509 was selected initially, testing with the Neu 1509-1820 and Neu 1112-1750 revealed that the Neu 1112-1750 was a better choice. This was because the Neu 1509's continuous power rating of 750W was unnecessary due to internal battery resistance decreasing the output voltage from 32V to 19V when current draw was high. Therefore, the battery pack could only produce a maximum of about 475W. Testing revealed the lighter Neu 1112 with a lower kV rating would be more suitable and less resistive.

8.1.2 Wing

The wing-tip test was successfully completed. As can be seen in Figure 8.2, the deflection is the wing is minimal, but smooth across the entire span of the wing. There were no obvious discontinuities or large stress concentrations. Post-test visual inspection revealed no cracks or fractures. The wing-tip test validated the decision to reinforce the foam wing with carbon spars.
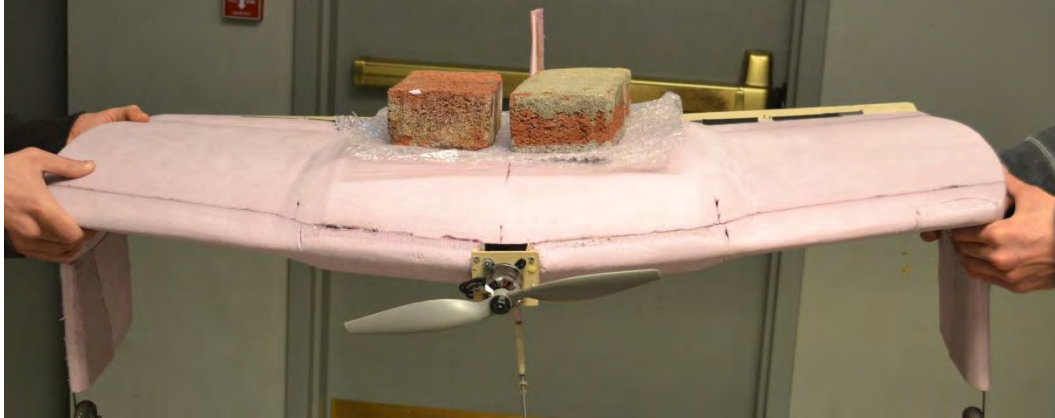
Figure 8.2: Wing tip test.

8.1.3 Landing Gear

The landing gear test was successful. There were no fractures in the struts or attachments or permanent deformation in the landing gear even after the heaviest test loads were applied. The landing gear flexed correctly, demonstrating its ability to withstand a hard landing on the runway. Figure 8.3 shows the results of the test.
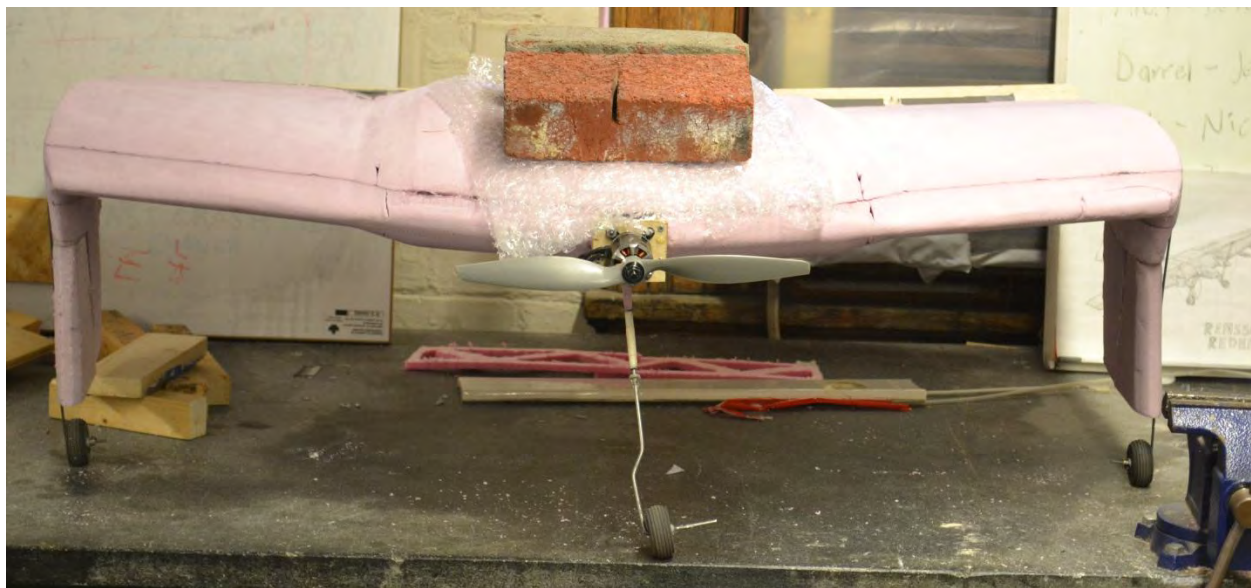
Figure 8.3: Landing gear test.

8.1.4 Payload

The payload test verified the payload attachment methods. All types of payload could be securely attached. The payload stayed attached to the aircraft during all simulated loads and vibration. Figure 8.4 shows the internal stores resting in their flight arrangement in the cargo area.
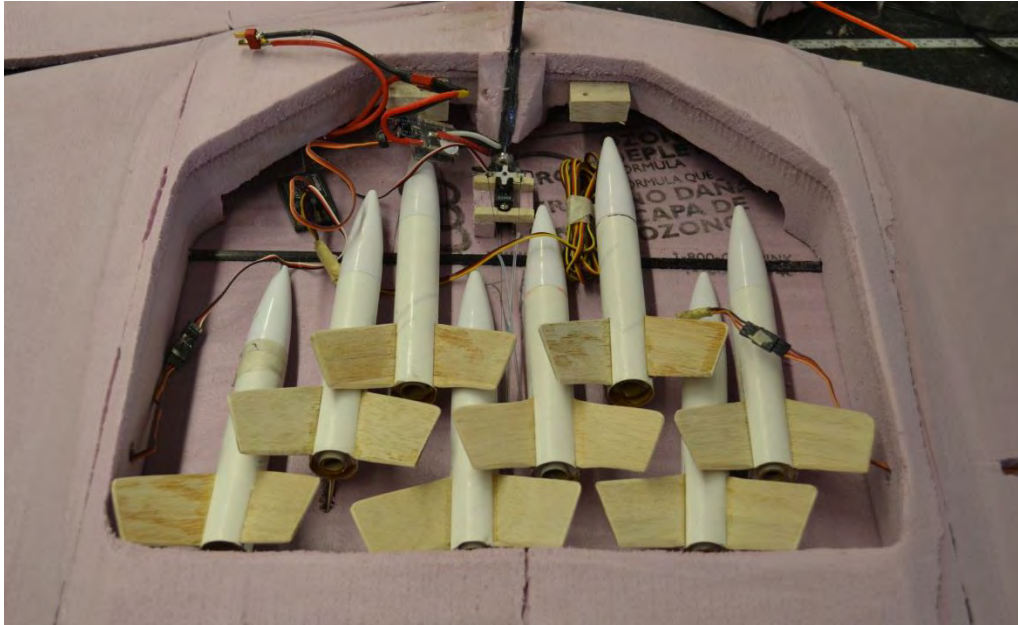
Figure 8.4: Payload installation test

8.1.5 Assembly

The final pre-flight test was also completed successfully. The team member selected for assembly was able to construct the aircraft from its pre-flight configuration to the flying configuration (including payload loading) in an average time of 2 minutes 15 seconds. No single trial took more than the allotted 5 minutes.

8.2 Flight Test Results

8.2.1 Prototype 1

The first prototype easily verified the foam structure could be manufactured and was strong enough for both the wing and vertical surfaces. This prototype had good flight characteristics which verified the design code for use in the competition plane design.

This prototype was loaded with aluminum bars to simulate the weight of the rockets. When fully loaded, the power system would not allow the aircraft to take off in 30 feet and climbing was difficult.

The power system of the final design was designed to be much stronger than this initial prototype power system. Thus, the final propulsion system utilized a different motor and battery selection.

During one of the test flight landing approaches, the aircraft demonstrated a slight unstable oscillating motion. It was theorized that this was caused due to insufficient vertical stabilizer area causing instability. Other than this the flight characteristics were satisfactory.

8.2.2 Prototype 2

Initial flight characteristics were very positive. The aircraft easily rotated for takeoff and gained altitude quickly. The elevons needed some up-trimming, since the plane initially wanted to pitch down

when the elevator control stick was centered. Once trimmed the aircraft maintained straight and level flight.

Each additional increment of weight required the use of a higher throttle setting to climb and maintain altitude. However, this prototype was able to takeoff in 30 feet and easily climb when fully loaded. The airframe itself, however, proved to have adequate maneuverability. It was able to complete a loaded practice mission with relative ease.

When the rudder was deflected it induced roll in the opposite direction. The cause of this turned out to be an adverse aerodynamic effect of the winglets below the wings. This will be corrected by adding winglet surface area above the wing and only have the vertical stabilizer and rudder be above the wing.

Otherwise, the airframe performed as designed. The maneuverability and ease of elevator and aileron control during flight gave reassurance that aerodynamic calculations were correct. The plane is highly sensitive in roll. The power system was also adequate.

After several attempts at inducing an unstable mode, the aircraft did not demonstrate any unusual instability. The oscillation was determined to be a pilot induced movement and not a deficiency in the aerodynamic stability.

The aircraft structure never exhibited any cracks during inspections or any undesired characteristics during flight. It was found that the CG location needed for stability was impractically far forward and so sweep will be added to bring the AC back, allowing a further aft CG.

Figure 8.5: Test flight of the second prototype

9.0 Works Cited

[1] R. F. Anderson, "Report No. 572: Determination of the Characteristics of Tapered Wings," NACA, 1937.

[2] "UIUC Airfoil Coordinates Database," University of Illinois at Urbana-Champaign Department of Aerospace Engineering, [Online]. Available: http://www.ae.illinois.edu/m-selig/ads/coord_database.html. [Accessed 2012].

[3] B. W. McCormick, Aerodynamics, Aeronautics, and Flight Mechanics, John Wiley and Sons, 1995.

[4] R. C. Nelson, Flight Stability and Automatic Control, Boston: McGraw Hill, 1998.

[5] Drela, "XFLR5," Novermber 2012. [Online]. Available: www.xflr5.com.

[6] M. Hepperle, "Javafoil," 2006. [Online]. Available: http://www.mh-aerotools.de/airfoils/javafoil.htm.